Numerical modelling and mechanical analysis of the machining of large aeronautical parts : Machining quality improvement

Xavier Cerutti

ParisTech
INSTITUT DES SCIENCES ET TECHNOLOGIES
PARIS INSTITUTE OF TECHNOLOGY

MINES ParisTech

École doctorale nº 364 : Sciences Fondamentales et Appliquées

Doctorat ParisTech

THÈSE

pour obtenir le grade de docteur délivré par

l'École Nationale Supérieure des Mines de Paris

Spécialité "Mécanique Numérique"

présentée et soutenue publiquement par

Xavier CERUTTI

le 04 décembre 2014

Modélisation numérique et analyse mécanique de l'usinage de grandes pièces aéronautiques: Amélioration de la qualité d'usinage

-

Numerical modelling and mechanical analysis of the machining of large aeronautical parts: Machining quality improvement

Directrice de thèse : **Katia MOCELLIN**

Jury

M. Philippe LORONG, Professeur des universités, Arts et Métiers ParisTech, PIMM	Président
M. Pedro-José ARRAZOLA ARRIOLA, Professeur des universités, Université de Mondragon	Rapporteur
M. Jean-Michel BERGHEAU, Professeur des universités, ENISE, LTDS	Rapporteur
M. Emmanuel DUC, Professeur des universités, IFMA, Institut Pascal	Examinateur
Mme. Katia MOCELLIN, HDR, Maître de Recherche, MINES ParisTech, CEMEF	Examinateur
Mme. Myriam BOUET-GRIFFON, Chef de projet R&D, Constellium Technology Center	Invité

MINES ParisTech
CEMEF - UMR CNRS 7635
1 Rue Claude Daunesse, 06904 Sophia Antipolis, France

THESE

Remerciements

Pour commencer, je souhaiterais remercier tous ceux qui m'ont formé, aidé et suivi et qui ont donc contribué à la réussite de ce projet.

Premièrement je tiens à remercier l'ensemble de la direction du CEMEF pour m'avoir donné la possibilité et donné les moyens de réaliser ce travail.

Je tiens également à remercier ma directrice de thèse, Katia MOCELLIN, pour son encadrement remarquable, sa disponibilité ainsi que sa bonne humeur! Nos discussions furent pour moi une grande source de motivation et ce fut vraiment un grand plaisir de travailler avec elle durant ces trois années. J'ai beaucoup appris. Merci!

Je tiens ensuite à remercier tous les membres de mon jury. Pedro-José ARRAZOLA ARRIOLA et Jean-Michel BERGHEAU pour avoir accepté et eu la patience de lire avec attention ce manuscrit ainsi que Philippe LORONG pour avoir accepté de présider ce jury. Ce fut un plaisir de vous rencontrer et de pouvoir discuter avec vous. Merci également à Emmanuel DUC et Myriam BOUET-GRIFFON pour avoir pu vous rendre présents ce jour.

Ces travaux ont été réalisés dans le cadre du Projet OFELIA. Je tiens donc également à exprimer ma gratitude à tous les acteurs de ce projet ayant contribué à sa réussite : Myriam BOUET-GRIFFON et Sylvie ARSENE (Constellium CRV), Ludovic BOURGEON et Arnaud BLANCKAERT (Aubert&Duval Issoire), Abel KHAMALLAH (Constellium Issoire), Arnaud BOIVIN (Rexiaa) ainsi que Emmanuel DUC et Sami HASSINI (IFMA). Je tiens à remercier ce dernier pour avoir partagé ses connaissances de l'usinage, des logiciels FAO et sans qui il n'aurait pas été possible d'obtenir les mesures expérimentales nécessaires pour la validation de l'outil numérique.

Je tiens également à remercier toutes les personnes ayant fait de ces trois ans de thèse au CEMEF un moment agréable et enrichissant: François BAY, Yannick TILLIER, Pierre Olivier BOUCHARD, Marie-Françoise GUENEGAN, Patrick COELS et tous les autres. Je tiens bien évidemment à remercier également tous mes collègues doctorants et post-doctorants pour toutes les discussions sur nos thèses et travaux et pour tous les bons moments passés: Olivier, Ali, Dorian, Antoine, Sabrina, Romain(s), Victor, Simon, Colin et tous les autres.

Enfin, je tiens à remercier tout particulièrement mes proches, pour tout le temps avoir été présents ainsi que pour m'avoir soutenu et encouragé et sans qui rien de tout cela n'aurait été possible. Merci pour tout!

Contents

Introduction

Contents

Aeronautics

According to forecasts, air traffic is expected to more than double over the next 15-20 years with an increase of approximately 4.7% [1] per annum. The aerospace industry is therefore booming and is facing an increasing demand [2]. This represents a need for approximately 30,000 new planes, a third of them replacing older ones. The aviation industry is thus very healthy and presents a high potential of economical growth (see Figure 1).

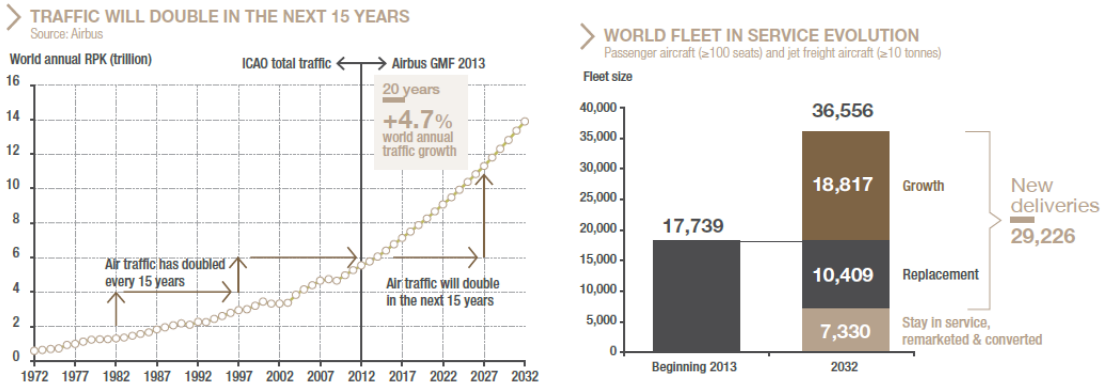

Figure 1: Forecasts of the development of air traffic and the number of new aircrafts needed by 2032 [1]

Aeronautics requires the implementation of sophisticated technologies with an absolute security, resulting in the need of a high mastery of every process which has led the aviation industry to significant investments into R&D programs. For example, the technological progresses made during the last 40 years have already allowed to reduce the fuel consumption and CO_2 emissions by 70% as well as noise by 75% compared to levels in 1970, while passengers benefit from an increasing level of comfort [1]. This progress results in a continuous improvement of technologies used in the construction of aircrafts which is itself the result of the numerous R&D programs. Competition in the aviation industry is therefore increasing and industries face many challenges to produce even more efficient parts with increasingly shorter lead times, using the most advanced materials. The production of relatively small series requires production flexibility, making the fulfilment of these expectations even harder.

The aim to improve the efficiency and to minimise the environmental impact of planes has become a priority and therefore a major area of research and innovation in aeronautics. One way to achieve the objective of more efficient and more environmentally friendly planes is the manufacturing of lighter parts with better mechanical properties and the use of the smallest amount of resources (material, energy) possible to produce them. Both the development of new grades and the optimisation of the manufacturing processes are therefore solutions. This need has already led to an increase in the use of composite materials for aircraft construction. However, in new planes aluminium still represents up to 20% of the weight (see Figure 2) and with the arrival of new alloys this percentage may well increase.

The necessity to improve planes is also one of the reasons which led to the fact that most

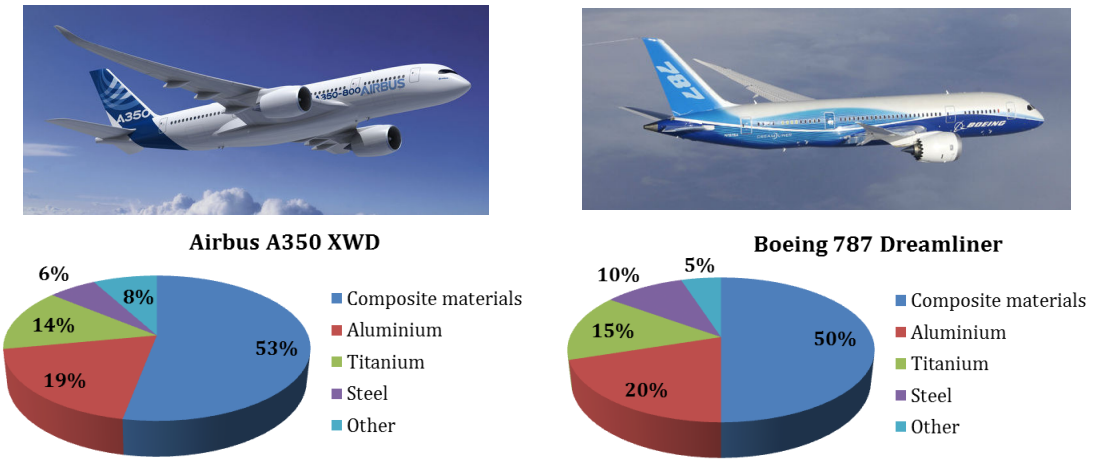

Figure 2: Distribution of materials by percentage of weight of the aircraft [3, 4]

structural parts made of aluminium are large monolithic parts, thereby lowering the weight of the parts in minimizing the use of assembly equipment (bolts, screws, etc). The manufacturing of increasingly larger monolithic parts in aeronautics is also intensified by the need to reduce the assembly costs which can represent up to 50% of the total costs of delivered parts [5]. These large monolithic parts are usually made from aluminium prismatic blocks or from preformed parts (forging, stamping) of which up to 90% of the weight of the raw material is removed by machining operations. One of the terms commonly used to express this characteristic is the "buy-to-fly" ratio, which represents the ratio between the weight of raw material purchased to manufacture the part and the weight of the final part (flying part). Some examples of structural aluminium alloy aircraft parts are presented in Figure 3. The large monolithic structural parts usually present a high "buy-to-fly" ratio and a lot of added value due to the manufacturing steps and to the amount of material required to obtain the final part. These parts are thus very expensive to produce. Machining is the last manufacturing step where the finished product is obtained and is therefore a crucial step in the global manufacturing of aeronautics aluminium alloy parts.

Aluminium-Lithium Alloys

Among new aluminium alloys developed to meet these new challenges the Al-Cu-Li alloys have reached the leading position. Al-Li and especially Al-Cu-Li alloys are very interesting for aeronautics. With lithium (the lightest metallic element) these alloys present a lower density as well as higher elastic properties compared to conventional high strength alloys such as the 2XXX and 7XXX series. Using 1% lithium of the total mass, the alloy density drops by about 3% while its Young's modulus will be increased by about 6% (valid for a Li content of up to 3%) [7, 8].

The use of lithium as an additive element in aluminium is not new. As shown in Figure 4, the

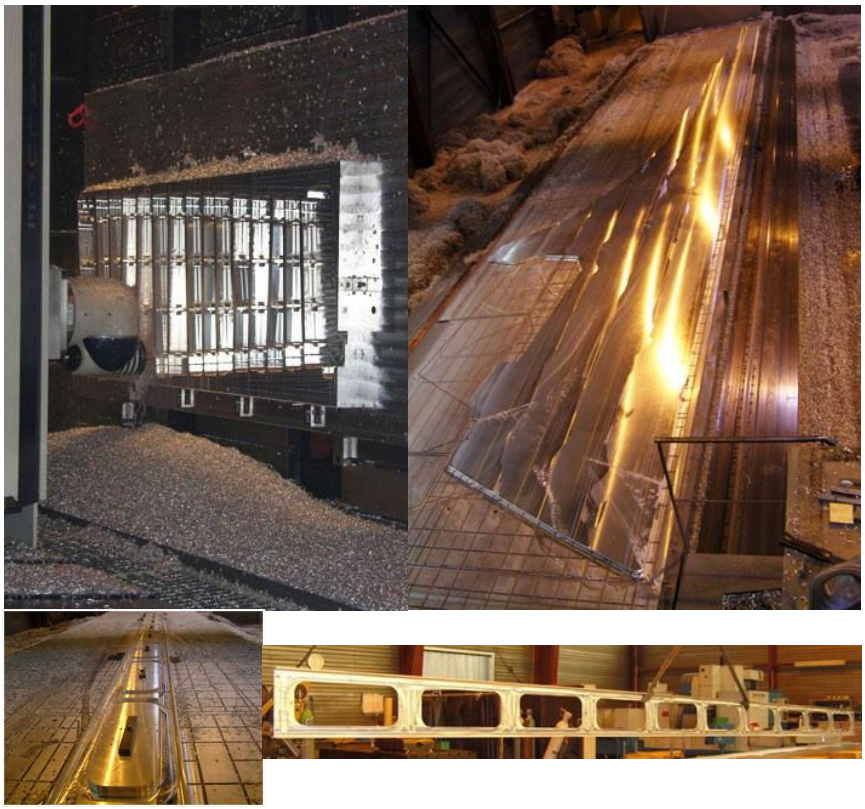

Figure 3: Machining examples of large aerospace monolithic parts made of aluminium alloy [6]

first appearances of lithium in aluminium alloys go back to the 1920s, but the first generation of aluminium-lithium alloys has emerged only in the 1960s with the arrival of the AA2020 alloy (Alcoa in 1958, USA) and then VAD23 (1961, USSR) [9].

However, the development of modern aluminium-lithium alloys (second generation) really began after the oil-shocks of the late 1970s and early 1980s. This second generation comprised mainly the alloys AA2090, AA2091, AA8090 and AA8091. These alloys contained more than 2% of lithium in their weight and therefore had lower densities (about 7-10% compared to conventional alloys of the same strength used at that time). They were used primarily for military applications and achieved very limited commercial success, mainly because of technical problems due to the strong anisotropy and to the particularly low toughness and corrosion resistance under stress causing many cases of rupture during riveting operations for example [7].

The alloys of the new generation that emerged in the 1990s contained less lithium than previous alloys, thereby avoiding the technical problems encountered before. The first alloy of the new-generation alloys was the Weldalite 049 (AA2094) followed by a refined version of the original AA2195 alloy. This alloy was selected for the Space Shuttle (U.S. Space Shuttle Super Light Weight Tank) allowing a reduction in weight by 3,400 kg of a total weight of the

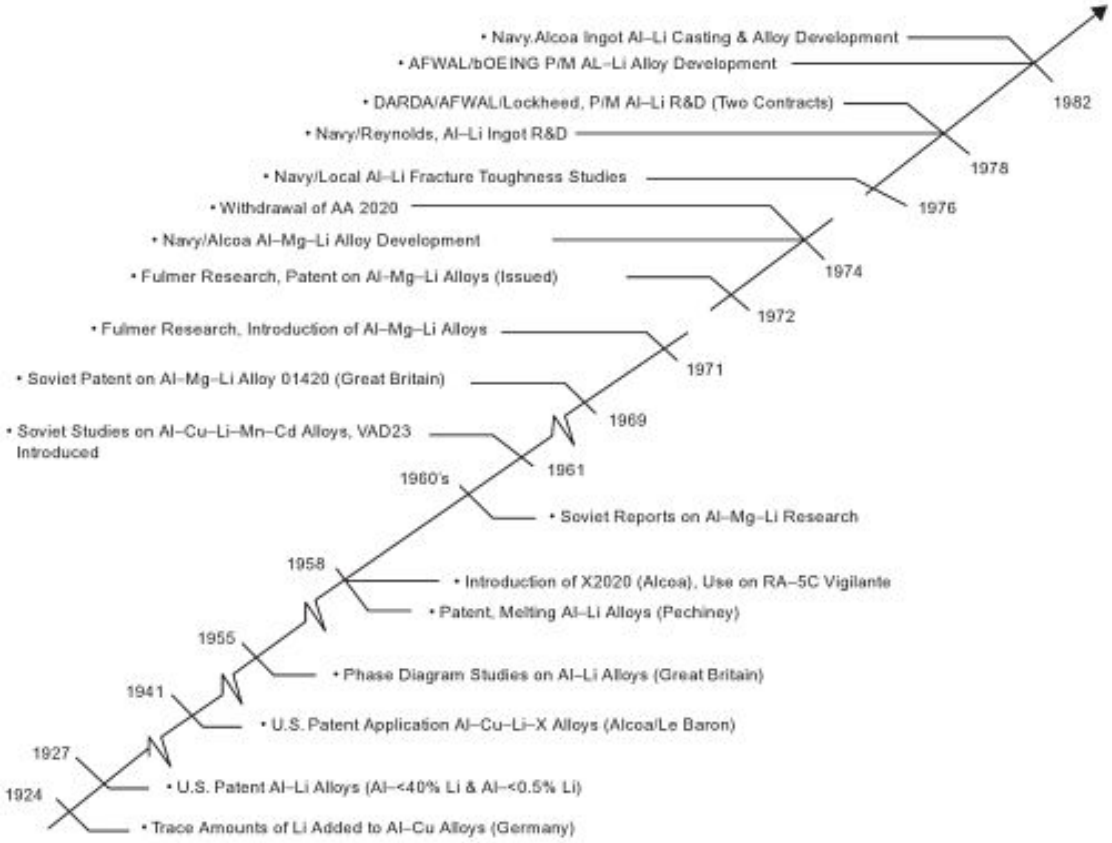

Figure 4: The first developments and uses of lithium in aluminium alloys [9]

space shuttle of 27,000 kg. Three other alloys of the new generation were then developed: AA2096, AA2097 and AA2197. These alloys exhibit improved fatigue properties which allow for example to double the service life of parts such as the BL 19 Longeron of the F16 military aircraft compared to the alloy used previously (2124) [10]. Despite the fact that these alloys are more expensive than conventional alloys they are more economical on the long term. It has for example been shown that the AA2098 has an improvement in life time of the factor six compared to the AA2024. This alloy was then selected for the fuselage of the F16 military aircraft [8].

In the past, aluminium-lithium alloys have not achieved a great commercial success because in addition to the problems encountered in the mechanical properties of these alloys (anisotropy), they were also difficult to produce. The arrival of new and more efficient addition techniques of lithium [11] have given a fresh boost to these alloys making them one of the cutting-edge materials for aerospace.

Among the new aluminium-lithium alloys, the ones using the AIRWARE® technology developed by Constellium are the most advanced. They have been specially developed for aeronautics and space and combine uniquely strength, lightness, durability and recyclability.

They have notably been chosen by Bombardier for the fuselage of the CSeries aircraft and by SpaceX for the Falcon 9 rocket.

The product range includes the AIRWARE® 2050 alloy for thick products. It is an alloy offering a high strength and high damage tolerance. The chemical composition of the AIRWARE® 2050 alloy, which is presented in Table 1, has been specially chosen to obtain a very good balance in its properties and at the same time to avoid element additions which can cause undesired behaviour. In other words, the AIRWARE® 2050 alloy has been developed using an optimised chemical composition allowing to ensure thermal stability, to achieve the required strength level and to maximise the strength-toughness balance.

Table 1: The AIRWARE® 2050 alloy's chemical composition

% by weight	Si	Fe	Cu	Mn	Mg	Zn	Li	Ag	Zr
Min			3.2	0.20	0.20		0.7	0.20	0.06
Max	0.08	0.10	3.9	0.50	0.60	0.25	1.3	0.70	0.14

The mechanical properties of the AIRWARE® 2050 alloy (the main ones being summarised in Table 2) substantially exceed those of conventional alloys including the 7050 alloy very commonly used in aeronautics. For more details on the choice of the addition elements interested readers can refer to [12]. The AIRWARE® 2050 alloy is particularly used in the manufacture of large structural parts where significant machining operations are generally performed. More specifically, the alloy used for these parts is the AIRWARE® 2050-T84 alloy. This state of the AIRWARE® 2050 alloy is obtained by performing multiple thermo-mechanical treatments after the forming process (which are described later in this dissertation in Section 1.1.3). Within this document the AIRWARE® 2050-T84 alloy will always be cited as the AIRWARE® 2050 alloy.

Table 2: Main mechanical properties of the AIRWARE® 2050 alloy at room temperature (20 °C)

Young's Modulus (E)	Poisson's Ratio (ν)	Density (ρ)	Tensile Yield Strength
75000 MPa	0.33	2693 kg/m^3	500 MPa

The OFELIA Project: Motivation

Presentation of the OFELIA Project

The work presented in this dissertation has been carried out in the framework of the **OFELIA** project which aims to optimise the eco-efficiency of the AIRWARE® alloys sector for the aeronautic industry ("**O**ptimisation d'une **F**ilière **E**co-efficiente Aluminium **Li**thium pour **A**éronautique" in French). The OFELIA project is labelled by the "Pole de Competitivité

Viaméca" in the scientific topic of "Advanced manufacturing processes". Its main objective is to develop an optimised manufacturing chain for complex aeronautics parts made of AIRWARE® 2050 alloy. More specifically, the project objective is to optimise the global manufacturing going from the semi-finished product (forged part, rolled plate) to the recycling of the machining chips. The improvement of the eco-efficiency of the sector aims to minimise both the environmental impact by optimising the use of resources and the costs (economic efficiency).

The OFELIA project gathers three industrial (Constellium, Aubert&Duval, Rexiaa) and three academic (Cemef, IFMA, SPIN) partners and is structured in five tasks. More information on the project organisation and partners can be found in Appendix A.

Involvement of this Work in the Project: Problematic

The work presented in this dissertation has as main objective the prediction of the machined part quality depending on the machining process plan used in order to develop machining process plans taking into consideration the mechanical behaviour of the workpiece due to its manufacturing history and therefore to improve the machining quality.

The machining quality can be defined as the machining process plan's capability to produce parts with the desired geometrical and dimensional characteristics. The fewer differences between the final machined part and the designed one (CAD) occur the better the quality of the part. The machined part quality is defined by macro-geometrical properties such as the accuracy of dimensions, form and position of geometrical elements [13]. The part quality is strongly governed by the parameters of the machining process which can all cause disturbances. Five different machining parameters can be defined:

- The fixture
- The tool path
- The machining sequence
- The cutting conditions
- The mechanical state and the dimensions of the initial workpiece

All these parameters can have a more or less significant influence on the global part quality. In a traditional industrial environment, the choice of the machining parameters is often based on the experience and expertise of the process engineers and machinists. There is therefore almost no rule available based on scientific analysis in the definition of machining process plans.

Influences of parameters such as the manufacturing technique (forged part or rolled plates) of the initial workpiece are often not taken into account in the definition of the machining process plan. The consequences of neglecting some of the machining parameters and their influence on the machined part quality can lead to several costly machining trials to validate a machining process plan, to unexpected extra conforming steps after machining to obtain a conforming part or in the worst case to reject. To improve the cost-efficiency of the machining

processes, the initial workpiece is often chosen to have the shortest machining time and the smallest amount of material used as possible, despite the fact that the choice of the initial workpiece has a significant influence on the machining quality. The workpieces having undergone several manufacturing steps (forming processes and/or heat treatments) always contain residual stresses. When a section of a workpiece that possesses residual stresses is removed by machining, the initial equilibrium state of the block (plate or preformed part) is broken. A new state of static mechanical equilibrium is therefore obtained resulting in part distortion. Depending on the manufacturing steps performed previously to the machining, the workpiece exhibits different residual stress distributions. A change in the choice of the initial workpiece can therefore have a significant influence on its behaviour during the machining process.

In the past, several studies have been realised on the influence of the different machining parameters but most of them are applied on parts with simple geometries and are not adapted to our industrial problematic (large and complex structural parts with multiple machining features) [14, 15, 16]. Only a few studies have been performed on the combined effects of the parameters and their impact on the global part quality [17, 18]. These studies have nevertheless shown some limitations:

- The numerical method used to perform the material removal makes it difficult to simulate the machining of large and complex aluminium alloy aerospace parts (the size of the simulated part is often decreased and the geometry often simplified).
- The numerical methods (material removal technique, element type) used make it difficult to simulate the machining of aluminium alloy aerospace parts made from workpieces obtained with different manufacturing methods (like forging).
- Only the post-machining distortions are predicted. The dimensional and geometrical variations due to the workpiece deflections during the machining depending on the machining process plan used are neither considered nor predicted.

The main objective of this work is therefore the development of a numerical approach and tool to predict deflections during machining as well as post-machining distortions of large and complex aerospace parts depending on the machining process plan used. In other words, this numerical tool has to be able to predict the final shape and dimensions of the parts to analyse the quality of the machining process plan. This work aims to offer an evolution in the establishment of machining process plans of aluminium structural parts by proposing rules of chronological sequencing of the machining operations and of the choice of the fixture-layout depending on the residual stresses in the workpiece and the geometry of the designed part. The need for this study is further enhanced by the use of new alloys such as the AIRWARE® 2050 alloy whose machining behaviour has not been extensively studied. This work therefore presents both scientific and economic challenges.

Scientific challenges:
The numerical tool developed will allow to understand the various phenomena occurring during the machining of large and complex AIRWARE® 2050 alloy aerospace parts and the

influence of the different parameters. This work will therefore enable to determine the parameters of first order (with the biggest influence) and to determine rules to ensure the desired machining quality. In addition, it will allow to accurately predict the final geometry and the stress state of the parts at the end of the manufacturing line. This will give the possibility to model the behaviour of a part in service in taking into account its whole manufacturing history (including machining). It will be possible to study for example the influence of the final geometry on the assembly process and stress state of the global structure, the influence of the final stress state of the part on the mechanical strength (fatigue, crack growth) as well as the optimisation of the entire life cycle of a part.

Economic challenges:
By predicting the machining quality, the numerical tool developed will provide a better control of the machining process and the possibility to optimise the machining process plan to ensure the accuracy and quality aimed at. This will avoid the rejection of parts due to the non-conformity with dimensional and geometrical specifications as well as the realisation of extra-conforming steps to decrease the post-machining distortions and to make the part compliant with the tolerance specifications. The prediction of the machining quality and the optimisation of the machining process plan will therefore help to enhance both the productivity and the machining process robustness.

A strong collaboration between project stakeholders was necessary to fulfil the objectives of the work presented in this dissertation:

- With Aubert&Duval and Constellium CRV: to determine the residual stress state of the workpiece before machining (rolled plates or forged parts) as well as the main thermo-mechanical characteristics of the AIRWARE® 2050 alloy.
- With IFMA: to make the connection between CAD/CAM software and the numerical tool developed to predict the machining quality as well as the comparison between simulation and experimental results.
- With Constellium Issoire, REXIAA and LUSINA: to use their experience and knowledge of the machining of large aerospace aluminium alloy parts and to come as close as possible to the industrial problem.

Research Objectives

The main objective of this work is to meet needs of the aerospace industry in giving the possibility to optimise and to validate a machining process plan to obtain the desired part quality before going into real machining. If the predicted machined geometry lies outside the tolerance specifications, the part is defective and the parameters of the machining process plan have to be changed. The requirements are therefore to predict the workpiece deflections during the machining as well as the post-machining distortions of large and complex aerospace AIRWARE® 2050 alloy parts depending on the machining process plan parameters.

To fulfil this purpose, the research objectives of this Ph.D. work are:

- To review the literature on the machining of aluminium alloys and to establish assumptions on the machining parameters' influence on the machining quality.
- To develop a modelling approach to simulate the machining of complex and large AIRWARE® 2050 alloy aerospace parts based on the previously established assumptions.
- To develop numerical methods based on the approach chosen.
- To develop a numerical method which gives the possibility to use both experimentally and numerically determined residual stress distributions as input.
- To integrate all the numerical methods into the FORGE 2011® environment in order to obtain the numerical tool FORGE OFELIA: the version of FORGE® adapted to the simulation of the machining of large and complex parts made of aluminium alloys.
- To analyse the influence of the different parameters in order to develop a procedure for the definition of machining process plans adapted to the initial residual stresses and therefore to the mechanical behaviour of the workpiece.

Organisation of the Dissertation

The presentation of this research work on the prediction of the machining quality of large and complex AIRWARE® 2050 alloy aerospace parts revolves around five chapters.

In the first chapter, a review of literature is presented which constitutes a background for the whole dissertation. First, an introduction on the residual stresses and their development during the manufacturing is realised. The machining process plan parameters (the cutting conditions, the fixture and the machining sequence and tool path) are then presented and reviewed with a particular attention on the machining of aluminium alloys. Then the different numerical material removal techniques and models developed to simulate the machining are revised. Finally, conclusions are drawn from the reviews of literature and assumptions adapted to the objectives of this project are established.

Chapter 2 is dedicated to the numerical developments. In the first section, a brief summary on the mechanical problem and solving using the mixed velocity-pressure formulation of FORGE 2011® is performed. Details on the numerical methods used for contact modelling, automatic remeshing and field mapping are also briefly introduced. Then, the developments performed to create FORGE OFELIA, the version of FORGE 2011® adapted to the machining simulation, are described. The methods used for the computation of the initial residual stresses, for the material removal as well as the adaptation of the contact analysis are detailed. The implementation of these methods in FORGE 2011® is then discussed, followed by the parallelization of this procedure. The options developed to increase the accuracy of the cutting are also presented. The last section focuses on the different models which can be created using FORGE OFELIA followed by a numerical validation by comparing with literature results.

Chapter 3 presents the study of the residual stress state of two rolled plates with different thicknesses made of AIRWARE® 2050 alloy. First, the layer removal method used to determine the residual stress profiles of both plates is presented and the results obtained are analysed. Simulations of these experiments are then performed which allow a first experimental validation of the numerical tool. An example of the machining of a part is also simulated and compared to experimental results, showing again the validity of the approach and of the numerical tool for the prediction of the post-machining distortion. Then, a more in-depth study on a simplified machining case, on which the two main problems of machining non-quality are highlighted, is performed. An analysis of the influence of the initial residual stresses and of the machining sequence on the geometrical and dimensional errors is thus realised. The feasibility to improve the machining quality using the developed numerical tool is then demonstrated.

Chapter 4 is devoted to a complete analysis of the influence of the machining process plan parameters on the machining quality. The case studied is a more complex part requiring several machining steps. A complete analysis of the fixture, machining sequence and initial workpiece has been performed on this part. From the results observed, a classification of the parameter influences has been realised and a procedure as well as guidelines for the definition of the machining process plan taking into consideration the mechanical behaviour of the workpiece have been developed.

In Chapter 5, the developed numerical tool is tested on two industrial cases. The first case is a large and complex structural part machined from a rolled plate whereas the second one deals with a part machined from a forged workpiece. The objective is to show that the developed numerical tool can also be used to study and to optimise the machining of complex industrial parts.

Finally, conclusions of the present study are drawn and perspectives are presented.

Chapter 1

Review of Literature

This first chapter is dedicated to a complete review of literature on the different aspects linked to the prediction of the machining quality. This literature review is organised in three main sections and is used as a reference for the whole study.

In the first section a brief introduction on the residual stresses, their origins and the residual stress genesis during the manufacturing of aluminium parts is realised.

Then, in a second section, previous work realised on machining processes and more specifically on the milling of aluminium alloys and the parameters possibly influencing the machining quality is studied.

In the third section, the different numerical methods to simulate the material removals as well as the different models used to predict the machining quality are presented.

Finally, based on the literature review, assumptions have been established and are introduced.

Contents

1.1 Residual Stresses

In order to achieve a better understanding on the residual stresses, a brief introduction on their origins and influences is realised in this section. The residual stress genesis and control during the manufacturing of aluminium alloy parts is also presented.

1.1.1 Residual Stresses in Metals: Definition and Origins

Residual stresses can be defined as self-equilibrated stresses (tensile and compression stresses) existing in a solid material which is not submitted to any external load (thermal or mechanical). They can arise from different sources and can be structured in four different categories [19, 20].

- The two first sources are the unequal plastic deformations resulting from mechanical and thermal loads.
- The third source is the metallurgical structure changes. During solid state transformations a release of latent heat, change in dimensions and transformation plasticity occur, resulting in a change of the residual stresses inside the part. The difference in volume between two coexisting phases in the presence of an external load generates microscopic plasticity leading to macroscopic plastic flow [21].
- The last source of residual stresses is a mismatch in the thermal expansion coefficients.

Manufacturing processes being complex combinations of these sources [22], residual stresses cannot be avoided and can be considered as outcomes of the manufacturing processes. Figure 1.1 illustrates the coupling of temperature, stress and metallurgical changes (microstructure) which causes the development of residual stresses during manufacturing.

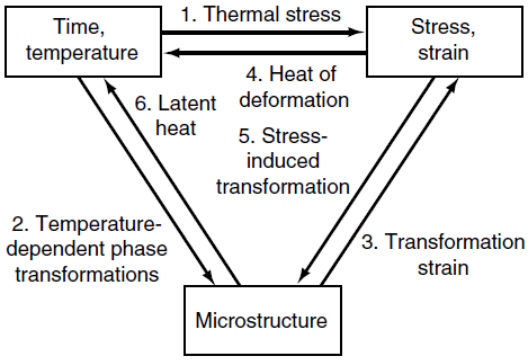

Figure 1.1: The coupling of temperature, stress and metallurgical changes [23]

Residual stresses are also categorised in three types in function of the length scale over which they act [19, 24].
"Type I" are macroscopic residual stresses and are almost homogeneous across distances equal to several grains. They affect a large number of grains or the whole mechanical part. The forces and moments associated are in equilibrium in any cross-sectional plane throughout the complete body. A change in this equilibrium will lead to macroscopic dimension changes.

"Type II" are homogeneous microscopic residual stresses. They act at the microstructure scale (grain size at maximum). The forces and moments associated are in equilibrium across a sufficient number of grains. They are almost always present in polycrystalline materials because of the heterogeneity and anisotropy of each crystal or grain (grain orientations). Changes in the microstructure therefore lead to the creation of "Type II" residual stresses. A change in the equilibrium will create microscopic deformations which can also cause macroscopic dimension changes.
"Type III" are heterogeneous microscopic residual stresses. The forces and moments associated are in equilibrium over a small part of the grain. Changes in the equilibrium will not lead to macroscopic dimension changes.

In Figure 1.2 illustrations of these three residual stress categories are shown.

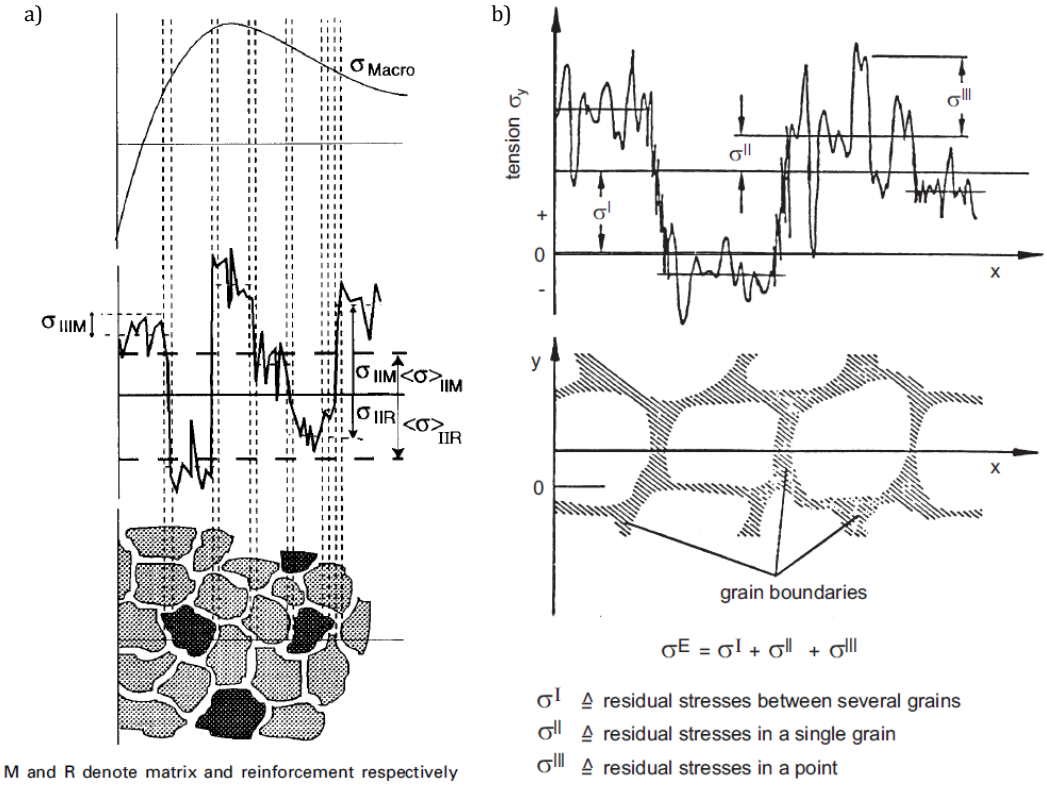

Figure 1.2: Illustration of the residual stress types: a) [25]; b) [24]

1.1.2 Residual Stress Influences

Whether it is to improve the final properties of parts or to optimise the manufacturing steps, the study of residual stresses and their effects on the mechanical behaviour of parts have become one of the major interests in the manufacturing industry. Because residual stresses are sources of manufacturing defects and problems and because they can significantly alter the mechanical behaviour of parts, the interest in mastering them and their effects is particularly high in aerospace [26, 20].

When a part containing initial residual stresses (σ_{IRS}) undergoes thermal or mechanical loads, in-service stresses σ_S are created in the part and will be added to the initial residual stress fields. The real stress state of the part σ_{Real} can therefore be defined as $\sigma_{IRS}+\sigma_S$, as illustrated in Figure 1.3.

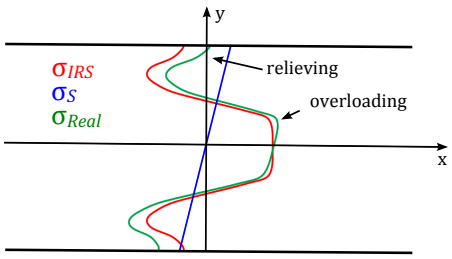

Figure 1.3: Illustration of the real stress state of a part linked to the addition of the residual stresses and in-service stresses

Residual stresses play therefore an important role in the mechanical strength, fatigue strength and stress corrosion cracking [26]. For example, the superposition of the residual stresses and cyclic stresses can have a significant influence on the fatigue strength of materials. Depending on the distribution pattern of residual stresses the fatigue strength and stress corrosion resistance of parts will be improved or degraded. Failure due to fatigue and stress corrosion are two mechanisms initiated in surface areas of parts. Surface compressive residual stresses allow to prevent failure [27]. Specific processes as shot-peening have therefore been invented and are used in order to generate uniform compressive residual stress patterns and to eliminate microscopic defects nearly without any changes in the geometry of the part [28, 29].

Because residual stresses lead to the distortion of parts, problems can also occur during the manufacturing and the assembly processes. As explained in the Introduction, the machining process is especially concerned with non-quality problems linked to the redistribution of residual stresses. The machining inaccuracies and distortions can also have a significant impact on the assembly process. A small distortion on each part can generate a domino effect and lead to significant residual stresses in the final structure or even to the impossibility to assemble the parts. Moreover, additional steps can sometimes be required for distortion correction, thus increasing the manufacturing costs.

The interest of mastering residual stresses and associated distortions is therefore very high. The incorporation of the residual stress effects into the design and the manufacture phases of parts can allow to significantly improve the quality and final properties of products.

1.1.3 The Aluminium Alloy Aerospace Part Manufacturing: Residual Stress Genesis

Aerospace parts are usually machined from rolled plates or forged parts. In a first step, the mix of alloying elements is melted and cast into an ingot. To obtain a plate, the ingot is then hot-rolled before being heat-treated and quenched. The quenching step allows to

avoid precipitation but also produces high levels of residual stresses. In order to decrease these residual stresses, a mechanical stress relief operation is realised by stretching [30]. It is performed in the rolling direction until a uniform plastic strain of about 4% is reached [12]. To achieve precipitation strengthening, thermal aging is finally performed. Figure 1.4 illustrates the needed successive manufacturing steps to obtain the AIRWARE® 2050-T84 alloy rolled plates.

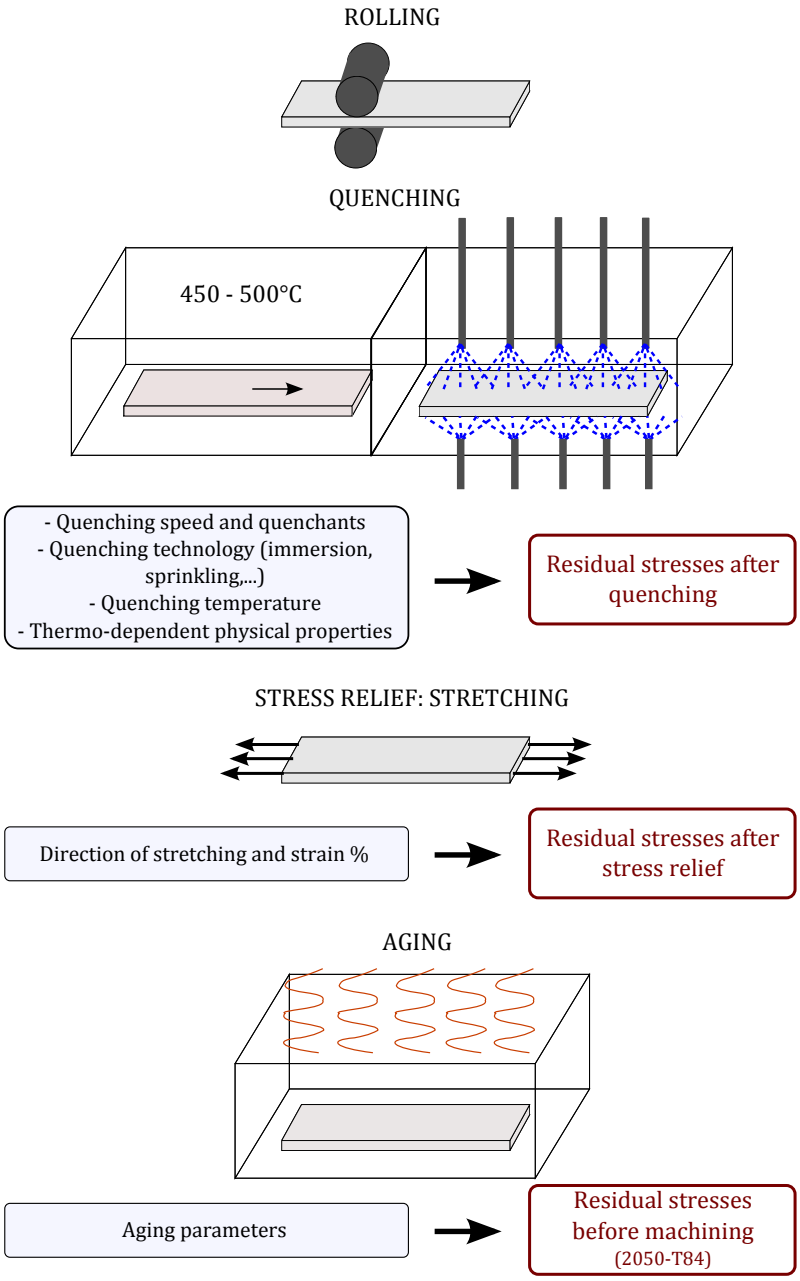

Figure 1.4: Illustration of the AIRWARE® 2050 alloy manufacturing line for rolled plates: the residual stress genesis

For forged parts, the forming is also performed with a hot working process. At the end of the forging, parts are heat-treated and quenched. Mechanical stress relief operations are also performed to suppress the high residual stresses induced during quenching. These operations are done by cold compression and then, depending on the case, thermal aging can be performed additionally. However, the residual stress patterns in a forged part are not uniform like they are in rolled plates. The determination of residual stresses is therefore more complex for forged parts than for rolled plates.

Overall, residual stress distributions are complex to determine. The multiple sources and their interactions (mechanical, thermal, metallurgical) make the use of analytical analyses almost impossible. The understanding of residual stresses can therefore only be realised by two approaches, the experimental trials and the numerical modelling. Purely experimental approaches being often expensive, numerical modelling and especially finite element modelling is nowadays commonly used in the numerical analysis of manufacturing processes and great progress has been made in this field during the last few decades. In addition, numerical modelling is a cost-effective approach allowing a closer and more in-depth understanding. However, the quality of the modelling is strongly governed by inputs like the material behaviour. Experimental and numerical approaches are therefore required when dealing with residual stresses and distortion [19].

To achieve the objective of a good understanding of residual stresses and their effects, several measurement methods have thus been developed. Depending on the residual stress type and the part's characteristics the measurement techniques used have to be adapted [31]. A list of possible measurement techniques can be found in Table1.1. Figure 1.5 allows to determine which method has to be used depending on the manufacturing process and the measurement depth.

Table 1.1: Different residual stress measurement techniques [31, 25]

Technique	Residual stress type	Comments
Hole drilling	Type I	Semidestructive
Sectioning	Type I	Destructive
Layer removal	Type I	Destructive
X-Ray	Type I, II & III	Non-destructive, only surface measurements, sensitive to grain size (difficult with aluminium alloys)
Neutron diffraction	Type I & II	Non-destructive, costly
Ultrasonics	Type I, II & III	Non-destructive, microstructure-sensitive
Magnetic	Type I, II & III	Non-destructive, microstructure-sensitive, for magnetic materials only

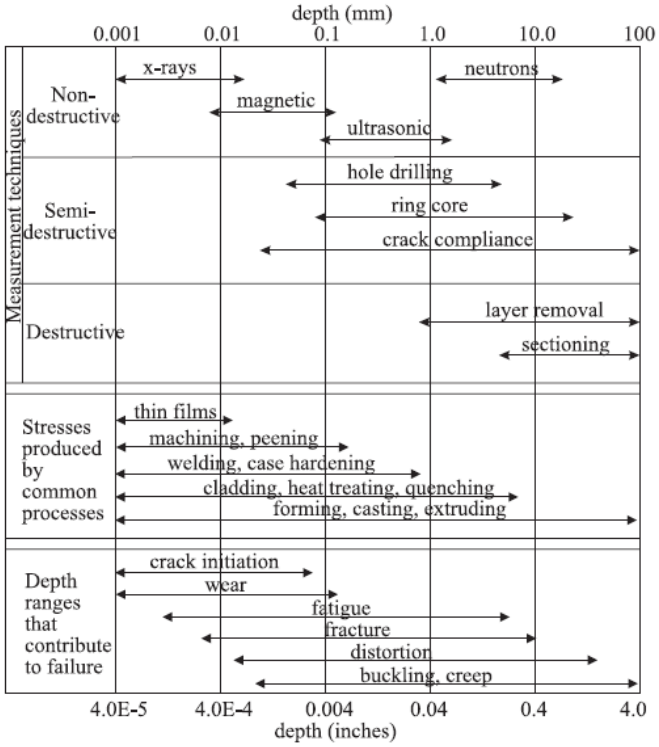

Figure 1.5: Measurement techniques depending on the processes, depth of measurements and failure [32]

1.1.4 Discussion on the Residual Stresses

Residual stresses are present in all manufactured parts and are created all along the manufacturing line. They can have both benefits and drawbacks for the final mechanical properties of the part. The determination of residual stresses can be realised using both numerical modelling and experimental measurements, the best approach being a mix of both.

In the OFELIA project, both experimental and numerical approaches have been investigated for rolled plates and a forged part. This work is partly described in Chapter 3 for the rolled plates. The prediction of the residual stress distribution of a forged part has been performed on a complex industrial case by one of the industrial partners. The results will be briefly discussed in Chapter 5.

1.2 Machining Processes

Machining processes are subtractive manufacturing methods which consist in the realisation of multiple removals of material by cutting an initial workpiece to obtain the desired final part. The machining gathers several kinds of processes which can be classified in four categories:

- The turning process

- The drilling process
- The milling process
- Specific machining processes

The three first categories are the machining processes commonly used in all industries. The last one is composed of all specific or relatively new machining processes such as grinding, sawing, electrical discharge machining (EDM), electro-chemical machining (ECM) or even the laser and water jet cutting processes. The machining process has to be chosen depending on the part geometry, surface texture and desired accuracy.

In aeronautics manufacturing industry, the milling process is most frequently used, especially when machining large aerospace aluminium alloy parts. This process is therefore the one considered in the whole study presented in this dissertation.

The milling process is a machining process where the removal of material is performed with a rotating cutting tool composed of several cutting edges (milling cutter). Usually the workpiece is moved against the rotating milling cutter, in function of the material removal required, to obtain the desired final geometry. In some cases, the milling tool can move against the fixed workpiece. Milling allows the machining of simple (plane surface) as well as of complex geometries (curved and irregular surfaces).

The first milling machine appeared in the 1810s and technologies have since never stopped evolving. The most significant evolutions in the machine tool industry occurred in the 1950s with the development of the first Numerical Control machine at MIT and then in the 1970s-1980s with the development and implementation of the Computer Numerical Control (CNC) in industry [33]. CNC technology has allowed a significant improvement in the manufacturing of parts by offering more flexibility, shorter delivery times and the capacity to produce an enormous range of geometrically complex parts for various kinds of materials and dimensions from micro- to multi-metre sized parts [34, 35]. To face the new challenges and the increasing need of productivity and quality, efforts to improve CNC machine tools are still made. Nowadays, CNC machine tools with multi-axes are adapted to High Speed Machining (HSM) and multi-process machine tools allowing drilling, milling, turning, laser hardening and grinding operations on a single machine in one part setup have been developed [36]. New machine tool kinematics are also explored as a new field of improvement with the development of Parallel Kinematic Machine Tools (PKM) for example [37, 38]. According to the CNC machine tools progress, Computer Assisted Design/Manufacturing (CAD/CAM) software products have also evolved, thus contributing to the increase of the productivity and quality of machined products. In order to fully use the capacities of the new CNC machine tools, these software programs allow now to automatically generate tool paths and machining programmes for complex geometries machining operations [34, 39]. They also allow to obtain a virtual representation of the machining and information such as the material volume removed and the machining time. Nowadays these software products are largely spread in industry and allow to make the link between the designed parts (CAD) and the production (machining program).

In the aerospace industry, usually five-axis milling machines are used to machine the large and complex aluminium alloy structural parts. Depending on the available resources and on the desired productivity, accuracy and complexity of the designed part the machining parameters have to be adapted. All of these are defined in the machining process plan.

1.2.1 Machining Process Plan

The machining process plan is a detailed plan with instructions specifying how a product has to be machined, depending on the characteristics of both the part and the available machining facilities. All needed information regarding the machining facility, processes and parameters which are to be used are therefore defined in it.

In the next section, previous research work related to the analysis of the influence of the different machining parameters with a specific emphasis on the machining of aluminium alloys is briefly presented. The machining parameters are here subdivided into three groups: the cutting conditions and more precisely their resulting effect on the material, the fixture and the machining sequence and tool path.

1.2.1.1 Cutting Conditions

As explained previously, in milling the material removal is performed by moving the workpiece against a rotating milling cutter. The cutting edges of the milling cutter therefore penetrate the surface of the workpiece. The material is plastically deformed and slides along the rake face of the cutting edge before breaking. This phenomenon is called chip formation [40]. Assuming that the deformation is two-dimensional because the major material flow occurs within the orthogonal plane, the mechanism can be illustrated by five deformation zones, as presented in Figure 1.6. The main deformation zone is located between the front of the cutting edge and the area of the free surface (primary shear zone).

For productivity reasons, a high material removal rate (MRR, in cm^3/min) is requested in industry. It can be obtained by varying machining parameters, especially the cutting speed, as shown in the equation 1.1.

$$N = \frac{1000 \times V_c}{\pi \times D} \quad ; \quad V_f = f \times Z \times N \quad ; \quad MRR = \frac{V_f \times a_p \times a_e}{1000} \tag{1.1}$$

with N being the spindle speed in (rpm), V_c the cutting speed in (m/min), D the largest tool diameter in (mm), V_f the feed speed in (mm/min), f the feed per tooth revolution in (mm/r), Z the number of teeth, a_p the axial depth of cut in (mm) and a_e the radial depth of cut in (mm).

The removal of material during machining by cutting being obtained by chip formation high levels of strains and strain rates can be observed depending on the machining parameters. The use of cutting conditions allowing a high MRR therefore results in an increase of the

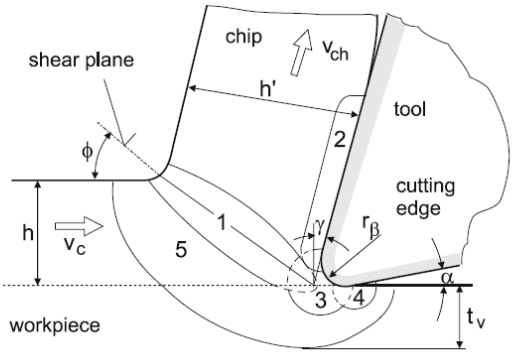

1 : primary shear zone
2 : secondary shear zone at the rake face
3 : secondary shear zone at the stagnation zone/seperativ zone
4 : secondary shear zone at the flank face
5 : preliminary deformation zone

γ : rake angle
α : clearance angle
ϕ : shear angle
t_v : deformation depth

Figure 1.6: Continuous chip formation illustration [40]

needed power to remove the material and in significant cutting forces and heat generation. These cutting forces and temperature can therefore have a direct impact on the mechanical behaviour of the workpiece during machining as well as they can induce residual stresses which can also affect the behaviour of the workpiece. In the next section, a review of models to describe the chip formation process and of past studies on the influence of the cutting parameters on the cutting loads and associated residual stresses is thus realised.

Cutting Forces

In this section, a brief description of past research work on the prediction of cutting forces with an outline of the most important models is realised. The cutting forces determine the needed machine power, the cutting tool life and can cause deflections of the tool, the workpiece and even of the machine tool [41].

Significant work has been performed in the past and several analytical models have been developed for the prediction of cutting forces in orthogonal cutting. Conditions can be described with a simple two-dimensional case of machining. These models can be classified in three types.

The first one is the shear plane model which is based on the Ernst and Merchant's theory [42]. In this model, the chip is formed by shearing along a single plane inclined at an angle ϕ (shear angle). The shear stress along the shear plane is assumed to be equal to the shearing flow stress of the material. Figure 1.7 shows the Ernst and Merchant cutting force diagram.

The second type of model is the slip-line field model developed by Lee and Shaffer [44]. In this approach based on plasticity analysis, the material is considered as rigid perfectly plastic (constant stress in the yielding area). The constructed slip-line field formed by the triangle ABC (plastic zone) is shown in Figure 1.8.

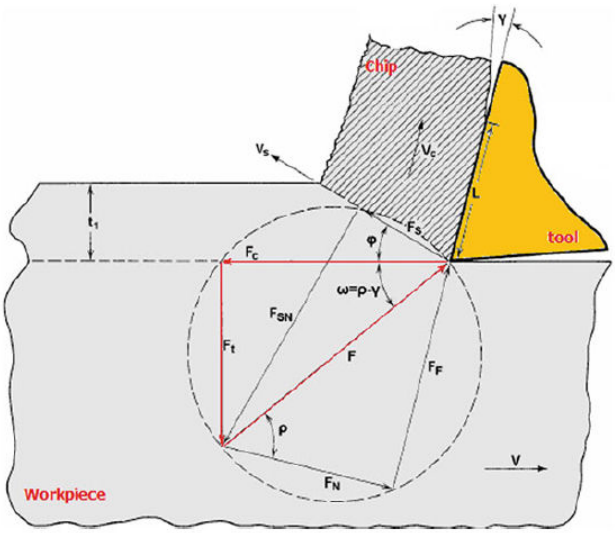

Figure 1.7: Ernst and Merchant's shear plane model of orthogonal cutting [43]

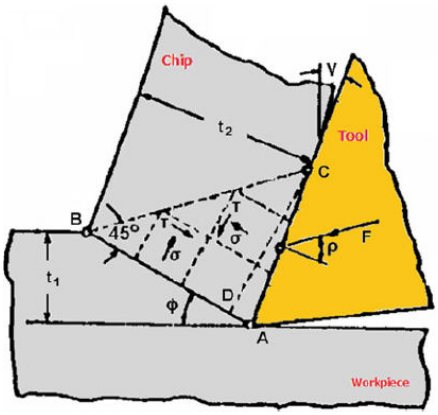

Figure 1.8: Lee and Shaffer's slip-line field model for orthogonal cutting [43]

Later, some researchers have also extended these two first models to three-dimensional oblique cutting [45].

These models show similar results while agreeing only relatively poorly with experimental results, principally due to the fact that the material is considered as rigid perfectly plastic and that friction is characterised by one constant friction coefficient.

The last kind of analytical model is the shear zone model, of which one of the best known is the Oxley's model [46]. It assumes that the deformation takes place in a narrow band centred on the shear plane, as illustrated in Figure 1.9.

This model is therefore an enhancement of the previous models and allows to consider strain hardening as well as the strain rate sensitivity and therefore the cutting speed influence. Cutting forces can then be calculated depending on the workpiece material properties, the tool geometry and the cutting conditions.

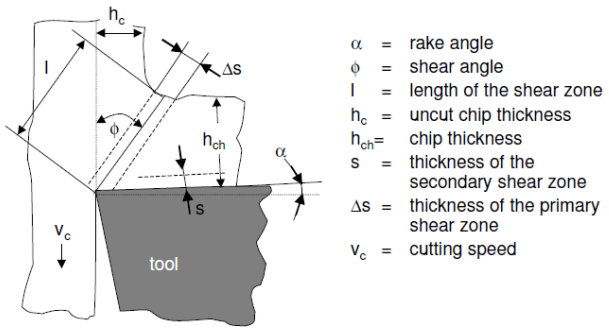

Figure 1.9: Illustration of the shear zone model of Oxley [47]

However, this model presents some limitations which makes its use in industry difficult:

- It is only valid for continuous chip formation and can therefore not be used to predict what type of chip formation will be obtained depending on the machining conditions.
- It cannot predict accurately the behaviour of the material in the chip formation area.
- It cannot be quickly applied to new materials, new machining methods or new phenomena due to the use of a new tool and new coating for example.

Analytical models presenting these drawbacks, an interest for the numerical modelling of cutting processes has grown. Among the numerical methods, the finite element models are the most commonly used to simulate the chip formation process and to predict cutting forces and the temperature depending on cutting conditions and tool geometry. Since the first models in the 1970s, significant work has been realised [48, 43]. Several commercial software products even offer special solutions for the simulation of the chip formation. The main benefits of the finite element models are:

- The type of chip formation can be predicted.
- They offer the possibility to analyse in detail the whole phenomenon in taking into consideration nonlinear effects linked to the material behaviour and tool-chip interface friction as well as the influence of the exact tool geometry. Fracture mechanisms can also be implemented into finite element models for chip breakage and tool wear prediction.
- The desired variables, such as the cutting forces, temperature and chip geometry are directly obtained from machining parameters such as the cutting conditions and the tool geometry.

However, the results obtained are strongly governed by the modelling assumptions and the modelling approach. For example, depending on the formulation employed (Lagrangian, Eulerian or Arbitrary Lagrangian–Eulerian) results obtained can vary but the most significant uncertainties are due to input parameters. Indeed, an accurate description of the input parameters is essential to overcome these uncertainties and particular attention has thus to be paid during their definition, which can be relatively time-consuming. These input parameters are: the material behaviour laws, the friction models, the fracture models and the wear models [48].

Prediction of cutting force during milling:
The milling process is an intermittent process making the prediction of cutting forces more difficult than in orthogonal cutting. Based on the above-mentioned studies, specific models for the milling process have been developed. In this section a brief summary of some predictive milling force models based on cutting theory is presented.

Young et al. [49] showed that the machining theory can be applied to predict the milling cutting forces depending on the workpiece material properties and cutting conditions. Later, authors in [50, 51] developed an approach based on Oxley's machining theory to predict the cutting forces in end-milling. In these studies, the milling cutter is considered as a multiple single-point cutting tool and the effect of intermittent cutting on temperature and workpiece material behaviour is taken into account. Measurements of experimental milling force components using a 3D dynamometer were then performed. Good agreements between the experimental and simulated results were obtained.

Based on the same machining theory, Li et al. [52] proposed a model to predict milling forces depending on the fundamental workpiece material properties, the tool geometry and the cutting conditions. In this approach a helical end milling cutter is discretized into a number of slices along the cutter axis, as illustrated in Figure 1.10.

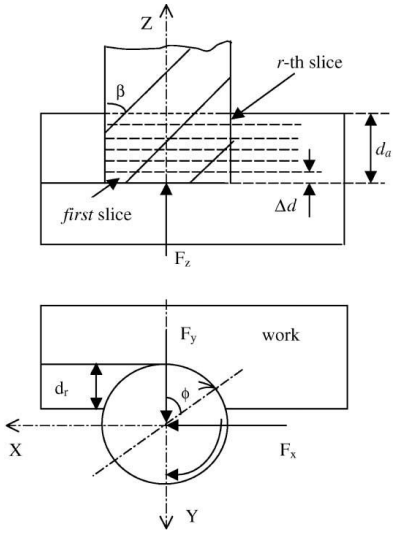

Figure 1.10: Illustration of the discretization of the milling cutter into slices [52]

The cutting force is then obtained on each slice using oblique cutting models and depending on the geometry of the milling cutter. The sum of the forces at all cutting slices of all teeth is then computed to predict the total cutting force acting on the cutter. The flowchart of the procedure is shown in Figure 1.11. Experimental milling tests have also been conducted in order to validate the approach. A good agreement between the experimental and simulated results was obtained, except for severe cutting conditions where vibrations occurred.

Using the same approach as proposed in [52], Rai et al. [18] implemented the mechanistic cutting force model into a finite element environment. In their approach, the computed forces

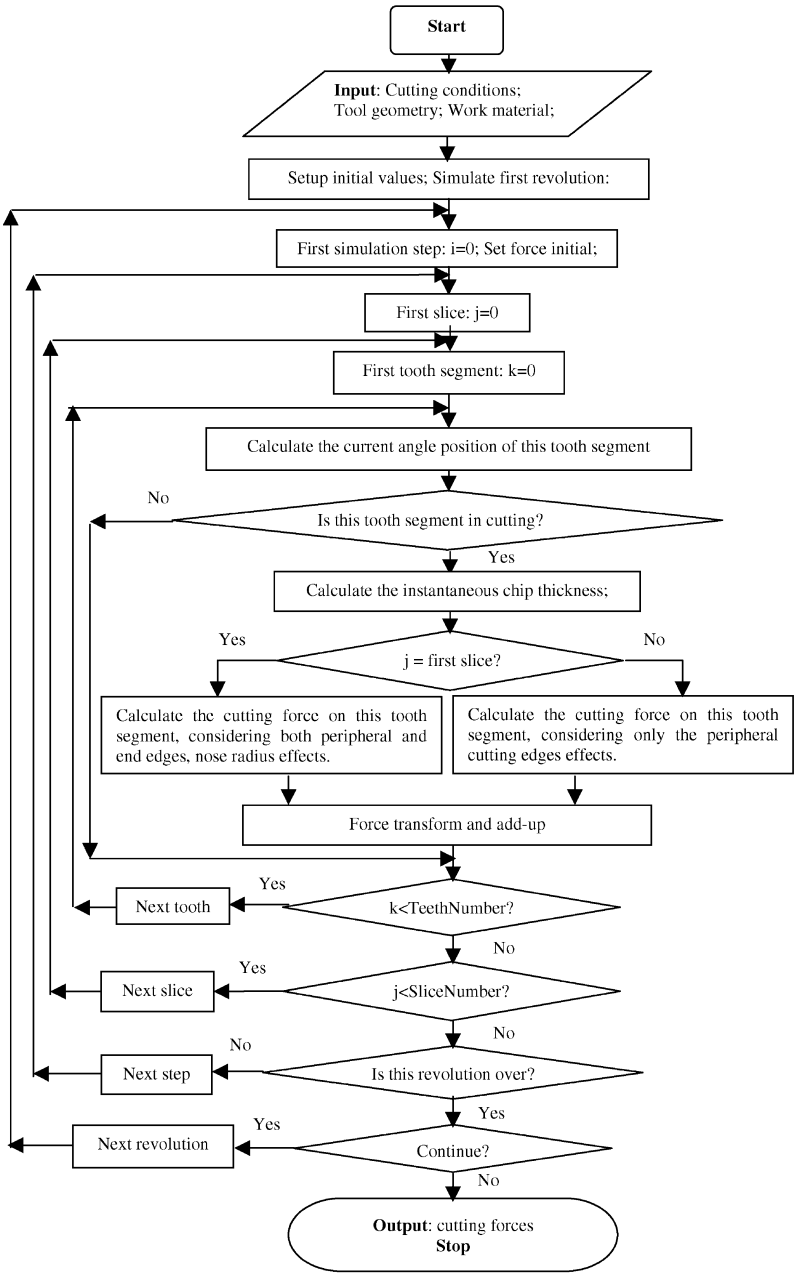

Figure 1.11: Flowchart of the simulation system proposed in [52]

are directly applied on the nodes of the mesh representing the workpiece in order to predict the deformations of the workpiece during milling (thin-walled parts).

Conclusion

Globally, the predicted forces are similar to the experimentally measured ones. These models therefore allow to achieve a good prediction of the milling forces. It can also be observed that the cutting forces are relatively small and that deflections due to the cutting forces occur only during machining of thin walls.

Heating During Cutting

During machining, almost all the energy needed to realise the metal cutting is converted into heat. The main part of this heat generation is due to plastic deformation in the shear zones, the rest being due to the friction between the tool and the chip as well as the tool and the workpiece [53, 41]. Most of the generated heat is considered to be carried out by the chip (~80%), the rest being dissipated in equal parts into the tool and into the workpiece (~10% each). Figure 1.12 illustrates the dissipation of the heat generated during machining depending on the cutting speed (for carbide tools).

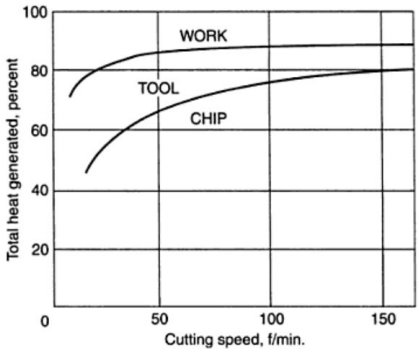

Figure 1.12: Amount of heat dissipated into the chip, tool and workpiece during machining [53]

Several researches have been performed in the past on the prediction of the heat dissipated into the workpiece during cutting. Specific mathematical models allowing to determine the surface heat flux into the workpiece depending on the cutting conditions have for example been developed and used for the prediction of the behaviour of the workpiece during cutting (drilling and milling operations) [54, 55]. However, they have not been used for the cutting of aluminium alloys.

In this section, a brief description of past research work on the prediction of heating during milling operations of aluminium alloys is given. Several techniques have been used in order to determine the cutting temperature. They can be classified into two categories, the experimental one and the analytical one [56, 57].

Due to the fact that chip formation is a localised phenomenon, high gradients of temperature can be observed. Accurate measurements of cutting temperatures are therefore difficult to perform. This is even more problematic for milling, where more difficulties are encountered due to the cutting tool rotation and confined work space. To face these difficulties, several specific measurement techniques have been developed to determine the cutting temperature during the milling of aluminium alloys.

In his thesis, L. R. de León García [58] performed tests to determine the surface temperature of a 7449-T7651 alloy workpiece during milling using an infrared thermocamera. The temperature is measured on the milled surface once the cutting tool has moved further.

Figure 1.13 shows the results obtained. A temperature range between 20°C and 65°C can be

observed. In these measurements, temperature cannot be clearly related to a defined body (tool, chip or workpiece) and the temperature near the cutting edges cannot be analysed. It is therefore difficult to analyse the results to evaluate local heating of the machined surface. Finite element models to predict the surface temperature have also been developed in [58]. These models consist in the application of a moving heat source reproducing the one observed during cutting on the machined surface. Both the thermal power and the heat source speed are computed in function of the machining parameters. Using this model, the cutting speed and feed per tooth influences on the surface temperature have been studied. Due to the low temperature observed, the author concludes that the thermal influence on the workpiece subsurface and on the induced residual stresses during milling is not significant.

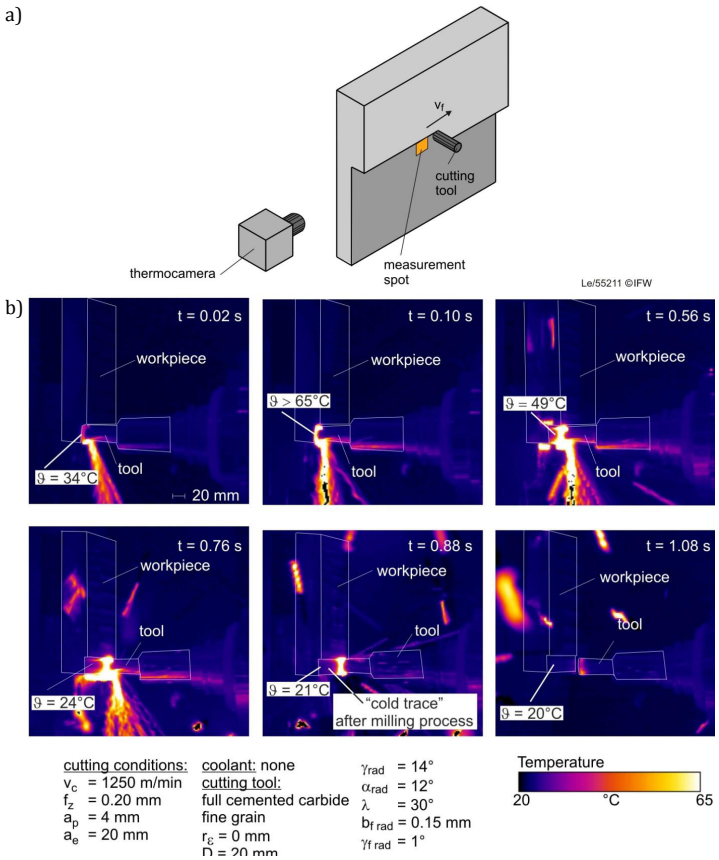

Figure 1.13: Temperature measurements using an infrared thermocamera: a) experimental setup; b) The surface temperature measured during milling [58]

In their study, Tang et al. [59] used infrared thermocamera measurements coupled to a finite element model. They initially performed the measurement of the evolution of the temperature in the chip during the machining of an alloy 7050-T7451 part with an infrared camera before using the data to develop and to validate a finite element model. By using this numerical model, they then studied the evolution of the workpiece surface temperature created during the machining and the influence of certain parameters. They found a temperature range between around 140°C and 200°C depending on the spindle speed and feed rate.

Richarson et al. [60] proposed an approach using only thermocouples placed at different depths from the machined surface in a block of 7449 aluminium alloy. They obtained a maximal temperature range from 35°C to 65°C depending on the cutting conditions. In their paper, they also showed that the bigger the cutting speed and feed rate the less heat is transferred to the workpiece.

In [61] authors used an infrared pyrometer and thermocouples to determine the cutting temperatures during the milling of aluminium alloys. A coupled experimental-numerical approach was established. In that work, the surface temperature measurements performed with an infrared thermometer have been used to compute inversely the average heat flux flowing into the workpiece during machining and to predict the cutting temperature in a 2024 alloy. Cutting conditions like the spindle speed have been studied and have shown to have a significant influence on the temperature. Examples of results obtained are shown in Figure 1.14. It has also been observed that the tool–workpiece interface temperature is influenced by the thickness of the workpiece, the surface temperature of a thin-walled part increasing with thickness decrease. The cutting temperatures are therefore more critical when dealing with thin walled parts than with massive parts.

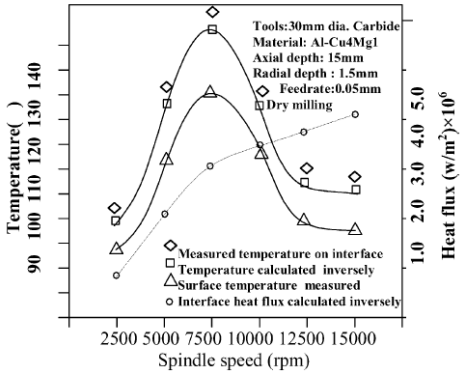

Figure 1.14: Values obtained for both measured and inversely computed temperatures [61]

In order to reach a better understanding of the influence of some parameters such as the tool corner radius on the cutting temperature, Denkena et al.[62] developed three-dimensional finite element simulations of milling. These simulations have been realised with material parameters linked to a 7075 aluminium alloy and using the finite element software Deform 3D. The model used and the analysis performed are shown in Figure 1.15. A maximum temperature of approximately 250°C was found at the machined surface at the time of material separation. A relatively high gradient in the first 400 μm of the machined subsurface is also observed.

In their studies, Rai et al. [17, 18] implemented the average shear plane temperature (Oxley's cutting temperature model) into a finite element environment to perform the transient thermal analysis and to obtain the transient temperature distribution in the workpiece during the material removal process. The thermal loads were applied with the cutting forces on the mesh representing the workpiece in the areas where the machining is in progress. The finite element model has been validated by experimental comparisons (measurements performed using thermocouples).

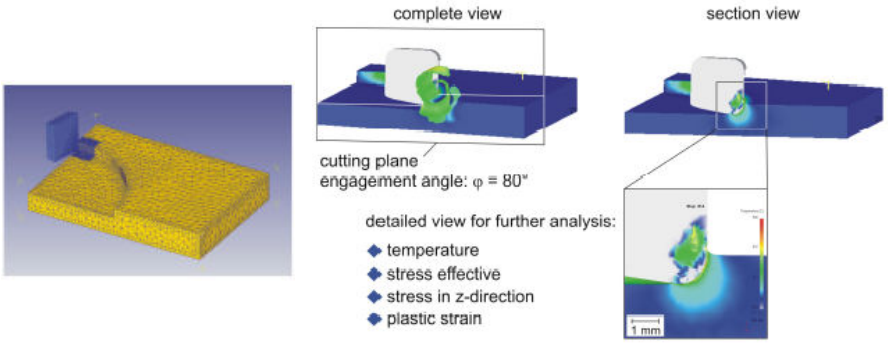

Figure 1.15: The finite element model used in [62]

Whereas only dry machining is considered in the other studies, Rai et al. [17] also analysed the influence of coolant on the heat dissipation rate. It was found that whereas the temperature profile rises gradually in dry machining due to the continuous heat flow into the workpiece, the rise of the temperature is negligible in wet machining, as illustrated in Figure 1.16. The temperature rise is therefore limited in industry where coolants are usually used.

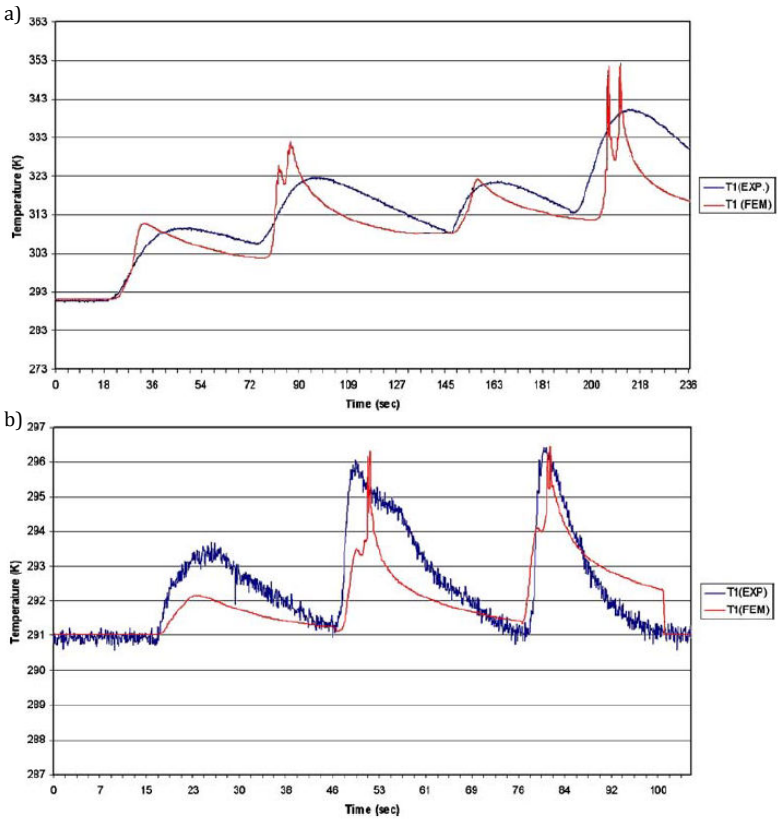

Figure 1.16: Comparison between predicted and measured temperature [18]: a) Test without coolant; b) Test with coolant

Table 1.2 presents a literature overview of the studies realised on the prediction of the temperature under the machined surface.

Table 1.2: Recap on the different studies realised on the prediction of the cutting temperature

Study	Year	Alloy	Cutting conditions	Results: Temperature max (°C)	
				Numerical	Experimental
[58]	2010	7449-T7651	Vc = 250; 750; 1250 m/min f = 0.05; 0.2; 0.35 mm.z^{-1} ap = 4 mm ; ae = 20 mm	$f(Vc)$ = 32; 39; 48 with f = 0.2 $f(f)$ = 37; 48; 52 with Vc = 1250	$\sim$ 65 with Vc=1250 and f = 0.2
[59]	2008	7050-T7451	N = 4000; 12000; 16000 rpm f = 0.1; 0.15; 0.2 mm.z^{-1} ap = 2 mm ; ae = 10 mm	$f(N)$ = 140; 175; 190 with f = 0.15 $f(f)$ = 175; 185; 200 with N = 12000	-
[60]	2006	7449	Vc = 300; 4750 m/min f = 0.2 mm.z^{-1} ap = 2 mm ; ae = 5 mm	-	$f(Vc)$ = 65; 35
[61]	2003	2024	N = 2500; 7500; 15000 rpm f = 0.05 mm.z^{-1} ap = 1.5 mm ; ae = 15 mm	$f(N)$ = 100; 130; 105	$f(N)$ = 105; 140; 110
[62]	2007	7075	Vc = 1250 m/min f = 0.3 mm.z^{-1} ap = 1.2 mm ; ae = 10 mm	$\sim$ 250	-
[17]	2008	7075	N = 25 rps f = 0.074 mm.z^{-1} ap = 6 mm ; ae = 9.5 mm	$\sim$ 80 (dry machining case)	$\sim$ 80 (dry machining case)

with: Vc = the cutting speed in (m/min) ; N = the spindle speed in (rpm) ; f the feed per tooth revolution in (mm/r) ;
a_p the axial depth of cut in (mm) and a_e the radial depth of cut in (mm)

Conclusion

It can be observed that depending on the material, the approach used to determine the temperature and the cutting conditions, various results are found in literature. However, it can be concluded that even if the machining parameters have a strong influence on the heat generated during the cutting, only the machined subsurface is affected. In addition, the temperature is lower when dealing with massive parts (without thin walls) and the heat is relatively quickly dissipated due to the thermal properties of aluminium. It has also been observed that with coolant, which is usually used in industry, the temperature stays really low and heat transfer can be neglected.

Residual Stresses Induced by Machining

As explained, the chip formation mechanism is provoked by plastic deformation of the material due to the combination of the mechanical and thermal cutting loads (cutting forces and temperature). Only the machined subsurface is affected by the cutting loads during the milling of aluminium alloys, resulting in unequal plastic deformations as well as in metallurgical transformations and therefore in residual stresses. These residual stresses can have a significant effect on the performance and fatigue strength of parts. As seen previously, the cutting loads depend on the different cutting parameters, as the cutting speed, the tool geometry and the feed rate. In order to predict residual stresses due to the machining and to study the influence of these parameters on the machining residual stress profiles, previous research based on experimental, analytical and finite element methods has been conducted.

Fuh et al. [63] were one of the first to propose an empirical model to predict the residual stresses produced by milling of an aluminium alloy (2014-T6). In their work the influence of cutting parameters such as cutting speed, feed rate, cutting depth, nose radius or even flank wear has been studied. However, no real physical relationship between the cutting parameters and the residual stresses induced during the milling could be determined. More recently, Su et al. [64] have proposed an analytical model using cutting parameters, cutting conditions, and workpiece material properties as inputs to predict the residual stresses induced during milling. In their model, cutting forces, cutting temperatures and the related residual stress magnitudes and profiles are predicted without needing calibration steps. The results have then been compared with experimental ones obtained by X-ray diffraction measurements on a titanium alloy (Ti 6Al-4V), showing a good agreement.

Regarding machining-induced residual stresses in aluminium alloys, considerable work has been realised by Denkena et al. [65, 62, 66, 67, 68]. In these studies, a combination of X-ray diffraction measurements and finite element simulations is used to study the milling-induced residual stresses in aluminium alloy workpieces. Analyses on the influence of cutting parameters and tool geometry have been conducted. They prove the influence of the cutting speed, the feed rate and cutting edge geometry on the residual stresses induced during machining. Tool corner radius and tool wear have also been found to be a parameter with a big influence on the residual stresses induced during the machining, even more significant

than the cutting speed and feed rate. In all cases, the affected depth is relatively small, staying below 250 μm. An example of results obtained in these studies is shown in Figure 1.17.

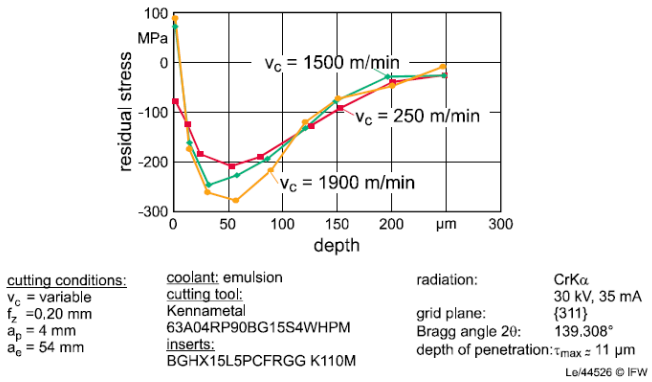

Figure 1.17: Example of milling-induced residual stress profiles in aluminium alloys [68]

Recently, another approach to predict residual stresses using numerical models has been developed. The hybrid approach consists in the computation of the mechanical and thermal loads linked to the chip formation and in the application of an equivalent thermo-mechanical loading on the machined surface of the part. This approach is illustrated in Figure 1.18. It has first been developed to predict residual stresses during the turning of steel [69] and more recently for the ball-end milling of steel [70]. A good agreement between predicted and measured residual stress profiles has been obtained. This approach has as a main benefit to avoid the time-consuming simulation of the chip formation. However, no application on aluminium alloys has been performed yet.

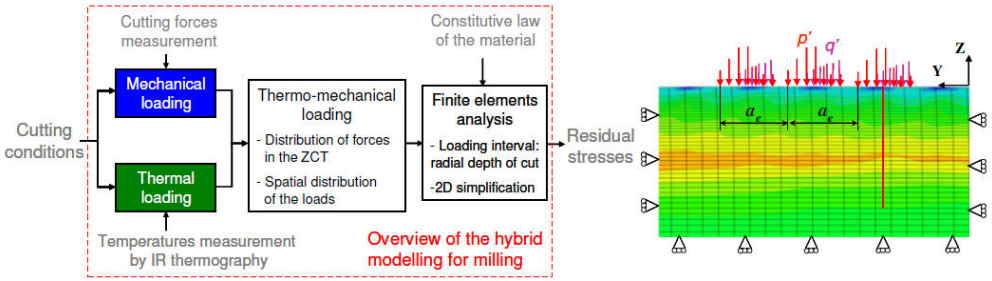

Figure 1.18: The hybrid approach developed for ball-end milling in [70]

Conclusion

Machining-induced residual stresses are strongly governed by cutting conditions and the tool geometry. A change in one of these parameters can lead to changes in the residual stress profiles (tensile or compression stress) and amplitudes. However, the depth affected by the residual stresses stays in all cases below 250 μm when dealing with the milling of aluminium alloys.

1.2.1.2 Fixture

Fixtures are fundamental devices in a manufacturing process and play an important role in the final product quality. In machining, the two objectives of fixture systems are to provide an accurate and repeatable location of the workpiece surfaces with respect to the machine tool axes, as well as to prohibit the motion, deflection and distortion of the workpiece during the machining [71, 72]. The fixtures used during the machining therefore have to be designed to counteract all loads which could provoke a change in the position and orientation of the workpiece as well as its deflections. During the machining, both cutting loads (forces and temperature) and the redistribution of the residual stresses can provoke such problems.

Fixture Elements

A fixture system is usually composed of several elements which can be classified into four groups: locators, supports, clamps and fixture body.

- *Locator*: A locator is a fixed element which allows to establish the position and orientation of the workpiece in the machine tool by restricting its degrees of freedom. The contact between the locators and the workpiece is realised on the datum surfaces of the workpiece. The accuracy of the workpiece positioning is therefore strongly governed by the choice of the locators. Some examples of locators can be seen in Figure 1.19.

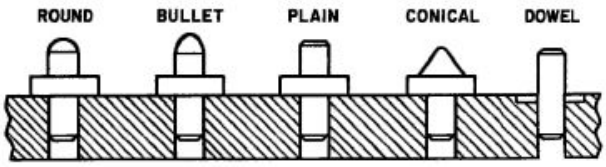

Figure 1.19: Examples of locators [73]

- *Support*: A support is a fixed or adjustable element which allows to restrict the movement and the deflection of the workpiece during the machining due to the cutting loads and the redistribution of the residual stresses. Some examples of supports can be seen in Figure 1.20.

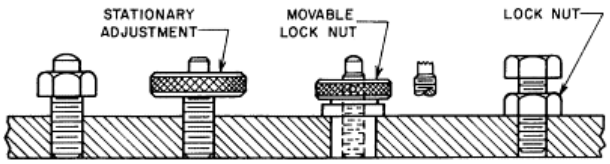

Figure 1.20: Examples of supports [73]

- *Clamp*: A clamp is a moveable element which allows to provide a holding force on the workpiece. Neither positional displacement nor deflection should be observed after clamping and during the machining. Clamping forces should be applied towards locators and support elements in order to ensure the desired workpiece location. Several

types of clamps exist: strap clamps (a), sliding clamps (b), swing clamps (c), hinge clamps (d) and multiple clamps (e) which can be seen in Figure 1.21.

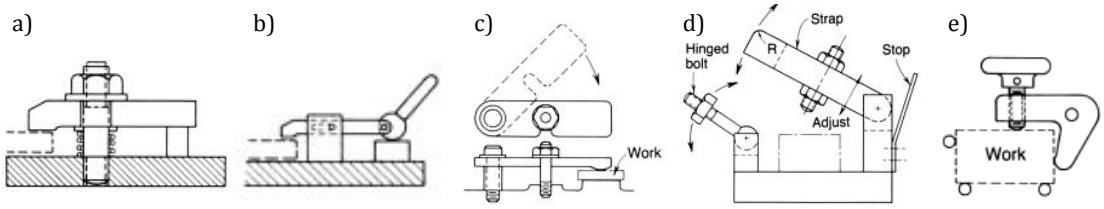

Figure 1.21: Examples of clamps [74]

- *Fixture body*: A fixture body is a rigid structural element which allows to maintain the spatial relationship between all the fixture elements and the machine tool.

Fixture Design

The fixture system has to be designed to fulfil three principal requirements. The first one is to constrain the workpiece in a precise location and orientation in a repeatable way for each machined part. There are twelve degrees of freedom (rigid body movements) in any workpiece (+/- movements), as shown in Figure 1.22. Locators therefore have to give a unique and accurate position and orientation of the workpiece in the spacial coordinate frame of the machine tool. The second requirement is that the fixture system has to withstand all possible loads which could occur during the machining in order to ensure an accurate material removal. The last requirement is to design the fixture as efficient as possible to optimise productivity [71].

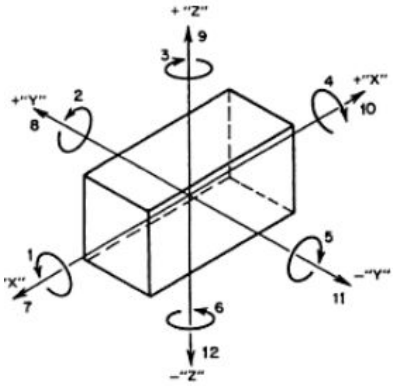

Figure 1.22: The twelve degrees of freedom of a workpiece [73]

These requirements have led to some basic rules and methods in fixture design which can be summarised in the following points [71, 74, 75, 72, 73, 41]:

- A 3-2-1 location is usually used to restrict the degrees of freedom of a prismatic workpiece. The 3 refers to 3 locators on the primary datum surface, the 2 to 2 locators on the secondary datum surface and the 1 to 1 locator on the tertiary datum surface. Nine out

of twelve degrees of freedom are restricted with this method. The three remaining ones should be restricted by clamps. An illustration of this method is shown in Figure 1.23.

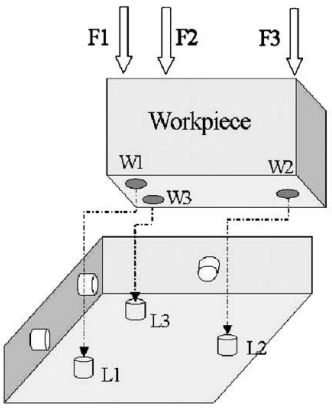

Figure 1.23: A 3-2-1 fixturing scheme [76]

- A 4-2-1 or N-2-1 location (with N > 3) can be used for large parts and to avoid vibration and deflection of the workpiece. However, the use of redundant locators can lead to bigger positioning variability during the setup. Adjustable supports should be used to respect the locating constraints. An illustration of this method is shown in Figure 1.24.

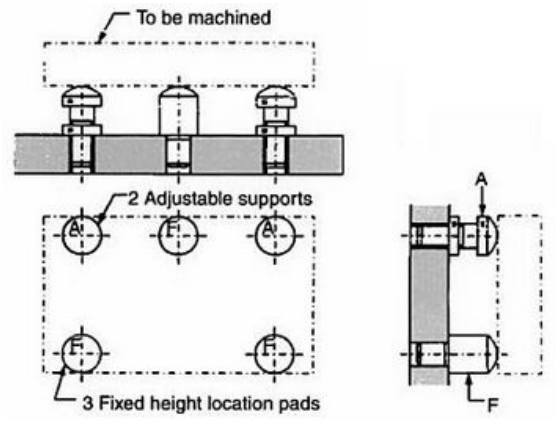

Figure 1.24: An N-2-1 fixturing scheme [75]

- Locators should oppose the majority of the loads during the machining.
- Clamping forces have to be directed towards locators and support. In addition, clamps have to be directly fixed on the fixture body.
- Clamping forces have to be set to the minimum force to overcome the maximum loads during the machining. The objective is to avoid undesirable effects like deflection and surface damage.
- If possible pneumatic and hydraulic clamping devices should be used. This allows to avoid all disadvantages of manual clamping like the variation in the clamping forces and needs a shorter clamping time. However, it is a more expensive method which also requires more space and maintenance.

- Fixture systems have to be designed to facilitate the locating, clamping and unclamping of the part as well as the cleaning (of chips) in order to optimise the setup time. A sufficient clearance should therefore be provided around the workpiece in order to ensure easy placing of the workpiece (avoid locating variations) and a good evacuation of the machining chips.
- Fixture systems have to be designed to optimise the number of features which can be machined within a fixture layout. The objective is to limit the number of required fixture systems to machine a part and therefore the global setup time.

These are only basic guidelines for fixture design and many other parameters have to be taken into account when dealing with fixture design. For example, fixtures have to be adapted to the workpiece geometry, the desired accuracy or even to the machining sequence. In Figure 1.25 Stephenson et al.[41] summarise the multiple factors which can influence the design of a fixture system.

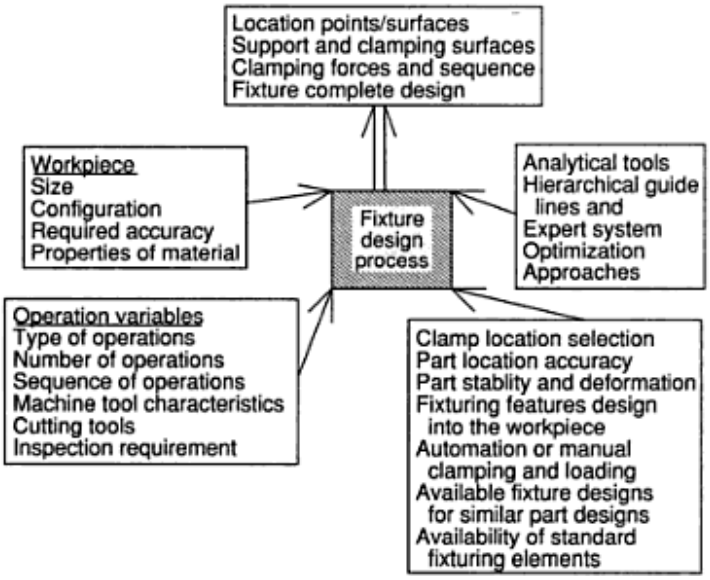

Figure 1.25: Parameters which influence the fixture design [41]

The main drawback of the commonly used fixture design rules is the validation step. The mechanical behaviour of the workpiece during machining due to its initial residual stresses being usually not taken into consideration during the fixture design, the realisation of several machining trials to validate a fixture layout can be required. Moreover, for each new initial workpiece (type, dimension and material) new machining trials have to be performed again as the mechanical behaviour of the workpiece can be different. The validation can therefore be a very time-consuming and expensive step.

Machining Fixture Analysis

Significant work has been performed in the past on fixture analysis using kinematic models,

discrete elastic contact models, finite element models and optimisation methods. In this section, a brief description of this past research work is presented with a particular interest on work realised on fixture layout design and fixture stability analysis using finite element models.

De Meter [77] proposed a rigid body fixture-workpiece model to determine locator and clamp positions as well as the minimum clamping forces. His algorithm is based on a min-max load model and allows to optimise the fixture layout (position of locators and clamps) and to determine the minimum clamp actuation intensities throughout a series of cuts to satisfy restraint requirements in taking into account the friction effect. Results have shown that it is possible to optimise the fixture element positions to obtain a feasible fixture layout allowing to minimise the maximum contact force. This algorithm's main benefit is to be a computation efficient tool, but the elastic behaviour of the workpiece is not taken into account and only prismatic geometries can be studied.

In their work Li and Melkote [78] developed a model allowing to minimise the location errors of the workpiece by optimising the position of the locators and clamps around it. The elastic deformation of the workpiece in the contact areas is taken into account, as illustrated in Figure 1.26a. It was shown that the optimised fixture layout allows to decrease the inaccuracy in the workpiece location due to the rigid body motion of the workpiece produced by the localized elastic deformation in fixture-workpiece contacts. Finite element models have also been developed and showed that this optimised fixture layout allows to minimise as well the overall workpiece deflections after clamping. Later, Li and Melkote used the same approach to minimize workpiece location errors and clamping forces in taking into consideration the influence of workpiece rigid-body dynamics during machining [79].

Asante [80] proposed a new approach combining a discretized contact elasticity model (see Figure 1.26b) and a finite element model to predict the contact load and pressure distribution at the contact interfaces of the workpiece. Using this model, he determined the optimal clamping forces to obtain adequate contact forces which allow to keep the workpiece in the desired position during machining.

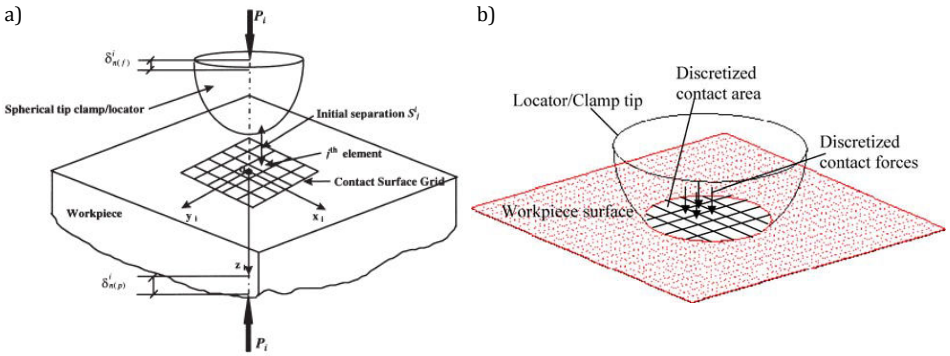

Figure 1.26: The contact interfaces with the discrete elastic contact model: a) [78]; b) [80]

Other work has been realised using exclusively finite element models. Since the first work

of Lee and Haynes [81] a considerable evolution has been seen. Satyanarayana and Melkote [82] demonstrated that the finite element method is well-suited for predicting workpiece deformations and reaction forces during clamping. They studied the influence of different boundary conditions and the influence of the mesh size in the contact areas for a single fixture–workpiece contact. They thus showed that surface-to-surface contact elements are best suited for modelling fixture–workpiece contacts and that the mesh size has to be adapted to ensure correct results. Siebenaler and Melkote [83] studied the influence of factors such as the contact friction, the mesh density and the fixture-body compliance on the prediction of workpiece deformation during clamping using finite element models. In a case study, it was found that 98% of the all-system-deformation could be captured by only modelling the workpiece and fixture tips and that such a modelling allows to divide the computation time by six compared to a case with a complete modelling of the fixture.

Wang et al. [84] used finite element simulations to study the workpiece deformation during clamping and machining of a part with a complex geometry (turbine blade). The machining (grinding) is simulated by applying the grinding forces on the machined areas, no numerical material removal step is performed. Using this model, they developed a numerical procedure to study the deformation of the fixture-workpiece system by comparing the displacements during machining with the displacements before machining and after machining. Their procedure is composed of five steps: the set up contact, the locating, the clamping, the machining and the release of the machining forces. However, a simplification of the part geometry still has to be performed.

Recently Siva Kumar and Paulraj [85] combined finite element analysis (FEA) and a genetic algorithm (GA) to optimise the locations of fixture elements in order to minimise the deformation of the workpiece. In their model the frictional contact behaviour between the fixture elements and the workpiece as well as the dynamic machining conditions are taken into account. They showed the feasibility to increase the machining quality by optimising the fixture layout.

Conclusion

These studies demonstrate the importance of the contact modelling when dealing with the machining quality prediction and the feasibility to improve the machining quality by adapting the fixture layout. Indeed, an adapted fixture layout allows to ensure an accurate workpiece location as well as the required stability to avoid deflections of the workpiece. An approach such as the one developed in [15, 14, 86], where simple restrictions of the degrees of freedom are performed in the fixture-workpiece contact areas, is therefore not the best suited for the prediction of the machining quality. These studies also give some relevant information regarding the fixture-workpiece contact modelling. For example, it has been demonstrated that an adapted mesh size was required to accurately predict the elastic deformations in the fixture-workpiece contact areas and the associated workpiece location errors and that it was possible to obtain accurate results by only modelling the workpiece and fixture tips.

1.2.1.3 The Machining Sequence and the Tool Path

The machining sequence and the tool path can be defined as follows:

- The machining sequence represents the order in which the machining features are going to be machined.
- The tool path represents how each feature is going to be machined (contour parallel path, zig-zag path, etc). Examples are shown in Figure 1.27.

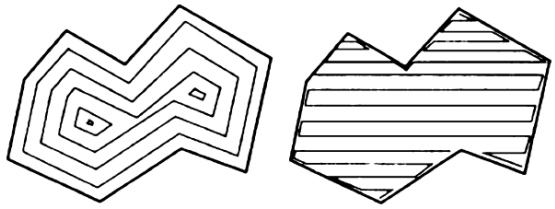

Figure 1.27: The two main types of tool path trajectories [87]

When dealing with CNC machining, the machining sequence and the tool path strategy chosen are directly defined in the program. The machining time and therefore the machining productivity are strongly governed by these two parameters. The main objective of past research work realised on the machining sequence and the tool path has therefore been related to the increase of the machining productivity.

For example, Pateloup et al. [88] developed a pocketing tool path method to minimise the machining time by taking into account the kinematic behaviour of the machine tool and the radial depth of the cut variation. Experimental validation has then been realised showing a machining time decrease of around 20% compared to the more conventional tool path resulting from CAM software programs.

Bieterman and Sandstrom [89] proposed a curvilinear tool path generation method for pocket machining. This method allows to reduce both the machining time and the tool wear when dealing with the cutting of hard metals.

Some work has also been realised to develop models allowing to adapt tool paths depending on unexpected relative movements between the workpiece and the tool. For example, Mayr et al. [90] used the Finite Difference Element Method (FDEM) to compensate the thermal effects on the machine tools. The finite difference method is used to compute the temperature distribution in the machine tool whereas the finite element method is used to compute the resulting deformation of the machine tool structure. The developed model is then used to compensate thermally-induced displacements at the tool centre point relative to the workpiece coordinate system in real time in order to improve the machining accuracy.

Poulhaon et al. [91] proposed an approach to correct the trajectory of the tool depending on the real workpiece geometry identified using on-line measurements. The cutting forces that the tool undergoes are monitored and used as input data for the numerical model from which the depth of cut and therefore an approximation of the geometry is derived. A correction of the

tool path is then computed and updated on the machine. More recently, Poulhaon et al. [92] developed another model to predict the impact of the initial residual stresses on the deflection of the workpiece during the on-going machining as well as the post-machining distortion. This method is based on the comparison of the geometry of the workpiece measured on-line to a reduced basis of mechanically admissible geometry evolutions extracted from a bigger database. Another database for the post-machining distortion of parts is also created. These databases are composed off-line using both simulation and experimental test results. The final objective is to be able to correct the tool path to ensure dimensional conformity in function of the measured displacements during machining and to make the planning of the possibly needed extra-conforming steps to correct the deviations due to the material removal easier.

Many other examples of research work on the minimising of machining time are available in literature. However, only few work has been focused on the influence of the machining sequence and of the tool path on the machining quality.

1.2.2 Discussion on the Machining Processes

As it has been shown, the milling process is a very complex process where a multitude of parameters can affect the machining quality. In this subsection a brief recap of the machining process parameters based on the literature review is realised.

During the machining, the cutting loads linked to the chip formation phenomenon are strongly governed by the cutting conditions and the tool geometry. Depending on these parameters varying cutting forces and temperatures are therefore obtained. However, the cutting loads usually affect only the machining accuracy of thin walled parts (deflection of thin walls).

The combination of mechanical and thermal loads is also the source of residual stresses induced in the machined subsurface. The residual stresses induced during the milling of aluminium alloys vary in function of the cutting conditions and the tool geometry but tend to be compressive and to affect a maximal depth of approximately 250μm. A typical milling-induced residual stresses profile in aluminium alloys is shown in Figure 1.28.

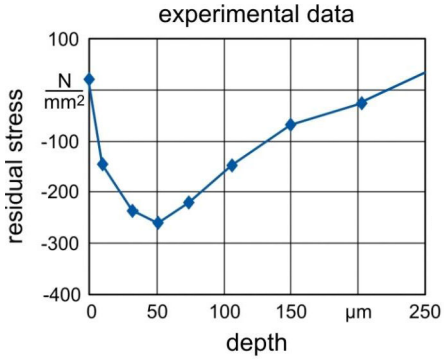

Figure 1.28: Typical subsurface residual stresses induced during milling of aluminium alloys [58]

The fixture is an important parameter which is crucial to ensure the desired machining quality. The fixture design activity includes three principal steps: the fixture planning, the fixture layout design and the fixture design verification. Past research has principally been focused on the minimisation of the workpiece location errors by optimising the position of the locators and clamps around the workpiece as well as on the development of fixture layout optimisation methods. However, only little attention has been paid to the development of models allowing to predict if the designed fixture is able to satisfy the machining quality desired (dimension and geometrical tolerance specifications). In addition, the mechanical behaviour of the workpiece (initial residual stresses) is usually not taken into consideration during the fixture design step.

The machining sequence and the tool path have been principally studied to improve the machining productivity. Their influence on the machined part quality has not been studied in detail.

1.3 Simulation of the Milling Process at Part Scale: Prediction of the Machining Quality

In this section, an overview of past research work on the prediction of machined part quality is presented. Different numerical methods used for the material removal simulation are briefly described and a summary of the finite element models developed is then realised.

1.3.1 Numerical Methods for Material Removal

Various techniques used for numerical material removal can be found in literature. Three types of methods can be distinguished: the deactivation or "death & birth" method, the massive removal approach and the so-called "level-set" method.

1.3.1.1 The Deactivation Method

The deactivation or "death & birth" method is the most widespread approach and has been developed by Wang et al. [15]. In this method, a structured mesh usually composed of hexahedral elements with the element size determined in function of the cutting parameters is used. To simulate the removal of material, elements are deactivated step by step in the machined zone. The material removal is therefore based on predefinition and deactivation of a set of elements generated on the ideal machined path. This method has been applied in several commercial finite element software products such as Abaqus [93, 94, 95, 86, 16, 96], Ansys [97, 98, 18] and MSC.Marc [15] using scripts. Most of these studies have been realised on the machining of aluminium alloys, but authors have also used this method on other materials like Yang et al. [96] who studied the machining of titanium alloy (Ti6Al4V) parts.

Among these studies, some have combined this method with local thermal and mechanical load applications at each new deactivation to model the workpiece-tool interaction [94, 95,

86, 16, 18, 96]. The loads (cutting forces and temperatures) are previously determined and applied to the nodes of the new free surfaces after each deactivation of a set of elements, as shown in Figure 1.29.

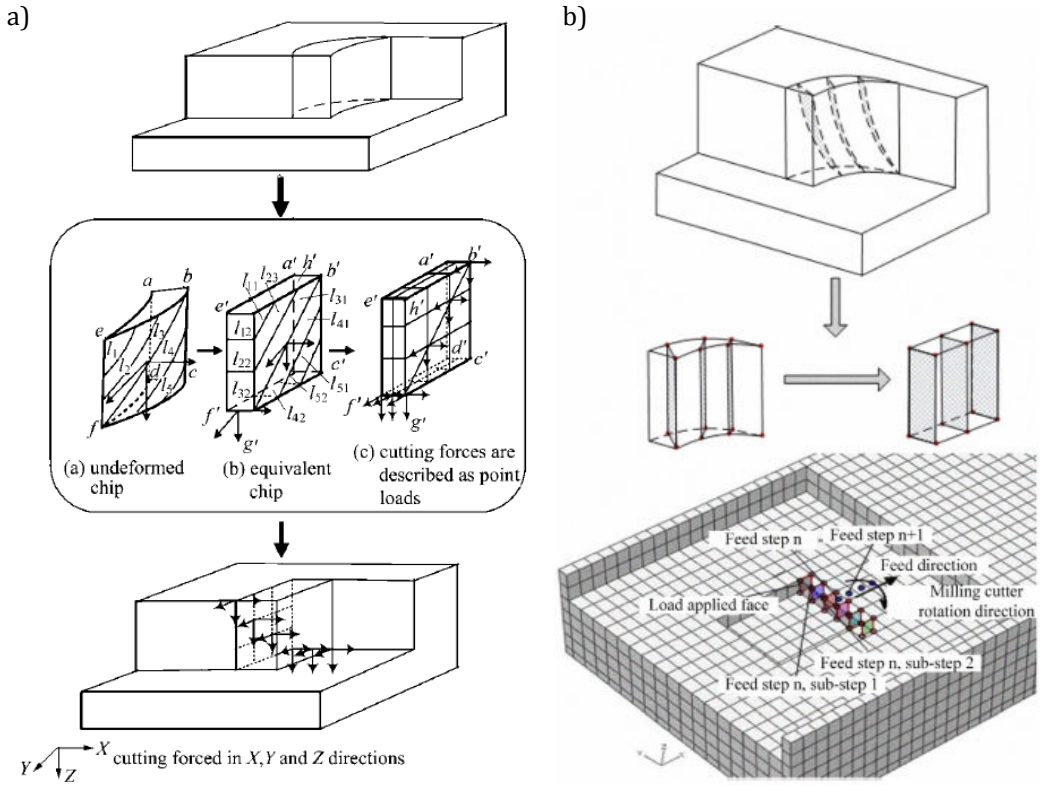

Figure 1.29: The deactivation method: simplification of the geometry of the chip and application of the cutting loads. a) Dong et al. [86] ; b) Bai et al. [95]

For each new deactivation of a set of elements the new residual stress state is computed. This method therefore allows to study the behaviour of the workpiece during the whole machining process.

However, this method is strongly dependent on the mesh and requires the use of structured meshes (usually composed of hexahedral elements) of defined size (depending on the cutting parameters). It is therefore difficult or impossible to simulate the machining sequence of large and complex parts such as structural aerospace parts, which can reach lengths of more than six meters. Indeed, the machining simulations of parts with irregular machining features (i.e. non rectangular) or with complex initial geometries (i.e. forged parts) seem difficult to be performed. In addition, large parts where parallel computing is required to deal with meshes comprising a significant number of nodes and elements have not been studied (no information is available on the parallelization of this removal method). Most of the studies were performed on parts of small dimensions (no real aerospace parts) where some authors have already highlighted problems associated with the mesh requirements. The increase in size and complexity of the part makes the mesh generation difficult, as well as it provokes

an increase in the number of nodes and elements resulting in longer computation time. To overcome these problems and to avoid mesh generation problems and the use of meshes composed of many nodes, some researchers developed the so-called restart-calculation method where remeshing steps are added [96, 86] in function of the machining sequence used. For each machined pocket a different mesh is generated. The mesh size is defined depending on the cutting conditions in the area where the material removal has to be performed and a coarser mesh everywhere else in the workpiece is used. Once the new mesh is obtained, a field transfer of the previous mesh to the new one is performed. A new phase of deactivation of elements and of computation of the residual stress redistribution can then be started. This amounts to a new simulation of deactivation of elements with a new mesh for each machining feature, as represented in Figure 1.30.

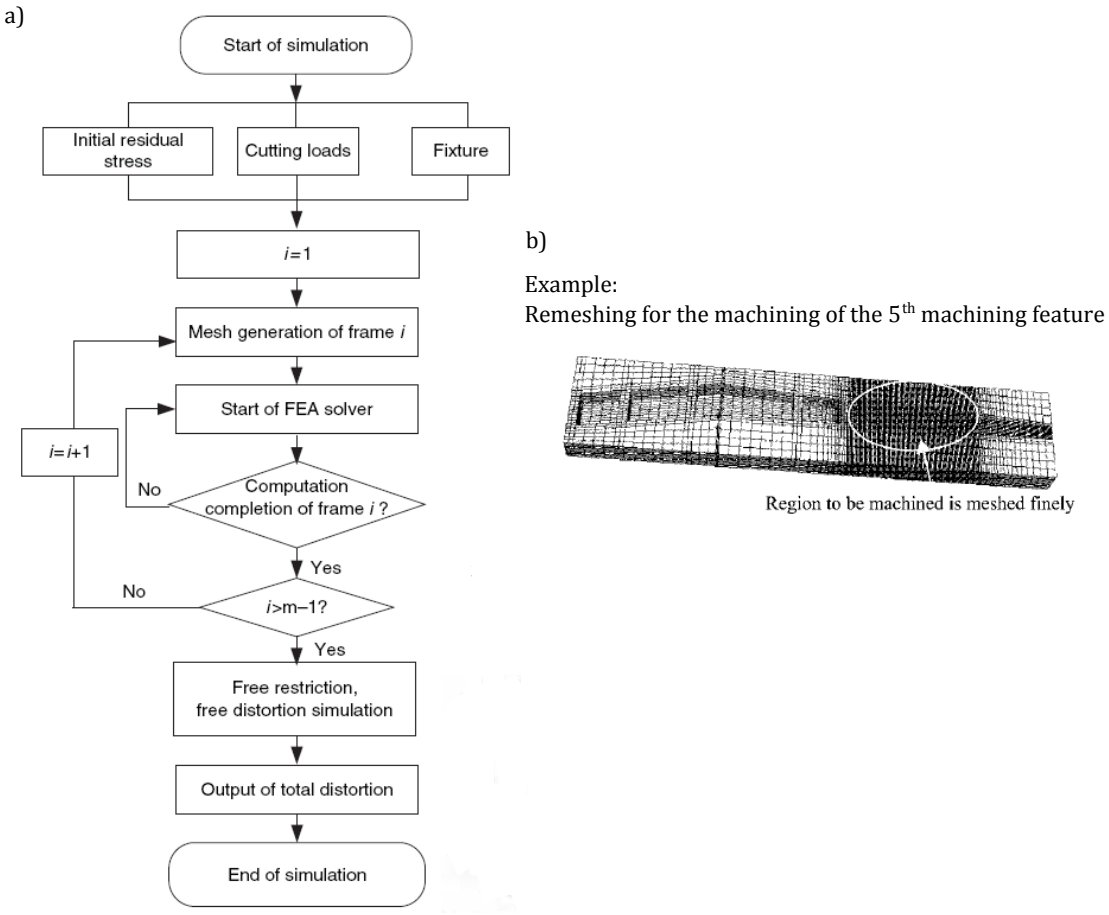

Figure 1.30: The so-called restart-calculation method: a) The principle [96]; b) Example of remeshing adapted to a machining feature [86]

1.3.1.2 The Massive Removal Approach

Recently, Ma et al. [99] have proposed three procedures to perform material removal that can all be classified as massive removal approaches.

The first procedure consists in the mapping of the initial residual stress state of the workpiece on the designed part (CAD) and in the computation of the redistribution of the residual stresses to obtain the post-machining distortion. This procedure is illustrated in Figure 1.31. A similar approach is used in [100] to predict post-machining distortions of thin-walled parts in taking into consideration both the initial residual stresses and the machining-induced residual stresses.

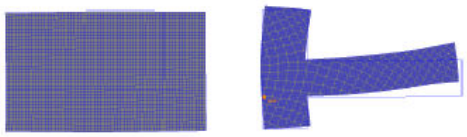

Figure 1.31: The One-step procedure [99]

The principle of the second procedure is quite similar to the method by deactivation, the principal difference being the amount of material removed at each step. With this procedure, the material is removed in several steps and material removals are based on a predetermined machining sequence. The workpiece is therefore composed of several sections meshed in advance which are removed step by step depending on the machining sequence, as illustrated in Figure 1.32.

Figure 1.32: The Multi-step procedure with predetermined material removal [99]

These first two procedures are rather simple and easy to implement, they avoid the remeshing associated with the modelling of each machining operation and allow to predict correctly the part distortion. However, material removals do not represent the real machining path because the influence of the shape changes during the machining on the fixture-workpiece interface and on the machining quality is ignored. In addition, with the second procedure the simulations have to be entirely redone if changes in the machining sequences have to be analysed.

The last procedure presented in this article is a procedure where the material removals follow the real machining path and where workpiece deflections and fixture-workpiece interactions are taken into account. The material removals are realised using a Boolean procedure. This means that for each material removal the new geometry is obtained by a subtraction operation between the current geometry of the workpiece and the machining path, as illustrated in Figure 1.33.

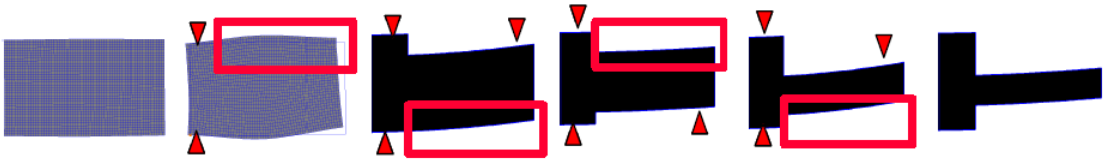

Figure 1.33: The Multi-step procedure with path-dependent material removal [99]

This new geometry is then remeshed before the computation of the new residual stress state and of the associated deflection. Two examples of material removals using a Boolean procedure are illustrated in Figure 1.34.

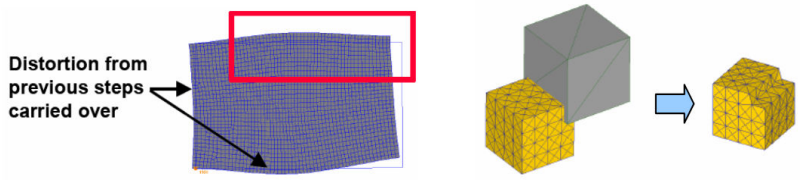

Figure 1.34: Illustration of the Boolean procedure [99]

This procedure is therefore a more realistic representation of the machining process and allows the simulations of complex parts by fully respecting the machining path. Its implementation is nevertheless more complex and remeshing steps are required.

1.3.1.3 The Level-Set Method

This method using level set functions to simulate the machining has been proposed by the Centre of Excellence in Aeronautical Research (Cenaero) and has been implemented into the software Morfeo [101, 102]. Level set functions are signed distance functions which in this case are used to represent the machining path.

At each machining step, the area which has to be machined is considered by modifying the free boundary conditions along the iso-zero of the level-set function representing the machining path. The new equilibrium and associated displacements are then computed. The main benefit of this method is the fact that no remeshing step is needed, but on the other hand the level-set function has to be recomputed on the updated configuration after each machining step. The authors also proposed an approach to consider cutting loads by directly adding typical machining-induced residual stress profiles to the initial residual stresses around the newly machined surface which is described by the level-set function.

1.3.2 The FE Models for the Prediction of the Machining Distortion

Several kinds of models can be distinguished in literature. Differences in the choice of the material removal techniques, in the application of cutting loads and in the boundary conditions (i.e. the fixture modelling) can be observed.

Table 1.3 presents a literature overview of the finite element models developed to predict machining distortions with their main modelling choices. It can be observed that the deactivation method is the main material removal method used and that in most of these studies the fixture-workpiece interaction is often modelled by simply restricting the degrees of freedom in the concerned zones. It also becomes obvious that the cuttings loads are not always taken into account.

Table 1.3: Recap of the different studies and models realised on the prediction of the machining distortions

Study	Year	Material removal method	Cutting loads	Fixture
[15]	2004	Deactivation	-	Restriction of the DoF
[93]	2006	Deactivation	-	Restriction of the DoF
[14]	2006	Deactivation	-	Restriction of the DoF
[86]	2006	Deactivation	Forces and temperatures	Restriction of the DoF
[16]	2007	Deactivation	Only forces	Restriction of the DoF
[101]	2008	Level-set	Machining-induced residual stresses	-
[102]	2008	Level-set	-	-
[17]	2008	Deactivation	Forces and temperatures	Contact modelling
[100]	2008	Massive removal (stress mapping)	Machining-induced residual stresses	-
[18]	2009	Deactivation	Forces and temperatures	Contact modelling
[94]	2009	Deactivation	Forces and temperatures	Restriction of the DoF
[95]	2010	Deactivation	Forces and temperatures	Restriction of the DoF
[99]	2010	Massive removal	-	-
[98]	2010	Deactivation	-	-
[97]	2011	Deactivation	-	Restriction of the DoF
[96]	2011	Deactivation	Cutting forces and temperatures	Restriction of the DoF
[103]	2011	Level-set	-	-
[104]	2012	Massive removal	-	-

1.3.3 Discussion on the Prediction of the Machining Quality

As seen in this literature study, various models using different numerical material removal and fixture-workpiece interaction modelling methods have been developed. All these models present benefits and drawbacks. The modelling approach therefore has to be adapted to the objectives, the part geometries, the machining process plan parameters which could influence the machining quality, the accuracy desired and the available resources.

It can be pointed out that one of the most advanced approaches is presented in the studies of Rai and Xirouchakis [17, 18]. In their model, both the cutting loads and the fixture-workpiece contact modelling are considered. This approach seems particularly well suited for the simulation of thin walled parts, where the effects of cutting loads can become of first order compared to the initial residual stresses. However, the use of the deactivation method makes it difficult to realise the simulation of large and complex aeronautical parts.

Regardless of the methods, the results obtained in all these studies seem to be approximately equivalent. Studies comparing simulation results with experimental ones give a percentage of error on the post-machining distortion varying between 15% and 30%. The assumption that the different numerical methods achieve approximately the same order of precision can therefore be made. Furthermore, the accuracy of the results is not only related to the numerical methods used but is strongly governed by the accuracy of the initial residual stress fields used as input of the simulations.

It is also important to point out that no study has been performed on the prediction of the final machined part geometry and of the machining quality (conformity with the geometrical and dimensional specifications). No prediction of the exact volume removed during the machining, where workpiece deflections are observed, is realised, only post-machining distortions are usually predicted.
Only Rai, in his thesis [105], developed an extra module to compute the final machined part geometry depending on the displacements observed on some nodes during the finite element simulation of the machining process. However, no comparison of the dimensional variations obtained to experimental results is performed and the final part geometry is not computed directly and requires the use of other software solutions like the CAM software Opencascade. Other authors like Masset et al. [106] focused on the prediction of form errors and developed a specific model. However, only form errors of part surfaces obtained by face milling and turning processes can be modelled with such an approach and the redistribution of the initial residual stresses is not taken into consideration. No prediction of the final machined part geometry and of the machining quality of a complex aerospace part can thus be performed with this model.

1.4 Establishment of the Assumptions

The conclusions drawn from this literature survey can be summarised as the following points:

- The intensity of the cutting loads principally affect the machining accuracy of thin walled parts.
- The subsurface residual stresses induced during the milling of aluminium alloys depend on the cutting parameters and the tool geometry and affect a maximal depth of approximately 250μm.
- The influence of the machining sequence and the tool path on the machining quality is often ignored.

- The influence of the initial residual stresses on the machining quality and on the machining process plan definition is often ignored.
- A proper fixture design is crucial to ensure the desired machining quality.
- Only little attention has been paid to the fixture layout optimization design to minimise the dimensional and geometrical errors due to workpiece deflections.
- Only the final post-machining distortion (global curvature of the part) is predicted in most of the finite element models.
- No finite element model allows to predict directly the machining quality (geometrical and dimensional errors).
- No finite element model allows to analyse the behaviour of large and complex parts made of aluminium alloys (rolled plates or forged parts).

The definition of a machining process plan allowing to ensure the desired machining quality is therefore a complex task. Currently, there is a lack of methodology to predict the geometrical and dimensional instabilities due to the combined effects of the redistribution of the residual stresses during machining and the other machining parameters. There is therefore a need in industry (especially in the aerospace industry) of a numerical tool allowing to predict the machined part quality in order to optimise and to validate a machining process plan before going into real machining.

In order to meet this need, the work presented in this dissertation has as an objective to propose a numerical tool allowing to analyse the machining process plan parameter influences and to increase the machining quality of thick, large and complex parts made of AIRWARE® 2050 alloy. Using the developed numerical tool, a methodology to ensure machining quality based on the phenomena observed and on scientific principles is then proposed. The numerical tool has to give the possibility to study the combined effect of the initial residual stresses, the fixture layout and the machining sequence on large and complex aeronautics structural parts made from rolled plates or forged parts. Furthermore it has to be possible to use both experimental and simulation results as input data (residual stress distribution).

Based on the literature review and the research work objectives, three main assumptions have been made:

I The initial residual stresses are the main reason of post-machining distortion and form errors and have therefore the biggest influence on the machining quality of aluminium alloy parts. Yang et al. [107] have recently demonstrated that the main cause of machining distortion for aluminium alloys are the initial residual stresses, which confirms our first assumption.

II The cutting loads and associated induced residual stresses will be ignored. This assumption is justified by the fact that the subsurface residual stresses induced by the milling only affect a maximal depth of approximately 250μm [58, 68] and have therefore a small impact on parts with relatively thick walls (at least 5 mm). The induced machining residual stresses are therefore of second order compared to the initial residual stresses. In addition, it would be difficult to numerically take into account such residual stress

profiles. The mesh would have to be able to capture the profiles in the subsurface (250μm) and would therefore require a high mesh density in these areas.

III Fixture layout and machining sequence have an important influence on the redistribution of the residual stresses during the machining and therefore on the machining accuracy. Depending on the material removal and fixture layout used, workpiece deflections can occur during the machining which lead to a loss of accuracy (overcut and/or undercut). The machining sequence furthermore has to be modelled by multiple material removals to be representative of the real machining behaviour.

In the next chapter an overview of the numerical tool developed to predict the machining quality of thick, large and complex AIRWARE® 2050 alloy parts based on the previous assumptions is realised.

1.5 Conclusion

This chapter is dedicated to the literature review and has been organised in four principal sections.

The first section focuses on the residual stresses. After a brief introduction on the residual stresses, their origins and influences, the residual stress genesis related to the manufacturing of aluminium alloy aerospace parts is detailed.

In the second section, a review of literature on the machining process and the parameters defined in a machining process plan is realised with a particular attention on the milling of aluminium alloys. These parameters are the cutting conditions, the fixture and the machining sequence and tool path.
Several studies have been performed in the past in order to determine the cutting forces and temperatures during machining as well as to determine the residual stresses induced by the cutting. It has been concluded that using typical cutting conditions, the cutting forces and temperatures are too small to provoke workpiece deflections (for the type of parts studied). Furthermore, the associated induced residual stresses affect a too small depth under the machined surface to influence the behaviour of the workpiece during the machining.
The review of literature on the fixture has shown the importance of the use of an adapted fixture layout to ensure a good machining accuracy. It has also allowed to obtain useful information on the modelling choice, like the fact that the modelling of the workpiece and fixture tips is sufficient to achieve an accurate prediction of the fixture-workpiece contact behaviour. Regarding the machining sequence and the tool path, most of the past studies focus on the development of machining tool paths to decrease the machining time. No clear trend of their influence on the machining quality has been found.

The third section is a review of the different models to simulate the machining of parts and their associated numerical method to perform the material removal. Three principal techniques to perform the material removal have been found: the deactivation method, the massive removal

approach and the level-set method. Depending on the material removal technique used as well as on the boundary conditions applied, several models have been developed in the past. However, no model allowing to predict the machining quality (dimensional and geometrical errors) or to simulate the machining of large aerospace parts is available.

Based on the conclusions drawn from the review of literature (on the material, the machining process and the modelling techniques) and depending on the objectives of the project, assumptions have been established and are introduced in the last section. All the developments realised in this Ph.D. thesis have then been based on these assumptions.

1.6 Résumé en Français

Ce chapitre est dédié à l'étude bibliographique et est organisé en quatre principales parties.

La première partie est une introduction sur les origines et influences des contraintes résiduelles ainsi que sur leur genèse au cours de la fabrication des pièces aéronautiques en alliage d'aluminium.

Dans la deuxième partie, une étude bibliographique sur l'usinage et les différents paramètres définis dans les gammes d'usinage est réalisée en accordant une attention particulière au fraisage d'alliages d'aluminium. Les paramètres étudiés sont les conditions de coupe, le montage ainsi que la séquence et les trajectoires d'usinage.

Plusieurs études portant sur la détermination des efforts de coupe et des températures pendant l'usinage, ainsi que sur la détermination des contraintes résiduelles induites par la coupe ont été réalisées dans le passé. Il a été conclu qu'en utilisant des conditions de coupe classiques, les efforts et températures sont généralement trop faibles pour déformer le type de pièces étudiées. Les contraintes résiduelles d'usinage affectent en effet une trop faible couche de matière sous la surface pour affecter le comportement de la pièce pendant l'usinage. L'étude bibliographique sur le montage a montré l'importance de l'utilisation d'un montage adapté pour assurer une bonne précision d'usinage. Cette étude a également permis d'obtenir des informations utiles sur les choix de modélisation. Par exemple, il a été démontré qu'il n'est pas nécessaire de modéliser entièrement tous les éléments du montage et leurs déformations au cours de l'usinage pour modéliser précisément le contact entre la pièce et le montage. En ce qui concerne les séquences et les trajectoires d'usinage, la plupart des études sont focalisées sur le développement de trajectoires d'outils permettant de diminuer les temps d'usinage. Aucune information de leurs influences sur la qualité d'usinage n'a pu être trouvée.

La troisième partie est consacrée à une étude bibliographique sur les différents modèles utilisés pour simuler l'usinage et les différentes méthodes numériques développées pour réaliser l'enlèvement de matière. Trois principales techniques ont été trouvées, la méthode de désactivation, la méthode par enlèvement massif de matière et la méthode dite "level-set". En fonction de la technique utilisée et du type de conditions aux limites appliquées, plusieurs modèles ont été développés. Cependant, aucun modèle permettant de prédire

la qualité d'usinage (erreurs dimensionnelles et géométriques) ou de simuler l'usinage de grandes pièces n'est disponible (aucun résultat montré dans la littérature).

A partir des conclusions tirées de cette étude bibliographique (sur le matériau, sur l'usinage et sur les techniques de modélisation) ainsi qu'en tenant compte des objectifs du projet, des hypothèses ont été formulées et sont introduites dans la quatrième et dernière partie de ce chapitre. Ces hypothèses sont :

I Les contraintes résiduelles initiales sont la raison principale de non-qualité d'usinage.

II Les efforts de coupe, l'élévation de température ainsi que les contraintes résiduelles induites pendant l'usinage affectent seulement une faible couche de matière sous la surface usinée et peuvent donc être négligés dans le cas d'usinage de grandes pièces aéronautiques en alliage d'aluminium ne présentant pas de parois minces comme traité dans cette étude.

III Le montage et les séquences d'usinage ont une influence sur la redistribution des contraintes résiduelles et donc sur la qualité d'usinage

Tous les développements réalisés dans ce travail de thèse sont donc basés sur ces hypothèses.

Chapter 2

FORGE OFELIA

This chapter is devoted to the development of FORGE OFELIA, the version of FORGE® adapted to the machining simulation and the prediction of the machining quality.

A brief description of the finite element software FORGE® and of its main characteristics is first performed with a particular attention to numerical aspects linked to our work.

In a second step, the numerical tool FORGE OFELIA is presented. Based on the assumptions established in Chapter 1, a modelling approach has been defined and is introduced. Then, the development of numerical methods, their implementation in FORGE® and the solver adaptation are discussed. Finally, the capacities of FORGE OFELIA and its models are presented and evaluated by comparison with a model found in literature.

Contents

2.1 The Finite Element Software FORGE®

As explained in the Introduction, the work presented in this thesis is realised in the framework of the finite element software FORGE® which has been developed at CEMEF since the 1980s. FORGE® is an implicit finite element software suitable for material forming simulations using the so-called MINI element (P1+/P1) with a mixed velocity-pressure formulation [108]. A small strain approach with the updated Lagrangian formulation is implemented in this software. The MINI element is a linear isoparametric tetrahedron element enriched with an additional degree of freedom in velocity at its center. This element ensures the Brezzi/Babuska condition (stability condition) of existence and uniqueness of solution [109] and offers a good compromise between computational cost and accuracy of results. To deal with distorted meshes during large strain simulations an automatic adaptive remesher is used [110].

In this section, a brief description of the formulation, the FE discretization and the characteristics of the software FORGE® is given. We will only focus on the aspects adapted, modified or impacted by our work. Interested readers can find further information in [111].

2.1.1 The Mechanical Problem

When dealing with the modelling of manufacturing processes inducing deformations different geometrical objects are interacting. Objects can be considered either as rigid or as deformable solids. Whereas the workpiece is always considered as a deformable solid, depending on the analysis objectives the tools and dies can be modelled as rigid or deformable solids. In our models, a deformable solid is considered as a finite domain $\Omega \subset \mathbb{R}^3$ with its boundary $\partial\Omega \subset \mathbb{R}^2$. It obeys material laws which can be described by the fundamental principles of continuum mechanics. The study of the mechanical problem consists thus in the determination of the physical quantities (at a time t) describing the evolution of the system (deformable solids). These physical quantities are displacements, stress and strain fields and are deduced from the computed velocity and pressure fields.

2.1.1.1 The Motion Description

Three principal approaches can be used in order to describe the motion of any point $\vec{x}$ of Ω: the Lagrangian approach, the Eulerian approach and the Arbitrary Lagrangian Eulerian approach, which is a combination of the two previous. In the Lagrangian approach the evolution of each point of the material is followed in time from the initial position to the current one whereas the Eulerian approach consists in the observation of the evolution of the material from a fixed point in space. In FORGE®, the updated Lagrangian approach is used. The configuration is therefore updated at each time step, i.e. the displacement of any node is computed from the last time step to the current one and not from the initial time step.

A solid occupying the domain Ω_0 at the initial moment $t = 0$ is considered. After a certain time t the solid has been deformed and occupies the domain Ω_t, as illustrated in Figure 2.1.

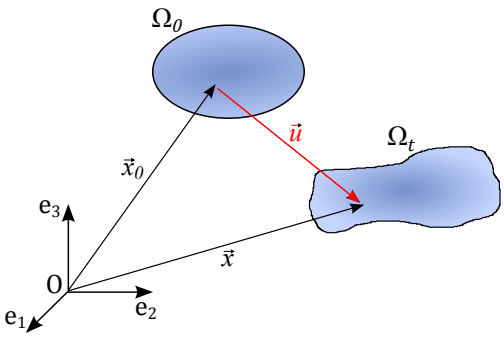

Figure 2.1: Motion description with the Lagrangian approach

A function φ exists, which is the bijection of Ω_0 on Ω_t, allowing to follow the motion of a material point of the solid. The position vector $\vec{x}$ of any material point at time t can therefore be defined as:

$$\vec{x} = \varphi(\vec{x}_0, t) \tag{2.1}$$

with $\vec{x}_0$ being the initial position of the material point at time t_0.

The motion of a material point being defined as the difference between its position at the current time t and its initial position, the Lagrangian displacement field $\vec{u}$ can be defined as:

$$\vec{u} = \vec{x} - \vec{x}_0 = \varphi(\vec{x}_0, t) - \vec{x}_0 \tag{2.2}$$

The displacement field $\vec{u}$ includes rigid body motions (translation and rotation) as well as the deformation of the solid.

With the updated Lagrangian approach, which is used in FORGE®, the motion is defined for each time interval by a function φ^t, similar to equation 2.1.

$$\vec{x}_{t+\Delta t} = \varphi^t(\vec{x}_t, t + \Delta t) \tag{2.3}$$

with Δt being small enough to be consistent with the small strain hypothesis (equation 2.4):

$$\epsilon = \frac{1}{2}(\vec{\nabla}\vec{u} + (\vec{\nabla}\vec{u})^T) \tag{2.4}$$

with ϵ the Cauchy strain tensor (infinitesimal strain tensor) and $\vec{\nabla}$ the nabla vector operator[1].

2.1.1.2 Fundamental Equations

The deformation of the deformable solid is governed at all instants by fundamental equations which are the mass conservation (equation 2.5) and the momentum balance (equation 2.6).

[1] As a reminder, $\vec{\nabla}$ is the nabla vector operator such that: the gradient of a scalar field s or a vector field $\vec{s}$ is expressed as $\vec{\nabla}s$ or $\vec{\nabla}\vec{s}$ and the divergence of a vector field $\vec{s}$ is written as $\vec{\nabla}\cdot\vec{s}$. Note that the divergence can operate on any tensor field of rank one and above.

Fundamental equations

$$\frac{\partial \rho}{\partial t} + \vec{\nabla} \cdot \rho \vec{v} = 0 \tag{2.5}$$

$$\vec{\nabla} \cdot \sigma + \rho(\vec{f} + \vec{\gamma}) = 0 \tag{2.6}$$

with σ being the Cauchy stress tensor, ρ the mass density, $\vec{v}$ the velocity, $\vec{f}$ the volumetric force (gravity) and $\vec{\gamma}$ the acceleration vector.

For an elastic-plastic constitutive model, the plastic incompressibility and elastic compressibility are taken into account, leading to another expression of the mass conservation equation:

$$\vec{\nabla} \cdot \vec{v} + \frac{\dot{p}}{K} = 0 \tag{2.7}$$

with $\dot{p}$ being the hydrostatic pressure rate and K the bulk modulus defined as $K = \frac{E}{3(1-2\nu)}$.

In the manufacturing process modelling the inertial and gravitational forces are often neglected. In our case, large and thick machined parts presenting a significant stiffness are considered. The assumption that the gravitational forces affect neither the behaviour of the workpiece during machining nor the post-machining distortion can thus also be made. In several tests, of which one is presented later in this dissertation (see Section 2.2.1.1), it has been shown that the same assumption can also be made for the inertial forces when dealing with machining simulations of such parts (dynamic aspects such as vibrations are neglected). The momentum balance equation then becomes:

$$\vec{\nabla} \cdot \sigma = 0 \tag{2.8}$$

2.1.1.3 Boundary Conditions

The above-mentioned equilibrium equations are verified in every point of the deformable solid and at every time, for whatever conditions applied on the boundary $\partial\Omega$. The boundary conditions determine the evolution of the equilibrium state of the solid and can be classified in four types of conditions. The boundary $\partial\Omega$ can therefore be decomposed in four parts ($\partial\Omega = \partial\Omega_f \cup \partial\Omega_v \cup \partial\Omega_T \cup \partial\Omega_c$), as illustrated in Figure 2.2.

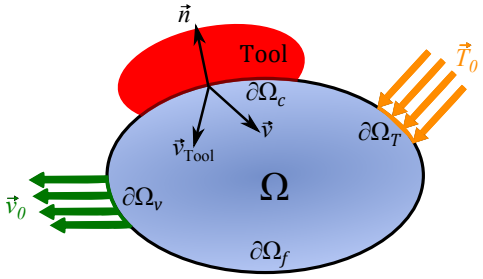

Figure 2.2: The four types of boundary conditions

These four conditions are:

1. The free boundary condition which is expressed as: $\sigma \cdot \vec{n} = 0$ on $\partial\Omega_f$

2. The imposed velocity condition which is expressed as: $\vec{v} = \vec{v_0}$ on $\partial\Omega_v$
3. The imposed stress condition which is expressed as: $\sigma \cdot \vec{n} = \vec{T}$ on $\partial\Omega_T$
4. The contact condition, on $\partial\Omega_c$, which can be decomposed into two categories: the unilateral contact condition and the friction condition.

The unilateral contact
The unilateral contact condition ensures that the deformable solid (workpiece) is not penetrated by the rigid tool. This condition is described by the Signorini's conditions (equation 2.9)

$$\begin{cases} (\vec{v} - \vec{v}_{Tool}) \cdot \vec{n} \leqslant 0 \\ \sigma_n \leqslant 0 \\ \sigma_n (\vec{v} - \vec{v}_{Tool}) \cdot \vec{n} = 0 \end{cases} \tag{2.9}$$

with $\vec{v_{Tool}}$ being the tool velocity and σ_n the normal stress (the contact pressure) defined as: $\sigma_n = (\sigma \cdot \vec{n}) \cdot \vec{n}$.
If there is no contact, the solids can have different velocities and the contact pressure is zero. When the deformable solid comes into contact with a tool, the contact pressure σ_n is not zero anymore and the contact points between two solids have an equal normal velocity.

The friction tangential component
The friction tangential component τ is given by the friction law according to:

$$\tau = \sigma \cdot \vec{n} - \sigma_n \cdot \vec{n} \tag{2.10}$$

To model the relative sliding movements which can occur between two solids, tribological laws are defined. Several friction laws are available in FORGE®. In this work, the Coulomb's law limited with a Tresca criterion is used. This law is defined as in equation 2.11.

$$\begin{aligned} \tau &= -\mu\sigma_n \frac{\Delta V_g}{|\Delta V_g|} \quad if \quad \mu\sigma_n < \overline{m}\frac{\sigma_0}{\sqrt{3}} \\ \tau &= -\overline{m}\frac{\sigma_0}{\sqrt{3}} \frac{\Delta V_g}{|\Delta V_g|} \quad if \quad \mu\sigma_n \geq \overline{m}\frac{\sigma_0}{\sqrt{3}} \end{aligned} \tag{2.11}$$

with μ being the Coulomb friction coefficient, $\overline{m}$ the Tresca friction coefficient (comprised between 0 and 1), σ_n the contact pressure, σ_0 the yield strength of the material and ΔV_g the relative sliding velocity defined as $\Delta V_g = v - v_{tool} - [(v - v_{tool})\vec{n}]\,\vec{n}$.

2.1.1.4 Constitutive Laws

Constitutive laws are essential to model the material behaviour during the manufacturing process. They allow to relate the stress tensor σ to the strain tensor ϵ, the strain rate tensor $\dot{\epsilon}$ and the temperature T.

The stress tensor σ can be decomposed into deviatoric (s) and volumetric parts (pI):

$$\sigma = s - pI \tag{2.12}$$

with p being the hydrostatic pressure expressed as $p = -\frac{1}{3} tr(\sigma)$ with $tr(.)$ being the trace of the tensor and I the identity matrix.
The equivalent von Mises stress is given by:

$$\overline{\sigma} = \sqrt{\frac{3}{2} s : s} \tag{2.13}$$

The strain rate tensor $\dot{\epsilon}$ is given by:

$$\dot{\epsilon} = \frac{1}{2}(\vec{\nabla}\vec{v} + \vec{\nabla}\vec{v}^t) \tag{2.14}$$

and the equivalent strain rate $\dot{\overline{\epsilon}}$ and equivalent strain $\overline{\epsilon}$ are given by:

$$\dot{\overline{\epsilon}} = \sqrt{\frac{2}{3}(\dot{\epsilon} : \dot{\epsilon})} \qquad \text{and} \qquad \overline{\epsilon} = \int_0^t \dot{\overline{\epsilon}} dt \tag{2.15}$$

Depending on the process, different constitutive laws are used. Elastic-plastic constitutive models are used for cold manufacturing processes where the elastic behaviour cannot be neglected. When dealing with the redistribution of residual stresses during machining, strains observed generally stay within the elastic domain. However, in order to capture a possible yielding which could occur due to an unsuitable fixture system during the clamping step or the machining step with a workpiece presenting a high residual stress level, an elastic-plastic constitutive model is used in this work. In this model, the linear elastic behaviour for an isotropic material is described by Hooke's law until the stress reaches the yield strength. The model is based on the law of strain additivity from the Prandtl-Reuss theory [112, 113, 114]. The total strain rate is therefore decomposed into elastic ($\dot{\epsilon}^e$) and plastic ($\dot{\epsilon}^p$) terms:

$$\dot{\epsilon} = \dot{\epsilon}^e + \dot{\epsilon}^p \tag{2.16}$$

The elastic behaviour is characterised by a linear and reversible behaviour, described by Hooke's law:

$$\begin{cases} \sigma = \underline{\underline{D}}\, \epsilon^e = 2\mu^e \epsilon^e + \lambda^e tr(\epsilon^e) I \\ \text{with:} \quad \mu^e = \dfrac{E}{2(1+\nu)} \quad \text{and} \quad \lambda^e = \dfrac{E\nu}{(1+\nu)(1-2\nu)} \end{cases} \tag{2.17}$$

where λ^e and μ^e are the Lamé parameters, E the Young's modulus and ν the Poisson's ratio.

The elastic-plastic model is based on the von Mises plasticity criterion which is defined by a yield criterion function f such as:

$$\begin{aligned} &f = \overline{\sigma} - \sigma_0 \\ &\text{If } f \leqslant 0 \Rightarrow \text{ Elastic behaviour} \\ &\text{If } f = 0 \Rightarrow \text{ Plastic behaviour} \end{aligned} \tag{2.18}$$

with $\overline{\sigma}$ being the equivalent von Mises stress defined as in equation 2.13 and σ_0 being the yield strength of the material. Plastic flow therefore occurs when $\overline{\sigma} = \sigma_0$.

The direction and the intensity of the plastic flow is determined using the Prandtl-Reuss model:

$$\dot{\epsilon}^p = \lambda^{pl} \frac{\partial f}{\partial \sigma} \tag{2.19}$$

with λ^{pl} the scalar plastic multiplier.
When associated with the von Mises criterion, the plastic flow becomes:

$$\dot{\epsilon}^p = \frac{3\lambda^{pl}}{2\overline{\sigma}} s \tag{2.20}$$

The elastic-plastic model can then be summarised by the following system of equations:

$$\begin{cases} \dot{\epsilon} = \dot{\epsilon}^e + \dot{\epsilon}^p \\ \dot{\epsilon}^e = \underline{\underline{\mathrm{D}}}^{-1} \dot{\sigma} \\ \dot{\epsilon}^p = \lambda^{pl} \dfrac{\partial f}{\partial \sigma} \\ f = \sigma - \sigma_0 \end{cases} \tag{2.21}$$

Only the elastic-plastic model is considered here, for more details on the different constitutive laws the reader can refer to [111, 112].

2.1.1.5 System of Equations to Solve

The mechanical problem to solve is defined by the system of equations composed of both the fundamental equations and the boundary conditions. Decomposing σ into deviatoric and volumetric parts, the strong form of the mechanical problem can be expressed by the following system of equations:

$$\begin{cases} \vec{\nabla} \cdot \sigma = \vec{\nabla} \cdot s - \vec{\nabla} p = 0 & \text{on } \Omega \\ \vec{\nabla} \cdot \vec{v} + \dfrac{\dot{p}}{K} = 0 & \text{on } \Omega \\ \sigma_n \cdot \vec{n} = 0 & \text{on } \partial\Omega_f \\ (\vec{v} - \vec{v}_{Tool}) \cdot \vec{n} \leqslant 0 & \text{on } \partial\Omega_c \\ \tau = -\mu \sigma_n \dfrac{\Delta V_g}{\mid \Delta V_g \mid} & \text{on } \partial\Omega_c \end{cases} \tag{2.22}$$

2.1.2 Finite Element Formulation

2.1.2.1 Weak Formulation

The weak formulation is a mixed velocity-pressure formulation. These two variables are considered as completely independent from each other. The functional spaces of kinematically admissible velocity fields V^{ka} and V_0^{ka} and the functional space of pressure P are introduced as follows:

$$\begin{aligned} V^{ka} &= \{v \in (H^1(\Omega))^3 / (\vec{v} - \vec{v}_{Tool}) \cdot \vec{n} \leqslant 0 \quad \text{on } \partial\Omega c\} \\ V_0^{ka} &= \{v \in (H^1(\Omega))^3 / \vec{v} \cdot \vec{n} \leqslant 0 \quad \text{on } \partial\Omega c\} \\ P &= L^2(\Omega) \end{aligned} \tag{2.23}$$

The weak formulation of the problem is obtained by multiplying the equations of the strong form by test functions $(\vec{v^*}, p^*)$ and with integration by parts. Using Green's theorem[2] , the problem becomes:
Find $(\vec{v}, p) \in V^{ka} \times P$, so that

$$\begin{cases} \int_\Omega s(\vec{v}) : \dot{\epsilon}(\vec{v^*}) d\Omega - \int_\Omega p(\vec{\nabla} \cdot \vec{v^*}) d\Omega - \int_{\partial\Omega_c} \vec{\tau} \cdot \vec{v^*} d\Gamma = 0 \\ \int_\Omega p^* (\vec{\nabla} \cdot \vec{v} + \dfrac{\dot{p}}{K}) d\Omega = 0 \\ \forall (\vec{v^*}, p^*) \in V_0^{ka} \times P \end{cases} \tag{2.24}$$

2.1.2.2 Spatial Discretization

In order to solve the above-mentioned weak form of the mechanical problem using the finite element method the continuous domain Ω is decomposed into multiple elements Ω_e. The combination of these elements forms the triangulation of Ω and defines the discrete domain Ω_h, which is therefore a discrete approximation of the continuous domain Ω.

$$\Omega_h = \bigcup_{\Omega_e \in \Omega_h} \Omega_e \tag{2.25}$$

Let V_h and P_h be the finite dimension sub-spaces such as $V_h \subset V^{ka}$ and $P_h \subset P$. The discrete problem can then be written as:
Find $(\vec{v}_h, p_h) \in V_h \times P_h$, so that

$$\begin{cases} \int_{\Omega_h} s(\vec{v}_h) : \dot{\epsilon}(\vec{v_h^*}) d\Omega_h - \int_{\Omega_h} p(\vec{\nabla} \cdot \vec{v_h^*}) d\Omega_h - \int_{\partial\Omega_{hc}} \vec{\tau} \cdot \vec{v_h^*} d\Gamma_h = 0 \\ \int_{\Omega_h} p_h^* (\vec{\nabla} \cdot \vec{v}_h + \dfrac{\dot{p}_h}{K}) d\Omega_h = 0 \\ \forall (\vec{v_h^*}, p_h^*) \in V_{0h} \times P_h \end{cases} \tag{2.26}$$

The accuracy of the results obtained during the resolution of the problem (equation 2.26)

[2] As a reminder, Green's theorem is written as: $-\int_\Omega \Delta\vec{u} \cdot \vec{v} = \int_\Omega \vec{\nabla}\vec{u} \cdot \vec{\nabla}\vec{v} - \int_{\partial\Omega} \frac{\partial \vec{u}}{\partial \vec{v}} \cdot \vec{v}$
with Δ the Laplace operator such that $\Delta\vec{u} = \vec{\nabla} \cdot \vec{\nabla}\vec{u}$

is directly linked to the choice of the interpolation functions associated with the unknown velocity and pressure. In addition, the interpolation of the pressure cannot be chosen independently from the interpolation of the velocity. These interpolation spaces have to satisfy the Brezzi-Babuska compatibility condition [109] which ensures the existence and uniqueness of the solution.

In FORGE® the P1+/P1 mixed velocity-pressure element is used, which is the element with the smallest interpolation degree ensuring the Brezzi-Babuska compatibility condition. It is a linear tetrahedral element on which the interpolation of the velocity field is enriched with an additional degree of freedom in the centre of the element, the so-called "bubble". The pressure is therefore linear whereas the velocity field is decomposed into a linear and a bubble part. The degrees of freedom of the P1+/P1 element are represented in Figure 2.3.

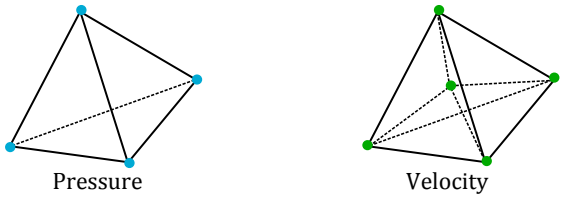

Figure 2.3: The velocity and pressure degrees of freedom of the P1+/P1 element

For more details on the particular formulation of the P1+/P1 element used in FORGE® (MINI-ELEMENT) and on the resolution of the problem, the reader can refer to [115, 116].

2.1.3 Contact Analysis

In this paragraph, a brief description of the method used in FORGE® to take into account the unilateral contact is given.

In order to determine which nodes have to be considered in the contact analysis, the distance between a surface node of the workpiece (deformable solid) and its projection onto the tool (rigid solid) is evaluated at each time step. When a node is in contact with a tool, the Signorini's conditions previously mentioned (equation 2.9) have to be imposed. To deal with potential new nodes arriving in contact, the contact condition is also computed for nodes located close to the tools' surfaces. Each node at a distance lower than a minimum distance d_{tool} is considered. The minimum distance is determined by default depending on the mesh size. This method is illustrated in Figure 2.4.

Considering an implicit formulation, the contact condition has to be respected at the end of the time step. This leads to the condition $d(t+\Delta t) \geqslant 0$.
This expression can then be linearised [117].

$$\begin{aligned} d(t+\Delta t) &= d(t) + \frac{\partial d(t)}{\partial t}\Delta t \\ &= d(t) + (\vec{v}_{Tool} - \vec{v}) \cdot \vec{n}(t)\Delta t \end{aligned} \tag{2.27}$$

with $d(t)$ the distance at time t, $\vec{v}_{Tool}$ the velocity of the tool and Δt the time step.

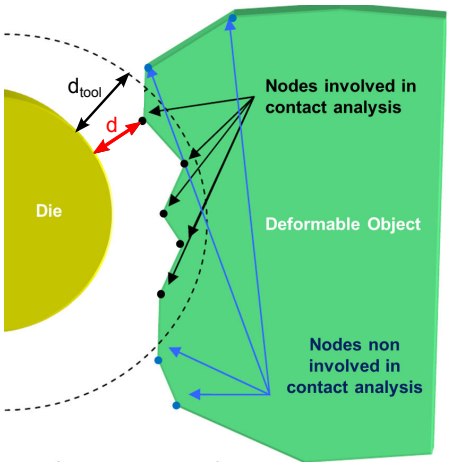

Figure 2.4: The contact analysis zone (taken from the FORGE® documentation [111])

The unilateral contact condition (first equation of 2.9) for the next time step becomes:

$$h(\vec{v}) = (\vec{v} - \vec{v}_{Tool}).\vec{n}(t) - \frac{d(t)}{\Delta t} \leqslant 0 \tag{2.28}$$

Although the contact condition is expressed at time $t + \Delta t$, this formulation is explicit because the normal $\vec{n}$ and the distance d are evaluated at time t and are considered constant during the whole time increment.

The condition in equation 2.28 is imposed as a discrete nodal condition and is therefore computed at each node k of the boundary surface.

$$h(\vec{v}_k) = (\vec{v}_k - \vec{v}_{Tool}).\vec{n}_k(t) - \frac{d_k(t)}{\Delta t} \leqslant 0 \tag{2.29}$$

$$\text{or } \langle h(\vec{v}_k) \rangle = 0 \qquad \text{with } \langle\,\rangle \text{ the Macaulay brackets}$$

In FORGE® the contact condition is imposed using a penalty method. The non-penetration condition is therefore imposed with the help of a penalty coefficient ρ_c. The weak formulation equation 2.30 of the mechanical problem can then be written as:
Find $(\vec{v}_h, p_h) \in V_h \times P_h$, so that

$$\begin{cases} \int_{\Omega_h} s(\vec{v}_h) : \dot{\epsilon}(\vec{v}_h^*) d\Omega_h - \int_{\Omega_h} p(\vec{\nabla} \cdot \vec{v}_h^*) d\Omega_h \\ \qquad + \rho_c \sum_{x_k \in \partial\Omega_{hc}} \langle h(\vec{v}_h(x_k)) \rangle \cdot S(x_k) - \int_{\partial\Omega_{hc}} \vec{\tau} \cdot \vec{v}_h^* d\Gamma_h = 0 \\ \int_{\Omega_h} p_h^* (\vec{\nabla} \cdot \vec{v}_h + \frac{\dot{p}_h}{K}) d\Omega_h = 0 \\ \forall (\vec{v}_h^*, p_h^*) \in V_{0h} \times P_h \end{cases} \tag{2.30}$$

with $S(x_k)$ being a surface associated with the node k, used to assign a weight proportional to the surface area of the adjacent triangles.

Outward-pointing normal vectors have therefore to be determined. They are computed at each contact node by projection of the node on the tool or rigid body surface. When nodes are exactly in contact, difficulties in determining these vectors can occur. In order to avoid problems during the computation of the normal vectors when nodes are exactly on the boundary surface, a penetration distance d_{pen} of the workpiece into the tool is authorised. This distance is chosen depending on the mesh size and is fixed to 1% of its size by default. The non-penetration condition can therefore simply be written as:

$$d(t+\Delta t) + d_{pen} \geqslant 0 \tag{2.31}$$

Physically the penalty method consists in the application of a repulsive force on the nodes penetrating the tool. This force is proportional to the distance of penetration.

The main benefit of this method is to impose mechanical conditions without increasing the number of unknowns. However, the exact solution being obtained for $\rho_c = \infty$, only an approximation of the contact problem solution can be achieved. The choice of the value of the penalty coefficient ρ_c is therefore very important. If the value of this coefficient is too big an ill-conditioned numerical problem might occur resulting in resolution problems [118]. The penalty coefficient thus has to be determined in function of the problem treated.
For more details on the contact analysis, interested readers can refer to [117, 119, 120].

2.1.4 Resolution

Whether it is due to the material behaviour or to the unilateral contact, the system to solve is in general non-linear. An iterative method is therefore required to solve it. In FORGE®, the resolution of the non-linear system is performed using the Newton-Raphson method. The non-linear problem is thus transformed into a series of linear problems. For each iteration of the resolution algorithm, the obtained linear system is then solved using the preconditioned conjugate residual method. An incomplete Cholesky factorisation preconditioner is used in order to improve the rate of convergence and therefore to decrease the CPU time. The solution of an increment is considered as being found when the convergence criterion is reached, which is based on the relative residual value. The relative residual represents the ratio between the error (or residual[3]) made after n Newton-Raphson iterations and the initial error (initial residual). In FORGE®, the relative residual threshold is fixed to 10^{-7} by default and can be written as:

$$\frac{|\,\text{Residual}_n\,|}{|\,\text{Residual}_0\,|} \leqslant 10^{-7} \quad (\text{relative residual threshold} = 10^{-7}) \tag{2.32}$$

with Residual_0 being the initial residual and Residual_n the residual after n iterations.

For more detailed information on the resolution, interested readers can refer to [116, 121, 111].

[3] As a reminder, a residual vector Residual of an approximate solution x_{app} to a linear system $Ax = b$ can be defined as: Residual $= b - Ax_{app}$

2.1.5 Automatic Remeshing and Field Transfer

As explained previously, in FORGE® P1+/P1 elements are used, meshes are therefore composed of tetrahedrons which are capable to describe accurately complex geometries. The simulation of manufacturing processes and especially forming processes generally involves large deformations. In case of an updated Lagrangian formulation (as in FORGE®) where the position of the nodes of the mesh is updated at the end of each increment, the mesh can quickly become distorted. The accuracy of the results is strongly governed by the mesh quality. In order to avoid the degeneration of the mesh, an automatic adaptive remeshing method is available in FORGE®. The mesh generation and remeshing method used are based on an iterative and local mesh optimisation procedure [122, 110]. The remeshing procedure has been fully parallelized and allows to generate unstructured meshes composed of tetrahedrons for all kinds of part geometries. Moreover, the remeshing can be triggered on several criteria: number of computed increments, mesh quality or even on the detection of a new contact zone with significant curvature.

Once the remeshing step is completed, the variable fields have to be transported into the new mesh. Due to the discretization order of the finite element formulation, two kinds of variables are used in FORGE®: the P1 variables defined at nodes like the velocity[4] and the pressure and the P0 variables defined at the element like the stress tensor components. Different methods of field transfer therefore have to be used in function of the variable type.

To perform a P1 variable transfer, the nodes of the new mesh are projected on the previous one. The objective is to detect which elements of the old mesh contain the nodes of the new one, as presented in Figure 2.5. When the localisation is realised, the variables defined at the nodes of the previous mesh are interpolated linearly on nodes of the new mesh.

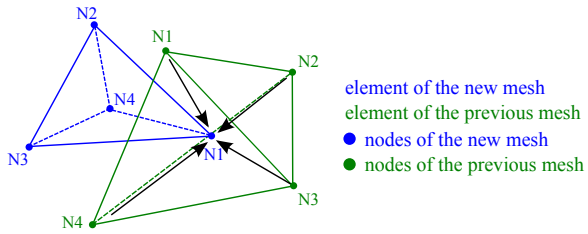

Figure 2.5: P1 variable transfer with P1+/P1 element

To perform the P0 variable transfer from the initial to the new mesh, P0 variables first have to be transformed into P1 variables, as illustrated in Figure 2.6. Using the same method as seen previously for the P1 variables, the P0 variables transformed into P1 variables are then interpolated on the new mesh. The operation is performed using a nodal smoothing technique with the least squares method which is equivalent to the minimisation of the following function [123]:

[4]The velocity is considered as a P1 variable and not P1+ due to the particular MINI-ELEMENT formulation [115, 116].

$$\Pi = \sum_{e=1}^{nbelements} V_e \left(\sum_{k=1}^{nbnodes} W_k \psi_k(\xi^e, \eta^e, \varsigma^e) - W_e \right)^2 \tag{2.33}$$

with W_e being the P0 variable defined on the element e, W_k the P1 variables defined at node k, V_e the volume of the element e, ψ_k the shape functions associated with nodes, $(\xi^e, \eta^e, \varsigma^e)$ the coordinates of the Gauss point, $nbelements$ and $nbnodes$ the number of element and nodes respectively.

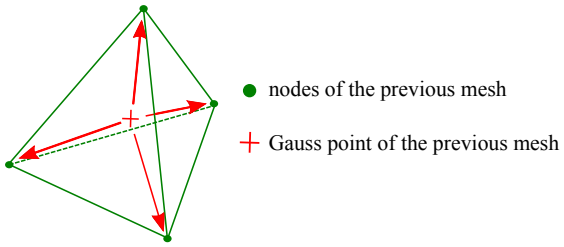

Figure 2.6: P0 to P1 variable transformation with P1+/P1 element

2.2 FORGE OFELIA [124]

In this section the developed finite element tool (FORGE OFELIA) allowing to predict the machining quality depending on the machining process plan used is introduced. The development of FORGE OFELIA has been realised in three main steps. The first one is the development of a modelling approach considering the previously mentioned assumptions on the machining conditions. The second step is to make FORGE OFELIA as computationally efficient as possible and the last step is the development of options allowing to increase the accuracy and flexibility of the numerical tool.

As a reminder, the three principal assumptions made are:

I The initial residual stresses are the main reason for machining non-quality.

II The cutting loads and associated induced residual stresses can be ignored.

III Fixture layout and machining sequence can have an important influence on the machining quality.

2.2.1 Numerical Approach for Machining

In this subsection the modelling approach chosen to simulate machining and to predict the machining quality is presented in detail. The development of this modelling approach has been organised around three main tasks. The first task is the validation of the mechanical model of FORGE® for the prediction of distortions. The second task is the development of a numerical procedure to perform material removal on unstructured tetrahedral meshes. The last task is the implementation of the developed modelling approach into FORGE® as well as its adaptation to the machining simulation.

2.2.1.1 Validity of the Mechanical Model

Linear tetrahedral elements, to which the P1+/P1 element belongs, are reputed as being relatively stiff for bending problems and could thus lead to the minimising of the distortions. When dealing with distortion predictions, Q1 elements are usually recommended and commonly used in literature [17, 95, 96, 94]. In order to evaluate the capability of the numerical tool to accurately predict distortions due to the redistribution of residual stresses, simple tests have been performed and results have been compared with results obtained using the finite element software Abaqus.

One of the tests consists in the application of a stress field on a plate and the comparison of the predicted distortions associated to its re-equilibrium. The plate is 200×40×10 mm and the initial stress profile is simply described by two layers. A tensile stress of 100 MPa is applied on the upper half section (half of the thickness) whereas the opposite stress is applied on the lower half section of the plate, as shown in Figure 2.7.

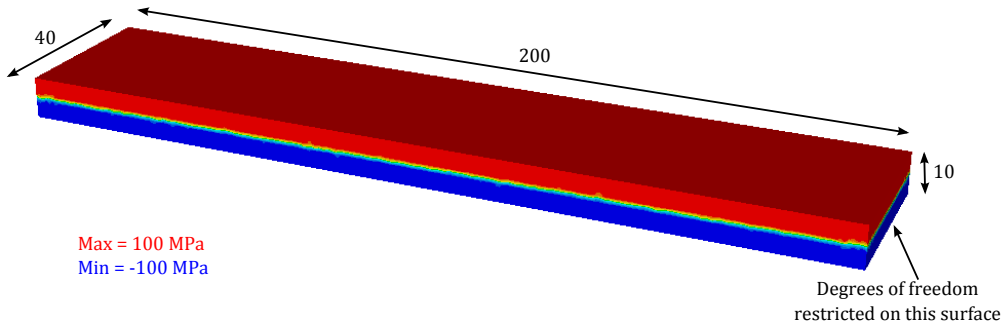

Figure 2.7: The geometry and its initial stress state used for the comparison between FORGE® and Abaqus

All the degrees of freedom at one of the lateral ends of the plate are restricted. The comparisons are performed based on the maximal distortion amplitude d, as illustrated in Figure 2.8.

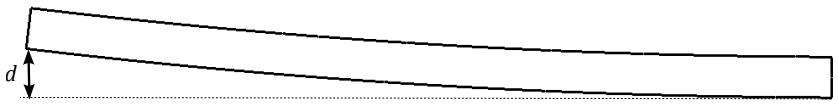

Figure 2.8: The distortion of the plate after the re-equilibrium: comparison of the maximal amplitude d

In FORGE® the inertia effect can be either considered or neglected. A first simulation considering the inertia effect (configuration by default in FORGE®) is performed. In this case, it has been observed that significant oscillations occurred and that a long simulation time was therefore required to reach the final solution. In our case, because tool-workpiece interactions are neglected, only the final solution is important. The same simulation has then been per-

formed without taking into consideration the inertia. It has been found that the same final solution was obtained in only one increment. For all the following simulations, the inertia has therefore been neglected, leading to the momentum balance equation form previously introduced (equation 2.8).

Simulations with FORGE® and Abaqus have then been performed in order to evaluate the influence of both the element type and the mesh size on the distortion predictions. A simulation using an initial mesh composed of Q1 elements has been performed with Abaqus and is considered as the reference solution. Several simulations have then been realised with FORGE® using mesh sizes of 3, 2, 1.25 and 0.8 mm, which represent a mean of 3, 5, 8 and 12 elements in the thickness of the plate respectively. The objective is to validate the small strain formulation and the element type (P1+/P1) used in FORGE® to simulate such problems.

As expected, for a given mesh size the P1+/P1 element (reputed to be relatively stiff) minimises the predicted distortion compared to the Q1 element. In fact, other tests have shown that simulation results from FORGE® are equivalent to the ones obtained with Abaqus and P2 elements. However, it has been found that by decreasing the mesh size, it is possible to reach similar results to the ones obtained with Q1 elements. The difference in percent between the predicted distortions with FORGE® and the ones with Abaqus (Q1) is summarised in Table 2.1.

Table 2.1: Comparison of the distortions predicted with FORGE® with the ones predicted with Abaqus and Q1 elements (the reference solution) in percent: mesh size influence

Number of elements in the thickness	Difference in %
3	12
5	8.5
8	4.5
12	3.5

Under certain conditions the formulation used in FORGE® therefore allows to reach results similar to Abaqus with the Q1 element. Two main conclusions can thus be drawn from the observations made and can be used to define two simple modelling guidelines:

- A mesh size allowing to obtain at least a mean of five elements in the thickness of the walls of the machined part has to be used to accurately predict distortions (error < 10%). This condition has to be fulfilled mainly in the walls causing the distortion (longitudinal walls for example). More information on the geometry analysis of a part and examples of meshes adapted to such simulations are given in Chapter 3 and Chapter 4.
- There is no clear benefit in defining a mesh size resulting in more than eight elements in the thickness of the walls of the machined part as the error reaches already less than 5% for eight elements and as the computation time would be impacted significantly.

2.2.1.2 Boolean Operation Strategy

As seen previously in Section 1.3.1, several approaches for the machining simulation are possible. To simulate the machining of large and complex parts based on FORGE®, the approach chosen also has to be adapted to unstructured meshes composed of tetrahedrons.

A method using a Boolean procedure and level-set functions has therefore been developed in this numerical tool. The new geometry (after material removal) is obtained by a subtraction operation between the current geometry of the part and a given volume (Figure 2.9*a*). The volume is characterised by a surface mesh describing the volume removed by the milling tool during a certain amount of time (Δt) of the real machining sequence. Volumes are automatically generated in STL (STereoLithography) format with a CAD/CAM software linked to the machining program (created by IFMA). The geometry of the milling tool (radius) is also considered during the generation of the volumes. They therefore represent exactly volumes swept by the milling tool during the machining sequence. It is important to point out that Δt is not obligatory constant and is usually defined as the time needed to machine a depth of cut of a machining feature (pockets, slots, holes, etc.). In order to simplify the computations, volumes in STL format are first automatically transformed into a table of coordinates and a table of connectivities which are more easily handled in the numerical tool.

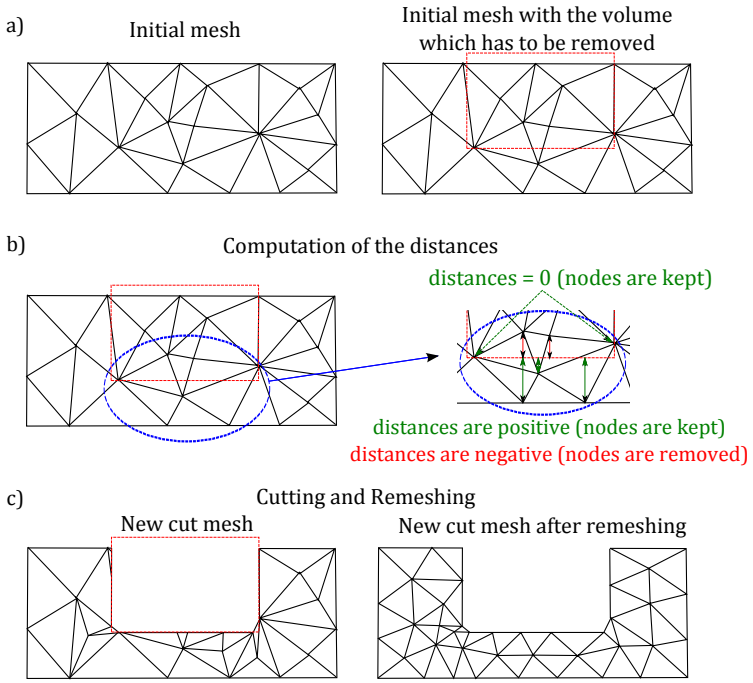

Figure 2.9: The principle steps of the method of massive removal of material with the Boolean procedure developed in the numerical tool [124]

At each new material removal step, a signed distance (level-set) between each node of the current mesh and its projection onto the geometry of the volume which has to be removed (surface mesh) is computed, as illustrated in Figure 2.9*b*.

The obtained distance field is then used to perform the Boolean operation. Depending on the sign of the distance, nodes are either removed or kept. If the distance is positive or zero, the node is not on the machining path and has to be kept. If the distance is negative the node is in the machining area (material removal area) and has to be removed. When an element has nodes that should be removed and kept, the element crosses the machining surface and has to be cut. Several cases are possible in three dimensions and each of those is analysed and treated in a particular way. For each cutting case new nodes on the cut edges and/or centroid nodes are created in order to obtain the new mesh. The four principal cases which can occur are presented in Table 2.2. Other specific cases can appear in function of the number of nodes having a distance equal to zero. In order to limit the generation of new or very small elements, if the distance is smaller than a given characteristic distance the node is projected onto the surface and kept. This characteristic distance is computed depending on the local mesh size defined at each node of the mesh (3% of the local mesh size). The different mesh sizes (refinement areas) which can be defined during data setting are thus taken into consideration. As illustrated in Figure 2.9*c* a remeshing is then performed to improve the quality of the new mesh.

Table 2.2: The main cases of element cutting [124]

Distances of the nodes	New nodes/ Total nodes	New elements	Illustration
3 distances < 0	3 / 4	1	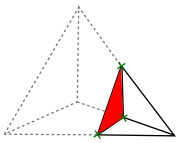
1 distance < 0 and 1 distance = 0	3 / 6	4	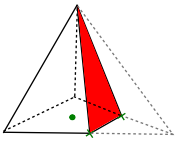
2 distances < 0	8 / 10	14	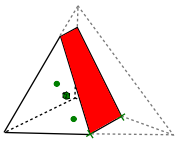
1 distance < 0	7 / 10	14	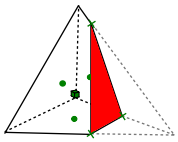
Cut-surface	× New node	● New node: Centroid of surface	New node: Centroid of prism

A simple example of a material removal step on a mesh is shown in Figure 2.10. The signed distance field computed on the initial mesh and its iso-zero surface are shown. As explained previously, the iso-zero surface represents the surface of the volume which has to be removed and is used to cut the mesh.

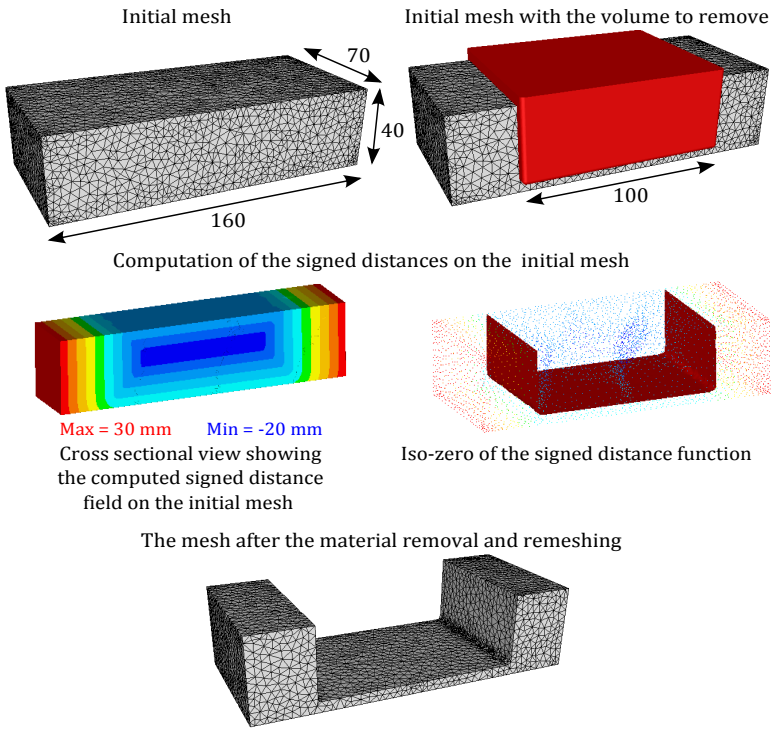

Figure 2.10: Example of material removal procedure on a mesh: the computation of the signed distances and the material removal

2.2.1.3 Multi-Step Modelling

In this section, the required steps for the implementation of the developed modelling approach into FORGE® as well as its adaptation to the machining simulation is presented.

2.2.1.3.1 Initial Residual Stress State Computation

According to the assumptions made, the initial residual stresses are the main input data for the prediction of the machining quality. When dealing with the machining simulation, the first step therefore consists in obtaining the initial mesh with its initial residual stress distribution. Depending on the initial workpiece (rolled plate or forged part), simulation or experimental results can be used. In case of a forged initial workpiece, the residual stresses can be determined by numerically reproducing the manufacturing steps (forging, quenching, stress relieving, etc.). The fields and the mesh are then used as input data for the machining simulation (transfer of a mesh between FORGE® simulations). When dealing with rolled plates, the residual stress profiles can also be determined numerically but experimental tests are usually used. The through-thickness residual stress profiles are, in this case, quite simple as they are almost similar everywhere in the plate excluding boundary condition effects [12, 125].

For this last case of rolled plates, a specific script has been developed in order to use the experimental through-thickness residual stress profiles as input data for the simulation of the machining. It allows to compute through-thickness residual stress profiles on a mesh

using the coefficients of polynomial functions which approximate the experimental profiles. A point-to-point curve with linear interpolation can also be directly computed. An example of experimental values and of their associated polynomial functions which can be used to approach the residual stress profiles is shown in Figure 2.11. Complex residual stress profiles can therefore be approximated and computed on a mesh furthermore allowing to obtain a continuous residual stress field.

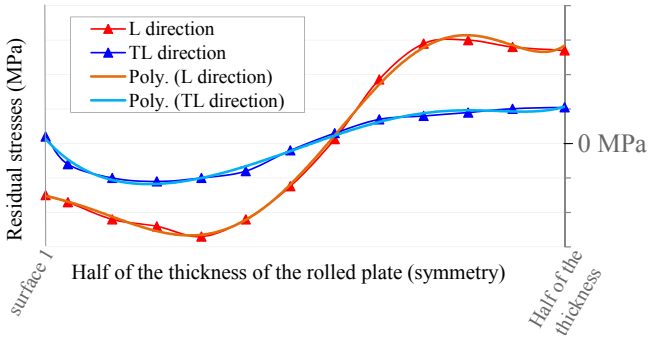

Figure 2.11: Example of polynomial functions used to approximate experimentally measured residual stress profiles in rolled plates. Only one half of the residual stress profiles is illustrated over the thickness direction because of the symmetrical distribution. The L direction represents the longitudinal axis (rolling direction) and the TL direction represents the transverse direction [124].

2.2.1.3.2 Iterative Computation Approach

As explained previously, at the end of the cutting and remeshing steps a new mesh is obtained (see Section 2.2.1.2). In order to compute the redistribution of the residual stresses and to predict the associated deformation, the residual stress state before the material removal has to be transported into the new geometry before computing the stress equilibrium. The same technique as the one presented in the Automatic Remeshing and Fields Transfer-section (2.1.5) is used to perform the fields transfer of both P1 and P0 variables. The new mesh with non-equilibrated stresses is then re-equilibrated to obtain the associated distortions. The modelling approach is thus based on massive removals of material and redistribution of residual stress computation steps.

When dealing with real machining, multiple massive removal and stress equilibrium computation steps are required to describe a machining sequence and to predict accurately the machining quality. To perform such machining simulations and to integrate this procedure the classical incremental operating of FORGE® has to be modified. The time step discretization is replaced by process steps (massive removal and stress equilibrium computation steps). Constant time steps are used and a new material removal is carried out giving a new mesh with non-equilibrium fields every two increments. Each material removal increment is then followed by an increment of computation to perform the stress re-equilibrium of the workpiece and to predict the associated deformation depending on the boundary conditions (fixture layout). At the end of the machining sequence, fixture elements are removed and a final equilibrium computation is performed to predict the post-machining distortion.

The procedure combining the massive removal steps and their associated residual stress redistribution computation is therefore particularly well adapted to the prediction of the machining quality as it presents the following main benefits:

- The volumes of material removed represent exactly the volume swept by the tool and therefore give a good representation of the real machining. The changes in the shape of the workpiece during the machining are taken into account. The volume of material removed during one step will therefore depend on the deformation after the previous step and on the machining process plan parameters used (the machining sequence and the fixture layout), as illustrated in Figure 2.12.

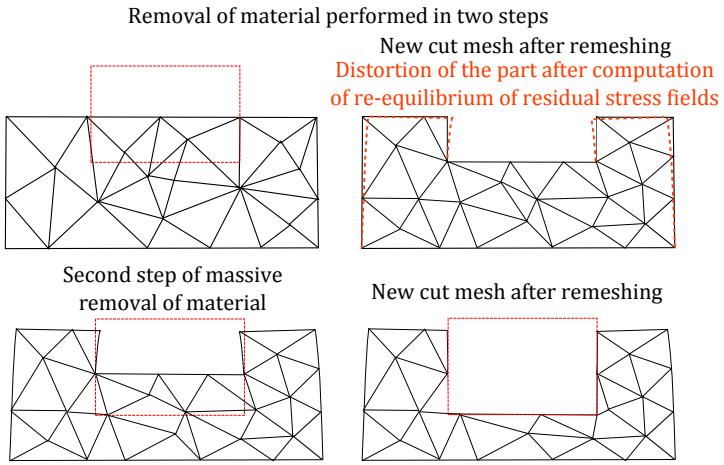

Figure 2.12: Illustration of the variation of the volume removed in function of the distortion of the part during the machining [124]

- The desired ratio between accuracy of results and computation time can be easily obtained by modifying the number of material removal steps to simulate a machining sequence. The higher the number of material removal steps used to describe the machining sequence, the more detailed and accurate the simulation will be.
- Machining of complex geometries can be realised using unstructured meshes composed of tetrahedral elements. In addition, the initial mesh does not need to be generated depending on the machining process plan.

Such an approach therefore allows to predict the machining quality by obtaining the exact final machined part geometry and its stress state. In addition, the machining simulation of all types of initial workpieces (forged part and rolled plates) can be performed, fully respecting the desired geometries. It also enables to give flexibility to the numerical tool with the possibility to easily obtain the desired ratio between accuracy of results and computation time.

The massive removal approach is nevertheless not especially well adapted to the simulation of machining of thin walled parts where local thermo-mechanical loads linked to the interaction between the tools and the workpiece cannot be neglected anymore. The surface thermo-mechanical loads are difficult to "globalise" on the new machined surface obtained after a

massive removal step. However, as it has been mentioned previously, on the parts considered in this work (large and thick parts) these solicitations are of second order compared to the initial residual stresses and can therefore be neglected.

2.2.1.3.3 Contact Parameter Adaptation

As seen in Chapter 1, the fixture-workpiece contact condition might have a major influence on the machining quality and therefore has to be taken into account. The penalty method mentioned previously (paragraph 2.1.3) is therefore used to model the unilateral contact between the fixture elements and the workpiece during the clamping (imposed clamping forces) and then the machining [119].

In order to avoid an ill-conditioned numerical problem and to ensure a good rate of convergence the penalty coefficient ρ_c (equation 2.30) has been adapted to the machining simulation. Indeed, during the simulation of machining, only small deformations occur. The terms linked to the contact modelling then become dominant compared to the terms linked to the material behaviour if the penalty coefficient is kept at its default value. Due to the difficulty to automatically adapt the penalty coefficient, it has been decreased (constant value) yet keeping the value big enough to ensure non-penetration of the workpiece into the fixture elements (determined empirically). This decrease of the penalty coefficient in general leads to the reduction of the number of Newton-Raphson iterations required to reach the desired convergence criteria and therefore of the computation time. In some cases the number of required iterations to reach the solution of an increment can be divided by more than two by dividing the penalty coefficient by 20, still keeping all contact conditions properly imposed. A Coulomb's law limited with a Tresca criterion (equation 2.11) is used for the friction modelling.

The penetration distance d_{pen} is one of the parameters which can also affect the accuracy of the fixture-workpiece contact analysis and therefore of the machining quality prediction. The same case of material removal as the one presented in Figure 2.10 shall be considered, with a mesh size of 2 mm and in taking into consideration the fixture layout. The clamping of the workpiece is performed by two clamps on the top surface applying a force of 10 kN each. As illustrated in Figure 2.13, depending on the value of d_{pen}, a bigger or smaller penetration depth of the nodes of the workpiece in the fixture elements can be observed. With a penetration distance d_{pen} of 0.1 mm, all the nodes of the bottom surface of the workpiece are considered to be in contact with the table. With a penetration distance d_{pen} of 0.001 mm, only the two ends of the bottom surface of the workpiece are in contact, which is coherent with the clamping areas and with the fact that the initial workpiece was not perfectly flat. The fixture-workpiece contact areas and the position of the workpiece within the fixture layout are therefore strongly influenced by the penetration distance d_{pen}.

Due to the inaccuracies in the positioning of the workpiece within the fixture layout caused by a too large value of d_{pen}, significant inaccuracies can occur during the cutting step. As shown in Figure 2.14, the inaccuracy induced during the clamping simulation results in an error of 0.1 mm in the thickness of the wall with a nominal dimension of 5 mm. With a smaller value of d_{pen}, the expected result is almost obtained as the error is only of 8×10^{-4} mm.

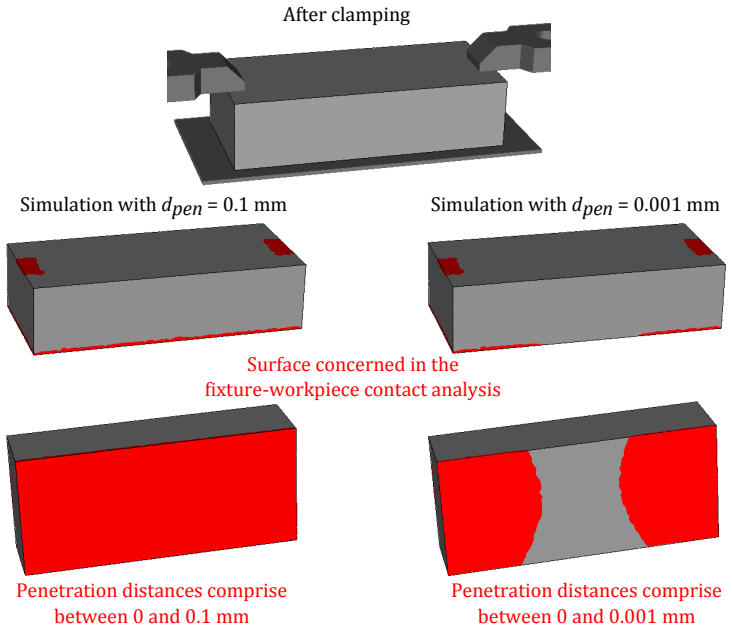

Figure 2.13: The influence of the penetration distance d_{pen} on the clamping simulation

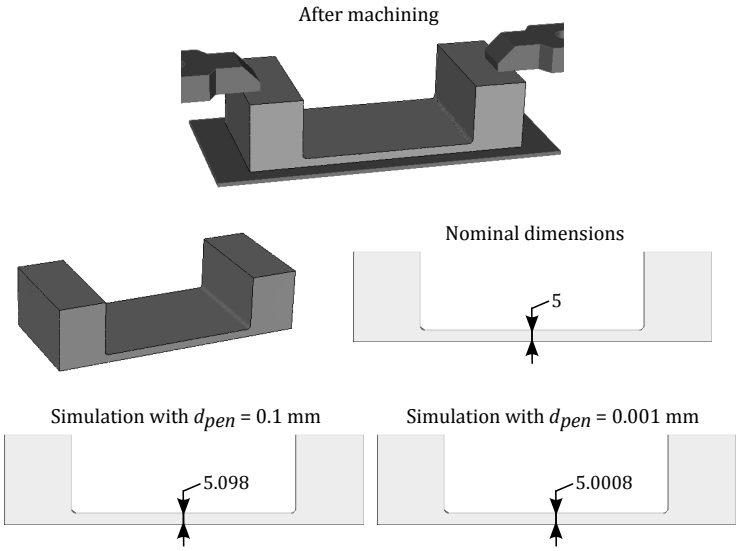

Figure 2.14: The influence of the penetration distance d_{pen} on the machining simulation

In order to achieve an accurate prediction of the machining quality, an accurate modelling of the fixture-workpiece contact is required. The value of d_{pen} has thus been fixed to a constant value of $1\mu m$ (inferior to the measurement uncertainties). The maximum error in the prediction of the dimensions of the machined part associated with the fixture-workpiece contact analysis should therefore not be bigger than this value.

2.2.2 Parallelization of the Code

FORGE® is a fully parallelized finite element software (solver and remeshing procedure) [126, 127] allowing to deal with industrial cases. The machining simulations of large and complex structural aeronautical parts involve large meshes and complex fixture layouts. Such simulations can therefore not be performed with a sequential program, at least not within an acceptable computation time. To improve the efficiency of FORGE OFELIA, the material removal procedure thus had to be parallelized.

The parallel strategy used in FORGE® and in FORGE OFELIA involves SPMD modules (Single Program Multiple Data) and the use of the MPI library (Message Passing Interface [128]). Depending on the number of available cores and on the mesh size, the initial mesh is automatically partitioned into subdomains. Each subdomain can then be mapped onto a core. Some nodes therefore belong to several cores. These nodes are called interface nodes and represent the boundary between the mesh subdomains and therefore the cores. Each core executes the same program and if needed a communication is performed between neighbouring cores to exchange information. Cores use their own local memory during computation and the exchange of data is performed by sending and receiving messages (MPI).

2.2.2.1 Subdomain-Cutting: Interface Nodes

In order to parallelize the procedure the cutting algorithm had to be modified to enable the cutting of each subdomain. The file representing the volume swept by the milling tool (surface mesh) is read by each core. The signed distances between the nodes of each subdomain and their projections onto the surface mesh are computed. The subtraction between each subdomain and the surface mesh using the signed distance field is then performed in taking into account the interface nodes. When an element is cut, new nodes are created on the cut edges (see table 2.2). An analysis on each node therefore has to be performed to determine all the interface nodes (nodes belonging to two or more cores). Four cases can be found:

- If nodes defining the cut edge are interface nodes, the new node created on this edge will also be a new interface node.
- If a new node has to be created on the centroid of a surface defined by interface nodes, the new node will also be a new interface node.
- If a node of an element is an interface node and has a positive distance (or a distance equal to zero), the node is kept as an interface node.
- Whether or not the node is an interface node, if it has a negative distance it is removed.

The list of interface nodes is then updated on each core, the main difficulty being that the lists on the neighbouring cores remain coherent. Indeed, at the end of the cutting, new subdomains are obtained (cut subdomains) with local node numbers (node numbers defined on each subdomain). An interface node therefore does not have the same node number depending on the subdomain considered.

2.2.2.2 Communication Between Cores: Coherent Global Mesh

In order to define a new coherent global mesh composed of the new subdomains, a communication step between cores has to be performed, during which each core sends and receives the interface nodes that it shares with its neighbours. At the end of this communication step, each core has updated its subdomain, its interface nodes and its neighbouring cores. A remeshing is then performed followed by a repartitioning (mesh migration) ensuring that each core runs the same number of nodes and that the computations are well distributed between the cores. Readers interested in the meshing-remeshing procedure used (introduced in subsection 2.1.5) can refer to [110].

Figure 2.15 illustrates the main steps of the removal of material procedure on the same problem as described in Figure 2.9 on two cores. The parallel procedure executed by each core during the simulation is summarised in the simplified Algorithm 1.

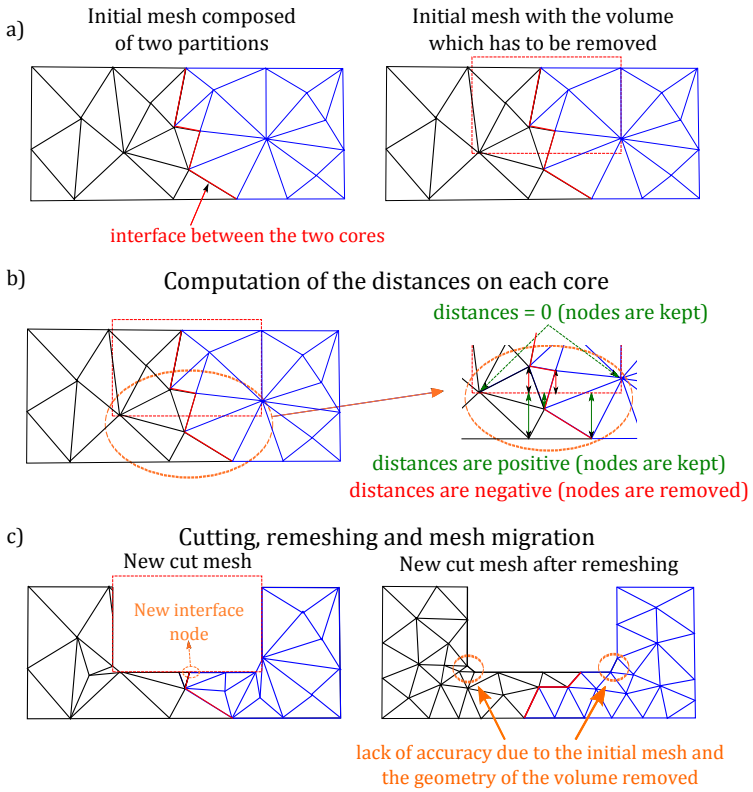

Figure 2.15: The main steps of the parallel massive removal of material method with Boolean procedure developed in the numerical tool [124]

Algorithm 1 Parallel finite element tool for machining simulation using massive removal of material with Boolean procedure [124]

```
Removal step = TRUE
Partitioning of the mesh                                   ▷ Depending on the number of cores used
while (Machining sequence is not finished) do
    if (Removal step) then
        Saving of the initial mesh partitions with initial fields        ▷ P0 and P1 fields
        Reading of the surface mesh: volume swept by the tool            ▷ Generated by CAM software
        Computation of the distances at partition nodes
        i = 1
        for (i = 1 to nb element) do
            if (all distances ≥ 0) then                    ▷ The element nodes are outside the tool path
                element is kept
                if (element has interface nodes) then
                    interface nodes are kept
                end if
            end if
            if (all distances < 0) then                    ▷ The element nodes are inside the tool path
                element is removed
            end if
            if (some distances are ≥ 0 and some < 0) then   ▷ The element nodes have positive and negative distances
                element is cut                             ▷ A specific algorithm is used in function of the case
                if (element has interface nodes) then
                    checking of the edges and surfaces which have to be cut
                    if (edge or surface is composed of interface nodes) then
                        new node → interface node
                    end if
                end if
            end if
            i = i + 1
        end for                                            ▷ New cut mesh partitions are obtained
        Building of the new partitions   ▷ New partitions with the new interface nodes and their neighbouring cores
        Remeshing of the new cut mesh
        Repartitioning                   ▷ Mesh migration ⇒ ensure that each core runs the same number of nodes
        Field transfer from the initial mesh to the new one
        Removal step = FALSE
    end if
    if (Not Removal step) then
        Computation of the reequilibrium of residual stresses ▷ Linearisation with Newton Raphson method and
                                                               resolution with preconditioned conjugate residual method
        Removal step = TRUE
    end if                                                 ▷ New residual stress equilibrium state and distortion of the part
end while                                                  ▷ Final residual stress equilibrium state and distortion of the part
```

2.2.2.3 Validation: Cutting Procedure Efficiency

The efficiency of the parallel algorithm has then been evaluated for several cases. First the focus has been set on the efficiency of the parallel cutting algorithm for a simple case of cutting. A layer removal case on a mesh with a parallelepiped shape has then been realised. The efficiency of the algorithm obtained in this case is summarised in Table 2.3. The test has been computed on four to twelve cores (PC with two processors: X5675 -3.07GHz-3.06GHz). The reference time is the time measured with four processors.

A good efficiency of the cutting algorithm has been obtained. However, it can vary depending on the location of the material removal with respect to the mesh subdomains. The computations can then be very unbalanced between the cores leading to a reduction of the efficiency.

Table 2.3: Efficiency of the parallel cutting algorithm

# cores	4	8	12
CPU time (s)	133.3	70.2	53.4
Speed-up	1	1.89	2.49
Efficiency	1	0.945	0.83

2.2.3 Automated Mesh Refinement

As explained previously, the initial mesh for the machining simulation may come from other forming simulations like forging. The initial mesh might therefore be adapted to this forming step but not be well adapted to machining simulations. The mesh size can for example be too large in some areas and can lead to inaccuracies when dealing with material removal for a complex geometry. Figure 2.15c illustrates this kind of problem. In this example, the curvature of the volume removed is very high in some areas (90 degree angles) and the mesh size is too large. The new nodes being created on the surface of the removed volume (iso-zero of the signed distance function), element edges may cross this volume in the areas where the removed geometry shows a high curvature.

A specific automatic mesh refinement procedure has therefore been developed to increase the accuracy of the material removal algorithm. The objective was to enable the adaptation of the mesh at each step of material removal depending on the geometry of the removed volume. The method is based on the computation of a curvature field on the mesh that is determined using the nodal signed distance field. This can be described as a level-set approach [129, 130].

Another remeshing option has been developed in order to obtain a global refinement of the mesh during the machining. Both these options are presented in the following sections.

2.2.3.1 Curvature

A signed distance function ϕ defined at the nodes of a mesh is considered. This function represents the signed distance between each node of the mesh and its projection onto the volume which has to be removed, as shown in Figure 2.15. The normal vector can therefore be computed from ϕ using equation 2.34.

$$\vec{n_\phi} = \frac{\vec{\nabla}\phi}{|\,\vec{\nabla}\phi\,|} \tag{2.34}$$

with $\vec{n_\phi}$ being the normal vector and $\vec{\nabla}\phi$ the gradient of the signed distance function.

In the case of a tetrahedral mesh, the gradient of the signed distance function $\nabla\phi$ can be computed for each element using equation 2.35.

$$\vec{\nabla}\phi_j = \sum_{i=1}^{3} (\phi^i - \phi^0)\left(MatLoc^{-1}(i,j)\right) \tag{2.35}$$

with i being the node of the element (four nodes per element numbered from 0 to 3), j the respective component in one of the three directions and $MatLoc$ the matrix defined as below:

$$\begin{pmatrix} x_1 - x_0 & x_2 - x_0 & x_3 - x_0 \\ y_1 - y_0 & y_2 - y_0 & y_3 - y_0 \\ z_1 - z_0 & z_2 - z_0 & z_3 - z_0 \end{pmatrix} \quad \text{with } (x_i, y_i, z_i) \text{ being the coordinate of node } i$$

At the end of these computations, the normal vector is defined for each element (P0 variable) before being computed at the nodes (P1 variable). This P0 to P1 transformation is done by computing the mean of the normal vectors of the elements containing the node.

The local curvature can also be computed on the mesh using the signed distance function ϕ. The local curvature defined by the zero iso-surface is expressed as in equation 2.36. The divergence can be computed for each element of the mesh using equation 2.37 and using the normal vectors computed in equation 2.34. In the case of material removal, the curvature therefore represents the curvature of the geometry of the volume that is to be removed.

$$\kappa = -\vec{\nabla} \cdot \frac{\vec{\nabla}\phi}{|\vec{\nabla}\phi|} = -\vec{\nabla} \cdot \vec{n_\phi} \tag{2.36}$$

$$\kappa = -\vec{\nabla} \cdot \vec{n_\phi} = -\sum_{j=1}^{3}\sum_{i=1}^{3} (n_{\phi j}^{i} - n_{\phi j}^{0}) \left(MatLoc^{-1}(i,j)\right) \tag{2.37}$$

To obtain the nodal value of the curvature, the same principle of P0 to P1 transformation like the one used for the normal vector is applied.

2.2.3.2 Refinement

Using the remeshing capabilities of the software [122], two options of refinement have been defined. One of these options is based on a global refinement of the mesh and the other is based on a local refinement depending on the geometry of the material removed.

Global Refinement

The post-machining distortion can be significantly dependent on the size of the mesh. An option enabling to compute a new mesh size in function of the removed volume at each step of massive removal has then been developed and introduced in the numerical tool. This new mesh size is computed as in equation 2.38 and allows to have a global refinement of the mesh keeping approximately the same amount of nodes and elements as the initial mesh during the whole simulation. The global refinement of the mesh enables to obtain a final mesh which allows an accurate prediction of the post-machining distortion while limiting the CPU time

compared to cases where the initial mesh is composed of many nodes.

$$H = H_{init}\left(\frac{Vol_{final}}{Vol_{init}}\right)^{1/3} \tag{2.38}$$

with H the new size of the mesh (size of the edges of the tetrahedral elements).

Local Refinement

In this option, the mesh size defined at each node is determined depending on the value of the curvature κ as defined above (see Section 2.2.3.1). In order to limit the CPU time to a reasonable amount, an additional constraint is added to the mesh size determination. The higher the curvature value, the more the mesh size decreases. As illustrated in Figure 2.16, the new mesh size decreases linearly with increasing curvature if the curvature is higher than the mean of all the computed curvatures (κ_{mean}) up to a ratio of four where the curvature is the highest (κ_{max}).

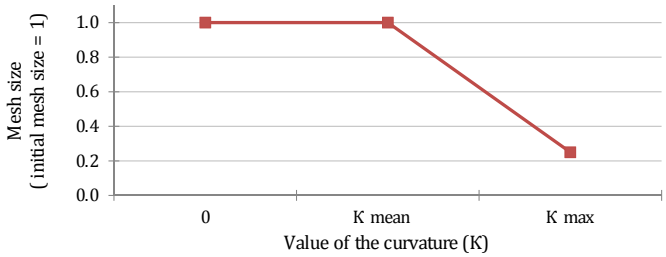

Figure 2.16: Evolution of the normalised mesh size in function of the local curvature value κ [124]

A mesh refinement is then performed depending on the computed curvature for each new removal step. The mesh is therefore automatically adapted to the geometry of the material removal allowing to increase the accuracy of the cutting.

Several tests have been performed to evaluate the benefits of this mesh adaptation procedure regarding the cutting accuracy. Results obtained for the simulation of the machining of the part shown in Figure 2.17 with one massive removal step are summarised in Table 2.4. Volumes of the simulated machined part with and without the mesh adaptation procedure have been compared with the CAD model of the desired machined part. It can be observed that the volume obtained in the simulation with the mesh adaptation procedure is very similar to the CAD model (nominal geometry). The error made is almost erased.

It is also important to notice that this accuracy can only be obtained using surface meshes precise enough. In this case, the volumes removed (surface meshes) are STL files generated with a tolerance of 0.025 mm in deviation and 8 degrees in angle.

As explained previously, one benefit of the methods used in this numerical tool to perform the removal of material is the possibility of taking into account the changes in the shape of

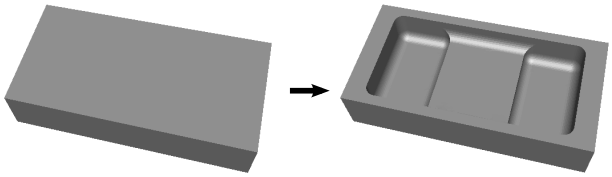

Figure 2.17: Initial and final geometries of the case studied to determine the influence of the mesh adaptation procedure on the accuracy of the cutting [124]

Table 2.4: Evaluation of the accuracy enhancement using the procedure of mesh adaptation in function of the curvature: Comparison of volume [124]

	Nominal volume (volume of the CAD geometry)	Without mesh adaptation	With mesh adaptation
Volume (mm^3)	880910	881062	880927
Difference (mm^3)	/	152	17
Difference (%)	/	0.0172	0.00192

the workpiece during the machining. Deformations of the workpiece due to the removal of material and due to the redistribution of initial residual stresses which can occur during the machining are therefore considered. In order to be able to observe the influence of these deformations on the volume of the material removed and therefore on the machining quality, the removal of material has to be as accurate as possible. The developed automated mesh refinement method gives the possibility to predict the volume of material removed more precisely enabling to be closer to the real machining.

Discussion

These options allow to improve the accuracy of the method in automatically adapting the mesh to the removed geometry. An academic example using the mesh adaptation method in function of the curvature is shown in Figure 2.18 where the removal of a complex volume (not a real machining geometry) is performed fully respecting the desired geometry. The computation has been run on three cores. This example shows the efficiency and the accuracy which can be obtained and thus confirms that the machining of more complex geometries can be simulated. However, this option of mesh adaptation increases the CPU time (about 50% for the case presented).

The geometry of the volumes removed is well respected and is therefore closer to the one removed during real machining. These improvements also make the numerical tool more flexible in giving the possibility to change the ratio between the accuracy of results and the computation time more easily.

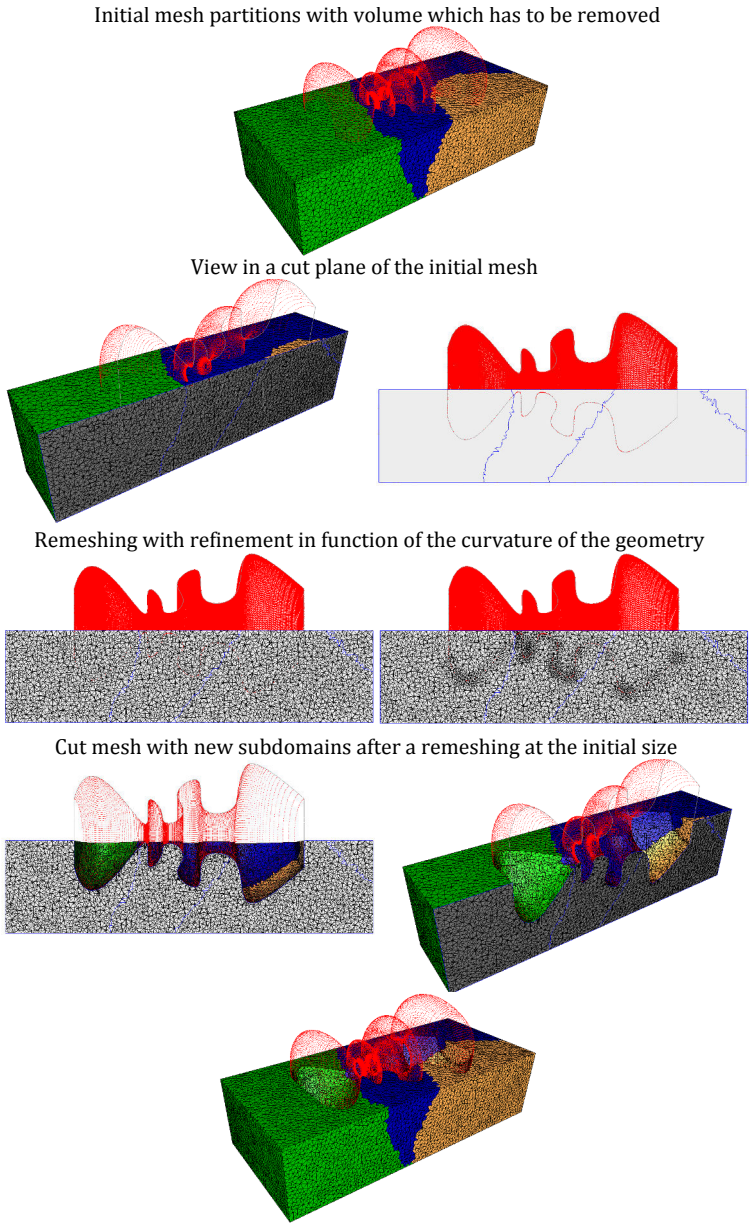

Figure 2.18: Removal of material with refinement of the mesh in function of the curvature [124]

2.3 The Different Levels of Modelling

FORGE OFELIA allows to develop models with various levels of accuracy depending mainly on the machining sequence discretization and on the contact modelling. The mesh size as well as the remeshing options mentioned above are also possibilities to reach a better accuracy. The ratio between the accuracy of results and the computation time can therefore be adapted to the analysis objective.

Without taking into account the automated mesh refinement options, the models which can be used with this numerical tool can be categorised in six principal types depending on the level of accuracy they enable to reach. The different model levels are represented in Table 2.5.

Table 2.5: The different models and levels of accuracy

	Level of accuracy of the model (level 1 = low / level 7 = high)					
	Level 1	Level 2	Level 3	Level 4	Level 5	Level 6
Initial worpiece		IRS Appl	IRS Appl	IRS Appl	IRS Appl	IRS Appl
Fixture layout No.1 (clamping)		Restr of the DoF	Contact mod	Contact mod	Contact mod	Contact mod
Machining No.1		1 MRS	1 MRS	f(features)	f(sequence, ap)	f(sequence, ap, tool path)
Unclamping No.1		✓	✓	✓	✓	✓
Fixture layout No.2 (clamping)		Restr of the DoF	Contact mod	Contact mod	Contact mod	Contact mod
Machining No.2		1 MRS	1 MRS	f(features)	f(sequence, ap)	f(sequence, ap, tool path)
Unclamping No.2		✓	✓	✓	✓	✓
⋮		⋮	⋮	⋮	⋮	⋮
Last fixture layout (clamping)		Restr of the DoF	Contact mod	Contact mod	Contact mod	Contact mod
Last machining		1 MRS	1 MRS	f(features)	f(sequence, ap)	f(sequence, ap, tool path)
Last unclamping		✓	✓	✓	✓	✓
Machined Part						

With: IRS Appl = initial residual stress application - Restr of Dof = restriction of the degrees of freedom - Contact mod = contact modelling - MRS = massive removal step - f(x) = removal of material in function of x - features = machining features - sequence = machining sequence - ap = depth of cut - ✓= prediction of the post-machining distortion linked to the machining step

- Level 1 is a model where the initial residual stress profiles are directly applied on the designed part (CAD). With this model, only the post-machining distortion can be predicted. Accurate predictions of the post-machining distortion can be achieved if the mesh size is small enough (see Section 2.2.1.1). In addition, computation times are short. However, the influence of the machining path and of the fixture layout on the machining quality cannot be studied.

- Level 2 is a model where fixture is considered by simply restricting the degrees of freedom of nodes in the fixture areas and where the machining is performed in one step. If several fixture layouts are used for the machining of a part, the same procedure is used again, as represented in Table 2.5. This kind of model enables to predict the post-machining distortion and to analyse the behaviour of the workpiece at the end of each machining step depending on the fixture areas. However, neither the evolution of the geometry during the clamping and the machining nor the friction and clamping forces are taken into account.
- Level 3 is a model similar to Level 2 but with the modelling of the fixture-workpiece contact. The simulation of clamping is therefore more realistic and the location and deformation of the workpiece for each fixture layout used before and after machining can be studied depending also on the clamping forces used. The computation time is nevertheless slightly longer than for Level 2 due to the contact modelling.
- Level 4 is a model where the fixture-workpiece contact is modelled and where the machining is performed in several machining removals. The removal steps are realised machining feature by machining feature (see Figure 2.19a) and therefore depend on the order in which they are machined. The deformation of the workpiece is computed for each machined feature. More information is therefore obtained on the behaviour of the workpiece during the machining and a verification of the fixture layout stability as well as an analysis on the machining sequence effect can be performed. However, only machining sequences where machining features are machined one by one can be performed (Z-level machining). The computation time is longer than for the above-mentioned models, especially for parts presenting a large number of machining features.

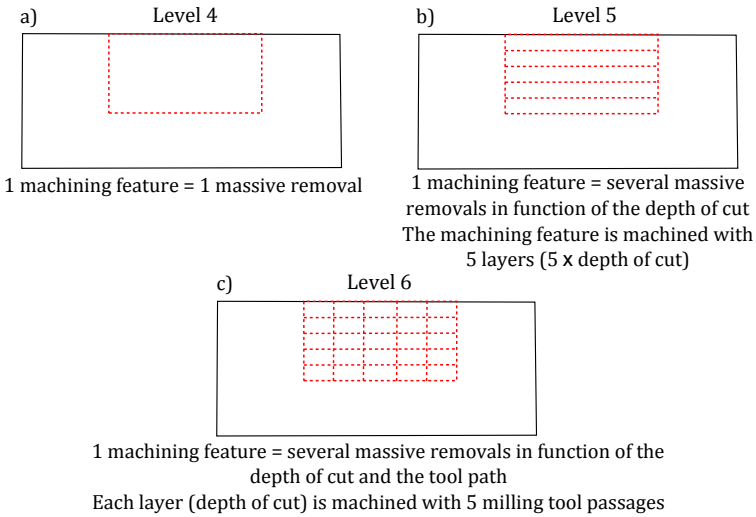

Figure 2.19: The discretization of the machining sequence depending on the modelling levels: a) Level 4 ; b) Level 5 ; c) Level 6

- Level 5 is a model equivalent to Level 4, the difference lying in the machining sequence

discretization. In this model, the machining sequence is discretized depending on the depth of cut, as illustrated in Figure 2.19b. A material removal is therefore realised for each new layer (depth of cut) of a machining feature. Complex machining sequences can thus be simulated using this kind of model giving a relatively accurate machining quality prediction. It is the first model which allows to predict accurately the machining quality (final dimensions and geometry of the part). However, the computation cost can be relatively significant.

- Level 6 is a model providing even more accurate machining quality predictions than Level 5. In this model, the layers removed with the Level 5 model are discretized in several volumes representing the tool-path strategy used, as illustrated in Figure 2.19c. This kind of model can be used in particular cases where Level 5 does not enable to obtain results accurate enough. However, this model is computationally expensive.

Optimised models allowing to decrease the computation time and to obtain the desired ratio between the accuracy of results and the computation time can be developed in some cases by mixing the different modelling options. Examples of these different modelling levels are presented later in this dissertation.

2.4 Numerical Comparison with a Different Modelling Approach

In order to validate the modelling approach, a simulation of a case taken from the Ph.D. thesis of J.K. Rai [105] has been realised. The results obtained by J.K. Rai using a model with the deactivation method have been compared to the results obtained using FORGE OFELIA and its massive removal approach.

2.4.1 Case Studied

The machining of the part depicted in Figure 2.20 made of Al7050-T74 is considered.

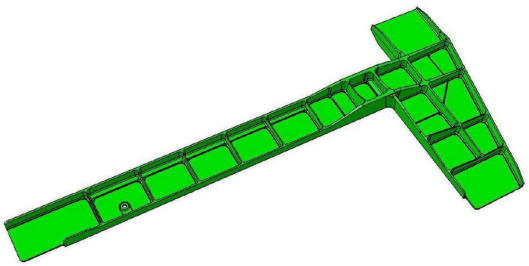

Figure 2.20: Presentation of the case studied taken from [105]

In order to simplify the analysis, the part dimensions have been reduced and its geometry has been simplified in [105], as shown in Figure 2.21. The initial residual stress distribution of the 35 mm thick plate used is applied layer by layer on the initial mesh.

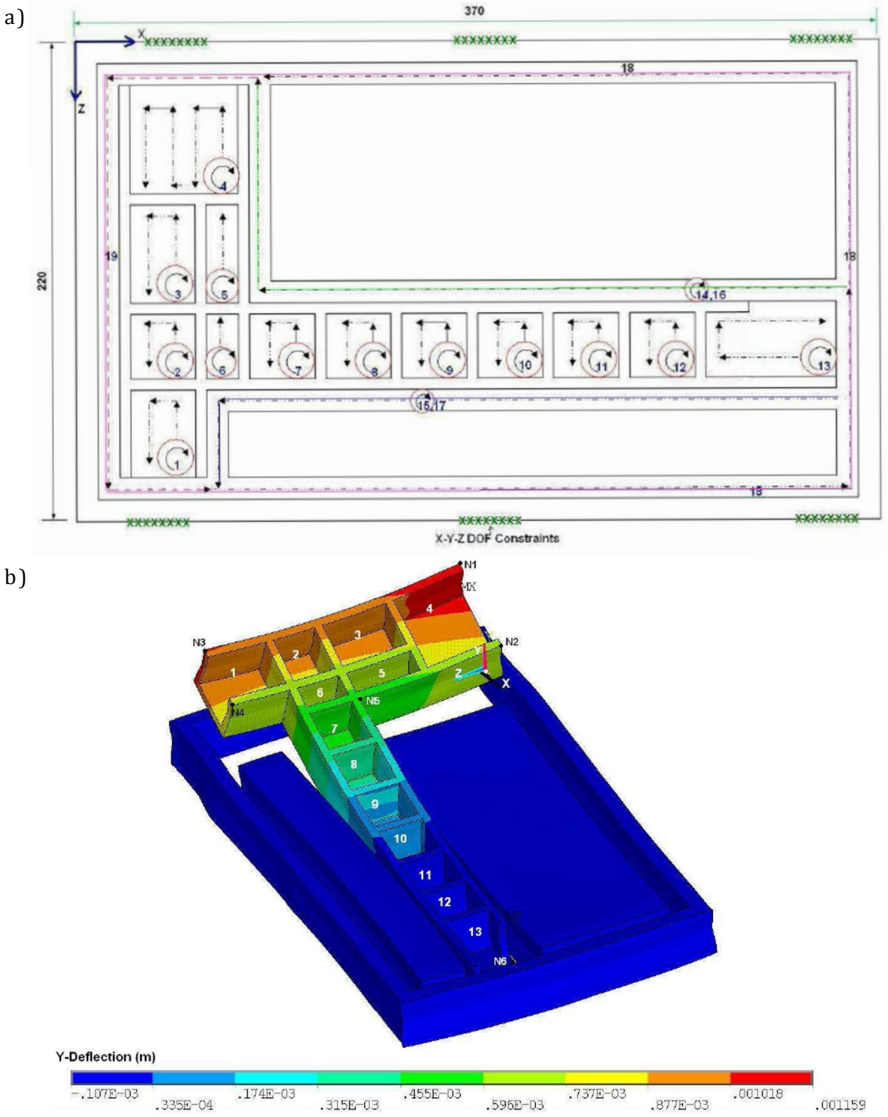

Figure 2.21: Presentation of the case studied taken from [105]: a) Geometry and machining features; b) Numerical sensor positions

The final part geometry is obtained by milling 19 features (pockets and slots). Slots are machined to detach the part from the plate. The fixture is considered by simply restricting the degrees of freedom in the areas represented by green crosses in Figure 2.21a. During the simulation six numerical sensors are positioned on the part in order to register the displacements. The positions of these sensors are represented in Figure 2.21b (N1 to N6).

2.4.2 The Model: Results

To simulate the machining of this part with FORGE OFELIA, a model where the machining features are removed in one step is created. This model is equivalent to a simplified Level 4

model because the fixture-workpiece contact is simply modelled by restricting degrees of freedom. The machining sequence is then decomposed in twenty-eight massive material removal steps. The pockets are in this example machined from pocket one to pocket thirteen.

Mechanical Computation: Adaptation of the Solver

In a first step, a simulation has been realised using the default solver configuration (preconditioner, relative residual threshold, maximal number of iterations for the resolution of the linear system). The initial mesh is composed of about 235,000 nodes and 1,250,000 elements. The displacements measured during the simulation with six numerical sensors are plotted in Figure 2.22. At the end of the increment step number 57, all the material removals and residual stress redistribution computations are performed. However, significant instabilities can be observed from step 57 to step 100, raising also questions about the validity of the deflections computed during the machining (from step 1 to 57). Moreover, many Newton-Raphson iterations have been required during the computation showing the difficulty of convergence leading to an increase in the computation time.

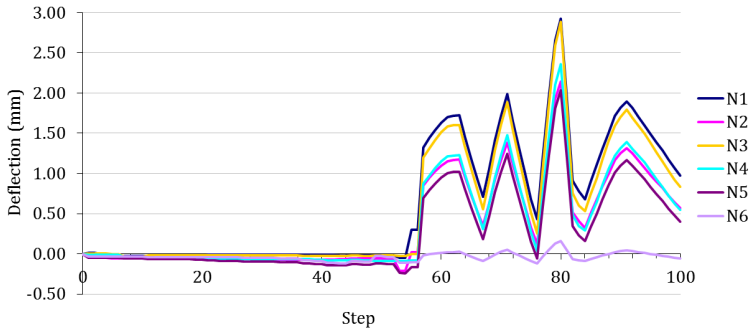

Figure 2.22: Displacements measured on the six numerical sensors during the machining: results with stability issues

In order to ensure a good stability and the validity of the computations as well as a computation time as short as possible, some parameters of the solver have been adapted to the machining simulation. Three parameters have been modified:

- The first parameter is the maximal number of iterations for the resolution of the linear system (see section 2.1.4) which is by default fixed to 3000 in FORGE®. It has been multiplied by more than 10 to ensure the convergence at each Newton-Raphson iteration. The convergence being reached leads to a decrease of the number of Newton-Raphson iterations needed to reach the relative residual threshold (convergence criteria) as well as to a decrease of the computation time.
- The second parameter is the relative residual threshold which is by default fixed to 10^{-7} (see section 2.1.4). This default relative residual threshold is often sufficient when dealing with material forming simulations where yielding and non-linearity due to the material behaviour are observed. In most cases, no yielding occurs when dealing with residual stress redistribution computations. Elastic problems can require more precise

computations in order to achieve the final solution. To improve the accuracy and to capture all phenomena linked to the residual stress redistribution, the relative residual threshold has therefore been decreased to 10^{-10}. However, this modification results in a slightly bigger computation time.

- The third parameter is the preconditioner. An incomplete Cholesky factorisation is used by default in FORGE®. Such a preconditioner is usually introduced to consider high extra-diagonal terms coming from the contact analysis which is not used in this study. In cases where no contact analysis is performed, it appears that the use of simpler preconditioners can reduce the computation time. The use of a preconditioner built using only the diagonal terms of the local matrix like the preconditioner "PRECONDVAD" of FORGE® or even the preconditioner "PRECONDIVP" which is built by inverting the 3×3 matrix (velocities) and by using $-p$ as the last term of the diagonal can therefore be relevant. More information on preconditioners can be found in [126, 117].

The use of the first two parameters allows to ensure a good accuracy and stability of results as well as to decrease the computation time. In this case a reduction of the computation time of approximately 40% is obtained compared to the case with the default parameters. The preconditioner can be modified and allows to decrease again the computation time by approximately 5% in cases where the contact modelling is not taken into account. Such preconditioners therefore have to be used when dealing with models of Level 1 and 2 as well as during the final residual stress redistribution computation (unclamping).

Using the new solver parameters adapted to the machining simulations, the computation has been performed again. Results obtained are depicted in Figure 2.23b and can be compared to the ones found in [105] in Figure 2.23a.

Similar results have been obtained for the two models. The displacements of the six numerical sensors show similar trends with still some differences due to the fact that each machining feature has been removed in one step. In addition, a good agreement is obtained between the post-machining distortion predicted in [105] and the one predicted with FORGE OFELIA, as shown in Figure 2.24.

Efficiency of FORGE OFELIA

This representative example has then also been used to evaluate the efficiency of the global numerical tool (mesh cutting and computation of the new residual stress state). The twenty-eight material removal files used as well as the evolution of the mesh subdomains for the simulation performed with twelve cores are depicted in Figure 2.25.

Table 2.6 shows the efficiency of the parallel algorithm on this example which has also been computed from four to twelve cores (PC with two processors: X5675 -3.07GHz-3.06GHz). The reference time is the time measured with four processors. A good efficiency of this developed parallel numerical tool to simulate machining is again obtained. It can also be observed that the global efficiency of the algorithm is not really affected by the unbalanced amount of computations between the cores that can occur during the cutting.

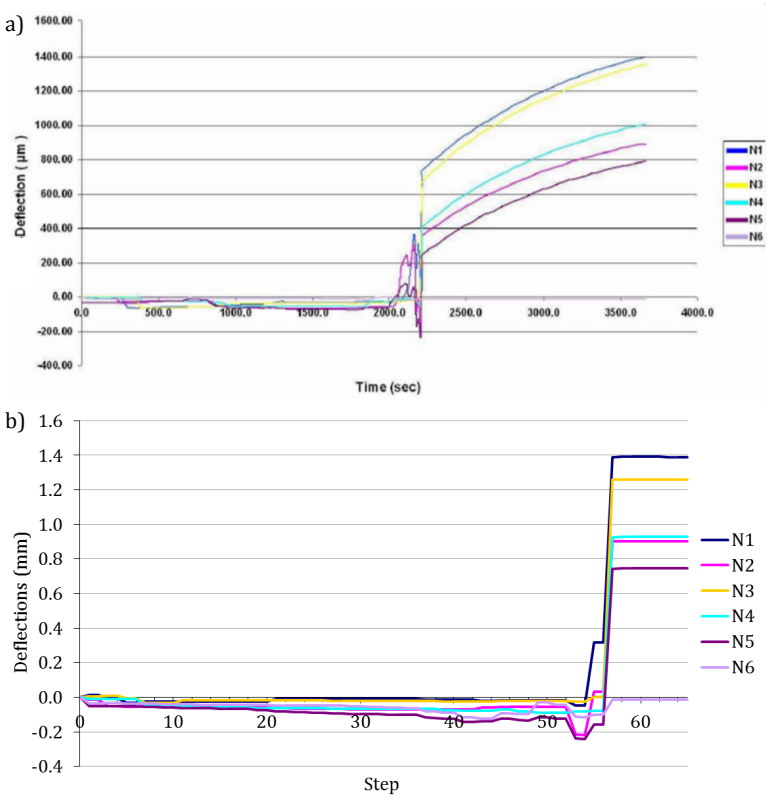

Figure 2.23: Displacements measured on the six numerical sensors during the machining: a) Results obtained in [105] ; b) Results obtained with FORGE OFELIA and 28 massive material removal steps

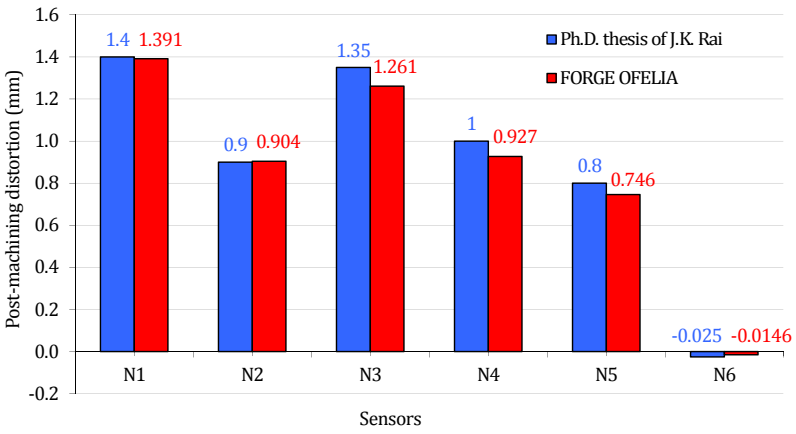

Figure 2.24: Post-machining distortion measured on the six numerical sensors

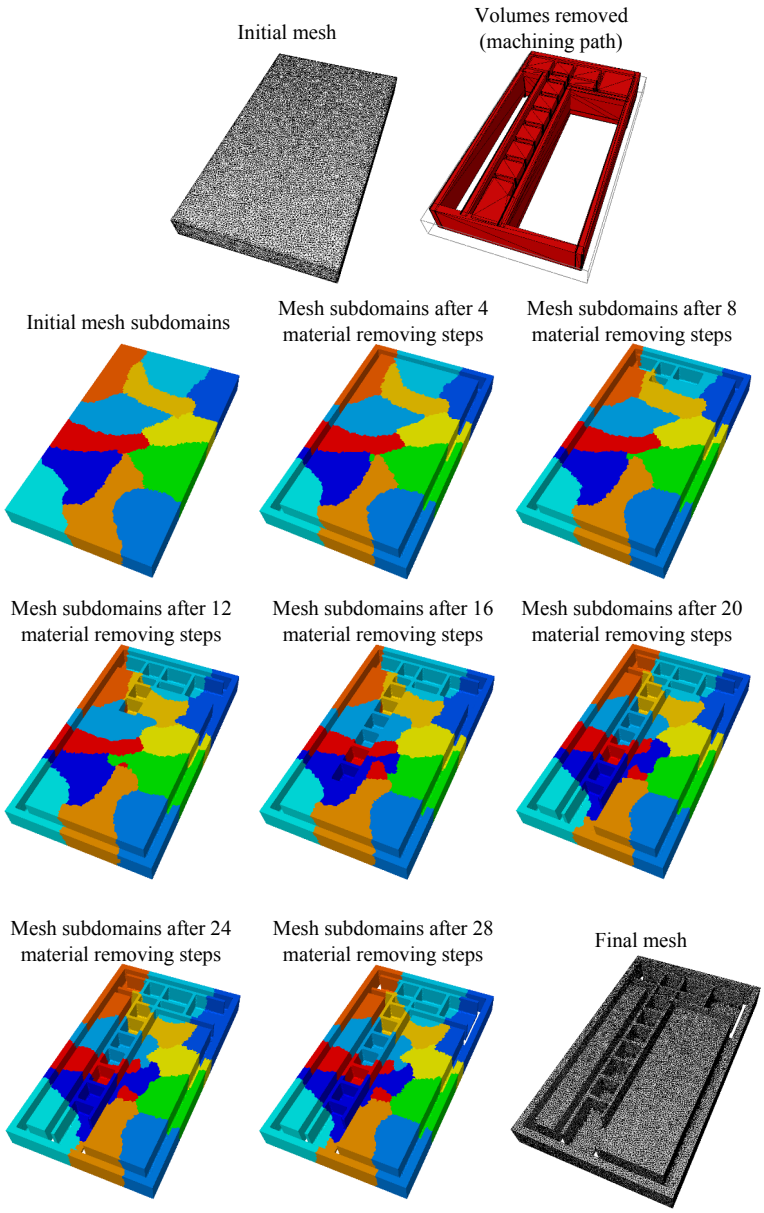

Figure 2.25: Evolution of the mesh partitions during a material removing simulation [124]

Table 2.6: Efficiency of the parallel numerical tool [124]

# cores	4	8	12
CPU time (min)	185	101	75
Speed-up	1	1.83	2.46
Efficiency	1	0.91	0.82

2.5 Conclusion

This chapter is dedicated to the developed numerical tool and is presented in three principal sections.

In the first section, a review of the finite element software FORGE® is realised. This review allows to give the essential information about the mechanical problem to solve, starting from basic continuum mechanics notions to the introduction of the mixed velocity-pressure formulation, the FE discretization and the contact analysis method used in FORGE®. This review has as an objective to clarify and introduce the important characteristics of FORGE® which have been used during the development of FORGE OFELIA, the version of FORGE® adapted to the machining process simulation.

In the second section the numerical developments are detailed. In a first step, a modelling approach has been defined. The numerical methods used for the computation of the initial residual stresses and the numerical material removal as well as the adaptation of the contact analysis are then presented. The implementation of these methods in FORGE® is also discussed. In a second step, the required modifications for the parallelization of the material removal procedure are detailed. A validation case showing the efficiency of the paralellization is also presented. In a third step, the numerical options developed in order to improve the accuracy and flexibility of the numerical tool are explained. These options are based on the automatic adaptation of the mesh (refinement) at each material removal step. The refinement is performed depending on the geometry of the material removal volume which is described by a signed distance function. A case showing the increase of accuracy using this option is also presented. Another option based on the refinement of the mesh depending on the volume removed at each step has also been developed and is presented in this section. This option has as an objective to obtain a good compromise between the computation time and the accuracy of the post-machining distortion predictions.

The last section is dedicated to the presentation of the different models which can be created using FORGE OFELIA. Six principal levels of accuracy of models have been defined. Each of these levels represents an improvement in the accuracy which on the other hand results in a longer computation time. However, with a combination of these models it is possible to obtain the best compromise between accuracy of results and computation time. A numerical comparison of results obtained on a case found in literature with a different modelling approach is then presented. After the adaptation of the solver parameters to the machining simulation, similar results to the ones in literature are observed. The efficiency of the global numerical tool is also studied on this case. These results are used as a first validation of the numerical tool. However, these are only comparisons between numerical models.

The developed numerical tool is therefore a computationally efficient tool allowing to simulate automatically complex machining operations in taking into account the influence of the coupled effect of the initial residual stress redistribution, the fixture layout and the machining sequence.

2.6 Résumé en Français

Ce chapitre est dédié à la présentation de l'outil numérique et est organisé en trois principales parties.

La première partie est consacrée à la présentation du logiciel éléments finis FORGE®. Les informations essentielles sur le problème mécanique à résoudre sont données, avec notamment l'introduction de la formulation mixte en vitesse-pression, de la discrétisation éléments finis et de la méthode pour l'analyse du contact utilisées dans FORGE®. L'objectif de cette section est de clarifier et introduire les caractéristiques importantes de FORGE® qui ont été utilisées pour le développement de FORGE OFELIA, la version de FORGE® adaptée à la simulation d'usinage.

Dans la deuxième section, les développements numériques sont détaillés. Dans un premier temps, une approche de modélisation a été définie. Les méthodes numériques utilisées pour l'application des contraintes résiduelles initiales sur les maillages, pour l'enlèvement de matière ainsi que l'adaptation de l'analyse de contact sont ensuite présentées. L'implémentation de ces méthodes dans FORGE® est également discutée. Dans un deuxième temps, les modifications nécessaires à la parallélisation de la procédure d'enlèvement de matière sont détaillées. Un cas de validation montrant l'efficacité de la parallélisation est également présenté. Dans un troisième temps, les options numériques développées en vue de l'amélioration de la précision et de la flexibilité de l'outil numérique sont expliquées. Ces options se basent sur l'adaptation automatique du maillage (raffinement) à chaque enlèvement de matière. Le raffinement est réalisé en fonction de la géométrie du volume de matière enlevé qui est décrit par une fonction distance signée. Un cas montrant le gain de précision en utilisant cette option est également décrit. Une autre option basée sur le raffinement du maillage en fonction du volume de matière enlevé à chaque étape a également été développée et présentée dans cette section. Cette option a pour objectif d'obtenir un bon compromis entre le temps de calcul et la précision des résultats.

La dernière section est consacrée à la présentation des différents modèles pouvant être créés avec FORGE OFELIA. Six principaux niveaux de précision ont été définis. Le niveau 1, le plus simple, est un modèle où les profils de contraintes résiduelles sont directement appliqués sur le maillage de la géométrie de la pièce usinée (CAO), permettant ainsi de prédire la distorsion finale de la pièce usinée. Le niveau 6, le plus complexe, est un modèle d'usinage "réaliste" où la géométrie de la pièce initiale et son état de contraintes sont pris en compte, où l'évolution du contact entre la pièce et le montage est modélisée et où la séquence d'usinage est discrétisée finement afin de modéliser précisément l'ordre dans lequel la matière est enlevée en fonction des trajectoires d'outils utilisées et des profondeurs de passes choisies. Chaque niveau représente une amélioration de la précision des résultats ainsi qu'une augmentation des temps de calculs. Cependant, la combinaison de ces modèles est possible pour obtenir le meilleur compromis entre temps de calculs et la précision des résultats. Une comparaison numérique des résultats obtenus sur un cas trouvé dans la littérature avec une approche de modélisation différente est ensuite présentée. Après une adaptation du solveur à la simulation

d'usinage, des résultats similaires à ceux obtenus dans la littérature sont observés. L'efficacité de l'outil numérique complet est également évaluée sur ce cas. Ces résultats servent donc de première validation de l'outil numérique.

FORGE OFELIA est donc un outil numérique efficace et permettant de simuler automatiquement des opérations d'usinage complexes en prenant en compte l'influence des contraintes résiduelles initiales, du montage et de la séquence d'usinage.

Chapter 3

The AIRWARE® 2050 Alloy Residual Stress Distribution

In Chapter 1, a review of literature is performed and modelling assumptions are introduced. Based on these assumptions, a specific numerical tool for the prediction of the machining quality has been developed and is detailed in Chapter 2. The present Chapter is devoted to the study of the residual stresses inside workpieces taken from AIRWARE® 2050 alloy rolled plates and their influence on the machining quality. To perform such a study, the work has been organised in four steps.

First, the experimental tests performed to determine the residual stress distribution of rolled plates made of AIRWARE® 2050 alloy are presented and results are analysed. Then, using the developed numerical tool, simulations of these experimental tests are realised and comparisons between numerical and experimental results are drawn. In a third step, a comparison of the predicted and the measured post-machining distortion on a small part is performed. To conclude, after the validation of both the numerical tool and the initial residual stress profiles, a more in-depth analysis of the influence of the residual stresses on the machining quality is realised on a simplified case. All along these simulations, the different models and their abilities are also discussed.

Contents

3.1 The Layer Removal Method

As explained in Section 1.1.3, several measurement methods can be used to determine residual stresses. In order to obtain the residual stress profiles of the AIRWARE® 2050-T84 alloy rolled plates, the layer removal method has been used in this project. More precisely, a similar method developed by the Constellium Technology Center which can be used on beams [30, 131] has been employed. With this method it is assumed that only one stress component is not equal to zero. Two beams therefore have to be used to determine the residual stress profiles, one in the rolling and another one in the transverse direction. In this section, the residual stress profiles of two AIRWARE® 2050-T84 alloy rolled plates determined using this method are presented and analysed.

More information on the principle of the layer removal method and on the redistribution of the residual stresses can be found in Appendix B.

3.1.1 Experimental Results: AIRWARE® 2050 Alloy Residual Stress Profiles

3.1.1.1 Methodology

The residual stress profiles of both a 70 mm and a 90 mm thick AIRWARE® 2050-T84 alloy rolled plate have been determined using the layer removal method. Successive removals of 3 mm thick layers on two beams, one taken from the rolling direction and the other from the transverse direction, are performed, as shown in Figure 3.1a. After each removal, the beams are unclamped and strain measurements are performed, as illustrated in Figure 3.1b.

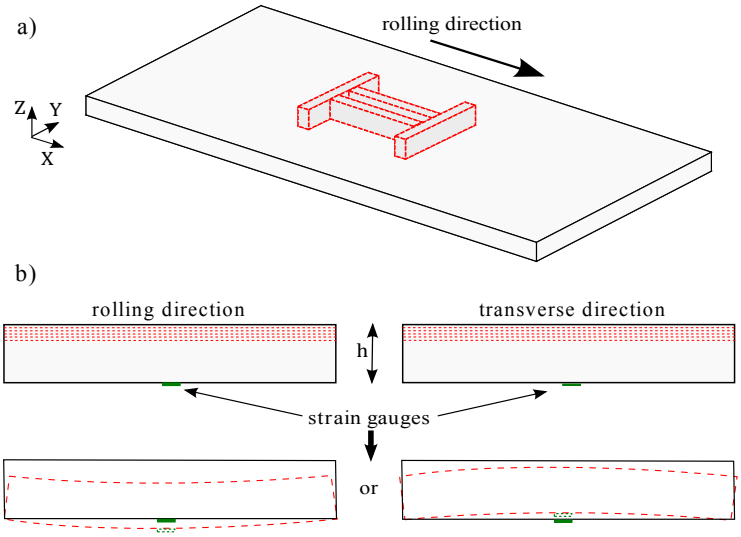

Figure 3.1: Illustration of the layer removal method on beams taken from rolled plates: a) Beams (×4) taken from the middle of the plate to avoid all side effects b) Deformation which can be observed after layer removal and redistribution of the initial residual stresses

Measurements have been realised by the Constellium Technology Center using both strain gauges and indicators (distance amplifying instruments) in order to compare and to validate the measurements. The successive layer removals are performed by machining, as shown in Figure 3.2. To ensure that the machining does not disturb the initial residual stresses the smooth specific machining parameters summarised in Table 3.1 are used. The clamping forces are also set to a value which ensures that the specimens are held in the desired position and which ensures that the initial residual stresses are not modified (prevent yielding).

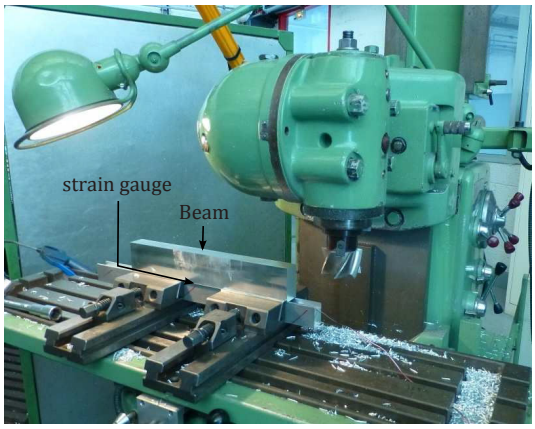

Figure 3.2: The experimental set-up used to perform the layer removal method

Table 3.1: Description of machining parameters

Tool diameter (mm)	63
Cutting speed (m/min)	280
Feed rate (mm/min)	400
Depth of cut (mm)	3

As explained in [30, 131], using the measured strain and considering the equations 3.1 the average stress inside the removed layer of the beams can be computed for the layer 1 to $n-1$ (with n the number of removed layers). $u(i)_{RD}$ is the average stress in the removed layer i on the beam taken from the rolling direction (RD) and $u(i)_{TD}$ the average stress in the removed layer i on the beam taken from the transverse direction (TD). They can be expressed as:

$$\begin{aligned} u(i)_{RD} &= -E\frac{(\epsilon(i+1)_{RD}-\epsilon(i)_{RD})h^2(i+1)}{[h(i)-h(i+1)][3h(i)-h(i+1)]} - S(i)_{RD} \\ u(i)_{TD} &= -E\frac{(\epsilon(i+1)_{TD}-\epsilon(i)_{TD})h^2(i+1)}{[h(i)-h(i+1)][3h(i)-h(i+1)]} - S(i)_{TD} \end{aligned} \tag{3.1}$$

with

$$\begin{aligned} S(i)_{RD} &= E\sum_{k=1}^{i-1}(\epsilon(k+1)_{RD}-\epsilon(k)_{RD})\left[1-\frac{3h(k)(h(i)+h(i+1))}{[3h(k)-h(k+1)]h(k+1)}\right] \\ S(i)_{TD} &= E\sum_{k=1}^{i-1}(\epsilon(k+1)_{TD}-\epsilon(k)_{TD})\left[1-\frac{3h(k)(h(i)+h(i+1))}{[3h(k)-h(k+1)]h(k+1)}\right] \end{aligned}$$

with E being the Young's modulus, $\epsilon(i)$ the measured strain linked to the layer removal i and $h(i)$ the thickness of the beam before the layer removal i.

Using the two stress profiles in the beams computed with equations 3.1, the residual stress profiles in the rolled plate can be obtained using equations 3.2.

$$\begin{aligned}\sigma(i)_{RD} &= \frac{u(i)_{RD} + \nu u(i)_{TD}}{1-\nu^2} \\ \sigma(i)_{TD} &= \frac{u(i)_{TD} + \nu u(i)_{RD}}{1-\nu^2}\end{aligned} \tag{3.2}$$

with $\sigma(i)_{RD}$ and $\sigma(i)_{TD}$ being the initial residual stresses in the rolled plate for the layer i and ν the Poisson's ratio.

3.1.1.2 70 mm Thick AIRWARE® 2050 Alloy Rolled Plate

Twenty-two steps of layer removals have been performed to determine the residual stress profiles along the whole thickness of the beams taken from a 70 mm thick rolled plate. Experiments have been realised four times in each direction to analyse the repeatability and to validate the measurements. For some tests, the beams have also been taken from various positions in the plate (avoiding the position near the sides of the plates) to analyse a possible deviation in the residual stress profiles depending on the position in the length of the plate (~ 7 m long).

The results obtained for the four tests are depicted in Figure 3.3. Due to the low level of measured strain, the residual stress profiles in the transverse direction are more difficult to determine and thus present some fluctuations. However, relatively low deviations are visible between the different residual stress profiles in the rolling direction. Results nevertheless have to be analysed in order to choose the most representative residual stress profiles for the simulations.

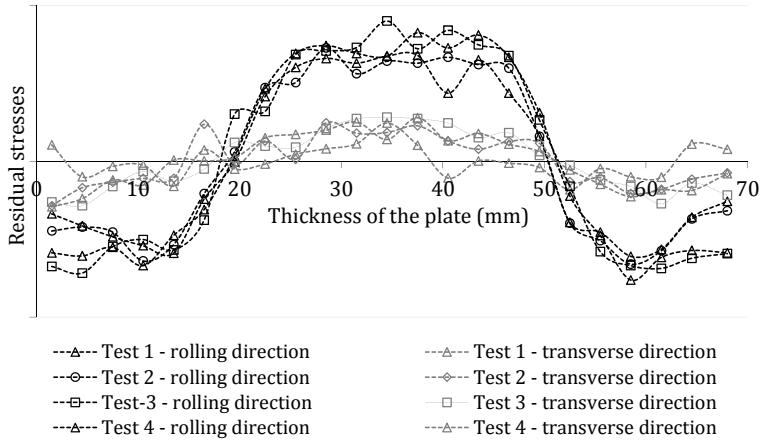

Figure 3.3: Residual stress profiles computed using measured strains in four tests realised with samples taken from a 70 mm thick AIRWARE® 2050 alloy rolled plate

It is sufficient to consider only one half of the residual stress profiles with the assumption of a symmetrical distribution. The upper half of the residual stress profiles has been chosen

because it can be assumed that it is usually more accurate due to the fact that it represents the first twelve layers removed and that the samples (beams) are therefore less distorted during the first layer removals than during the last ones.
Afterwards the residual stress profiles have to be analysed. The residual stress amplitudes being higher in the rolling direction, the choice of the most representative profile is important to be done in function of this direction. It is possible to observe that some profiles show less fluctuations than others. For example, non-physical fluctuations are clearly visible in the profile of test 3. The criterion to chose the profile has thus been defined by analysing the smoother profiles, i.e. where clear trends can be observed. It has been determined that the profile of test 1 represents the smoothest distribution. In addition, this profile is almost a mean value of all the profiles (see Figure 3.4), except close to the surface where differences are visible between all the profiles. It nevertheless represents a smooth profile in this section, showing a clearer trend than the mean value. The residual stress profile of test 1 is thus chosen.

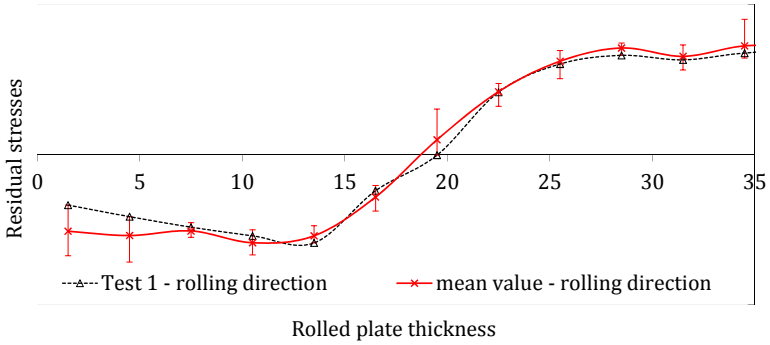

Figure 3.4: Comparison of the residual stress profiles in the rolling direction of test 1 with the mean value of all profiles

As mentioned above, all residual stress profiles in the transverse direction show almost the same fluctuations. The residual stress profile in the transverse direction has therefore been chosen on the same test selected for the rolling direction, i.e. test 1.

The typical initial residual stress profiles in the rolling and transverse directions obtained are shown in Figure 3.5. Globally small deviations in the residual stress profiles depending on the position of the beams in the plates have been observed, showing a relatively low uncertainty in the residual stress profiles determination.

3.1.1.3 90 mm Thick AIRWARE® 2050 Alloy Rolled Plate

Similarly, the residual stress profiles of a 90 mm thick AIRWARE® 2050 alloy rolled plate have been determined. Twenty-eight steps of layer removals have been performed. Experiments have been realised twice in each direction and a good repeatability has been observed, validating the residual stress profiles. The typical initial residual stress profiles obtained are

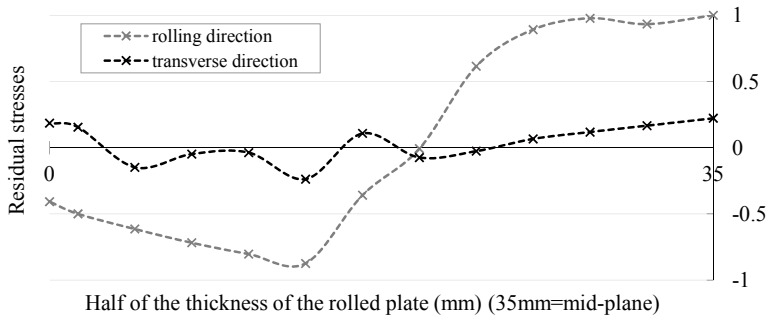

Figure 3.5: Typical residual stress distribution of a 70 mm thick AIRWARE® 2050 alloy obtained using the layer removal method with the strain gauge technique measurement (normalised residual stresses)

shown in Figure 3.6. Also only one half of the residual stress profiles is illustrated along the thickness direction in this case because of the symmetrical distribution. Some fluctuations are visible for both the residual stress profiles in the rolling and in the transverse direction. These fluctuations are, like for the 70 mm thick plate, more significant in the transverse direction.

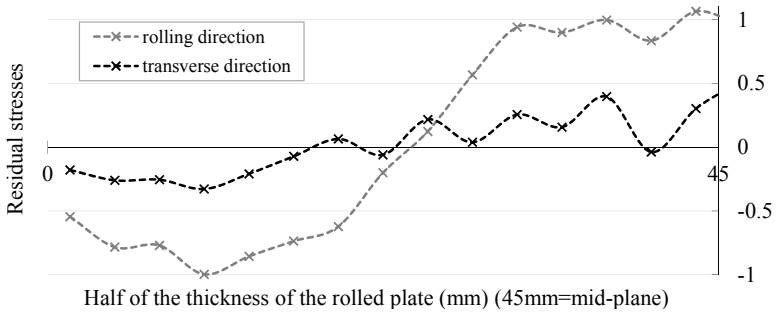

Figure 3.6: Typical residual stress distribution of a 90 mm thick AIRWARE® 2050 alloy obtained using the layer removal method with the strain gauge technique measurement (normalised residual stresses)

3.1.2 Analysis of the Residual Stress Profiles

To characterise and evaluate the global residual stresses in a rolled plate, a specific indicator defined as the mean stored elastic energy per unit volume has been created in [30, 132]. This stored elastic energy density W can be used to evaluate the potential risk of distortion and can be expressed as in equation 3.3.

$$W = \frac{1}{H}\int_0^H \frac{\sigma_{RD}^2 - 2\nu\sigma_{RD}\sigma_{TD} + \sigma_{TD}^2}{2E} \tag{3.3}$$

with W being the stored elastic energy density in kJ/m^3 and H the thickness of the plate.

Experience has shown that a low risk of distortion is expected with a stored elastic energy density lower than $1\,kJ/m^3$, that a risk of significant distortion could occur for materials

containing a stored elastic energy density higher than $2\,kJ/m^3$ and that large distortions are expected when the stored elastic energy density is higher than $4\,kJ/m^3$ [30]. This indicator therefore enables to give an order of magnitude of the distortion risk linked to the machining of a part taken from a rolled plate and to determine if particular attention has to be paid to the definition of the machining process plan. For more information on the distortion risk, a stress range indicator (difference between the maximum and the minimum stress) can also be used. However, as mentioned in [133], because the part geometry and its position within the workpiece are not taken into consideration in both of these indicators, no precise evaluation of the post-machining distortion risk can be done.

To take into account the anisotropy of the residual stresses in the plate the stored elastic energy density W can be divided into two terms, one principally representing the rolling direction energy W_{RD} and one the transverse direction energy W_{TD}. These differentiated stored elastic energy densities are computed using equations 3.4 [30].

$$W_{RD} = \frac{1}{H}\int_0^H \frac{\sigma_{RD}^2 - \nu\sigma_{RD}\sigma_{TD}}{2E} \qquad W_{TD} = \frac{1}{H}\int_0^H \frac{\sigma_{TD}^2 - \nu\sigma_{TD}\sigma_{RD}}{2E} \qquad (3.4)$$
$$\text{with } W = W_{RD} + W_{TD}$$

Using equations 3.4 the stored elastic energy densities W_{RD} and W_{TD} of both the 70 mm thick and the 90 mm thick AIRWARE® 2050 alloy rolled plate have been computed. The total stored elastic energy density being mainly due to the residual stresses in the rolling direction, a significant anisotropy can be observed as represented in Figure 3.7.

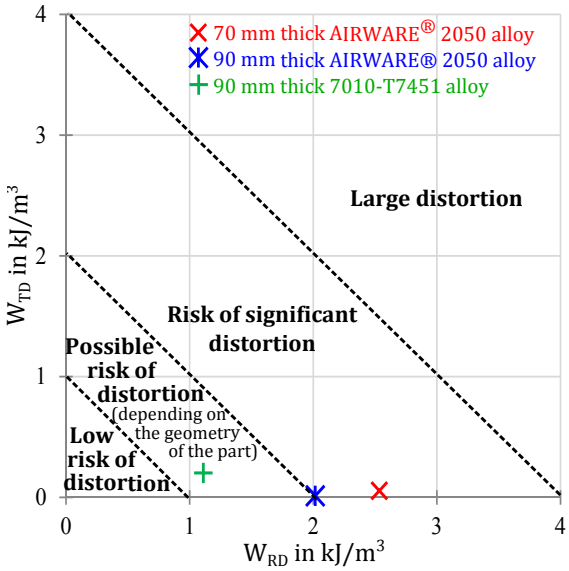

Figure 3.7: Stored elastic energy density for typical residual stress distributions of a 70 mm thick and of a 90 mm thick AIRWARE® 2050-T84 alloy rolled plate: comparison with an aluminium alloy of the 7XXX series

Note that the magnitude and the anisotropy of the stored elastic energy density vary in function of the alloy but also in function of the thickness of the plate. For example, in the alloys of the 7XXX series the highest values obtained are usually in a plate thickness range of 60-90 mm [132].

Figure 3.7 also shows that a part selected from a 70 mm thick or a 90 mm thick AIRWARE® 2050-T84 alloy rolled plate should have a low distortion if the initial workpiece is taken in the transverse direction (i.e. if the principal direction of the part is selected in the transverse direction) and that the risk of distortion is expected to be higher when dealing with workpieces taken in the rolling direction. In most cases, the parts are machined in the rolling direction. This is even more applicable for large aeronautical parts which are often too large to be machined in the transverse direction. The study of the behaviour of the workpiece due to the redistribution of the residual stresses during the machining is therefore relevant and can be helpful to define an appropriate machining process plan.

3.2 Simulation of the Layer Removal Method

In order to evaluate the accuracy of the developed numerical tool and of the experimental residual stress profiles, simulations of the layer removal method have been performed. Reverse analyses of the layer removal experiments have then been realised by simulations, as illustrated in Figure 3.8.

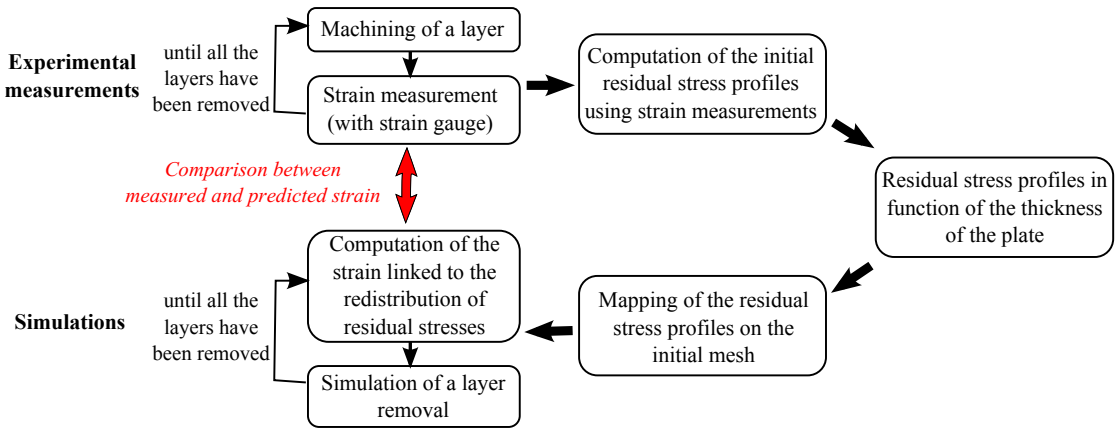

Figure 3.8: Illustration of the simulation and the experimental analysis of the layer removal method

As explained previously, the layer removal method and associated initial residual stress profile computations are based on strain measurements. In the simulation the residual stress profiles obtained experimentally (like the ones shown in Figure 3.5 and in Figure 3.6) are used as input data. During the simulation, layer removals as well as the computation of the associated redistribution of the residual stresses and strains are then performed. Comparisons between experimentally measured (with strain gauge) and computed strains can thus be drawn.

The initial beam geometries are 350×30×70 mm and 450×30×90 mm and are sampled from the rolled plates. The thickness of each removed layer is 3 mm, like for the experimental tests. The mechanical properties of the AIRWARE® 2050 alloy used in simulations are as presented in Table 2 in the Introduction.

3.2.1 Polynomial Approximation of the Residual Stress Profiles

To use the experimental residual stress profiles obtained as input data of the simulations, polynomial approximations have been done. Polynomial functions have been chosen to represent the residual stress profiles as this allows to smoothen the experimental results and to obtain a continuous residual stress distribution in the part. Figure 3.9 and Figure 3.10 show the polynomial functions used to describe the experimental residual stress profiles in Figure 3.5 and Figure 3.6. Using the specific script mentioned in Section 2.2.1.3.1, the initial meshes with their initial residual stress fields are computed using the coefficients of the polynomial functions determined previously. No distortion of the meshes can be observed during the computations of the initial residual stress profiles on the initial meshes, which proves that the initial residual stress profiles are balanced.

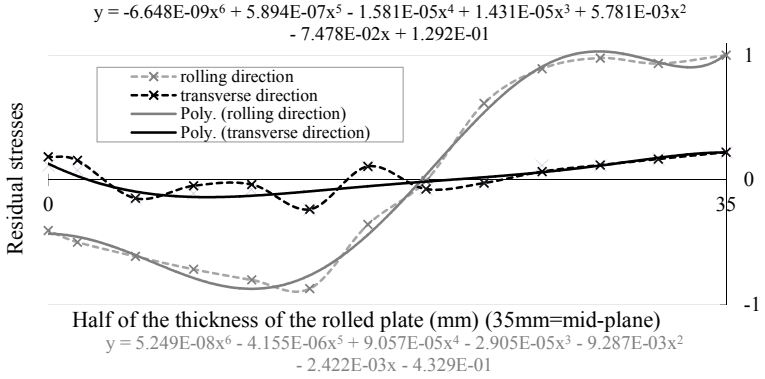

Figure 3.9: Polynomial functions used to apply the residual stress profiles on the initial mesh for the 70 mm thick rolled plate (normalised residual stresses)

3.2.2 The Numerical Approach

To ensure a good description of the through-thickness residual stress distribution and an accurate computation of the strain field, a small mesh size is used. As shown in Figure 3.11a, the initial element size (1.25 mm) is chosen to ensure a high number of elements along the total thickness. Depending on the removed volume, a new mesh size is computed at each remeshing step using the remeshing options previously introduced in Section 2.2.3.2. The mesh size is therefore smaller than what could be used but the objective being to use this case as a reference validation, a certain number of elements in the thickness had to be kept during the whole simulation. This mesh size therefore ensures accurate computations of the evolution of the residual stress profiles and of the associated strains.

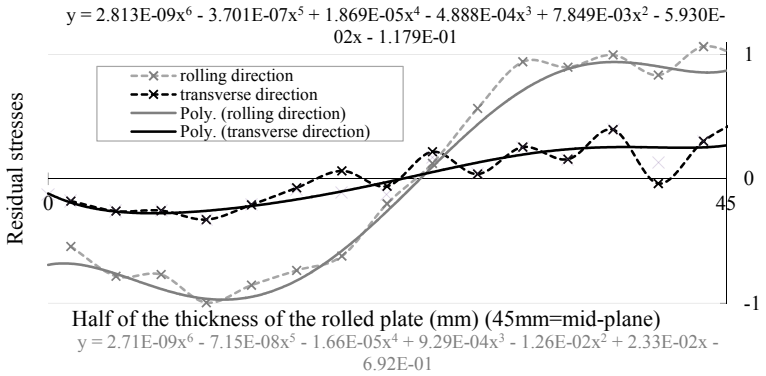

Figure 3.10: Polynomial functions used to apply the residual stress profiles on the initial mesh for the 90 mm thick rolled plate (normalised residual stresses)

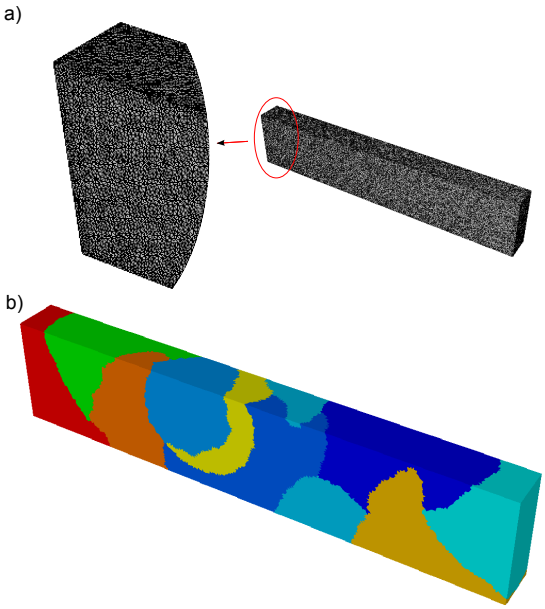

Figure 3.11: Initial mesh of the 70 mm thick specimens: a) Initial mesh composed of about 407,000 nodes and 2,269,000 tetrahedral elements, b) Initial subdomains of the mesh (simulation launched on 10 cores: one color per core)

The clamping is modelled by simply restricting the degrees of freedom of nodes in the clamping areas to reproduce the experimental clamping conditions (small clamping forces). After each layer removal the clamping condition is removed and strains linked to the redistribution of the residual stresses are computed. Figure 3.12 is a simplified flow chart of the procedure used to simulate the layer removal method.

Simulations have been performed on ten cores, the mesh thus being divided automatically in ten subdomains as shown in Figure 3.11b. Twelve and fifteen layer removal steps have been simulated for the 70 mm thick and 90 mm thick rolled plates respectively. A numerical sensor has been positioned on the mesh at the strain gauge location.

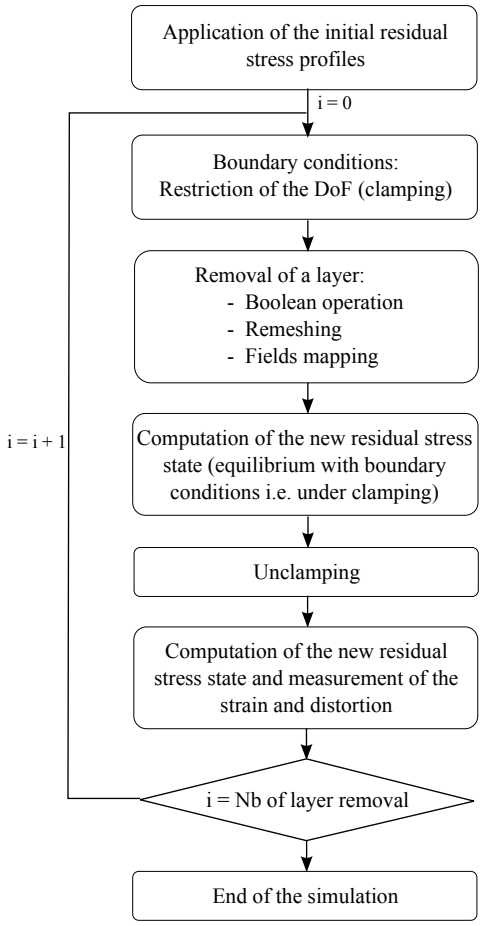

Figure 3.12: Flow chart of the simulation of the layer removal method procedure

The evolution of the elastic strain, the shape of the specimens (distortion) and the residual stress state are obtained for each removed layer, as shown in Figure 3.13.

3.2.3 Simulation Results

As explained previously in Section 3.1.2, due to the residual stress distribution anisotropy particular attention has to be paid when dealing with the machining of workpieces taken in the rolling direction. Using the developed numerical tool and experimental results, simulations of the layer removal method of beams taken from 70 mm thick and 90 mm thick rolled plates in the rolling direction have been performed. Only half of the thickness of the specimens has been machined in the simulations due to symmetrical considerations.

3.2.3.1 70 mm Thick Rolled Plate

Results of strains obtained for all twelve removals are depicted in Figure 3.14. A good agreement between experimental and simulation strains is achieved. The difference between

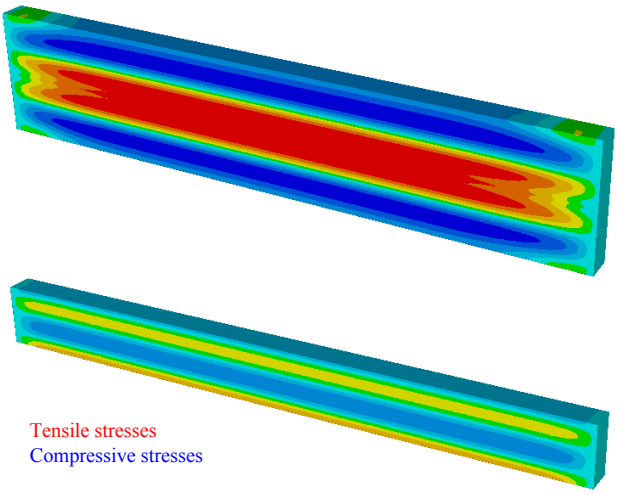

Figure 3.13: Evolution of the longitudinal residual stress field for the 70 mm thick specimen taken in the rolling direction. Comparison between the initial residual stress field and the one after 12 material removing steps

measured and predicted strains stays below 10% (except for the first layer where the strain is really low) with a majority even close to 5%.

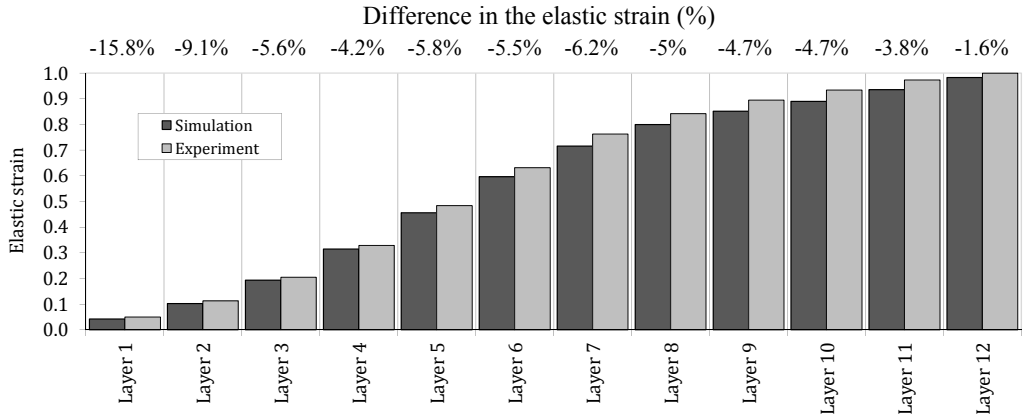

Figure 3.14: Evolution of the elastic strain during the layer removal method of the 70 mm thick specimen (normalised elastic strain). Comparison of simulation and experimental results (test 1). The difference in the elastic strain obtained by simulation and experiment in percent is also given.

The evolution of the curvature of the beam for each removal step can be observed in Figure 3.15. The cross represents the maximal displacement observed experimentally after the first twelve steps. A maximum value of 0.33 mm for the predicted and of 0.32 mm for the experimental test is obtained, which represents a difference of only 3%. The final predicted distortion is thus similar to what has been observed experimentally. A bigger increase of the curvature during the layer removals 4 to 8 can also be observed. These layers correspond to the area of a bigger gradient of the initial residual stress profiles, as can be seen in Figure 3.9.

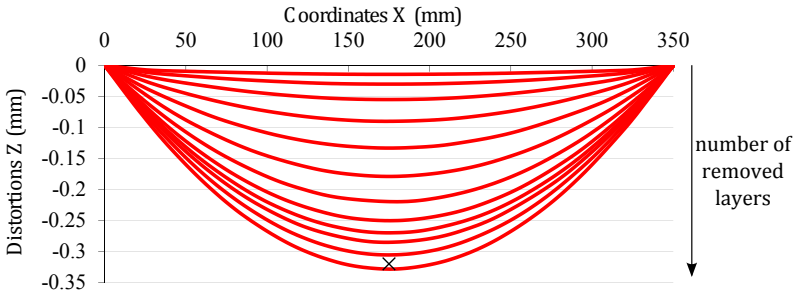

Figure 3.15: Evolution of the curvature of the 70 mm thick specimen during the twelve removals of layers. The cross represents the maximum displacement observed experimentally after the twelfth layer removal.

In addition to the good agreement between predicted and measured strains of test 1 (in Figure 3.3) the polynomial approximations of the typical residual stresses allow to have a relatively small error between the predicted and the mean of the measured strains (mean strain of the four tests). Moreover, this error is almost constant for each layer removed which shows that the same trends are obtained. The polynomial functions used are therefore a good approximation of the residual stress profiles of a 70 mm thick AIRWARE® 2050-T84 alloy rolled plate.

3.2.3.2 90 mm Thick Rolled Plate

Similarly to the 70 mm thick plate, the results obtained in terms of strains for all fifteen removals are depicted in Figure 3.16 for the 90 mm thick plate. A good agreement between experimental and simulation strain is also achieved. The difference between measured and predicted strains stays below 10% (except for the first layer where the strain is really low) with a majority even below 5%.

The evolution of the curvature of the beam for each removal step can also be observed in Figure 3.17. A difference of less than 7% is obtained between the maximum displacement measured experimentally and the one predicted. A bigger increase of the curvature during the layer removals 5 to 10 can also be observed, which corresponds to the area of a bigger gradient of the initial residual stress profiles.

3.2.4 Discussion

The predicted and measured strains show similar trends during the layer removal test. Knowing the initial residual stresses, the developed numerical tool therefore enables to predict the redistribution of the initial residual stresses and the associated distortion due to the removal of material. These simulations therefore allow a first experimental validation of FORGE OFELIA. They have also allowed to validate the polynomial functions defined to represent the typical residual stress profiles in a 70 mm and in a 90 mm thick AIRWARE® 2050-T84 alloy rolled plate.

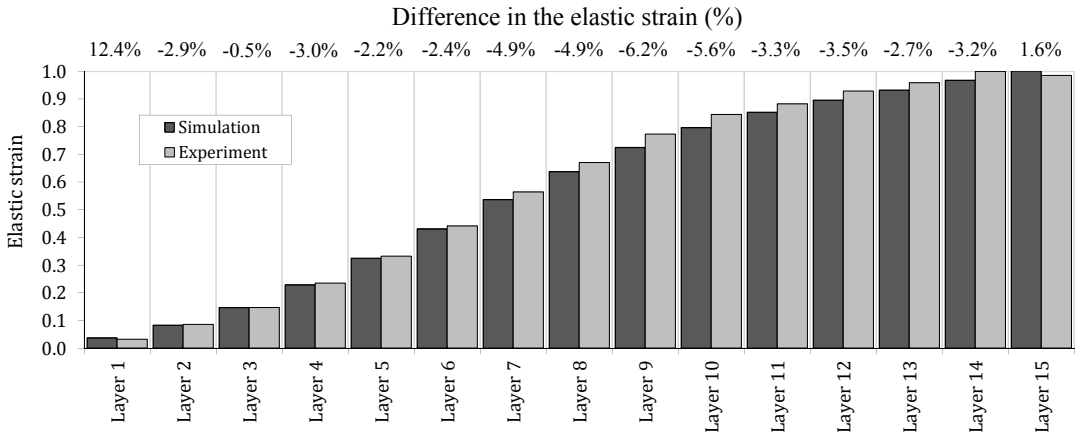

Figure 3.16: Evolution of the elastic strain during the layer removal method of the 90 mm thick specimen (normalised elastic strain). Comparison of simulation and experimental results. The difference in the elastic strain obtained by simulation and experiment in percent is also given.

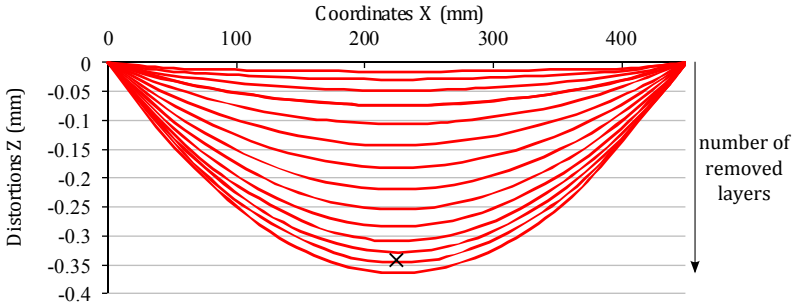

Figure 3.17: Evolution of the curvature of the 90 mm thick specimen during the fifteen removals of layers. The cross represents the maximum displacement observed experimentally after the fifteenth layer removal.

Such an approach could also be developed in industry, where databases of typical residual stress profiles of alloys and their associated polynomial functions could be developed and furnished by suppliers. For each new machining part, simulations could then be performed in order to study the influence of the residual stresses and to optimise the machining process plan.

This kind of simulation furthermore opens some new perspectives. Using the layer removal method and this numerical tool, it could be possible to improve the accuracy in the evaluation of residual stress profiles. Indeed, with this method the beams are machined layer by layer and strains are measured after each removed layer and the associated unclamping. Depending on the residual stress profiles and magnitudes, beams will bend and the next removed layers will therefore not be exactly of a constant thickness. In the theoretical analysis with the present technique a constant thickness of layers is considered for the evaluation of the residual stresses. In some cases, a relatively high level of residual stresses and gradients in their profiles can

be observed resulting in a significant curvature of the beams during the experiments (as-quenched plate for example), an uncertainty in the computation of the residual stress profiles can therefore be introduced. In most cases, the assumption of a constant thickness of the layer is almost respected during the whole experiment, the maximum amplitude of distortion being relatively low, as in this study (~ 0.3 mm). The uncertainty is thus limited in these tests.

In any case, one way to decrease this uncertainty would be to use the residual stress distribution obtained in the theoretical analysis as a basis and to use the numerical tool taking into account distortions of the beams at each step of the experiments (i.e. taking into account the non-constant thickness removals) to perform inverse analysis. This could be performed using an optimisation module like the one already integrated in FORGE®. An optimised residual stress distribution allowing to be closer to the measured strain could therefore be obtained. However, the feasibility of such an approach would still have to be studied, especially regarding the computation time of the inverse analysis. Indeed, a simulation of the layer removal method as shown in this chapter required a computation time of approximately ten hours and with the multiple coefficients to optimise, such an inverse analysis could be very time-consuming. However, as explained previously, the mesh size used could be optimised as the one used in these studies has been set to a small value to obtain results as accurate as possible to validate the numerical tool. An appropriate mesh size could therefore be determined, enabling to perform an inverse analysis.

3.3 Post-Machining Distortion Prediction: Validation Tests

Several simulations have then been performed and compared to experimental results to evaluate the capability of FORGE OFELIA to predict the post-machining distortion of AIRWARE® 2050 alloy parts. In this section an example of machining of a small part taken from a 70 mm thick rolled plate is presented.

The dimensions of the initial workpiece are 500×100×70 mm. The initial residual stresses are applied on the initial mesh using the polynomial functions represented in Figure 3.9. A 1 mm layer is then removed on both the upper and the lower part of the initial workpiece. Two other removals at both ends of the workpiece are also performed to obtain the prepared geometry shown in Figure 3.18. The initial mesh is composed of about 3,200,000 elements and 630,000 nodes (mesh size of 1.9 mm).

3.3.1 Machining of an "Open Pockets" Case [124]

The studied machined part is shown in Figure 3.19. Ten different machining features can be identified, they are numbered as depicted in Figure 3.19.

The simulations of the clamping and the machining of the ten features have been performed on twelve cores. The fixture layout is composed of three locators and the part is maintained in position with two clamps as shown in Figure 3.20. Clamps, locators and the table are

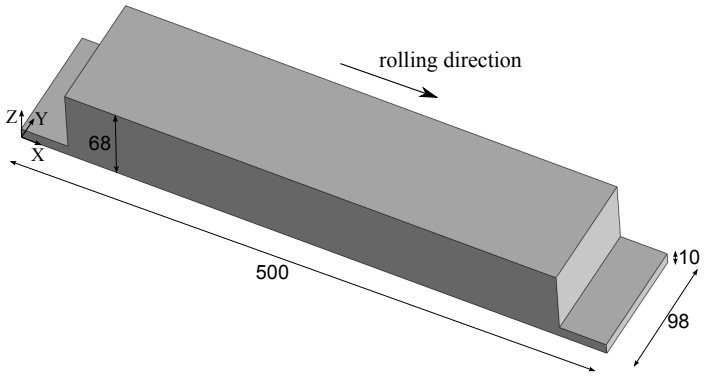

Figure 3.18: Geometry of the workpiece after the preparation steps

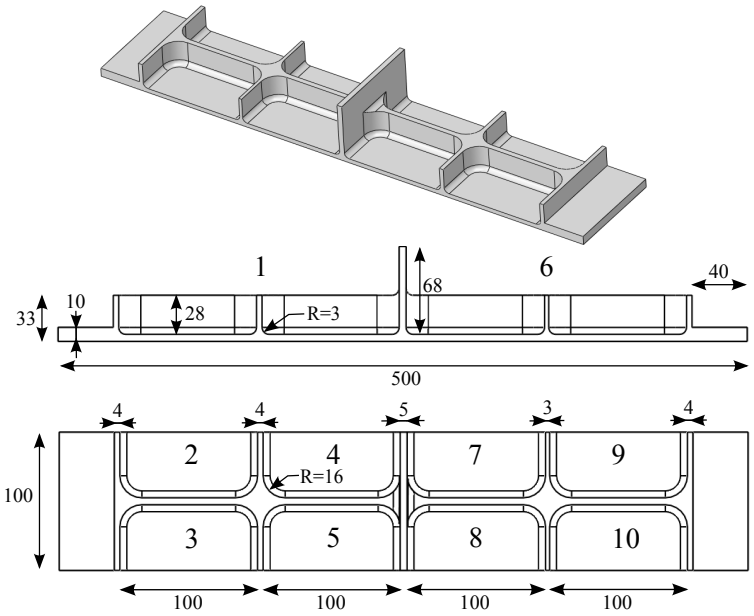

Figure 3.19: Geometry of the part and machining feature numbers [124]

considered as rigid solids and the clamping force is 11 kN per clamp. During the clamping simulation the clamps are displacement controlled and a maximum force criterion equal to the desired clamping force is defined as the criterion to stop the simulation.
During the machining simulation, the fixture elements are still considered as rigid solids but are this time fixed. Sliding between the workpiece and the fixture elements can therefore occur but no displacement of the clamps is possible. However, the evolution of the force applied on each fixture element is still computed. The assumption that the possible displacement and deformation of the fixture system which could occur during the machining can be neglected is based on the conclusions deduced from the review of literature presented in Section 1.2.1.2.

The simulation of the ten machining features has been performed with a model of Level 5

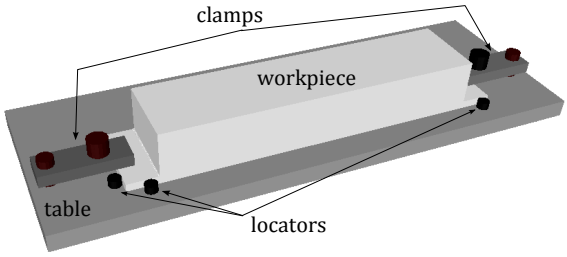

Figure 3.20: Fixture layout used for the simulation of machining [124]

(see Section 2.3). The machining sequence of the ten machining features has been discretized in forty-two layers with a thickness equal to the depth of cut, which is fixed to 7 mm (representative of what can be used in industry). This type of model allows therefore to be as close as possible to a real machining process still keeping reasonable computation times. The machining features are machined depending on the numbering defined previously in Figure 3.19.

At the same time, experimental machining tests have been performed by the French Institute for Advanced Mechanics (IFMA). Two parts have been machined with the same parameters as in the simulation (depth of cut, radius of the tool, fixture layout). Distortion measurements have been performed (by IFMA) on the bottom surface of the part using a coordinate-measuring-machine (CMM). The distortions of the parts can therefore be compared to the one resulting from the simulation. Figure 3.21 is an illustration of the measurement layout used to determine the curvature of the part.

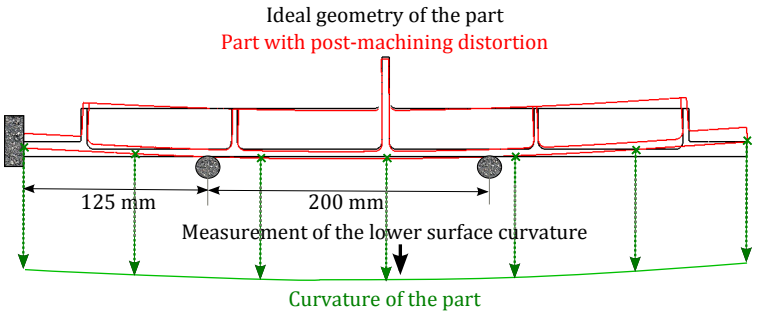

Figure 3.21: Description of the measurement layout used on the CMM [124]

Figure 3.22 shows the evolution of the displacement of the workpiece and the mesh subdomains at different steps of the simulation of the machining. It can be seen that the displacements due to the residual stress re-equilibrium during the machining go up to a maximum amplitude of 0.14 mm. Due to these workpiece deflections, the material removed is not exactly the same as the expected one. A difference of about 2% on the final volume of the part can be observed between the perfect geometry (CAD geometry) and the predicted one.

Figure 3.22: Evolution of the workpiece displacement (mm) and mesh partition during the simulation of the machining [124]

The evolution of the mesh subdomains can also be observed and the number of nodes which compose each of these subdomains at the different steps shown in Figure 3.22 can be seen in Table 3.2. The maximal difference compared to the average number of nodes on each core stays below 15%. The difference remaining below 10% most of the time, it can be concluded that the mesh migrations ensure a good evolution of the subdomains in repartitioning approximately the same amount of nodes of the mesh on each core after each removal step. Without using the options introduced in Chapter 2 a clear decrease in the number of nodes composing the mesh can also be observed.

Table 3.2: The evolution of the number of nodes composing the different subdomains shown in Figure 3.22

	Initial	Step 1	Step 2	Step 3	Step 4	Step 5	Step 6
subdomain 1	52145	33741	31142	29694	17916	13263	8717
subdomain 2	50214	34836	30454	26940	15777	13478	8944
subdomain 3	51049	34682	30856	27085	15813	12412	9076
subdomain 4	50886	34521	30672	27115	15763	12376	9111
subdomain 5	54634	34427	30522	27167	15841	12030	9302
subdomain 6	50490	32920	32129	30246	18783	13944	9408
subdomain 7	51856	35394	31464	27746	16003	12220	8461
subdomain 8	50253	34409	30114	27123	16734	13698	9517
subdomain 9	53694	34625	30863	26886	16241	12269	9047
subdomain 10	51079	34093	29702	26237	17459	13865	9454
subdomain 11	55649	35410	31343	27102	15657	12049	8651
subdomain 12	50860	34881	30691	27060	16550	12757	8990
average number of nodes	51900	34494	30829	27533	16544	12863	9056
maximal difference/average	7.2%	4.5%	4.2%	9.8%	13.5%	8.4%	6.5%

To be as close as possible to the experimental tests, measurements of the post-machining distortions have also been performed by modelling the experimental measurement layout used to obtain the curvature of the part (see Figure 3.21). With these results a direct comparison of the predicted and the measured post-machining distortion can be performed, as shown in Figure 3.23. It can be seen that the numerically predicted distortion is in good agreement with the measured ones. Deviations can only be observed at the two ends of the parts. Indeed, a change in the curvature of the part can be observed experimentally in an area of 40 mm on each side of the part. These areas correspond to the clamping zones. In the simulation no change in the curvature of the part can be observed. These differences could be due to severe machining conditions during the preparation machining steps.

The post-machining distortion predicted by the numerical tool is therefore a good representation of what can be observed during real machining, showing only small differences in the magnitude of the distortion.

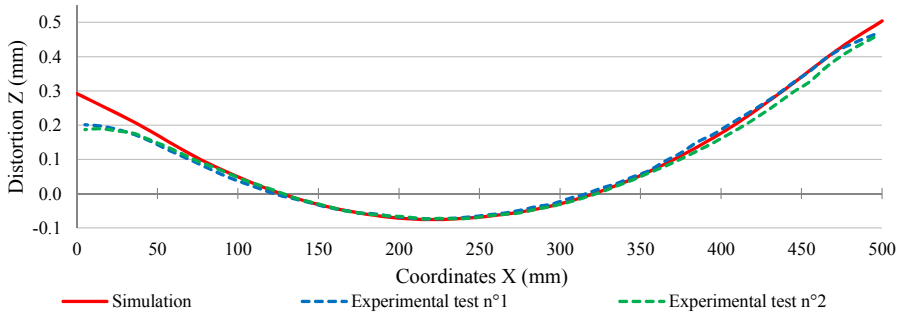

Figure 3.23: Comparison between experimentally measured and predicted post-machining distortion [124]

3.3.2 Discussion

Several other cases, presenting different geometries and machining feature types, have also been studied, as for example the one presented in Appendix C. The tests and comparisons with experimental results have allowed to validate the developed numerical tool and its capability to predict the post-machining distortions in function of the initial residual stress state and the geometry of the part.

Simulations with different levels of models have also been performed, showing no influence of the model level on the predicted post-machining distortions. The variation in the removed volume of the part has therefore no influence on the post-machining distortion in this case. A model of Level 1 is thus sufficient to predict accurately the post-machining distortion. In addition, the post-machining distortion being mainly driven by the longitudinal wall, a relatively coarse mesh size can be used to predict it. Results obtained regarding the mesh size influence on the predicted distortion with a model of Level 1 are summarised in Table 3.3. However, with this model level no information on the behaviour of the workpiece during machining depending on the machining process plan is obtained. In addition, even if the mesh size has only a small influence on the prediction of the post-machining distortion in this case, if a precise evaluation of the machining behaviour of the workpiece is required a relatively small mesh size (for example 1.9 mm in this case) should be used to capture the workpiece deflections as shown in Figure 3.22.

Table 3.3: Mesh size influence on the predicted distortion amplitude with a model of Level 1

Mesh size (mm)	Nb nodes	Nb elements	Difference on the predicted distortion amplitude in %
1	399274	2044525	reference
1.9	84032	382109	0.68
3	28573	113740	2.22
4	15889	58837	4.436
5	10764	37794	6.6
6	8045	27034	8.72

When dealing with post-machining distortion predictions, simple models can therefore be used. In order to determine the influence of the different machining parameters on the machining behaviour of the workpiece and on the machining quality, more in-depth analyses have to be performed.

3.4 Machining Part Quality Analysis: Initial Residual Stresses and Machining Sequence Influence

Based on the previous conclusions (Section 3.3), a specific study with a more in-depth analysis has been conducted. In this study, the influence of both the initial workpiece and the machining sequence on the post-machining distortion and on the machining accuracy is analysed.

3.4.1 Definition of the Case Study

3.4.1.1 The Part Geometry

In order to simplify the analysis of the influence of residual stresses on the machining quality and the development of a first method to optimise machining, a simplified but representative example of a part made of AIRWARE®2050-T84 alloy has been defined in collaboration with IFMA. The part is of small dimensions (500×98×68 mm) in order to limit the computation time and the amount of material. The size thus allows the simulation of different cases and enables an easier analysis of the results.

A specific part geometry has to be defined to be as representative as possible of the machining of large aeronautical parts. The chosen geometry therefore has to enable the observation of the same phenomena as on large aeronautical parts, i.e. measurable post-machining distortion as well as workpiece deflections during the machining.

The proposed geometry is composed of seven features and is presented in Figure 3.24.

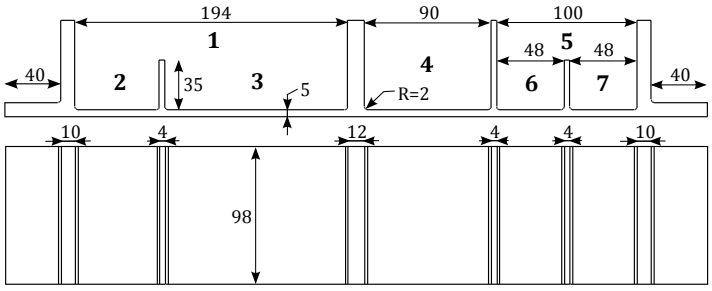

Figure 3.24: The geometry of the part (in mm) and its seven machining features

The geometry has been chosen after a long experimental and computational study. The main reasons which have lead to the choice of this geometry are summarised in the following points:

1. Despite the small dimensions, it allows to observe workpiece deflections during the machining due to the redistribution of the residual stresses without machining vibration problems.
2. It enables to obtain measurable post-machining distortion.
3. More than 84% of the initial workpiece volume is removed to obtain the designed part, which is representative of aeronautical configurations.
4. It enables to verify that the effects of the initial residual stresses on the phenomena observed during the machining are of first order.
5. The use of a simple fixture layout is possible. During the whole study the fixture layout remains fixed. No analysis of the influence of the fixture layout on the machining quality is performed. This study only focuses on the influence of the initial residual stresses and of the machining sequence on the part quality.

3.4.1.2 The Process Plan: The Set Parameters

In this section, the machining process plan parameters which are set for the whole study are introduced. The first step of the machining process plan is the preparation of the workpiece. It is the same as for the case presented in section 3.3. Each block is selected from an AIRWARE® 2050-T84 alloy rolled plate in the rolling direction and is prepared as explained previously in order to obtain the geometry shown in Figure 3.18.

The same fixture layout as the one presented in Figure 3.20 has been used for the whole study. The clamping force is set to 11 kN on each clamp. This fixture layout also allows to simplify the analysis because only overcuts can occur during the machining.

Furthermore, some machining parameters have been set for the simulations. The tool diameter is 32 mm with a nose radius of 2 mm. The depth of cut is, in a first step, fixed to a value of 7 mm. Based on a model of Level 5, the machining of the seven machining features of the part has been divided depending on the value of the depth of cut, giving thirty-seven layers. The discretization of the machining sequence is illustrated in Figure 3.25.

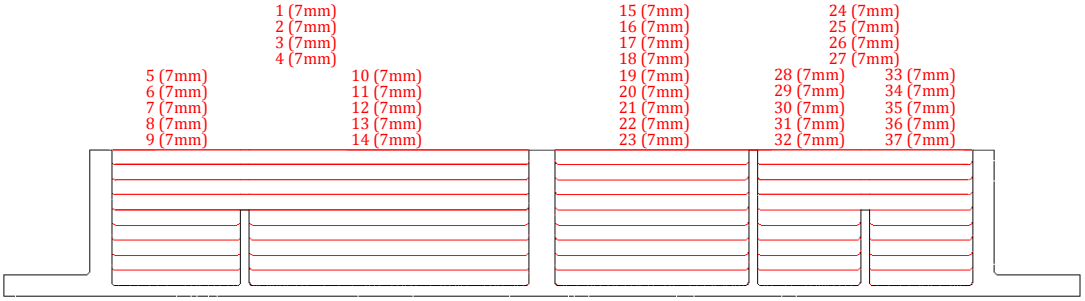

Figure 3.25: Discretization of the seven machining features in thirty-seven layers

3.4.2 Reference Machining Case

The case presented below represents the simplest and quickest machining process plan to machine the part. It would thus be the first choice to machine the part in an industrial context. This case is therefore used as a reference case during the whole study.

3.4.2.1 Initial Residual Stresses

In order to minimise the amount of material removed a rolled plate with a thickness as close to the part thickness (68 mm) as possible has to be used. A 70 mm thick rolled plate has therefore been chosen for this case.

The same residual stress profiles as the one presented in Figure 3.9 are used and applied with the specific script introduced in section 2.2.1.3.1.

At the end of the simulation, the initial block of material of 500×98×70 mm with the equilibrated initial residual stress state is obtained. This mesh therefore represents the initial state of the workpiece. Using this initial mesh, the simulation of the preparation step is then performed to obtain the prepared workpiece with its initial residual stress state.

3.4.2.2 Machining Sequence

The thirty-seven layers in Figure 3.25 are machined from layer one to layer thirty-seven, thus minimising the length of the global tool path and therefore the machining time.

The final part quality is strongly dependent on the machining of the last depth of cut of each feature, i.e. the layers 9, 14, 23, 32 and 37. To be as close as possible to the real machining the removals of these layers have to be therefore divided into several massive removal steps which are performed in function of the tool path used for the machining (contour augmentation). These layers are removed in several steps whereas all the others are removed in one. A removal of material is performed for each passage of the milling tool. Both the tool path and the associated machining sequence discretization are illustrated in Figure 3.26. This machining sequence discretization corresponds therefore to a combination of a Level 5 and a Level 6 model (Level 5-6).

3.4.2.3 Results

In a first step, an influence analysis of the mesh size on the post-machining distortion predictions has been performed using a model of Level 1. This analysis has as an objective to determine the final post-machining distortion as well as to determine an appropriate mesh size for the simulation using a model of Level 5-6. The results obtained are summarised in Table 3.4.

This analysis shows that with this part geometry, a high mesh density in the 5 mm thick bottom

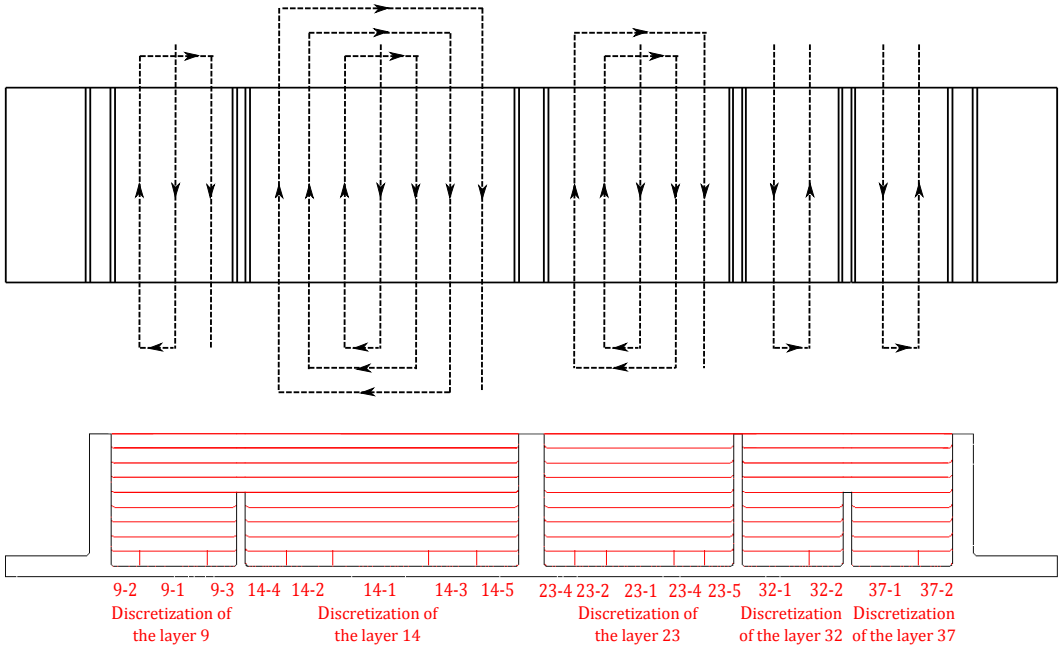

Figure 3.26: Illustration of the tool path used for the machining of each layer and the machining sequence discretization used for the simulation

Table 3.4: Mesh size influence on the predicted distortion with a model of Level 1

Mesh size (mm)	Nb nodes	Nb elements	Predicted distortion amplitude	Difference in %
0.75	1453955	7929969	0.468	reference
0.9	861021	4628834	0.463	0.96
1	359544	1833688	0.451	3.52
1.5	177478	877834	0.425	9.2
2	79344	373887	0.4	14.58
3	27056	114317	0.334	28.62
4	12747	48409	0.246	47.47

wall is required to obtain a convergent solution and that almost no more evolution between a mesh size of 0.75 mm and 0.9 mm can be observed. As mentioned previously in the modelling guidelines (see Section 2.2.1.1), a minimum of five elements in the thickness of the wall is required. A mesh size smaller than 0.75 mm seems difficult to be used as a significant number of nodes and elements is already generated with this mesh size.

The initial mesh has therefore been adapted to the geometry and is composed of about 830,000 nodes and 5,200,000 elements. Different mesh sizes have been defined in order to capture accurately the post-machining distortion and the phenomena which could occur during the last depth of cut, as shown in Figure 3.27. This mesh also allows to ensure a good description of the residual stresses as well as to have a good ratio between the computation time and the accuracy of results. Using this mesh, the simulation of the machining reference case has

then been performed. The whole computation has been realised automatically on a 12-core computer and took about two days.

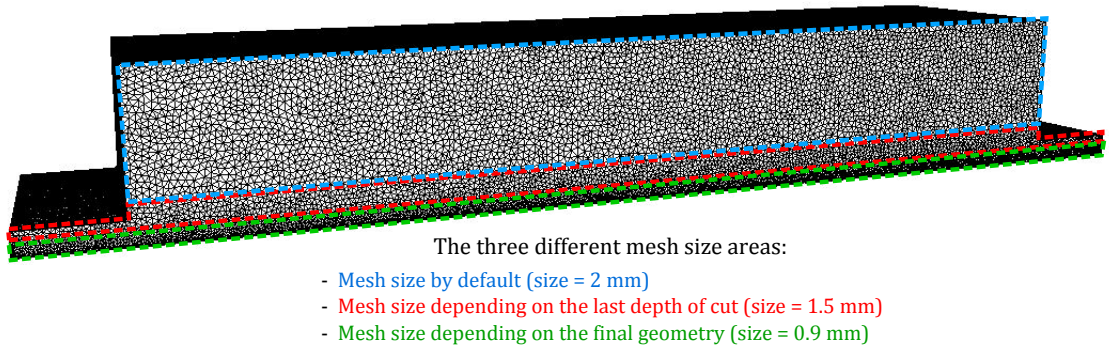

Figure 3.27: The initial mesh representing the prepared workpiece

After the unclamping and the final re-equilibrium computation, the machined part geometry is obtained. Measurements can then be realised to evaluate the quality of the machining process plan. Two kinds of measurements are performed. The first one is the measurement of the post-machining distortion in the middle of the bottom surface (Y = 49 mm) of the part (curvature of the part). The second one is the measurement of the thickness of the bottom wall. The thickness of the wall is measured at two different Y-coordinates (Y = 25 mm and Y = 73 mm) and at eighteen different coordinates along the X-axis. The comparison between the measured thickness variations and the nominal value of 5 mm can then be performed. Both measurement types are illustrated in Figure 3.28.

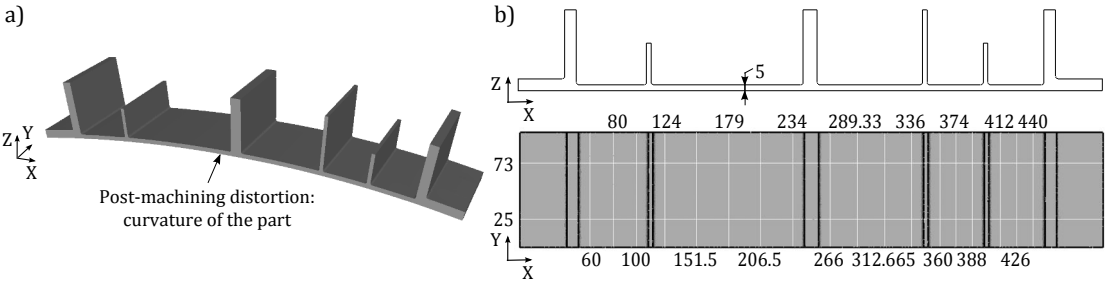

Figure 3.28: The different types of measurements realised for the machining quality evaluation: a) The post-machining distortion (curvature of the part); b) Coordinates for thickness measurements of the wall of 5 mm

Experimental machining tests have also been performed to validate this reference case. They have been realised by IFMA on a PCI METEOR-10 machine tool. The same parameters as in the simulation (depth of cut, radius of the tool, fixture layout) have been used for the experimental machining. Using a coordinate-measuring-machine (CMM), measurements of the post-machining distortion and of the thickness of the bottom wall have been performed. Comparisons of the predicted distortion and of the thickness variations with the experimental measurements have then been realised. The results are depicted in Figure 3.29. As it can be

observed, the deviation between simulation and experimental measurements is of the same order as the experimental uncertainty and similar trends are obtained, validating the reference case. These results also allow to complete those already discussed in [124] and therefore allow to validate again the approach developed in the numerical tool as well as its capacity to predict the machining quality.

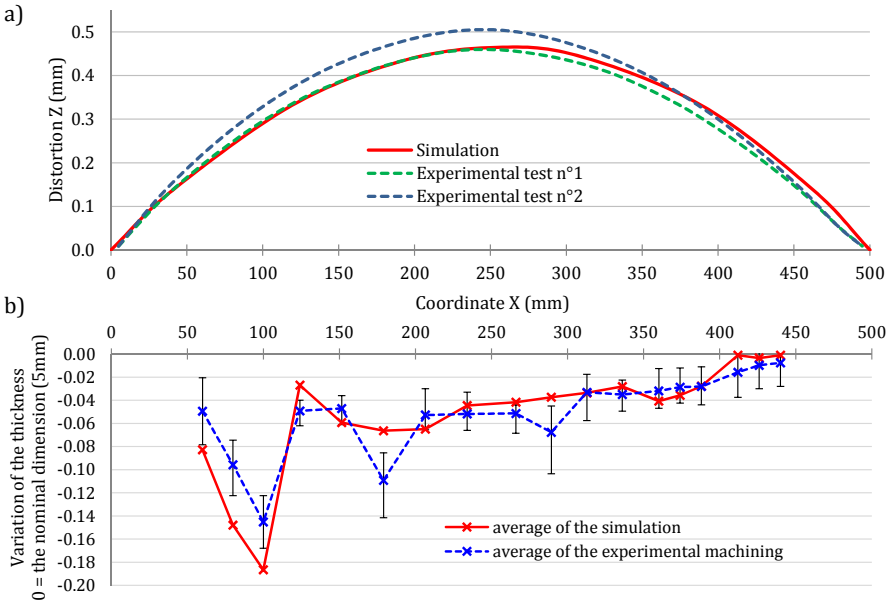

Figure 3.29: Comparison between experimental and simulation results: a) Post-machining distortion of the part (curvature) ; b) Variation of the thickness of the wall with a nominal dimension of 5 mm

With this reference case, which represents the simplest and quickest way to machine the part, two different machining problems are highlighted. The first one is the post-machining distortion (curvature) of the part after the unclamping and the second one is the lack of accuracy during the machining, causing variations in the thickness of the bottom wall. This lack of accuracy is due to overcuts linked to the workpiece deflections during the machining. To improve the quality of the machining process, the process plan has therefore to be adapted to limit these two problems.

3.4.3 Machining Part Quality Improvements

Part quality is industrially expressed as the post-machining distortion (curvature) of the part and the accuracy of the cutting. These two phenomena are dependent on different parameters. The post-machining distortion is mainly governed by the part geometry (designed part) and the initial residual stresses of the workpiece. The accuracy of the cutting, which can be affected by overcuts or undercuts in some areas of the part, depends on the initial residual stresses of the workpiece and on the evolution of the geometry of the part during the machining. This

evolution may depend on the machining sequence and on the fixture layout. This second parameter is not considered in the present case.

In this section, a study on the numerical tool and on the levels of models which can be used to predict the machining quality is performed. The objective is to evaluate the capability of the numerical tool to capture the different phenomena observed depending on the initial workpiece and machining sequence used. Applying the different models presented above (Level 1 and Level 5-6), numerical tests where these two parameters vary have been performed with the objective to improve the machining quality. This case can be considered as a representative example of some industrial machining cases where only few configurations of fixture layouts are possible and where the machining tools and cutting conditions cannot be modified (cutting parameters to optimise the tool-life and the costs). The fixture layout can therefore not be adapted to limit the workpiece deflections during the machining.

In the numerical tests described here, the two phenomena observed are uncoupled. Using a model of Level 1, a first analysis on the initial workpiece and its initial residual stress state is realised in order to determine its influence on the post-machining distortion. Then, using a model of Level 5-6, which is one of the most accurate models which can be used, the influence of the machining sequence on the accuracy of the machining is analysed.

To define a desired part quality, geometrical and dimensional tolerance specifications have been chosen. The tolerance specifications have been set to 5 ± 0.075 mm for the bottom wall thickness variations and to 0.2 mm for the planarity of the bottom surface of the part (post-machining distortion), i.e. that the bottom surface of the part has to lay between two parallel planes which have a distance of 0.2 mm. These tolerance specifications can also be considered as representative of the industrial tolerances as they have been adapted to the dimensions of the part. However, it can be noted that due to the smaller dimensions of the part, the phenomena observed could still be minimised compared to cases of machining of large and complex aerospace parts.

3.4.3.1 Post-Machining Distortion

The post-machining distortion is governed by the part geometry and the initial residual stresses of the workpiece. Because the final part geometry cannot be modified, the initial residual stress profiles have to be chosen in a way to limit the post-machining distortion in order to improve the machining quality. To change these initial residual stress profiles, a thicker AIRWARE® 2050-T84 alloy rolled plate can be used. In this case, the plate chosen is 90 mm thick. The residual stress profiles are the same as the one presented in Figure 3.10.

The use of this plate gives the possibility to change the so-called part-offset. The offset represents the position within the initial workpiece (90 mm) in which the final part geometry of 68 mm of thickness is machined [132, 12]. The offset value indicated in this report represents the distance between the bottom surface of the machined part and the one of the plate. Depending on the offset, the part has therefore not the same residual stress state, as illustrated in Figure 3.30.

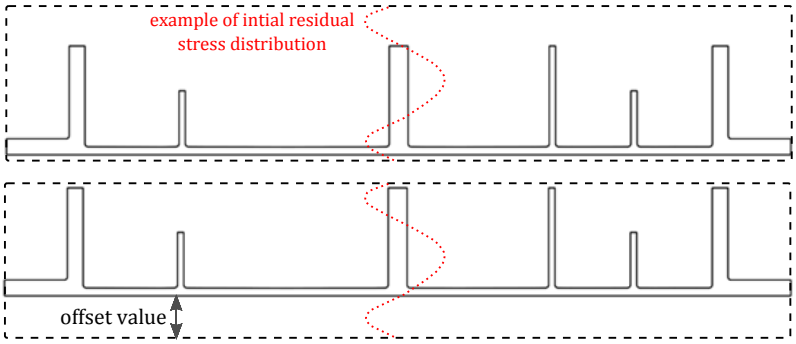

Figure 3.30: Illustration of part-offset: the position within the initial machined plate (90 mm) at which the final part is machined

To prevent the post-machining distortion, the residual stress state in the bottom wall has to be chosen to minimise the redistribution of the residual stresses. The post-machining distortion of the part being due to the bending moment, the bottom wall has to be located in a position within the workpiece where the bending moment is almost zero. Using the residual stress profiles and because the geometry of the part simplifies the analysis, it is possible to predict an offset which allows to obtain an almost non-existing bending moment. Indeed, as shown in Figure 3.31, an offset of 9 mm would enable to have no gradient of residual stresses between the lower and upper surfaces of the bottom wall. With this offset, the bending moment should therefore be zero like the post-machining distortion.

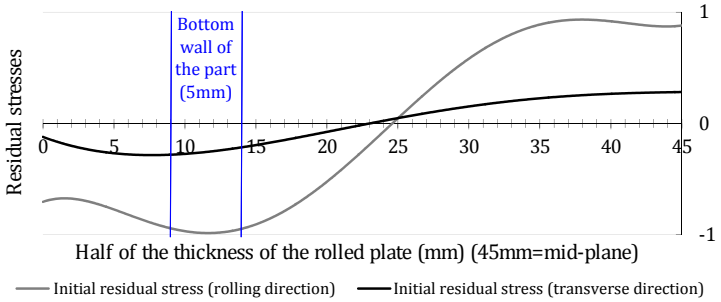

Figure 3.31: Determination of the optimal offset by analysis of the initial residual stress profiles and the final part geometry

In order to validate this analysis and the optimal offset found, a numerical analysis of the offset has also been performed. Furthermore, in the case of a complex part geometry the previous simple analysis is difficult, thus requiring the use of a numerical tool. The numerical offset analysis consists in multiple simulations. As demonstrated previously, a model of Level 1 can be used for the prediction of the post-machining distortion. In these simulations the residual stress profiles are therefore directly applied on the designed geometry of the part in taking into account its position within the initial workpiece. The offset analysis simulations are thus rather simple and quick to perform. As discussed in Section 3.4.2.3, an appropriate mesh size has to be used to accurately predict the post-machining distortion. In this case, a mesh size of

0.9 mm is thus used. The results of the offset analysis are depicted in Figure 3.32.

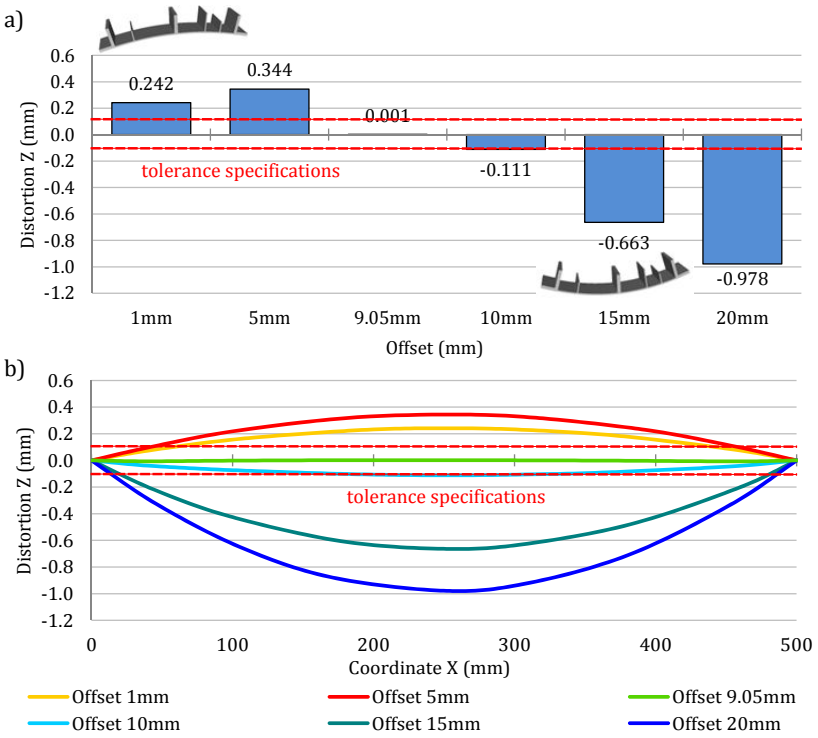

Figure 3.32: Numerical analysis of the offset: a) Maximum distortion observed in function of the offset ; b) Post-machining distortion of the part in function of the offset

An inversion in the curvature can be seen for an offset of around 9 mm, which confirms that the optimal offset is around this value. More precisely, a maximum distortion of about 1 μm is obtained for an offset of 9.05 mm.

Using this offset and the model of Level 5-6, the simulation of the machining of the part with the same machining sequence as for the reference case has been performed. The only modification concerns the phase of preparation of the workpiece, where the surface milling operations are realised to obtain the correct position of the workpiece within the 90 mm thick initial block. When the preparation phase is finished, the workpiece is slightly distorted due to the offset but is correctly put in contact with the table during the clamping.

At the end of the machining, the same measurements as the ones for the reference case are realised. Results obtained are depicted in Figure 3.33. As shown in Figure 3.33a a clear decrease of the post-machining distortion is achieved from a maximum distortion of about 0.5 mm for the reference case to 0.04 mm for the case with the optimal offset. The tolerance specification for the post-machining distortion is thus respected. Regarding the variation in the thickness of the bottom wall, it can be observed in Figure 3.33b that in several areas of the part overcuts occurred. These overcuts are bigger than the tolerance specification, leading to geometrical non-conformity and then rejection of the part.

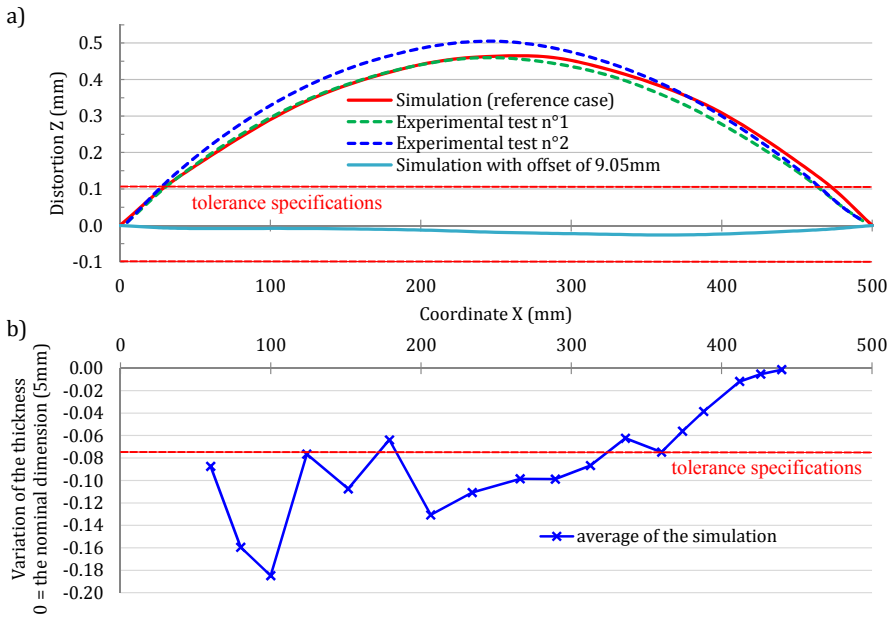

Figure 3.33: Simulation of the machining with an offset of 9.05 mm: a) Post-machining distortion of the part (curvature) ; b) Variation of thickness of the wall with a nominal dimension of 5 mm

3.4.3.2 Machining Accuracy

In this section, the influence of two machining parameters on the machining accuracy is studied. In a first step, the influence of the machining sequence on the workpiece deflections during the machining is analysed with the objective to prevent overcuts. In a second step, the capability of the numerical tool to detect the influence of a change in the depth of cut is evaluated. These studies are realised using a model of Level 5-6.

3.4.3.2.1 Machining Sequence

The quality of the part and the machining accuracy are governed by the initial residual stress profiles, the clamping (which is fixed in this study) and the evolution of the geometry of the part during the machining which depends on the machining sequence. To determine the different phenomena which could appear during the machining of the last depths of cut a first quick analysis of the residual stress profiles can be realised.

In Figure 3.34, the bottom wall of the part (5 mm) as well as the last two depths of cut (7 mm) have been represented. With the optimal offset determined previously, the bending moment in the part is zero. It can also be observed that the bottom wall is located in an area with compressive residual stresses, which means that the part will become longer during machining and that the clamping has to be able to stop these unexpected displacements.

Whereas the bending moment is zero in the bottom wall of the part, the bending moment in the last two depths of cut is significant. Indeed, a notable variation in the residual stress

profiles can be observed in these areas. For the last depth of cut, the bottom layer of the workpiece will be only 12 mm thick (5 mm of the wall plus 7 mm of the depth of cut). The coupled effect of the decrease of rigidity of the workpiece during the machining and the bending moment due to the gradient of residual stresses in this layer can therefore lead to the deflection of the workpiece during the machining.

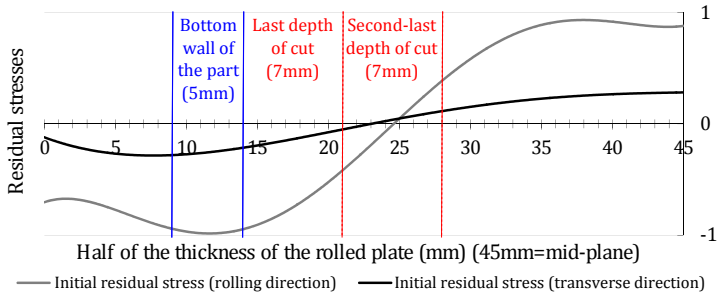

Figure 3.34: Analysis of the initial residual stress profiles to determine the different phenomena which can occur during the machining of the last depths of cut

In Figure 3.35, the deflections along the Z-axis observed during the simulation of the machining of the layer number 9 in Figure 3.25 with the same machining sequence as in the reference case are shown. Displacements of 0.2 mm can be observed. It is in this area that the biggest displacements occur, which corresponds also to the area where the biggest variations in thickness are observed in Figure 3.33b. The same phenomena can also be noted during the machining of the reference case, this confirms that the overcuts are only linked to the redistribution of the residual stresses during the machining.

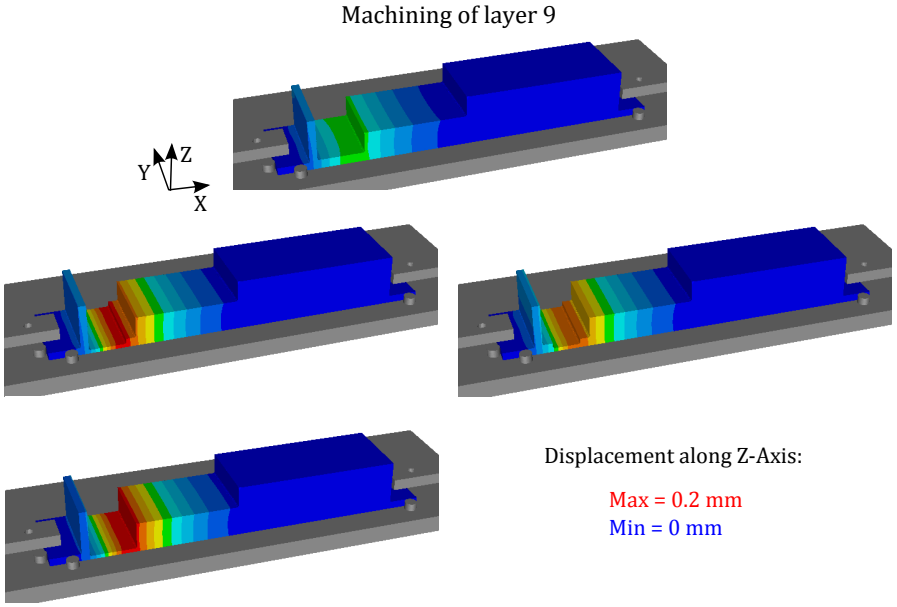

Figure 3.35: Simulation of the machining of the layer number 9 with an offset of 9.05 mm and the same machining sequence as in the reference case

In order to improve the accuracy of the machining process and to limit the phenomenon of overcutting, the redistribution of the residual stresses during the machining has to be mastered. The residual stresses therefore have to be redistributed gradually during the machining by taking into account the clamping areas and the dimensions of the machining features. A big feature placed in the middle of the part is rather subject to deflections during the machining than a small one next to a clamping area. For example, layer number 14 in Figure 3.25 will be more difficult to machine with the aim to avoid deflection than layer number 37. To obtain a progressive redistribution of the residual stresses during the machining, the machining sequence (tool path) has to be modified. The machining sequence used in the reference case did not take into account residual stresses and their possible effects on the machining accuracy. Only the simplicity of implementation and the machining time were considered. However, the workpiece deflections during the machining cannot be totally avoided. The new machining sequence has to be defined in a way such that the evolution of the geometry during the manufacturing only provokes small deflections all along the part instead of bigger deflections localised in the area where the machining is in progress.

A specific machining sequence has then been developed. This machining sequence is illustrated in Figure 3.36. The numbers represent the order of the machining. For each depth of cut, the milling tool will start the machining by crossing the workpiece at path No. 1, then No. 2, then No. 3 and so on.

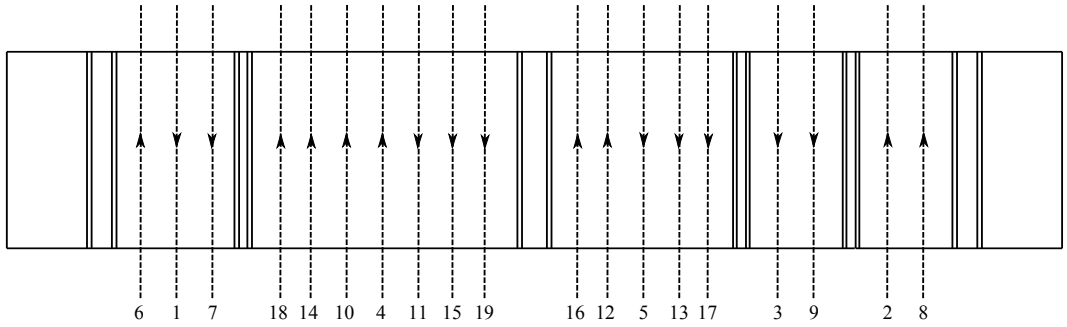

Figure 3.36: Illustration of the optimised tool path to take into account the residual stress redistribution effects on the machining accuracy. The numbers represent the order in which the passages of the milling tool are performed.

In this machining sequence, a first removal is performed near one clamp (path No. 1) before removing material near the other clamp (path No. 2 and No. 3). These removals allow to redistribute a part of the residual stress in keeping small deflections thanks to clamping. The following removals concern the layers located at the center of the part with one passage of the milling tool each. Each passage of the tool (No. 4 and No. 5) is located in the middle of the machining features. At the end of this step, the milling tool has realised one passage in each layer resulting in small deflections all along the part. The same procedure is then repeated to remove the rest of the layers.

As previously explained for the optimised offset, a simulation of the machining of the part

combining the optimised offset and the optimised machining sequence has been realised. Results obtained are depicted in Figure 3.37. As shown in Figure 3.37a the post-machining distortion is about 0.04 mm. The tolerance specification is therefore still respected. Regarding the variations of the thickness of the bottom wall, it can be observed in Figure 3.37b that the variations have clearly decreased, overcuts being almost zero all along the part.

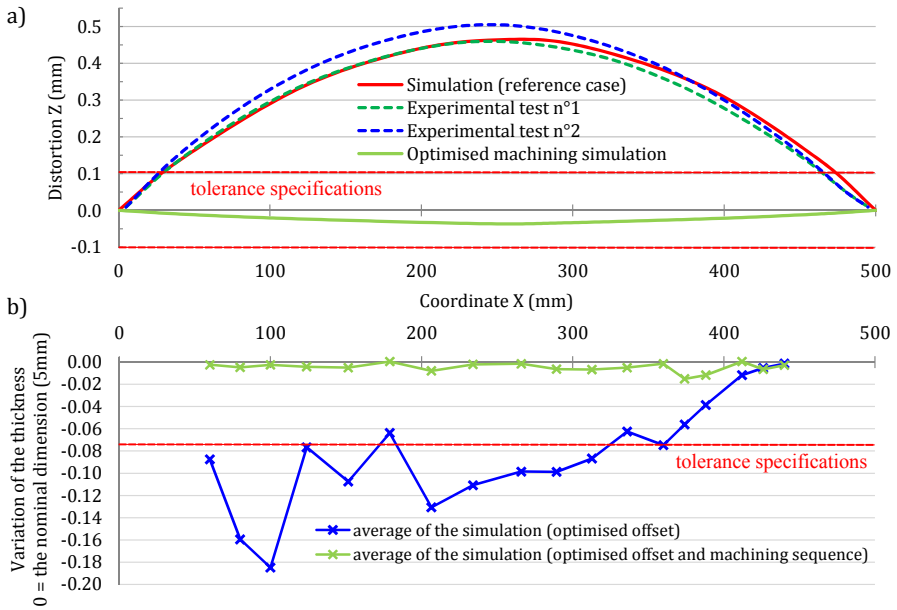

Figure 3.37: Simulation of the machining with an optimised offset and optimised machining sequence: a) Post-machining distortion of the part (curvature) ; b) Variation of thickness of the wall with a nominal dimension of 5 mm

The deflections observed during the simulation of the first five removals (numbered in Figure 3.25) of the last depth of cut with the optimised machining sequence can be seen in Figure 3.38. The biggest deflections occur during these removals.

In order to verify that the workpiece deflections during the machining are decreased using this optimised machining sequence, five numerical sensors have been placed along the X-axis of the part, as shown in Figure 3.39a. The displacements observed during the simulation of the machining with the optimised offset and the machining sequence of the reference case are depicted in Figure 3.39b. Significant displacements can be observed. It can also be seen that the deflections are indeed related to the machining sequence. In this case, the machining is first realised in the area of sensor 1 where the first significant displacements occur resulting in overcuts. It is then performed equally for sensor 2 and so on. Only small displacements are observed on sensor 5, which is placed in the last machined area. These small displacements are linked to the fact that the main part of the residual stresses has already been redistributed when the machining of this area is done. The displacements observed during the simulation of the machining with the optimised offset and the optimised machining sequence are depicted

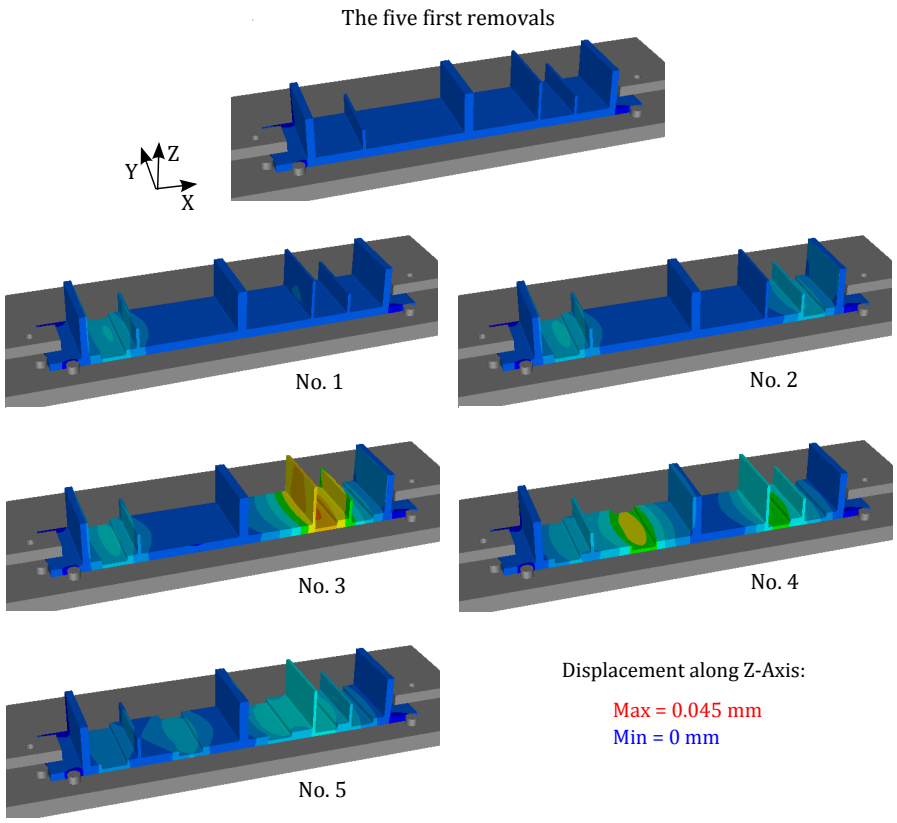

Figure 3.38: Simulation of the machining of the part with an offset of 9.05 mm and the optimised machining sequence: The deflections observed during the machining of the first five removals of the last depth of cut

in Figure 3.39c. A clear decrease in the displacements during the machining can be observed between the two machining sequences. All sensors have detected displacements during the machining with the optimised machining sequence but they are very small. The maximum amplitude of displacement is below 0.04 mm. This ensures that the maximum overcut which could occur during the machining stays below this value and that the tolerance specifications are thus respected.

These results show the feasibility to use the developed numerical tool and its associated models to predict the workpiece deflections during the machining as well as the post-machining distortion. A method based on numerical analysis to define or to validate a machining process plan and to improve the machining quality in taking into account the effects of the initial residual stresses is therefore possible. In varying important parameters of the machining process like the geometry of the initial workpiece, the offset and the machining sequence, it is possible to ensure the desired machining quality and to improve the robustness of the process. In addition, the CAD/CAM software product used to generate the removed volumes also allows to compare the machining time of each machining sequence. Using the same machine tool and cutting conditions as in the experimental machining of the reference case, the machining time for the two machining sequences (machining of the 37 layers) has been compared. The

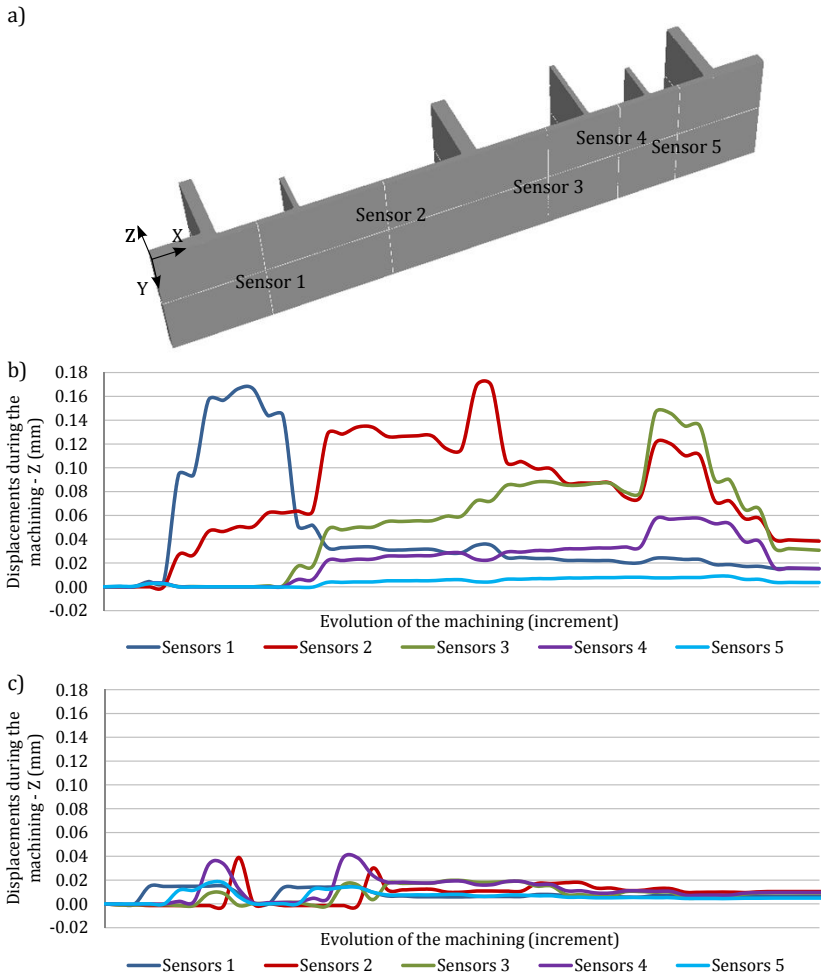

Figure 3.39: Analysis of the displacements during the machining depending on the machining sequence: a) The position of the numerical sensors to measure the displacements along the Z-axis ; b) Measurements of the displacements on the 5 sensors during the machining simulation with the optimised offset and the reference machining sequence ; c) Measurements of the displacements on the 5 sensors during the machining simulation with the optimised offset and optimised machining sequence

machining sequence of the reference case has a machining time of approximately 11 minutes whereas the optimised one has a machining time of about 14 minutes and 30 seconds. Using both the simulation results and CAD/CAM software, it can therefore be possible to define a machining sequence allowing to obtain the best compromise between machining quality and machining time.

3.4.3.2.2 The Depth of Cut

In order to ensure a better machining accuracy, in industry the last depth of cut of a machining feature is often chosen smaller than the previous ones. To evaluate the capability of the numerical tool to detect such an influence, a brief analysis of the depth of cut on the machining

accuracy is realised in this section. The simulation of the optimised machining process plan (optimised offset and machining sequence) with a depth of cut divided by two for the layers 9, 14, 23, 32 and 37 has been performed. The same tool path as the one presented in Figure 3.36 is used. The last 7 mm of material (depth of cut used previously) are therefore removed in performing two times a depth of cut of 3.5 mm. Note that the simulation and machining times are therefore doubled. Displacements during the machining have been measured using five numerical sensors located at the same positions as the ones in Figure 3.39a. The displacements observed during the machining simulation of the layers 9, 14, 23, 32 and 37 with the optimised machining sequence and with the depth of cut of 3.5 mm are depicted in Figure 3.40.

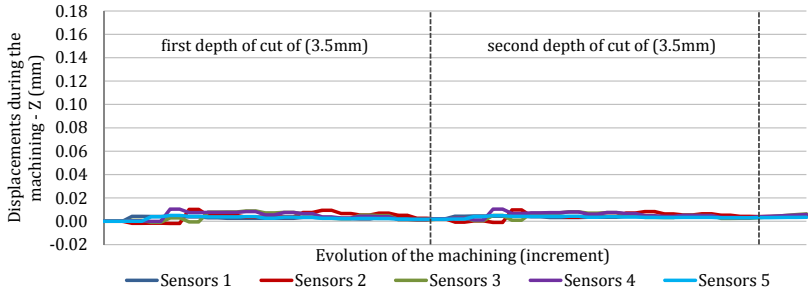

Figure 3.40: Analysis of the displacements during the machining with the optimised machining sequence and a depth of cut divided by two (3.5 mm) of the layers 9, 14, 23, 32 and 37

As expected, the decrease of the depth of cut gives a more gradual redistribution of the residual stresses during the machining. Almost no deflections can be observed during the whole machining simulation. It also become obvious that almost the same behaviour of the workpiece is obtained during the machining of the two steps (two times a depth of cut of 3.5 mm). The reduction of the depth of cut combined with the optimised offset and the optimised machining sequence allows to obtain nearly the geometry that has been designed (CAD).

3.4.4 Discussion

Two machining problems linked to the coupled effect of fixture layout, machining sequence and initial residual stresses have been highlighted in this simplified case. The first one is the post-machining distortion, which depends on the designed part geometry and the initial residual stresses. The second one is the deflections of the workpiece during the machining, resulting in overcuts and non-conformity of the part with the geometrical specifications. Using the developed numerical tool and appropriate models (models of Level 1 and Level 5-6), it has been shown that it is possible to adapt the machining process plan in order to take into consideration the effect of residual stresses on the machining quality.

It has thus been shown that a bigger initial workpiece with an optimal offset can be used to prevent the post-machining distortion of the part. Theoretically, the post-machining distortion can be suppressed in using the optimal offset, but due to the uncertainty in the residual stress

profiles it is difficult to guarantee that using the optimised offset the part will stay perfectly flat. However, the optimised offset allows to obtain a significant reduction of the post-machining distortion and to respect the tolerance specification (planarity). To determine the optimal offset, a relatively quick numerical analysis using a model of Level 1 can be performed.

In the case of the machining of a part where the fixture layout cannot be modified, an analysis of the critical steps of the machining, i.e. the areas where the workpiece deflections occur during the machining, can be realised. Depending on the phenomena observed, it has been shown that a machining sequence allowing a gradual redistribution of the residual stresses during the machining and therefore a minimising of the workpiece deflections during the machining can be found. This machining sequence allows to limit overcuts and to increase the accuracy of the machining while keeping the same cutting conditions and therefore to ensure the conformity of the part with the tolerance specifications. Such an analysis requires nevertheless accurate numerical models. A model of Level 5 or of Level 6 in some cases has to be used.

This study therefore shows the feasibility to use the developed specific numerical tool to optimise the machining process plan to improve the machining quality and to ensure conformity of the part with the geometrical and dimensional specifications in taking into consideration the initial residual stresses inside the workpiece and the geometry of the designed part. Simulations thus give the possibility to validate the process plan before going into real machining and to improve the accuracy and robustness of the machining process.

It has also been demonstrated that the numerical tool is able to exhibit the influence of the depth of cut on the machining quality and that this parameter can also be used to improve the machining accuracy in cases where the fixture cannot constrain the workpiece enough to limit the deflections during the machining.

3.5 Conclusion

In this chapter, the influence of the residual stresses inside workpieces taken from an AIRWARE® 2050 alloy rolled plate on the machining quality is studied.

In a first section, the layer removal method with strain gauge measurements used to determine residual stress profiles in a rolled plate is presented. The residual stress profiles of both a 70 mm thick and a 90 mm thick rolled plate are then obtained with this method. A strong anisotropy in the residual stress distributions can be observed. It can be concluded that while post-machining distortions could occur for parts machined from workpieces taken in the rolling direction, the risk of post-machining distortion in the transverse direction is relatively low.

In a second section, using the developed numerical tool, simulations of the layer removal method have been performed. A good agreement between experimentally measured strains and predicted strains is obtained, validating (with experimental results) the developed numer-

ical tool as well as the method to determine the initial residual stress profiles. This kind of simulation also opens new perspectives in the determination of the residual stress profiles.

Then an example of simulations for the prediction of the post-machining distortions is presented. The predicted distortion of the part is similar to the experimental ones, the only difference being observed at the two ends of the part (clamping areas). This example demonstrates again the validity of the developed numerical tool which enables to predict the post-machining distortion in function of the initial residual stress state and the geometry of the part. However, no difference on the post-machining distortion has been observed between a model of Level 1 and a model of Level 5. More in-depth analyses are therefore required to determine the influence of the different machining parameters on the machining quality.

In the last section, a machining case in which the two main problems of machining non-quality due to the redistribution of residual stresses are highlighted is presented. The first problem is the post-machining distortion and the second one is the deflections of the workpiece which occur during the machining and which can lead to dimensional as well as geometrical errors. The results obtained have demonstrated the capability of the numerical tool to predict the exact final part geometry. Indeed, a comparison with experimental measurements has shown that similar results are obtained for both the post-machining distortions and the dimensional errors. Then the feasibility to improve the machining quality using the developed numerical tool and appropriate models has been demonstrated. The influence of the initial workpiece, the machining sequence and of the depth of cut on the machining quality has then been observed.

3.6 Résumé en Français

Dans ce chapitre, l'influence des contraintes résiduelles présentes dans des blocs de matière prélevés dans des tôles laminées en alliage AIRWARE® 2050 sur la qualité d'usinage est étudiée.

Dans une première partie, la méthode par enlèvements de couches de matière (méthode du barreau) avec mesures par jauges de déformations qui est utilisée pour déterminer les profils de contraintes résiduelles dans des tôles laminées est présentée. Les profils de contraintes résiduelles d'une tôle de 70mm et 90mm sont ensuite obtenus avec cette méthode. La distribution des contraintes résiduelles montre qu'en fonction de la géométrie de la pièce usinée, des distorsions après débridage pourraient se produire, surtout si les pièces sont prélevées dans le sens de laminage.

Dans une deuxième partie, des simulations de la méthode par enlèvements de couches de matière ont été réalisées en utilisant l'outil numérique précédemment développé. Un bon accord entre les déformations prédites et mesurées expérimentalement est obtenu, validant ainsi l'outil numérique et la méthode pour déterminer les profils des contraintes résiduelles initiales. Ce type de simulations permet également d'ouvrir de nouvelles perspectives dans la détermination des profils de contraintes résiduelles.

Un exemple de simulation pour la prédiction de distorsions est présenté. La distorsion prédite est similaire à celles observées expérimentalement, la seule différence étant observée aux extrémités des pièces (zones de bridage). Cet exemple démontre de nouveau la validité de l'outil numérique développé qui permet de prédire les distorsions après débridage en fonction de l'état de contraintes résiduelles et de la géométrie de la pièce. Cependant, aucune différence sur les distorsions prédites entre un modèle de Niveau 1 et un modèle de Niveau 5 n'a pu être observée. Des analyses plus approfondies sont donc nécessaires pour déterminer l'influence des différents paramètres d'usinage sur la qualité d'usinage.

Dans la dernière partie de ce chapitre, on traite un cas d'usinage de pièce pour lequel les deux principaux problèmes de non qualité d'usinage dus à la redistribution des contraintes résiduelles sont présentés. Ces problèmes sont les distorsions obtenues après usinage et débridage de la pièce et les déformations pendant l'usinage qui peuvent conduire à des imprécisions d'usinage et donc des erreurs dimensionnelles et géométriques sur la pièce finale. Les résultats obtenus ont ainsi permis de démontrer la capacité de l'outil numérique à prédire la géométrie exacte de la pièce usinée. En effet, des résultats similaires à ceux obtenus lors de tests expérimentaux ont été obtenus, que ce soit pour les distorsions ou les variations d'épaisseurs (erreurs dimensionnelles). La faisabilité d'améliorer la qualité d'usinage en utilisant l'outil numérique développé a ensuite été démontrée. A l'aide de modèles appropriés, l'influence du choix du bloc initial de matière, de la séquence d'usinage et de la profondeur de passe sur la qualité d'usinage ont ainsi pu être étudiées.

Chapter 4

Machining Process Plan Optimisation

In order to determine the influence of the initial residual stresses, the fixture layout and the machining sequence on the machining quality of a part machined from an AIRWARE® 2050-T84 alloy rolled plate, a complete study has to be performed. In this Chapter, such a study applied on a part requiring several machining steps is presented.

After a validation of the models by comparison with experimental results, multiple machining process plans are numerically tested. Results are then analysed and a classification of the influence of the parameters can be done.

A methodology for the definition of machining process plans adapted to the mechanical behaviour of the workpieces (initial residual stresses) and allowing to obtain the desired machining quality is then presented.

Contents

4.1 Influence of the Parameters

In a first step, a preliminary study has been realised to determine a specific part geometry allowing the definition of multiple machining process plans and requiring multiple machining steps. This part is depicted in Figure 4.1 and can be considered as a representative example of a structural aeronautical part (at a smaller scale) both in terms of percentage of the volume of material removed during the machining (~ 80%) and of machining feature geometries.

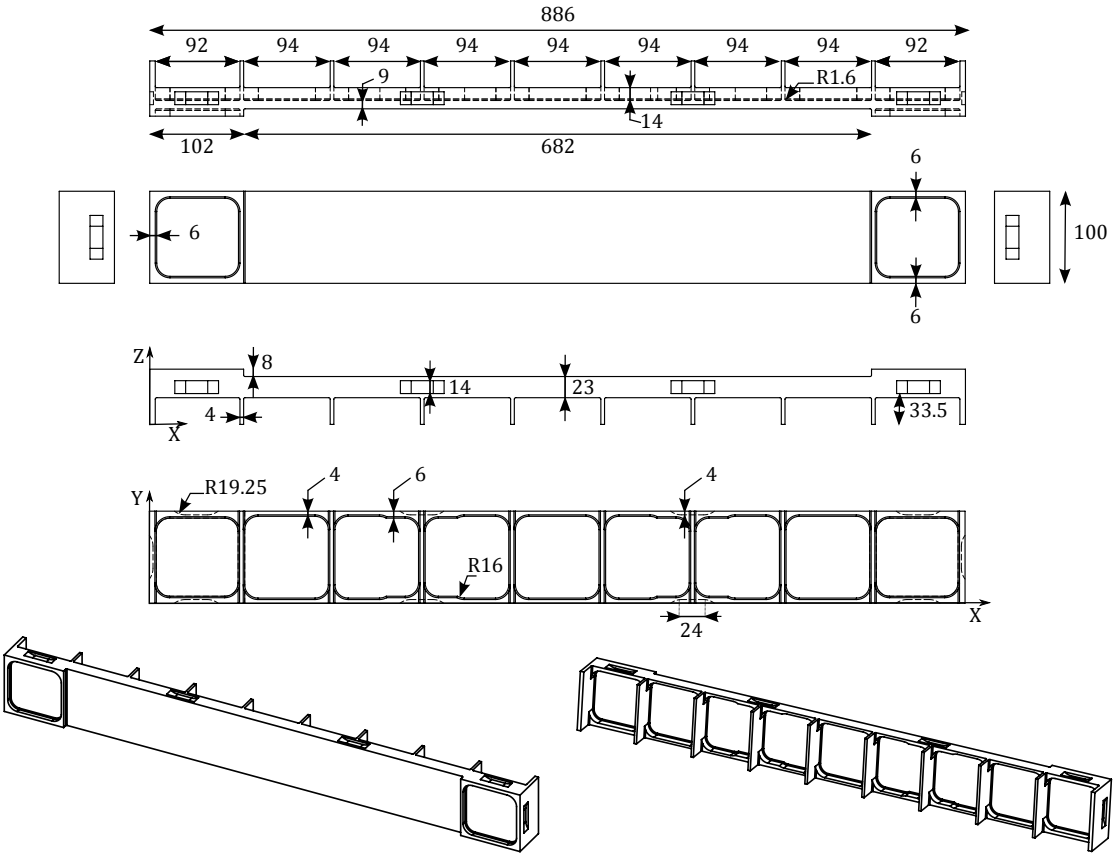

Figure 4.1: The part geometry

4.1.1 Machining Process Plan Parameters

In this section, the various fixture layouts and machining sequences used in this study to machine the part depicted in Figure 4.1 are presented in detail.

4.1.1.1 Machining Sequences

In order to obtain the final part geometry presented in Figure 4.1 two machining steps are required. However, before starting these machining steps the initial workpiece has to be

prepared. This consists in face-milling operations to reduce the thickness of the initial block of material taken from the rolled plate to 60 mm and in the machining of ten clamping grooves of 24×4×14 mm on the sides of the workpiece, as illustrated in Figure 4.1. At the end of this preparation step the initial workpiece of 886×100×60 mm represented in Figure 4.2 is obtained.

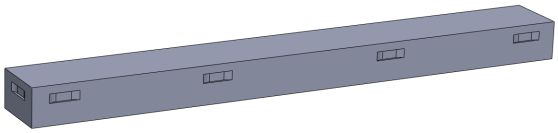

Figure 4.2: The initial workpiece (prepared initial block of material)

After preparing the initial workpiece, two machining steps have to be performed to obtain the final part. The first step consists in the machining of the three machining features located on the top surface of the workpiece. Based on the numerical approach and a model of Level 5, the material removed during this machining step has been discretized in six numerical material removal steps, as illustrated in Figure 4.3. During this machining step, the depth of cut has been fixed to 4 mm.

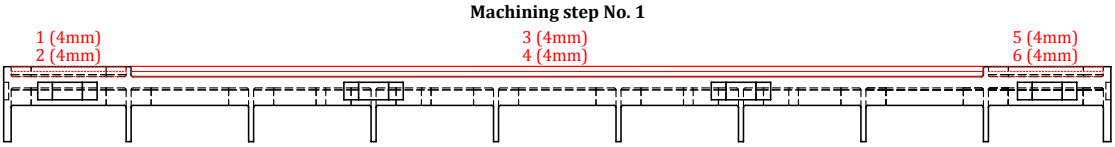

Figure 4.3: The discretization of the first machining step: six material removals with a depth of cut of 4 mm are used to numerically machine these machining features

When the first machining step is finished, the workpiece is flipped in order to perform the second machining step, during which most of the material is removed. By also considering a model of Level 5, this machining step has been discretized in sixty-three numerical material removal steps, as illustrated in Figure 4.4.

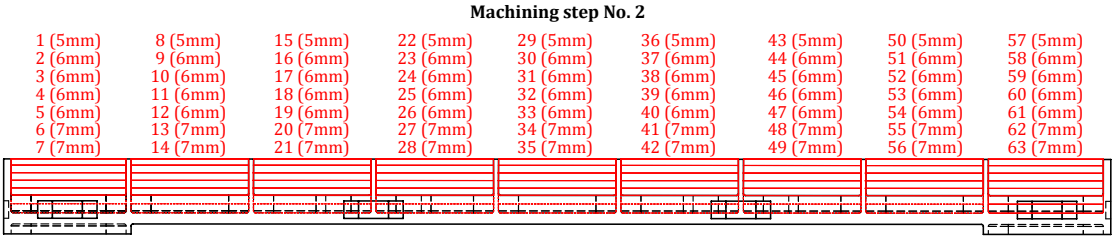

Figure 4.4: The discretization of the second machining step: sixty-three material removals with varying depths of cut (from 5 to 7 mm) are used to numerically machine these machining features

Based on these machining step discretizations, two different machining sequences have been defined. Depending on the machining sequence used, the order in which the numbered

material removals in Figure 4.3 and 4.4 are removed will be different. The machining sequences used in this study are given in Table 4.1.

Table 4.1: Description of the two machining sequences: order of the material removals (S = machining sequence)

Machining step No. 1	S1	1 - 2 - 3 - 4 - 5 - 6
	S2	3 - 1 - 5 - 4 - 2 - 6
Machining step No. 2	S1	1 - 2 - 3 - 4 - 5 - 6 - 7 - 8 - 9 - 10 - 11 - 12 - 13 - 14 - 15 - 16 - 17 - 18 - 19 - 20 - 21 - 22 - 23 - 24 - 25 - 26 - 27 - 28 - 29 - 30 - 31 - 32 - 33 - 34 - 35 - 36 - 37 - 38 - 39 - 40 - 41 - 42 - 43 - 44 - 45 - 46 - 47 - 48 - 49 - 50 - 51 - 52 - 53 - 54 - 55 - 56 - 57 - 58 - 59 - 60 - 61 - 62 - 63
	S2	29 - 36 - 22 - 15 - 43 - 50 - 8 - 1 - 57 - 30 - 37 - 23 - 16 - 44 - 51 - 9 - 2 - 58 - 31 - 38 - 24 - 17 - 45 - 52 - 10 - 3 - 59 - 32 - 39 - 25 - 18 - 46 - 53 - 11 - 4 - 60 - 33 - 40 - 26 - 19 - 47 - 54 - 12 - 5 - 61 - 34 - 41 - 27 - 20 - 48 - 55 - 13 - 6 - 62 - 35 - 42 - 28 - 21 - 49 - 56 - 14 - 7 - 63

For both machining sequences, similar machining times are observed (estimated with CAM software products). The machining time for the first machining step changes from 6 min 25 s for sequence S1 to 6 min 38 s for sequence S2. For the second machining step, the machining time evolves from 38 min 26 s for sequence S1 to 40 min 03 s for sequence S2.

4.1.1.2 Fixture Layouts

The machining of this part requiring two machining steps, the fixture influence on the machining quality is enhanced. Using the ten grooves machined during the initial workpiece preparation step, four fixture layouts have been defined. Each fixture layout is composed of one table and three locators. The number of clamps used in each fixture layout varies from two to ten, as shown in Figure 4.5a. The clamping force is fixed to 12 kN per clamp. When an eight or ten clamps configuration is used, supports are added for the second machining step in order to ensure a good positioning and to avoid deflections of the workpiece due to the clamping forces, as illustrated in Figure 4.5b. During all the simulations the fixture elements are considered as rigid bodies.

4.1.2 Machining Quality Evaluation: Measurements

As in Chapter 3, the evaluation of the machining quality is performed based on two criteria. The first one is the post-machining distortion, which is measured at the end of each machining step (after the unclamping). The post-machining distortion represents the curvature of the part and is measured on the top and bottom surfaces, as represented by the arrows in Figure 4.6a. The second criterion is the dimensional variations, which represents the machining accuracy and which is evaluated by measuring the thickness variations of the wall with a nominal dimension of 9 mm (parallel to the top and bottom surfaces of the workpiece). These

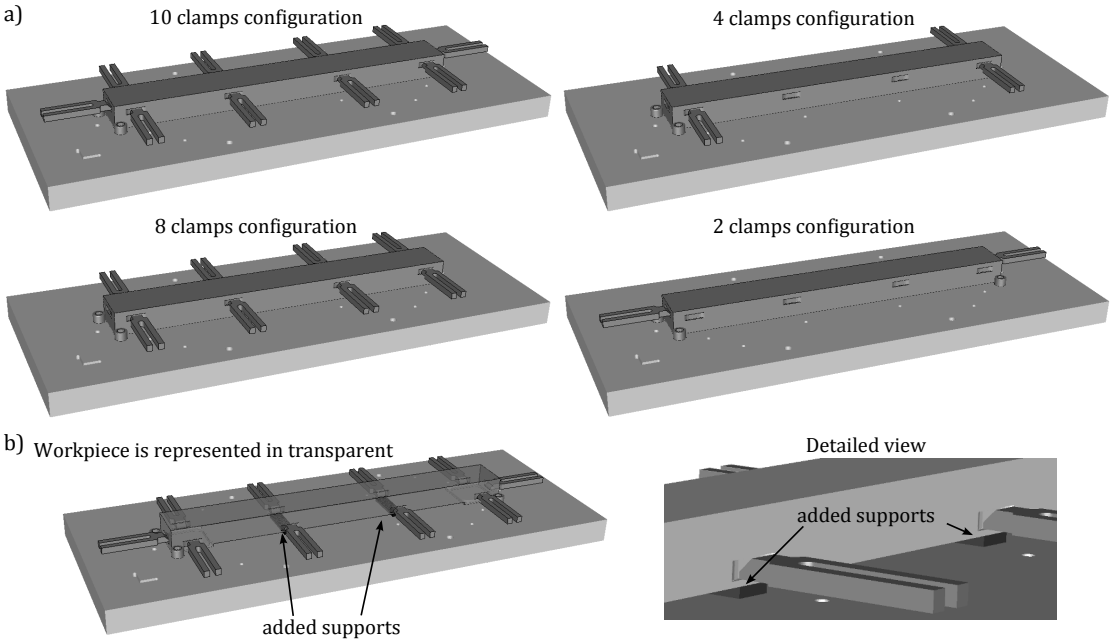

Figure 4.5: Fixture: a) The four different fixture layouts in function of the number of clamps used ; b) Supports are added for the eight and ten clamps configuration for the second machining step

measurements therefore allow to analyse the overcuts and/or undercuts which can occur during the machining due to the workpiece deflections. Twenty-seven thickness measurements are realised throughout the length of the part, as represented in Figure 4.6b.

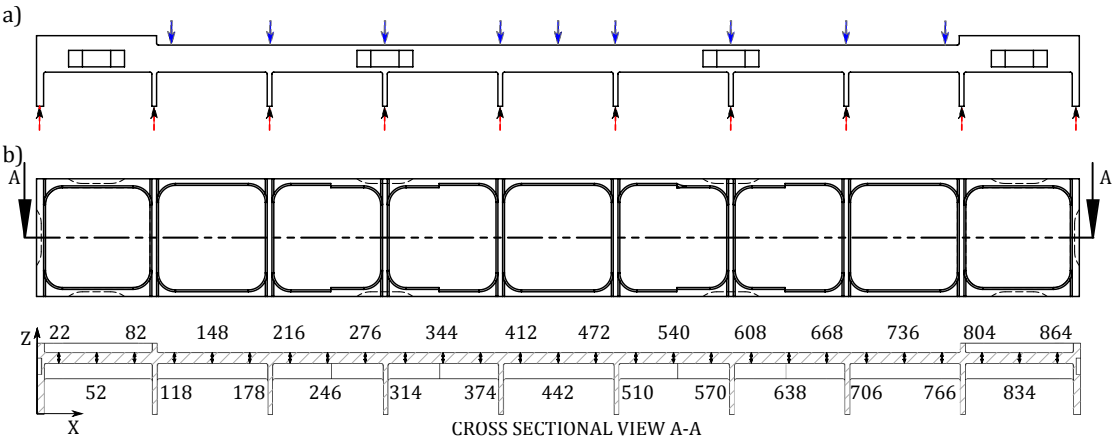

Figure 4.6: Representation of the measurements performed for the machining quality evaluation. The arrows represent the measurement zones: a) Post-machining distortion measurements on the top and bottom surfaces of the part ; b) Coordinates for thickness measurements of the wall with a nominal value of 9 mm

4.1.3 Machining Process Plans with a 70 mm Thick Rolled Plate: Minimal Use of Material

In this section, a complete analysis of the influence of the parameters by combining the four fixture layouts and the two machining sequences is realised. A total of eight machining configurations have therefore been tested. In a first step, the simulation of the initial workpiece preparation is realised once and the simulation of the first clamping step is performed once per fixture layout. Then, for each machining configuration, the first machining step and its associated unclamping are simulated. The workpiece is then flipped and the simulations of the clamping, of the second machining step and of the unclamping are realised. Due to the large number of configurations, only a few of these have been experimentally performed. All the experimental tests and associated measurements have been realised at IFMA.

An initial block of 886×100×70 mm taken from a 70 mm thick AIRWARE®2050-T84 rolled plate in the rolling direction is considered. This configuration allows a minimal use of material. The residual stress profiles used are the ones presented in Figure 3.9 (Section 3.2.1). The initial block of material being 70 mm thick, 5 mm on both the top and the bottom surface are removed during the preparation step to obtain the 886×100×60 mm initial workpiece.

At the end of the preparation step, the initial workpiece with its residual stress state and its mesh adapted to the simulation of the machining of the part is therefore obtained. In order to ensure an accurate capture of the phenomena which could occur during the machining as well as to ensure an accurate fixture-workpiece contact modelling in the clamping zones different mesh sizes have been defined depending on the part geometry, as shown in Figure 4.7.

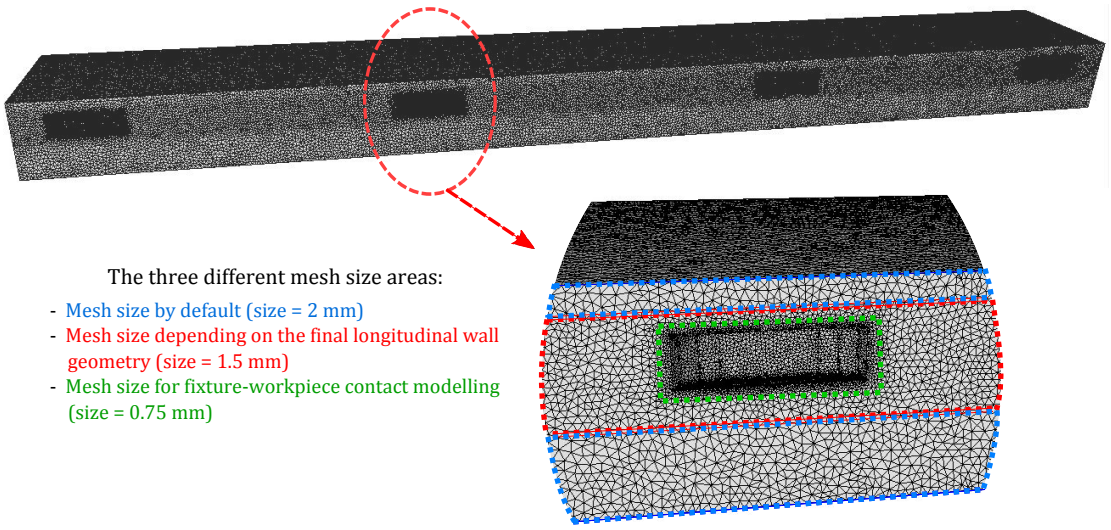

Figure 4.7: The initial mesh representing the prepared workpiece: Different mesh sizes have been defined depending on the final part geometry and the fixture-workpiece contact

4.1.3.1 Experimental Validation

Eight machining configurations have been numerically evaluated using this initial workpiece. As mentioned previously, due to the large number of configurations only a few of them have been experimentally tested. In a first step, experimental machining tests have been conducted using three different fixture layouts with the machining sequence S1. In a second step, one of these experimental tests has been performed again using the other machining sequence. Table 4.2 summarises the numerical and experimental tests realised with the initial workpiece taken from a 70 mm thick rolled plate.

Table 4.2: The numerically and experimentally tested machining configurations

Configuration	Numerical machining process plans		Experimental Tests
	Fixture layout	Machining sequence	
No. 1	2 Clamps	S1	✓
No. 2	2 Clamps	S2	✓
No. 3	4 Clamps	S1	✓
No. 4	4 Clamps	S2	-
No. 5	8 Clamps	S1	✓
No. 6	8 Clamps	S2	-
No. 7	10 Clamps	S1	-
No. 8	10 Clamps	S2	-

In a first step, three different machining process plans have been defined to machine this part. In these tests, the machining sequence S1 and three different fixture layouts are used (configurations No. 1, 3 and 5). The machining steps and measurements have been performed both numerically and experimentally (tests at IFMA). Using a CMM, the post-machining distortions after each machining step are measured and thickness measurements are performed on the final machined part. Whereas machining configurations No. 3 and 5 have been repeated several times, the configuration No. 1 has been performed only once.

Results obtained for the simulations and the experimental tests are depicted in Figure 4.8. For both machining steps a good agreement is obtained between experimental and simulation post-machining distortions (see Figures 4.8a and 4.8b). The same post-machining distortions are observed numerically for the three machining tests. Experimentally, only small variations in the post-machining distortion amplitudes are observed without clear trends. A change in the curvature is also visible when comparing the first and the second machining step.

Regarding the thickness variations, depicted in Figure 4.8c, similar trends between experimental tests and simulations are obtained depending on the fixture layout used. As mentioned previously, error bars are only depicted for configurations No. 3 and 5 as they have been tested several times experimentally. Principally positive values are observed for the three tests, i.e. the measured dimensions are greater than the 9 mm expected and mainly undercuts occur during the machining. Some differences between the experimental and numerical results are visible and can be partly explained by the experimental uncertainty.

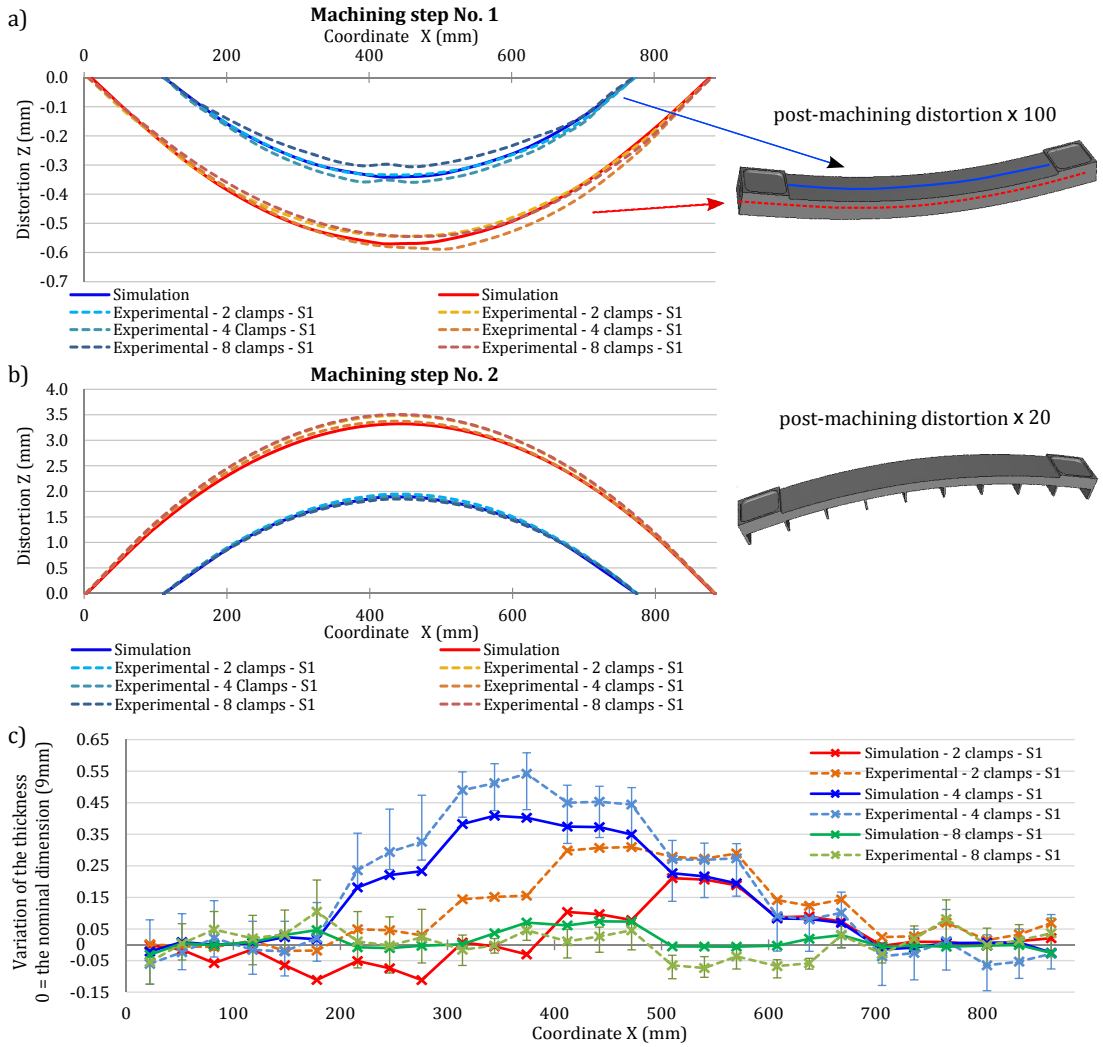

Figure 4.8: Comparison between experimental and simulation results with different fixture layouts and using the machining sequence S1: a) Post-machining distortion after the machining step No. 1 ; b) Post-machining distortion after the machining step No. 2 ; c) Variation of thickness of the wall with a nominal dimension of 9 mm (0 = nominal dimension)

In a second step, a machining process plan using a fixture layout with two clamps and with the machining sequence S2 has been tested (configuration No. 2). As for the configuration No. 1, it had only been possible to perform one experimental test. The objective is to compare experimental and simulation results depending on the machining sequence. Similarly to the first three tests, the post-machining distortion after each machining step as well as the thickness variations on the final machined part have been measured, as illustrated in Figures 4.9a, b and c. Similar results between experimental and simulation results are also obtained in this case, as well as no change in the post-machining distortion amplitudes. However, clear differences in the thickness variations of the wall can be observed between the two machining sequences. Whereas principally undercuts are obtained for the machining sequence S1, overcuts occur

during the machining with the machining sequence S2. The reasons of these differences are discussed later in Section 4.1.3.2.

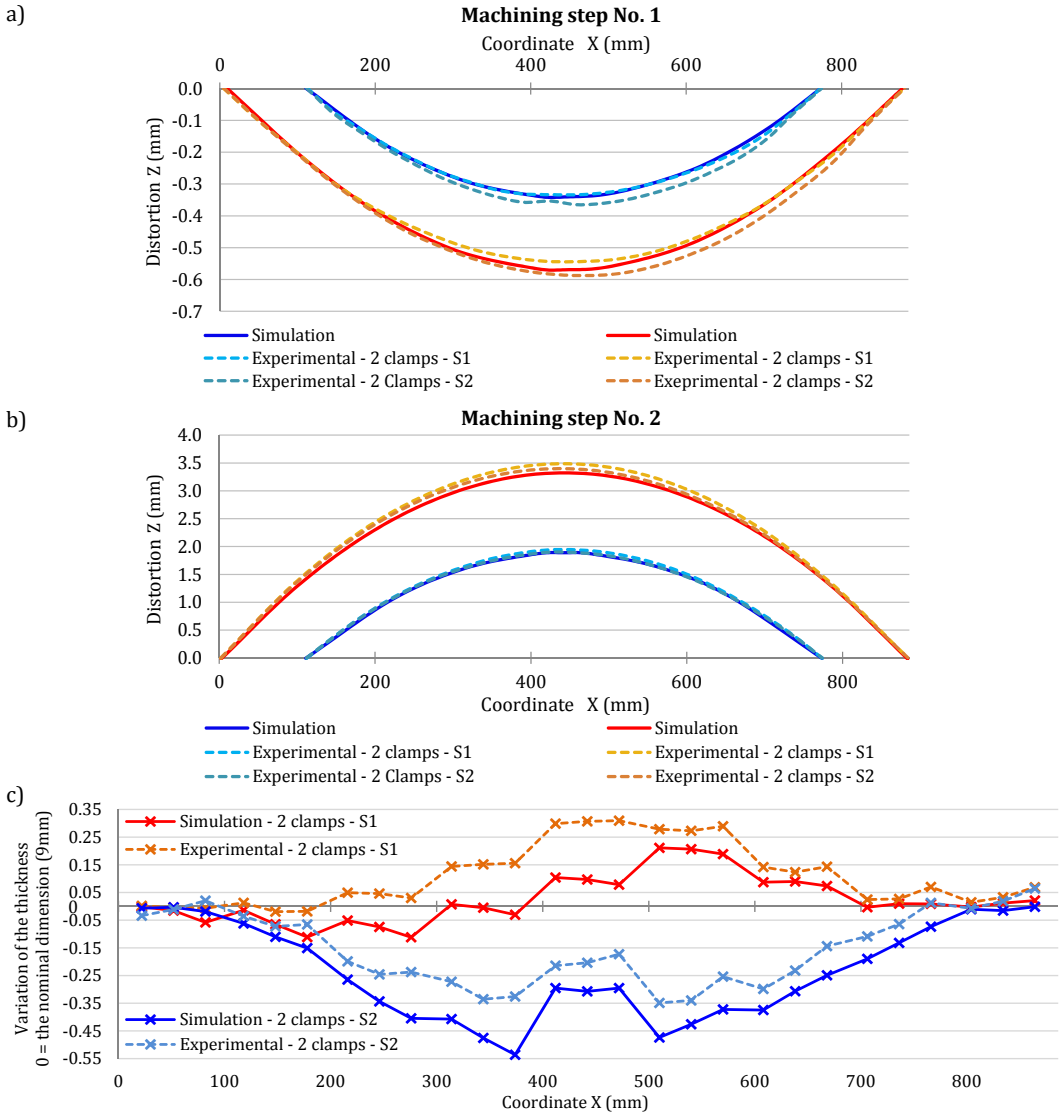

Figure 4.9: Comparison between experimental and simulation results with different machining sequences and using the two clamps fixture layout: a) Post-machining distortion after the machining step No. 1 ; b) Post-machining distortion after the machining step No. 2 ; c) Variation of thickness of the wall with a nominal dimension of 9 mm (0 = nominal dimension)

No influence on the post-machining distortion but clear effects on the machining accuracy can be observed in these tests (experimentally and numerically). In Figure 4.10 the fixture layout influence (a) and the machining sequence influence (b) on the maximal thickness variation obtained experimentally and numerically are compared. This criterion has been chosen because the maximal thickness is one of the criteria enabling to determine if the final part geometry conforms with the desired dimensional specifications. It can be observed

that the predicted influences of the parameters on the machining quality are similar to the experimental ones.

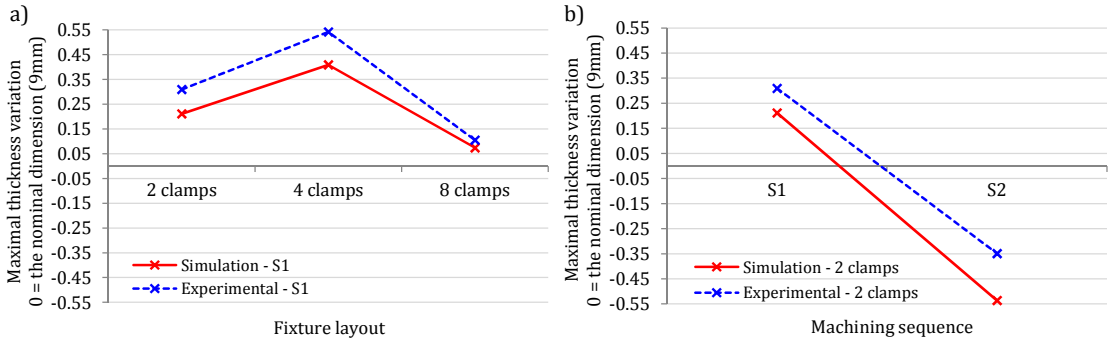

Figure 4.10: Comparison between the machining process parameter influence obtained experimentally and numerically: a) Influence of the clamping fixture on the machining accuracy ; b) Influence of the machining sequence on the machining accuracy

The numerical and experimental results are qualitatively and quantitatively similar in terms of post-machining distortions and dimensional variations. It can be concluded that the developed numerical tool is able to predict both the post-machining distortions and the workpiece deflections during the machining and can thus predict the final part geometry depending on the machining process plan used. The numerical tool can therefore be used to perform a complete influence analysis on the machining process plan parameters.

4.1.3.2 Influence Analysis

The predicted machined part geometries having been validated in the tests presented above, the remaining machining process plans defined in Table 4.2 have been simulated.

As for the previous tests, neither the fixture layout nor the machining sequence have an effect on the post-machining distortion. In all the cases, similar post-machining distortions to the ones observed in Figures 4.8 and 4.9 are obtained for both machining steps. However, a clear impact of the two parameters on the machining accuracy can be observed. This can be explained by the fact that the thickness variations do not change the residual stress state of the machined part strongly enough to observe a clear impact on the post-machining distortions. The different results observed in the thickness variations (machining accuracy) for the eight machining process plans simulated are depicted in Figures 4.11 and 4.12. Results plotted in function of the machining sequences can be found in Figures of the Appendix D.1.

It can be observed that mainly undercuts are obtained with the machining sequence S1 (see Figure 4.11) whereas mainly overcuts are obtained with the machining sequence S2 (see Figure 4.12). This phenomenon shows the influence of the redistribution of the residual stresses on the behaviour of the workpiece during the machining.

To illustrate this behaviour, the cases of the second machining step with the configurations

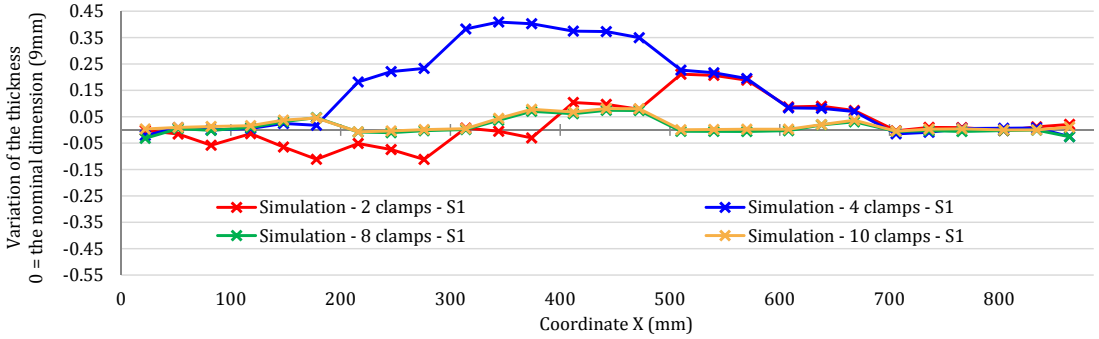

Figure 4.11: Thickness variations of the wall with a nominal dimension of 9 mm with the machining sequence S1 and four different fixture layouts

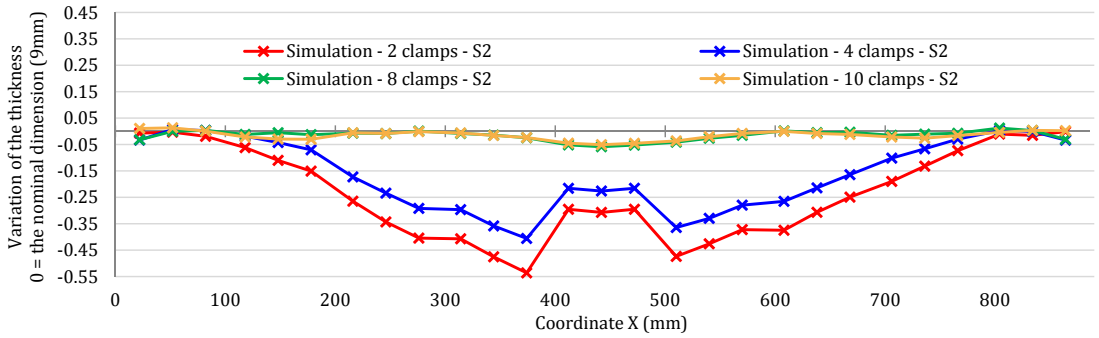

Figure 4.12: Thickness variations of the wall with a nominal dimension of 9 mm with the machining sequence S2 and four different fixture layouts

No. 3 and No. 4 are considered. The workpiece is therefore held with two clamps at each end (4 clamps in total). Depending on the machining sequence the material is removed differently. For the machining sequence S1, the material is removed from one end to the other. In the middle of the machining sequence, a significant difference in the behaviour of the workpiece is therefore obtained between the workpiece section which has already been machined and the one which has not yet been. Whereas the machined section wants to distort in a "∪" shape due to the residual stresses (bending moment) the other section resists and even wants to distort in the other direction, like after the first machining step. The clamping prevents any deflection at the ends of the workpiece but not in the central section. The machining with the sequence S1 causes deflections resulting in a "wave" which progresses along the workpiece together with the material removals, as illustrated in Figure 4.13a.
For the machining sequence S2, the material is removed gradually depending on the depth of cut. In the middle of the machining sequence the wokpiece has therefore approximately the same behaviour and wants to distort in a "∪" shape. However, during the machining of the last depth of cut, deflections occur due to the fact that the last removals located in the middle of the part provoke a change in the residual stress state. The two ends are held by the clamps but still want to distort in a "∪" shape. In the middle section of the workpiece, the bending moment and the rigidity are less significant due to the removal of the last depth of cut. During

the machining with the machining sequence S2 the redistribution of the residual stresses therefore leads to a positive Z-axis displacement of the middle section of the workpiece, as illustrated in Figure 4.13b.

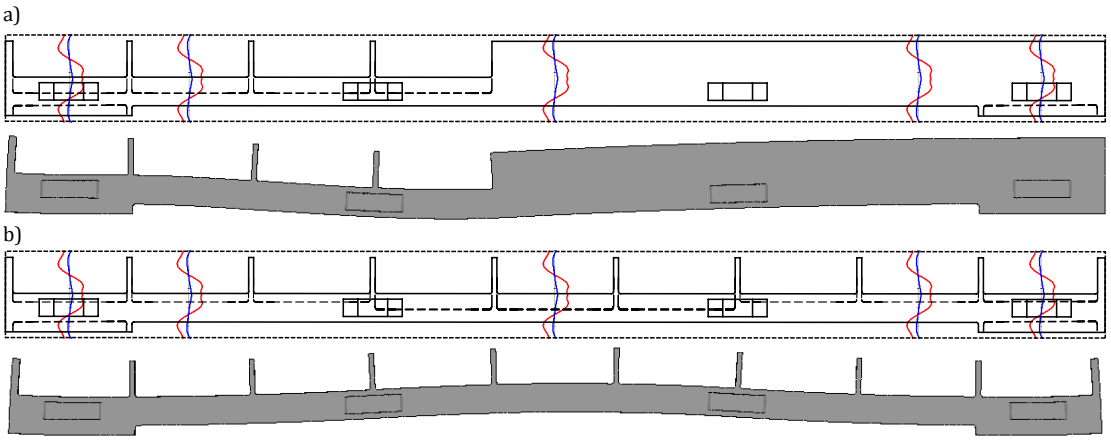

Figure 4.13: Deflections of the workpiece (× 25) observed during the second machining step with the two machining sequences: a) Machining sequence S1 leading to undercut ; b) Machining sequence S2 leading to overcut

The machining sequence can thus lead to an opposite behaviour of the workpiece and can lead to overcuts or undercuts. It can also be observed that the more clamps are used the smaller the deflections of the workpiece occurring during the machining become, leading to smaller overcuts or undercuts. In addition, the fixture layout plays also an important role in the machining accuracy by constraining the workpiece in the desired location. The importance of the fixture layout is even increased when dealing with machining of parts requiring multiple machining steps. Indeed, after the first machining step, the workpiece is unclamped and post-machining distortions are observed. The fixture layout used for the next machining step has then to ensure that the workpiece is constrained in the desired location and also with the desired shape, i.e. as if zero post-machining distortion had been obtained after the previous machining step. The fixture layout therefore has to allow to suppress the post-machining distortion due to the previous machining step when the workpiece is clamped. In Figure 4.14 the workpiece deflections observed after the clamping for the second machining step are depicted. It can be observed that for a two clamps configuration the post-machining distortions after the first machining step are not decreased and that for the eight and ten clamps configurations the desired shape of the workpiece is almost obtained.

The combined effect of the workpiece deflections after clamping and the deflections observed during machining with the configuration No. 1 (two clamps configuration) explains why the thickness variations are smaller than for the configuration No. 3 (four clamps configuration). Indeed, during the machining significant deflections are observed ($\backsim$0.6 mm in the case of the configuration No. 1). These deflections therefore compensate the deflection of the workpiece observed after clamping due to the post-machining distortion of the first machining step, as shown in Figure 4.14.

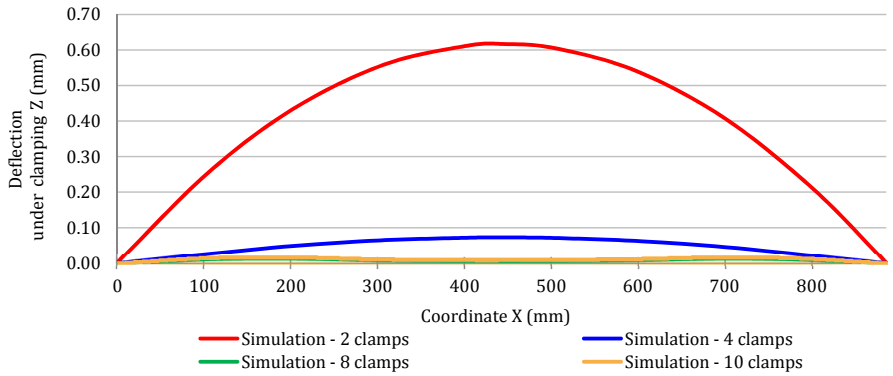

Figure 4.14: Deflections of the workpiece at the beginning of the second machining step (after clamping)

The influence of the machining sequence and of the fixture layout on the maximal thickness variations have then been studied. Results obtained are depicted in Figure 4.15. It can be observed that both these parameters can have an influence on the machining accuracy. A fixture layout allowing to strongly constrain the workpiece and to obtain the desired location and shape, like the eight and ten clamps configurations, can significantly improve the accuracy. The machining sequence also has a significant influence when a fixture layout ensuring only a minimal constrain of the workpiece is used. For this reason almost no more influence of the machining sequence is observed for the machining process plans with the eight and ten clamps configurations.

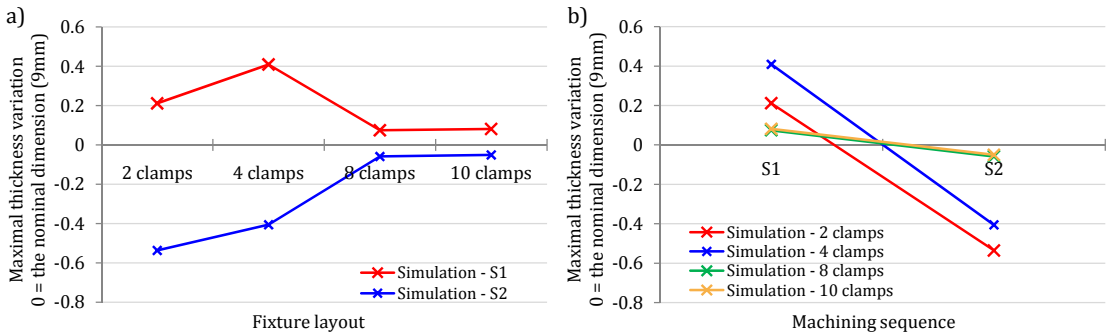

Figure 4.15: Influence of the machining process parameter obtained: a) Influence of the clamping fixture on the machining accuracy ; b) Influence of the machining sequence on the machining accuracy

4.1.4 Machining Process Plans with a 90 mm Thick Rolled Plate

An initial block of 886×100×90 mm taken from a 90 mm thick AIRWARE®2050-T84 rolled plate in the rolling direction is now considered. The residual stress profiles used are the ones presented in Figure 3.10 (Section 3.2.1).

4.1.4.1 Offset Analysis

The initial block of material being 90 mm thick, an offset analysis using the same method as presented in section 3.4.3.1 is performed. The objective is the determination of an optimal offset allowing to obtain a post-machining distortion of almost zero. The post-machining distortion being mainly due to the 23 mm longitudinal walls, the offset has to be defined in a way to obtain a bending moment of almost zero in these areas. A numerical analysis of the offset has thus been performed. The principal results of the offset analysis are depicted in Figure 4.16.

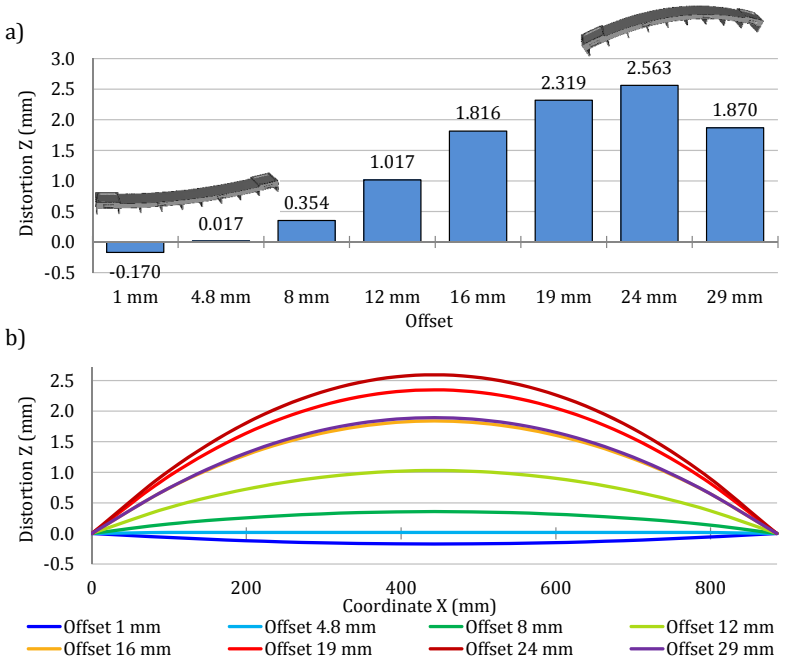

Figure 4.16: Numerical analysis of the offset: a) Maximum distortion observed in function of the offset ; b) Post-machining distortion in function of the offset

It can be observed that an inversion of the curvature is obtained depending on the offset used. An optimal offset can therefore be determined. As illustrated in Figure 4.17, an offset of 4.8 mm enables to obtain a bending moment of almost zero resulting in a significant reduction of the post-machining distortion. This offset can therefore be considered as the optimal one. Indeed, with this offset the longitudinal walls of 23 mm are almost centred on the neutral axis. The offset does not position the longitudinal walls perfectly centred due to the additional bending moments provoked by the residual stresses in the wall thickness of 9 mm and in the two ends of the part. These bending moments have to be compensated by slightly misaligning the middle of the longitudinal walls from the neutral axis.

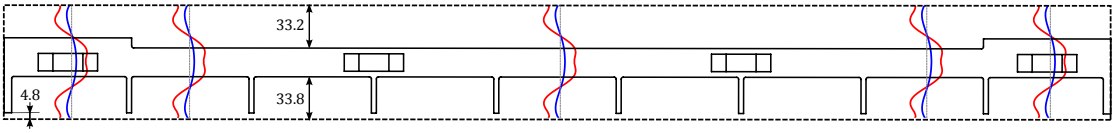

Figure 4.17: The optimal offset for the machining of the part in a 90 mm thick rolled plate with the residual stress profiles

4.1.4.2 Experimental Validation

The same machining process plans as used for the 70 mm thick initial workpiece have been numerically tested with this initial wokpiece. The configuration using four clamps and the machining sequence S1 (configuration No. 3) has also been experimentally realised (several times). This test had as an objective to validate the optimal offset determined previously with the offset analysis. A summary of the numerical and experimental tests is given in Table 4.3.

Table 4.3: The numerically and experimentally tested machining configurations

Numerical machining process plans		Experimental Tests
Fixture layout	Machining sequence	
2 Clamps	S1	-
2 Clamps	S2	-
4 Clamps	S1	✓
4 Clamps	S2	-
8 Clamps	S1	-
8 Clamps	S2	-
10 Clamps	S1	-
10 Clamps	S2	-

Simulation and experimental results obtained are compared in Figure 4.18. A good agreement is achieved for the post-machining distortions of both machining steps, as illustrated in Figure 4.18a and 4.18b. A maximum discrepancy of 0.06 mm is obtained between the experimental and the numerical final post-machining distortion (experimental value exceeding the numerical ones). A comparison can also be performed with the case of machining of the 70 mm thick rolled plate. Whereas the post-machining distortion after the first machining step is bigger with the 90 mm thick initial workpiece, the post-machining distortion obtained at the end of the second machining step is smaller, showing the validity of the optimal offset value. The maximal post-machining distortion goes from about 3.5 mm with the 70 mm thick rolled plate to almost zero with the 90 mm thick rolled plate.

Regarding the thickness variations, depicted in Figure 4.18c, similar trends between experimental and simulation results are visible. Some differences at one end of the part occur. Whereas the dimensions are almost equal to the nominal dimension in the simulation, overcuts can be observed experimentally. This could be partly explained by the experimental uncertainty which is linked to a small parallelism problem between the fixture body and the

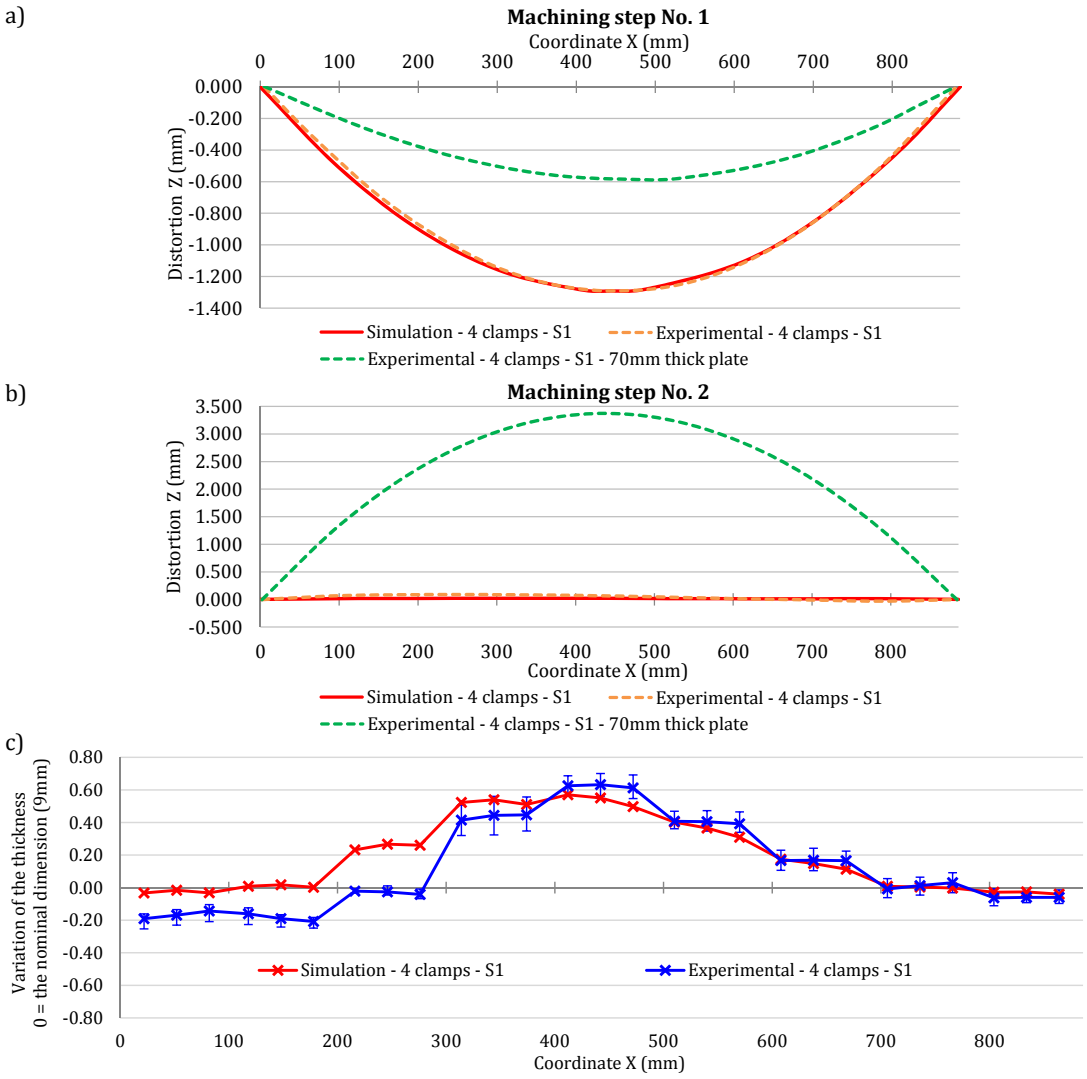

Figure 4.18: Comparison between experimental and simulation results for the machining process plan using a four clamps configuration and the machining sequence S1: a) Post-machining distortion after the machining step No. 1 ; b) Post-machining distortion after the machining step No. 2 ; c) Variation of thickness of the wall with a nominal dimension of 9 mm (0 = nominal dimension)

machine-tool table or even a small mistake in the tool-setting dimensions. It can also be observed that significant undercuts are obtained and that globally a good agreement between experimental and simulation results is reached.

4.1.4.3 Influence Analysis

The optimal offset being validated in the test presented above, the other machining process plans defined in Table 4.3 have been simulated.

No effect of the fixture layout nor of the machining sequence have been observed on the post-machining distortion after the first machining step. Figure 4.19 shows an example of the post-machining distortion obtained with the machining sequence S1 in function of the fixture layout used.

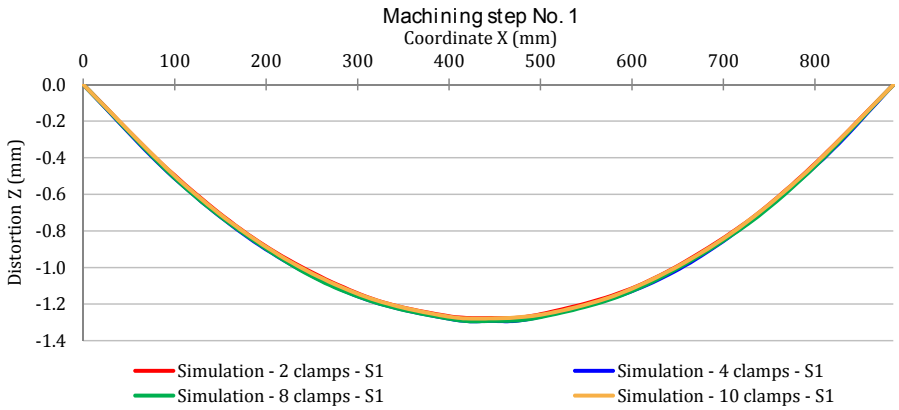

Figure 4.19: Influence of the fixture layout on the post-machining distortion after the first machining step with the machining sequence S1

After the second machining sequence, the post-machining distortions are almost zero. However, some differences can be observed depending on the machining process plan used. As illustrated in Figure 4.20, with the machining sequence S1 the fixture layout has an impact on both the global shape of the part and the distortion amplitude.

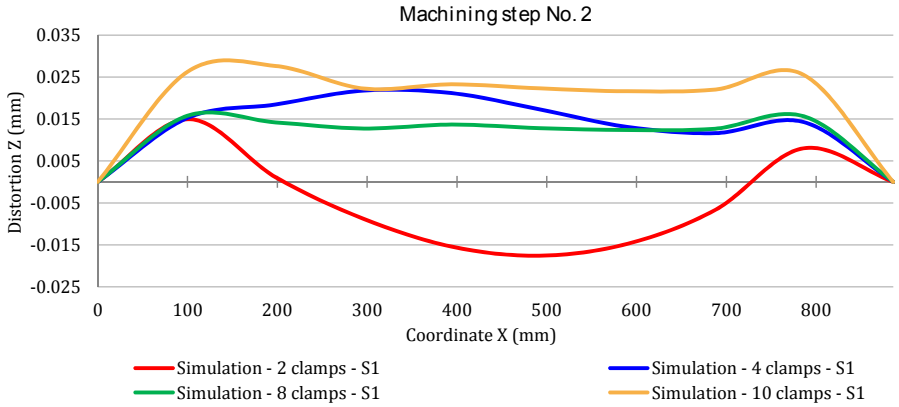

Figure 4.20: Influence of the fixture layout on the post-machining distortion after the second machining step with the machining sequence S1

In Figure 4.21, the post-machining distortions obtained with the machining sequence S2 are depicted. An influence of the fixture layout is also visible in this case. It can furthermore be observed that the machining sequence has an impact on the post-machining distortion, especially for the machining process plan with a two and a four clamps configuration. Figures showing the same results depending on the machining sequence can be found in Appendix D.2.

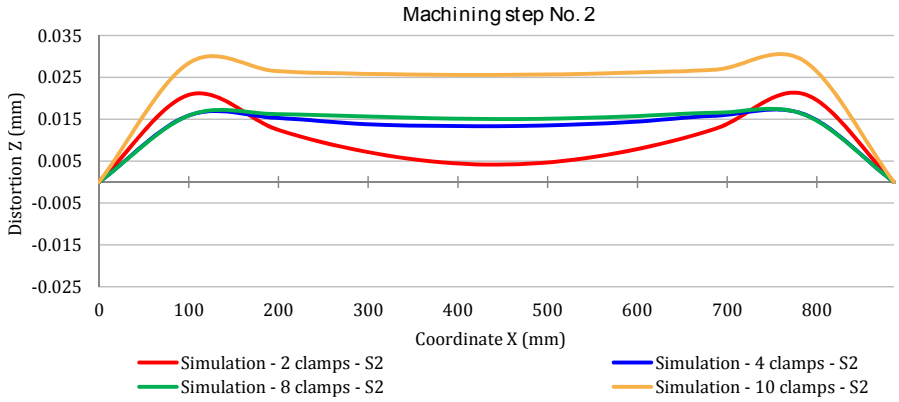

Figure 4.21: Influence of the fixture layout on the post-machining distortion after the second machining step with the machining sequence S2

Like for the machining with the 70 mm thick rolled plate, deflections of the workpiece after clamping also have an influence on the accuracy. The post-machining distortion after the first machining step being even bigger, significant deflections of the workpiece can be observed after the clamping for the second machining step, as illustrated in Figure 4.22. In addition, after the preparation step and due to the offset which breaks the symmetry of the residual stress profiles, the prepared workpiece is also slightly distorted. Workpiece deflections can therefore already occur after the clamping for the first machining step. These additional imprecisions can provoke a domino effect and can lead to significant dimensional and geometrical errors during the machining.

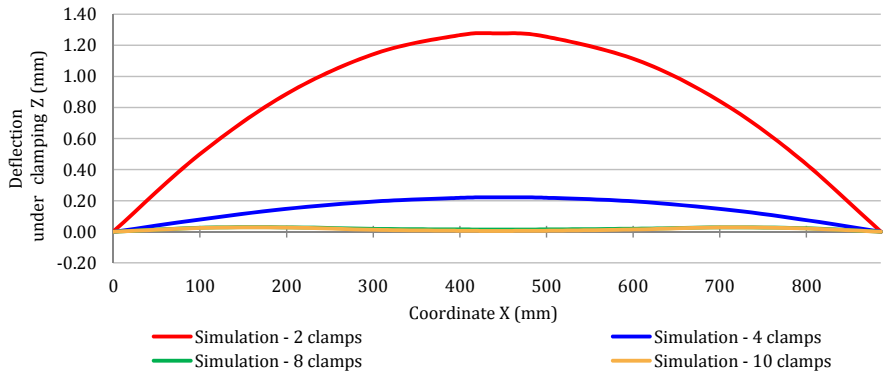

Figure 4.22: Deflections of the workpiece at the beginning of the second machining step (after clamping)

Regarding the machining accuracy, the thickness variations obtained depending on the different machining process plans used are depicted in Figure 4.23 and 4.24. The same results plotted in function of the machining sequences can be found in Appendix D.2. Apart from the machining sequence with a two clamps configuration where overcuts can be observed, only undercuts are obtained with the machining sequence S1 (see Figure 4.23). The case of overcuts occurs because significant deflections of the workpiece are still observable after the clamping step with a two clamps configurations ($\sim$1.2 mm). Overcuts of almost 0.8 mm are obtained in

the middle of the part, so during the machining of the features located at the middle of the part the initial clamping deflections have only been decreased by 0.4 mm. This is due to a significant difference in the behaviour between the workpiece section already machined and the initial one during the machining with sequence S1. The residual stresses in the machined section should almost not provoke any deflections (optimal offset) whereas the other section of the workpiece still has the same residual stress state as after the clamping step where a deflection of 1.2 mm was visible. For the three other fixture layouts used (four, eight and ten clamps configurations) the workpiece deflections obtained after the clamping step are already significantly decreased, the maximum amplitude being of about 0.2 mm. However, in the case of machining with a four clamps configuration undercuts of almost 0.6 mm are still obtained. For the machining with eight and ten clamps configurations, the undercuts are reduced but are still present.

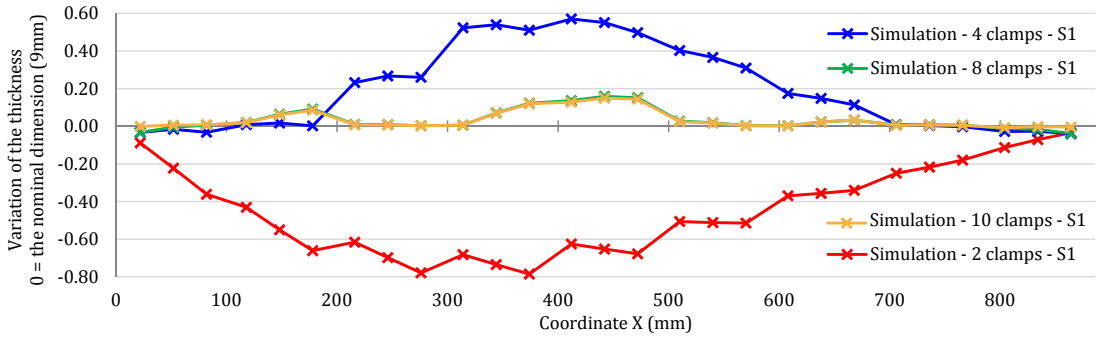

Figure 4.23: Thickness variations of the wall with a nominal dimension of 9 mm with the machining sequence S1 and four different fixture layouts

With the machining sequence S2, only overcuts are observed whichever fixture layout is used. The biggest overcuts are also obtained for the machining process plan with a two clamps configuration. However, the maximal overcut in this case is almost divided by two compared to the one obtained with the machining sequence S1. It can also be observed that for the fixture layout allowing to decrease the workpiece deflections after clamping, the thickness variations obtained with the machining sequence S2 are smaller compared to the ones obtained with the machining sequence S1. The machining sequence therefore has a clear influence on the machining accuracy in this case.

The thickness variations are also the cause of the variations in the post-machining distortion obtained in Figures 4.20 and 4.21. Indeed, at the end of the machining the part has almost zero distortion, a small difference in the wall thickness can therefore lead to a small bending moment and to a change in the post-machining distortion.

The machining sequence and fixture layout influences have then been analysed based on the maximal dimensional errors obtained for the 9 mm thick wall, as illustrated in Figure 4.25. Like it has been observed for the 70 mm thick rolled plate, both these parameters have an influence on the machining accuracy. Fixture layouts which strongly constrain the workpiece and allow to have a deflection of almost zero after the clamping improve the machining

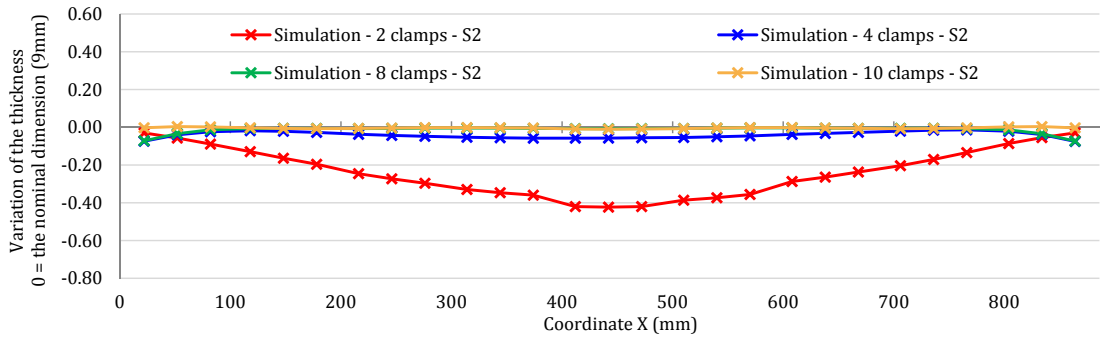

Figure 4.24: Thickness variations of the wall with a nominal dimension of 9 mm with the machining sequence S2 and four different fixture layouts

accuracy significantly. However, when the machining sequence S1 is used, no improvement of the machining quality is obtained between an eight and a ten clamps configuration. Regarding the influence of the machining sequence, it can be observed that a machining sequence allowing a gradual redistribution of the residual stresses (like the machining sequence S2) enables to improve the machining accuracy. However, only the combination of a ten clamps configuration with the machining sequence S2 allows to almost obtain precisely the designed part (maximal distortion of 0.03 mm and maximal thickness variation of 0.01 mm).

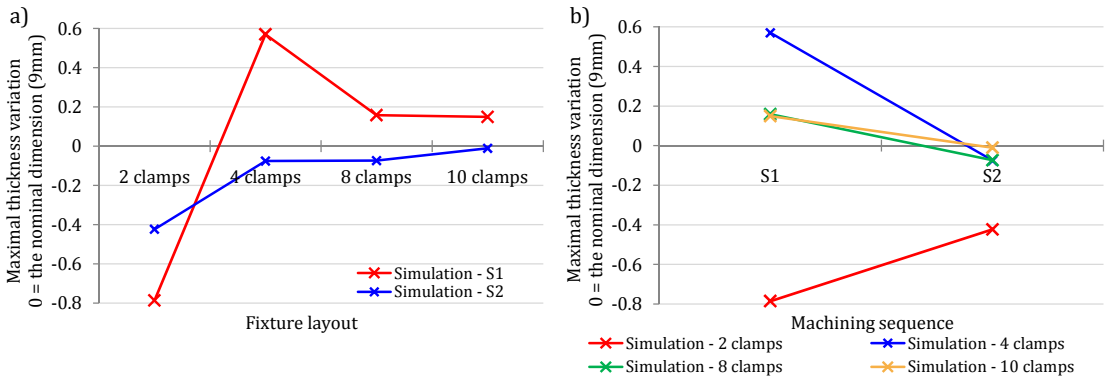

Figure 4.25: Influence of the machining process parameter obtained: a) Influence of the clamping fixture on the machining accuracy ; b) Influence of the machining sequence on the machining accuracy

It is also interesting to point out that, as explained previously in Section 3.3, during the machining simulations the evolution of the force applied on each clamp can be analysed. An increase of the force is predicted on the clamps located at the two ends of the workpiece during the first machining step. This phenomenon is due to the fact that the workpiece wants to distort in a "∪" shape while the machining is in progress. The maximal load predicted during the simulation could therefore be taken into account while dimensioning the different fixture elements. This could therefore allow to avoid the tearing out of fixture elements which can occur during the machining if they have not been appropriately designed. On the other hand, due to the fact that at the end of the second machining step a post-machining distortion

of almost zero is obtained, a decrease in the clamping force is observed during the machining. The predicted clamping force at the end of the machining represents approximately only a tenth of the initial one, raising questions about the validity of these predictions implying that the part is almost not constrained anymore. During the machining simulation the clamps are fixed. This modelling choice could therefore be the reason of such amplified phenomena. Indeed, with this modelling choice no displacement of the clamps is possible, the elasticity of the fixture system is therefore not taken into account which could result in the minimising of the force. In order to improve the prediction of the load on each fixture element, a more complex modelling of the fixture system has to be studied. One of the solutions could therefore be the use of the so-called floating dies in FORGE®. This modelling approach would consist in the modelling of the clamps as rigid solids mounted on springs. Each clamp would apply a constant load (initial clamping force) on the workpiece and the evolution of the load applied would depend on the stiffness of the fixture element. Such an approach could offer a good alternative to the complete modelling of the fixture system (deformable solid) which would result in a significant increase in the computation time. Further studies thus have to be performed in order to validate and to improve the prediction of the evolution of the force applied on each fixture element. However, the approach chosen in this study still enables to predict the important information of the maximal load applied on each fixture element as this is the basis of the fixture element design.

4.1.5 Discussion

The study presented in this section has allowed to analyse the influence of the machining process plan parameters on the machining quality. Both the dimensional and geometrical properties are used to evaluate the machined part quality. From the results obtained the following conclusions can be drawn:

- The use of a different initial workpiece with an optimal offset allows to significantly decrease the post-machining distortion.
- It is possible to use a machining sequence allowing a gradual redistribution of the residual stresses to improve the machining accuracy.
- The impact of the machining sequence is increased when a fixture layout applying small constraints on the workpiece is used.
- The deflection of the workpiece after clamping have a significant influence on the machining accuracy.
- The fixture layout can have a significant influence on the machining accuracy.
- A fixture layout which strongly constrains the workpiece allows to significantly decrease the deflections after clamping as well as during machining.
- Fixture layouts have to be adapted to the machining sequence to obtain an almost error-free machined part.

4.2 Methodology to Improve the Machining Quality

Influence of the Parameters

Using the results of the studies presented previously, a classification of the influence of the parameters has been realised. It is important to point out that this classification is therefore especially adapted to the machining of rolled plates as all previous studies deal with the machining of such workpieces.

It has been clearly observed that the use of an adapted initial workpiece and of an optimal offset is the only possibility allowing to decrease the post-machining distortion. The initial plate is therefore the parameter of first order to prevent post-machining distortion. Both the fixture layout and the machining sequence have an influence on the machining accuracy. The fixture layout has nevertheless a stronger influence because it plays a role in the clamping as well as in the machining steps. It has been observed that an adapted fixture layout allows to significantly reduce the deflections after the clamping as well as during the machining. However, both an adapted machining sequence and an adapted fixture layout are required to obtain an almost error-free machined part. Following these observations, influences of the different parameters have been classified as presented in Table 4.4.

Table 4.4: Classification of the parameters depending on their influence on the machining quality

	Initial workpiece (offset analysis)	Fixture layout	Machining sequence
Post-machining distortion	+++	+	+
Dimensional and geometrical accuracy	/	+++	++

with: +++ = significant influence (parameter of first order); + = small influence ; / = no influence

A procedure to improve the machining quality by defining machining process plans depending on the initial residual stresses has thus been created based on the classification mentioned above. Basic guidelines for the definition of machining process plans have also been determined. Both are presented in the following sections.

4.2.1 Procedure

The following procedure can be used in order to define, to validate or to optimise a machining process plan. It represents the order in which the analysis has to be performed depending on the influence of the parameters. The procedure created is established in four principal steps, presented in the following paragraphs:

1. **Initial workpiece and offset analysis**
   The previous studies have shown that the post-machining distortions are the main cause of machining non-quality and are linked to the initial residual stresses in the workpiece and the designed part geometry. The use of an adapted initial workpiece allows to significantly decrease the post-machining distortions and to obtain a part complying with the tolerance specifications. The offset is therefore the main parameter to improve the machining quality. To find the best compromise between the machining quality and the volume of material needed (dimensions of the initial workpiece), the following method can be applied.

   An initial workpiece as small as possible to machine the desired part first has to be evaluated using simple and quick simulations (Level 1 model). If too significant post-machining distortions are observed, the size of the initial workpiece has to be increased. For each initial workpiece tested an offset analysis has to be performed. The initial workpiece has to be chosen as the smallest one where an optimal offset allowing to obtain a zero post-machining distortion can be determined.

   At the end of the first step both the initial workpiece and the optimal offset are determined. To obtain the desired offset, particular attention has to be paid during the preparation step. The workpiece has to be strongly constrained with an adapted fixture layout to ensure the precise positioning of the part within the initial workpiece. In other words, accurate surface milling operations have to be carried out to obtain exactly the optimal offset. If inaccuracies during the preparation steps occur, the initial workpiece could have a different residual stress state resulting in higher post-machining distortion as well as in a different behaviour during the machining.

2. **Workpiece deflection analysis after clamping**
   When dealing with parts requiring several machining steps, it can be interesting to predict the post-machining distortion after each machining step and to simulate the clamping. These simulations can be done using models of level 2 or 3 or even by directly applying the initial residual stresses on the CAD part geometry which should be obtained after each machining step and under clamping conditions.

   Using these simulations, the post-machining distortions observed at the end of each machining step can be analysed and a fixture layout allowing to obtain an almost non-existing deflection after clamping can be designed. The minimal number of fixture elements as well as the minimal clamping forces to obtain a deflection of the workpiece of almost zero also have to be determined with these simulations. All these steps therefore enable to validate a first fixture layout adapted to the final part geometry and to the initial residual stresses. It is also important to note that a fixture layout leading to yielding has to be strictly avoided as it would modify the residual stress state and would deteriorate the part geometry and the clamping surfaces. In our studies, such cases have not been encountered.

3. **Workpiece deflections during the machining**
   Using the fixture layout chosen during the previous step, a machining sequence needing

the shortest machining time is tested first. If deflections of the workpiece occur during the machining, two possibilities have to be considered. The first one is the addition of fixture elements in the areas of the deflections. The second one is the adaptation of the machining sequence.

If simple fixture elements can be added, this solution is the one to prefer. Indeed, it will allow to improve the accuracy without creating a new machining program and without adding to much setup time (locating and clamping time of the workpiece). The machining process plan with the new fixture layout can then be tested again.

If no (or no more) fixture elements can be added or too complex fixture layouts would be required, the machining sequence has to be adapted. For this, the coupled effect of the fixture layout and the redistribution of the residual stresses has to be taken into account. The machining sequence has to provide a redistribution of the residual stresses as gradual as possible in taking into account the clamping areas and the geometry of the machining features. A machining sequence with material removals based on the same principle as the sequence S2 in Section 4.1.1.1 where gradual removals on each machining feature depending on the depth of cut are performed has therefore to be used. Regarding the order in which the machining feature layers have to be removed, no specific rules can be defined as this depends on the geometry of the part. However, it is usually better to perform the first material removals close to the clamping areas due to the fact that it is often during these ones that the redistribution of the residual stresses leads to the most significant deflections. The fixture elements can thus serve to limit these deflections and the most critical areas should be performed last (large machining features far from the clamping areas).

At the end of this step a machining process plan allowing to reach the desired machining quality has therefore been defined.

4. **Optimisation**
   Depending on the case, the optimisation of the machining process plan obtained above can be performed. It consists in the optimisation of both the fixture layout and the machining sequence. The objective is to find the best compromise between machining time and setup time to minimise the global time needed to machine the part with the desired quality.

   The machining time between the quickest machining sequence and the adapted machining sequence can then be compared using a CAD/CAM software. If a significant difference is observed, the adapted machining sequence can be optimised by minimising the tool-path length and therefore by regrouping some of the material removals of a machining feature. A machining sequence allowing a gradual redistribution of residual stresses in the most critical machining areas and a faster machining (e.g. Z-level machining) in areas where no deflection of the workpiece occurs can thus be created.

   The fixture layout can also be optimised by choosing the most suited fixture elements to constrain the workpiece in minimising the setup time. The type of clamps used and

the way they are positioned on the fixture body are two parameters which can influence the setup time. The simpler the clamping device and the bigger the clearance provided around the workpiece, the easier and the faster the clamping of the part will be.

It is also possible to remove some of the fixture elements or to render the machining sequence faster by degrading the machining quality in staying conform with the tolerance specifications. However, this approach can be risky and is not recommended due to the uncertainties related to the initial residual stress distribution and the small imprecisions during experimental machining which could result in a machined part non-complying with the tolerance specifications.

This procedure is based on the use of the developed numerical tool but some of these steps can also be performed without a numerical tool. The initial workpiece influence can be analysed and an approximation of the optimal offset can be found, especially when dealing with not too complex part geometries, as in Section 3.4. The workpiece deflections after clamping can also be analysed but cannot be evaluated precisely, only qualitatively. The use of a numerical tool is required to obtain precise results allowing to build a machining process plan (initial workpiece, fixture layout and machining sequence) adapted to the part geometry and to the desired quality.

4.2.2 Machining Process Plan Definition: Guidelines

Guidelines have also been defined based on the experience gained along this work and can be used as advices for the definition of machining process plans depending on the initial residual stresses. These guidelines are also helpful when going through the procedure introduced previously.

4.2.2.1 Initial Workpiece and Optimal Offset

The initial workpiece and its initial residual stress state is the main parameter which allows to reduce the post-machining distortion. The studies realised have led to the principal following observations:

- The post-machining distortions are directly related to the part geometry, whose analysis thus allows to obtain information on the geometrical characteristics which can lead to significant post-machining distortion. For example, in the geometry presented in Figure 4.1, the 23 mm thick longitudinal walls have a major influence on the post-machining distortion compared to the other geometrical elements.
- Based on the analysis of the geometry of the part, the initial workpiece has to be chosen in a way to minimise the bending moments in the most critical areas.
- The smallest initial workpiece allowing to obtain an optimal offset has to be used.
- The residual stress profiles in the transverse direction presenting a small risk of post-machining distortion, the initial workpiece should be taken in this direction if the

part dimensions are small enough and the mechanical properties are similar in both directions.

4.2.2.2 Fixture Layout

The fixture layout is the parameter with the biggest influence on the machining accuracy. In order to decrease the workpiece deflections and to reduce the resulting dimensional and geometrical errors, several advices have been defined. They are presented below and are completing the ones previously introduced in Section 1.2.1.2.

- The fixture layout has to ensure that the workpiece is correctly located with respect to the machine tool axes and that a deflection of the workpiece of almost zero is obtained after clamping. The distortions due to the previous machining steps have therefore to be suppressed by the clamping loads and no deflection due to the clamping is allowed to be observed.
- Clamping forces have to be set to the minimum value to cancel the potential previous distortions.
- Fixture elements have to be placed as regularly as possible along the workpiece to minimise the amplitude of the workpiece deflections which can occur during the machining.
- Support elements have to be used to avoid the workpiece deflections in unsupported areas. Supports can also be used to ensure the correct shape of the workpiece after clamping (example Section 4.1.1.2).
- If support elements are used, no contact between the supports and the workpiece is allowed before the clamping loads are applied.
- Clamping forces have to ensure that the workpiece is in contact with all the locators and potential supports.
- Fixture elements have to be placed in areas of the workpiece the least prone to deflections (most rigid areas).
- Whenever possible pneumatic and hydraulic clamping should be used. This kind of clamping ensures a better repartitioning of the clamping forces and therefore minimises the deflections. In addition, it increases the robustness of the process by always applying the same clamping loads.

4.2.2.3 Machining Sequence

The machining sequence can also have a major influence on the machining accuracy, especially when the optimisation of the fixture layout is not possible. In order to assist manufacturing engineers in the definition of the machining sequence, the following guidelines have been defined:

- A machining sequence with gradual material removals depending on the depth of cut

and on the machining features allows to obtain a gradual redistribution of the residual stresses and to reach a better machining accuracy.

- A machining sequence allowing a gradual redistribution of the residual stresses during the last two depths of cut is usually sufficient to improve the machining accuracy. Moreover, it allows to obtain a good compromise between the machining time and the machining quality.
- The biggest deflections are often obtained during the first removal of the last depths of cut (examples: layers 2, 4 for the first machining step and 6, 7, 14, 21, 28, 35, 42, 49, 56 and 63 for the second machining step in Figures 4.3 and 4.4). When dealing with the last machining step, these removals should be realised close to the clamping areas first and as far away from each other as possible.
- If too big deflections are still observed during the machining after adaptation of the fixture layout and the machining sequence, the depth of cut can be minimised. The decrease in the depth of cut leads to smaller material removals and therefore to a more gradual residual stress redistribution (smaller bending moments). The modification of the depth of cut results in a longer machining time and therefore has to be used as a last solution.

4.2.3 Application of the Methodology

In this section, an example of how the procedure and the guidelines can be applied to define a machining process plan adapted to the mechanical behaviour of the workpiece is presented. The part introduced in this chapter (Figure 4.1) is considered.

1. The first step consists in the choice of an initial workpiece and of the optimal offset allowing to obtain a post-machining distortion of almost zero. Based on the analysis presented previously, no optimal offset can be found with the 70 mm thick plate. A 90 mm thick rolled plate with an offset of 4.8 mm is therefore chosen as it represents the smallest initial workpiece allowing to obtain a post-machining distortion of almost zero after the second machining step (see Section 4.1.4.1).

2. The second step consists in the analysis of the workpiece deflections after the clamping steps. As it has been presented previously, after the first machining step, a post-machining distortion of approximately 1.3 mm is observed. Only the eight and the ten clamps configurations allow to almost suppress all the post-machining distortion and to obtain an almost deflection-free workpiece after clamping. The eight clamps configuration is therefore chosen because less fixture elements are required for an equivalent result. It can also be noted that with this fixture layout, the clamps are positioned regularly along the workpiece.

3. The third step consists in the analysis of the workpiece deflections during the machining. The machining of the part with the fixture layout chosen previously and the fastest machining sequence (sequence S1) is first simulated. As shown in Figure 4.23, significant dimensional errors (undercuts) due to deflections of the workpiece during the machining can be observed.

No fixture elements can be added in the areas where the undercuts occurred (middle section of the workpiece), the machining sequence therefore has to be modified. Using the same fixture layout, a machining sequence with gradual material removals (sequence S2) is tested. Results can be observed in Figure 4.24. Dimensional errors have been significantly reduced, however, overcuts appear at the two ends of the part. Two more clamps can be added in order to avoid these deflections during the machining. The results obtained with a ten clamps configuration with the sequence S2 can also be observed in Figure 4.24.
This machining process plan therefore allows to obtain the desired machined part with almost no errors. However, with this machining process plan a machining sequence with a bigger machining time than the one of sequence S1 and a fixture layout with many elements resulting in a significant setup time are used.

4. Based on the observations made on the simulations mentioned above and on the defined guidelines, the machining process plan is then optimised. It has been observed that with a machining sequence where gradual material removals are performed, the deflections of the workpiece during the machining are minimised and only small deflections at the ends of the workpiece occur. These deflections have been corrected by adding two clamps, one on each end. It is suggested to remove the four clamps next to these two added ones, resulting in a fixture layout with only six clamps, as shown in Figure 4.26.

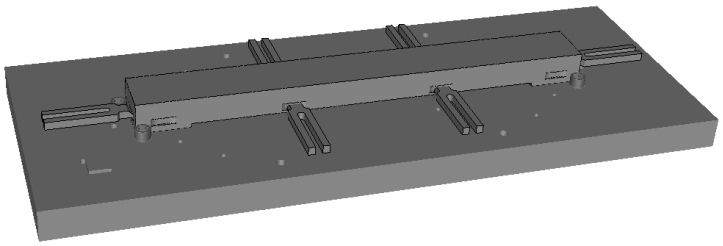

Figure 4.26: The optimised fixture layout

Using this fixture layout, the number of fixture elements as well as as the setup time are thus decreased. In addition, the clamps are positioned regularly along the workpiece, supports are used in the unsupported areas (middle section of the workpiece), no contact between the supports and the workpiece can be observed before clamping, the workpiece is in contact with all the fixture elements after clamping and only small deflections are observed after clamping, as shown in Figure 4.27.

Usually a gradual redistribution of the residual stresses during the last two depths of cut allows to significantly decrease the dimensional errors due to the workpiece deflections. The biggest workpiece deflections often occur during the first removals of these last depths of cut. These removals should therefore be realised close to the clamping areas and as far away from each other as possible to spread the deflections all along the workpiece and thus limit their amplitude. Based on these guidelines, the machining sequence has also been optimised in order to offer the best compromise between the machining time and the accuracy of machining. The optimised machining sequence is illustrated in Figure 4.28. In this machining

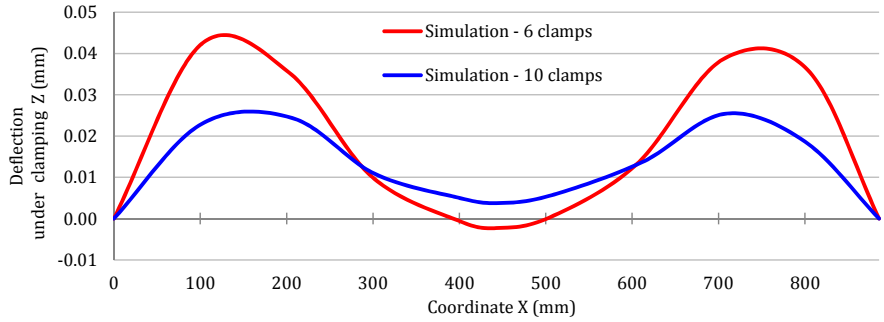

Figure 4.27: Deflection of the workpiece at the beginning of the second machining step (after clamping) with a 6 clamps configuration: comparison with a 10 clamps configuration

sequence, the removals are performed depending on the fixture layout. Z-level machining is used at the beginning to decrease the machining time and gradual removals in function of the depth of cut are then performed for the last two depths of cut.

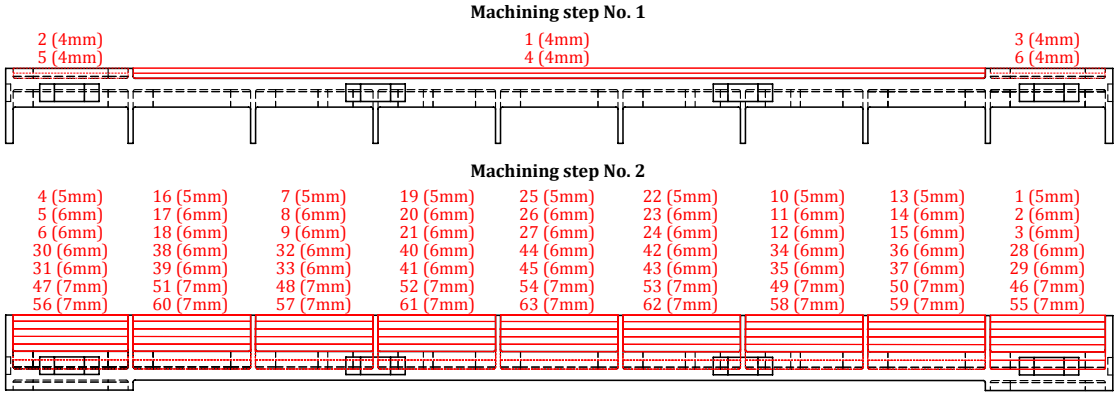

Figure 4.28: The optimised machining sequence for the two machining steps: the numbers represent the order in which the material removals are performed

Using this optimised machining process plan, the machining simulations of the two machining steps have been realised. The same results as with the ten clamps configuration and the machining sequence S2 are obtained after the first machining step. After the second machining step, only small differences between the two machining process plans can be observed. As they are almost only depending on the initial workpiece and its optimal offset, similar post-machining distortions are observed between the two machining process plans, as illustrated in Figure 4.29.

Regarding the machining accuracy, the thickness variations are depicted in Figure 4.30 and are very small in both cases. The optimised machining process plan nevertheless enables to divide the maximal dimensional error by two compared to the one obtained with the ten clamps configuration and the machining sequence S2. In addition, no distortion of the middle section of the part can be observed due to the fact that the thickness variations are almost zero along the whole part with the optimised machining process plan.

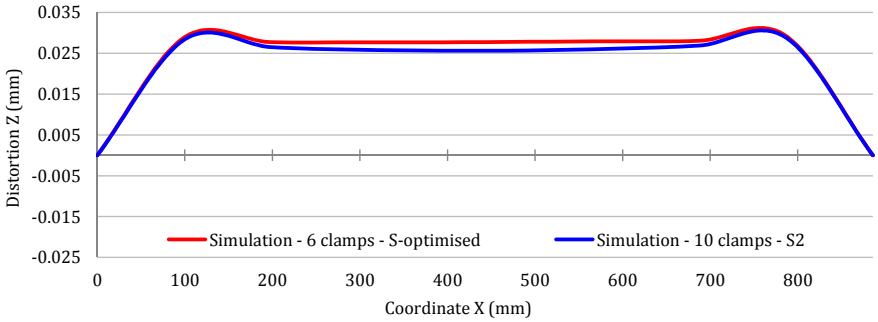

Figure 4.29: Comparison between the post-machining distortion observed after the second machining step with the optimised machining process plan and the machining process plan using the machining sequence S2 and a ten clamps configuration

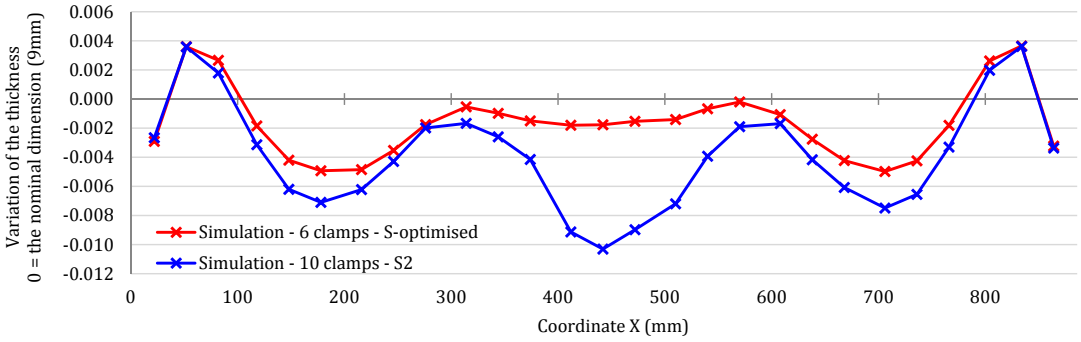

Figure 4.30: Comparison between the dimensional errors observed after the second machining step with the optimised machining process plan and the machining process plan using the machining sequence S2 and a ten clamps configuration

The use of this procedure and these guidelines therefore allows an easy and quick analysis of the machining phenomena and to optimise the machining process plan to ensure the desired machining quality. In this example, by only performing a few simulations, a machining process plan allowing an almost error-free machining has been developed without performing any costly machining trials. The use of such a machining process plan with a fixture layout with six clamps and an adapted machining sequence thus enables to decrease the global machining time (setup time and machining time) while increasing the machining quality.
However, no comparisons with experimental results have been performed with this machining process plan yet.

4.2.4 Discussion

The integration of this type of procedure into the machining process plan definition allows to take into account the mechanical behaviour of the workpiece. The machining process plan is therefore adapted to the resources (machine tools, cutting tools, etc.) as well as to the

material and the initial workpiece (mechanical behaviour). This has as an effect to increase the machining quality, the robustness of the process and to decrease the risk of non-conformity of the machined parts with the tolerance specifications.

As mentioned in the Introduction, this work has been performed in the framework of the OFELIA project. In this project, one of the objectives consists in the characterisation of an optimised machining chip for recycling improvements (see Appendix A). Specific cutting conditions have then been defined to obtain machining chips easier to recycle. The eco-efficiency of the machining process and the recycling can be enhanced by combining the cutting conditions with the adaptation of the machining process plan to the initial residual stresses.

The procedure and the guidelines are thus particularly adapted to industry and companies which desire to improve both the quality of their products as well as to decrease their impact on the environment. This is even reinforced by the use of materials allowing to obtain better mechanical properties (lighter parts) and which are also perfectly recyclable, like the AIRWARE® 2050 alloy. In this context, the use of numerical tools as the one developed and of the procedure presented is therefore relevant as it allows to obtain the desired machining quality and therefore to minimise rejection all in keeping set cutting conditions. These cutting conditions are defined to obtain the best compromise between productivity and recycling, resulting in the optimisation of the whole AIRWARE® 2050 alloy part manufacturing sector. However, the extension of the procedure and guidelines to initial workpieces presenting more complex initial residual stress distributions like forged parts will have to be studied in the future.

4.3 Conclusion

In this chapter, a complete study on the machining process plan parameters on a part requiring multiple machining steps is presented. As in Section 3.4, the two principal problems of machining non-quality due to the redistribution of residual stresses are also highlighted in this study. Both post-machining distortions and workpiece deflections during the machining and after the clamping can be observed on this part.

Results obtained have allowed to demonstrate again the capability of the numerical tool to predict accurately the final machined part geometry. Indeed, similar results to experimental tests are obtained for both the post-machining distortions and the dimensional errors. A criterion based on the maximal dimensional variation has also been defined and has allowed to analyse the influence of the machining parameters on the machining accuracy.

From these results, a classification of the parameter influences has been realised. It has been found that the parameters with the biggest influence on the post-machining distortion are the initial workpiece and the offset. The machining sequence has a significant influence on the machining accuracy but the fixture layout is even more important due to its role in both the clamping and the machining steps. Indeed, an appropriate fixture layout therefore allows

to prevent workpiece deflections after clamping as well as during the machining, resulting in more accurate removals of material. However, both the machining sequence and fixture layout have to be optimised in order to obtain an almost error-free machined part.

A procedure as well as basic guidelines to define machining process plans allowing to reach the desired machining quality have then been defined based on this classification. The use of such procedure and guidelines enables to take into consideration the mechanical behaviour of the workpiece, making therefore the definition of machining process plans ensuring the desired quality easier. The procedure is based on the use of a specific numerical tool like FORGE OFELIA allowing to validate a machining process plan before going into real machining in avoiding the realisation of the standard costly machining trials.

4.4 Résumé en Français

Ce chapitre présente une étude complète de l'influence des différents paramètres définis dans une gamme d'usinage qui a été réalisée sur une pièce nécessitant deux phases d'usinage. Dans cette étude, les deux principaux problèmes rencontrés lors de l'usinage liés à la redistribution des contraintes résiduelles pouvant affecter la qualité d'usinage sont mis en avant. En effet, des déformations après le bridage et pendant l'usinage ainsi que des distorsions après le débridage de la pièce peuvent être observées sur cette pièce et reliées aux défauts mesurés.

Les résultats obtenus ont ainsi permis de démontrer à nouveau la capacité de l'outil numérique à prédire la géométrie finale de la pièce usinée. En effet, des résultats similaires à ceux obtenus lors des tests expérimentaux ont été obtenus, que ce soit pour les distorsions ou les variations d'épaisseurs (erreurs dimensionnelles). Un critère basé sur la plus grande variation dimensionnelle a été défini, permettant ainsi d'analyser l'influence des différents paramètres sur la précision d'usinage.

A partir de ces résultats, une classification des paramètres en fonction de leurs influences a été réalisée. Il a été trouvé que les paramètres les plus influents sur les distorsions sont les dimensions du bloc de matière initial et l'offset utilisé. La séquence d'usinage a une importante influence sur la précision d'usinage mais le montage est encore plus important car il joue un rôle à la fois sur le positionnement de la pièce dans le montage et sur la limitation des déformations pendant l'usinage. Une procédure ainsi qu'une liste de recommandations pour la définition de gammes d'usinage permettant d'atteindre la qualité souhaitée a ainsi été définie en se basant sur cette classification. L'utilisation d'une telle procédure et de telles recommandations permet de faciliter la définition de gammes d'usinage assurant la qualité souhaitée. La procédure est basée sur l'utilisation d'un outil numérique spécifique comme FORGE OFELIA et permet ainsi de valider une gamme d'usinage sans réaliser de réels essais qui sont en général très couteux.

Chapter 5

Simulation of Large Aerospace Parts

This Chapter is dedicated to the machining simulations of real industrial parts using the developed numerical tool FORGE OFELIA.

In this project two industrial cases have been studied. The first case is a part machined from a rolled plate whereas in the second case, the part is machined from a workpiece which has been forged.

The main objective of these studies is to evaluate the capability of the developed numerical tool FORGE OFELIA to simulate such large and complex parts.

Contents

5.1 Machining of Rolled Plate

5.1.1 The Geometry

The structural part machined from a rolled plate is shown in Figure 5.1. Currently this part, intended to be used in the Airbus A330, is machined from a conventional aluminium alloy (7010-T7451). Following the development of the AIRWARE® 2050 alloy, it seems interesting to study the possibility to produce this part from this alloy. The same machining sequence and fixture layout as the current ones for the conventional alloy are used in this study. The behaviour of the workpiece made of AIRWARE® 2050 alloy during the machining is thus analysed and the machining process plan evaluated.

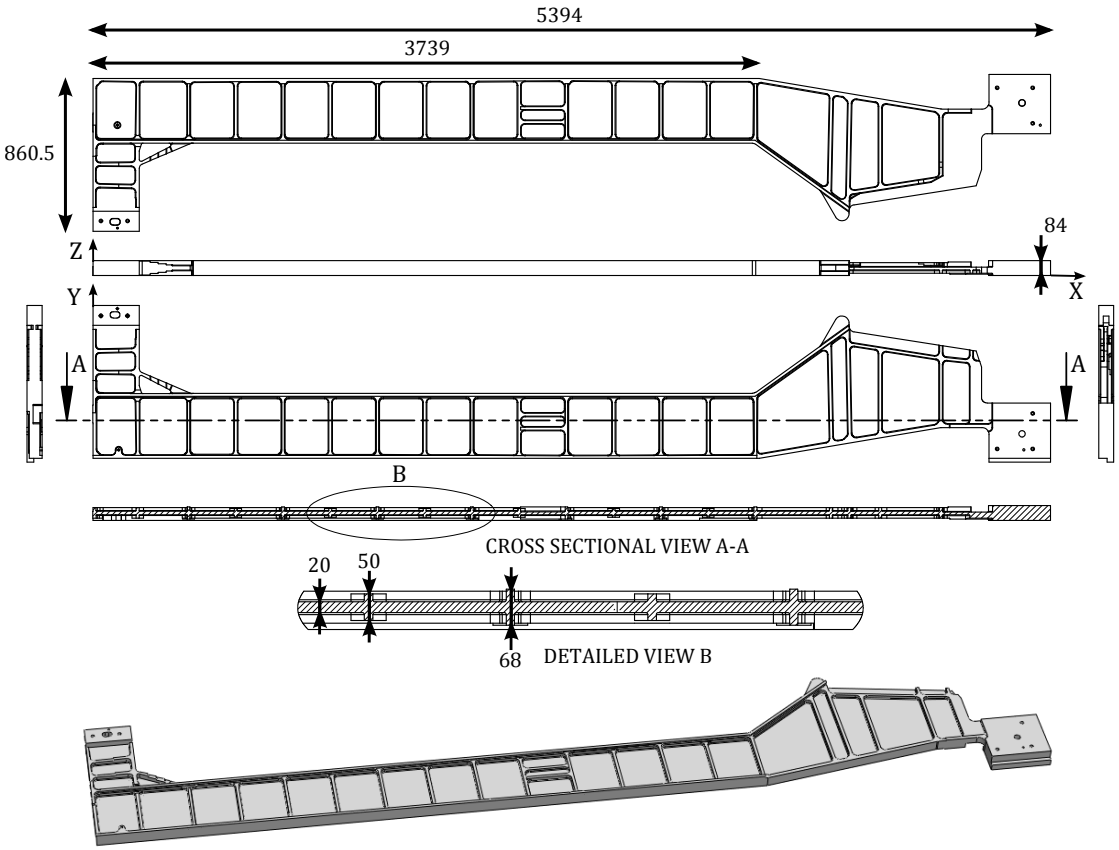

Figure 5.1: The geometry of the studied structural part and its main dimensions

5.1.2 Industrial Machining Process Plan

The final part being 84 mm thick and around 5400 mm long, an initial workpiece selected from a 90 mm thick AIRWARE® 2050 alloy rolled plate in the rolling direction is considered. The initial residual stress profiles are thus the same as the ones presented in Section 3.2.1.

For productivity reasons the parts are usually machined in pairs (top and tail) as shown in Figure 5.2. This type of machining increases the complexity of the process. It is thus harder to define a machining process plan ensuring the desired quality, reinforcing the need of a numerical tool allowing to predict the behaviour of the parts during the machining.

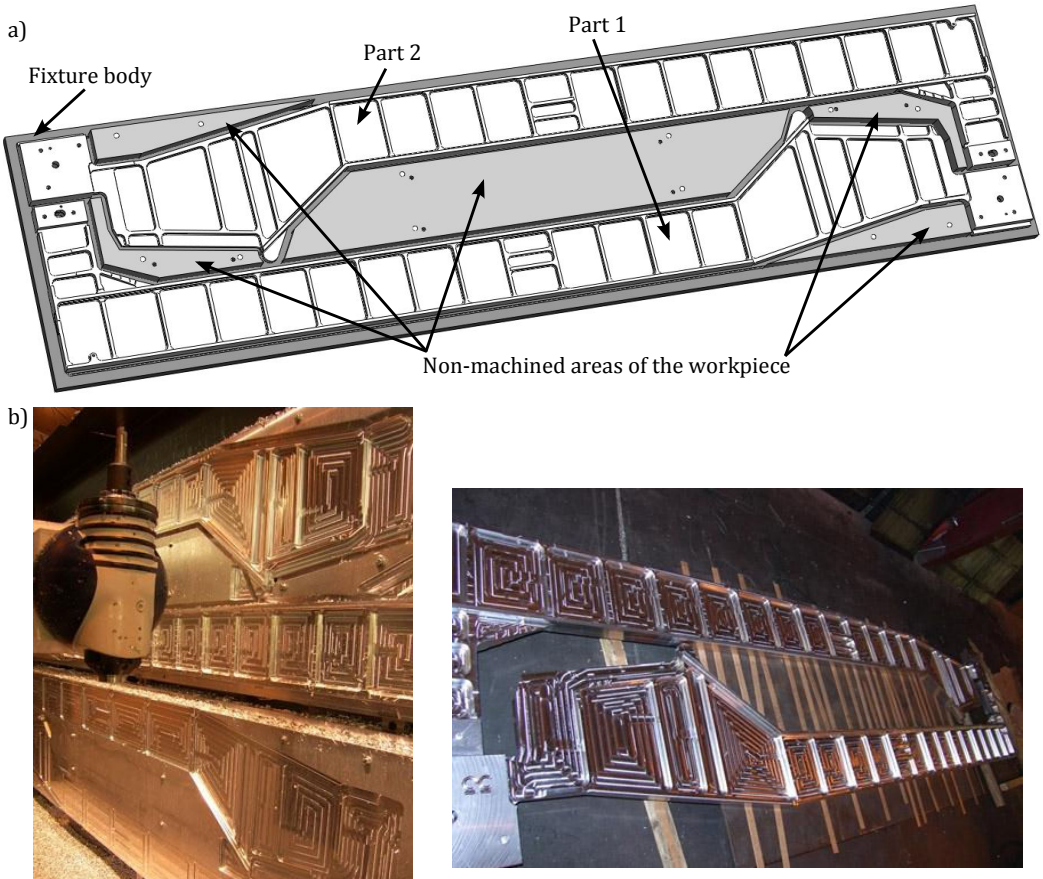

Figure 5.2: The machining of the structural part: a) The CAD representation of the machining in pairs ; b) real machining of the parts [6]

Before performing the two machining steps required to obtain the final part, the initial workpiece has to be prepared. In our case, the preparation step consists in face milling operations to reduce the thickness of the workpiece to 84 mm, in the machining of ten clamping grooves on the sides of the workpiece and in drilling operations, as illustrated in Figure 5.3. Both the grooves and the holes will be used for the clamping of the workpiece during the machining steps.

After the preparation, the two machining steps can be performed. The first step consists in the machining of all the machining features on the top surface of the workpiece. The machining of the contour of the parts at a depth of around 60 mm is also realised during this first machining step. Then the workpiece is flipped and the second machining step is performed. All the

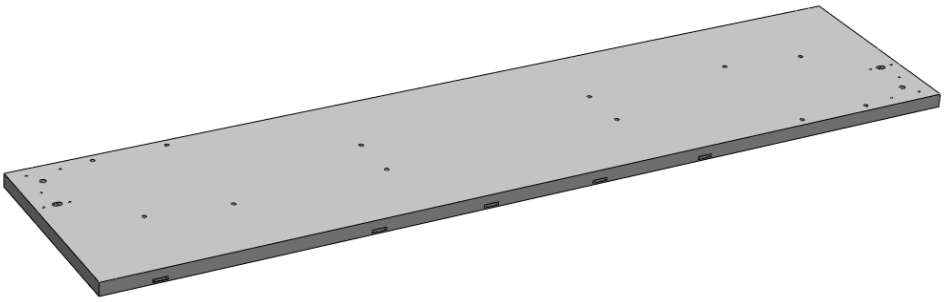

Figure 5.3: The initial workpiece (prepared initial block of material)

machining features on the opposite side are realised and the final machined parts are then detached from the workpiece by completing the contour started during the first step. For the simulations, the first and the second machining step have been discretized in 137 and 167 removal steps respectively.

5.1.3 Simulations

5.1.3.1 Geometry and Offset Analysis

The main source of non-quality being the post-machining distortions, an analysis of the geometry of the part is first realised. Due to the small residual stress amplitudes in the transverse direction, only the geometrical features of the part oriented in the rolling direction can be considered as having an effect on the post-machining distortion. It can be observed that the part is mainly composed of three geometrical features, two principal longitudinal walls and another wall constituting the bottom of the machining features (pockets). These walls should have a significant influence on the post-machining distortion. However, these walls are not at the same position within the workpiece, as illustrated in Figure 5.4.

In the first 3739 mm (see Figure 5.4a), whereas the 84 mm thick longitudinal wall and the 20 mm thick bottom wall are symmetrical, the 72 mm thick longitudinal wall is not. In the last 1655 mm of the part (see Figure 5.4b and c) important changes in the geometrical features and especially in the longitudinal wall thickness can be observed. All these particularities make a determination of an optimal offset difficult. A more detailed geometry and offset analysis has therefore to be performed.

Based on the same principle as the offset analyses previously presented, simulations of the application of initial residual stress profiles on the CAD geometry of the final part have been performed. Due to the small difference between the thickness of the final part and the thickness of the initial workpiece (6 mm), three offsets have been tested. In addition, a minimum layer of 0.5 mm has to be machined on each surface to ensure a correct quality of the datum surfaces. Offsets of 0.5 mm, 3 mm and 5.5 mm have thus been simulated and the post-machining distortions have been measured along the top surface of the longitudinal walls. The maximal values are depicted in Figure 5.5.

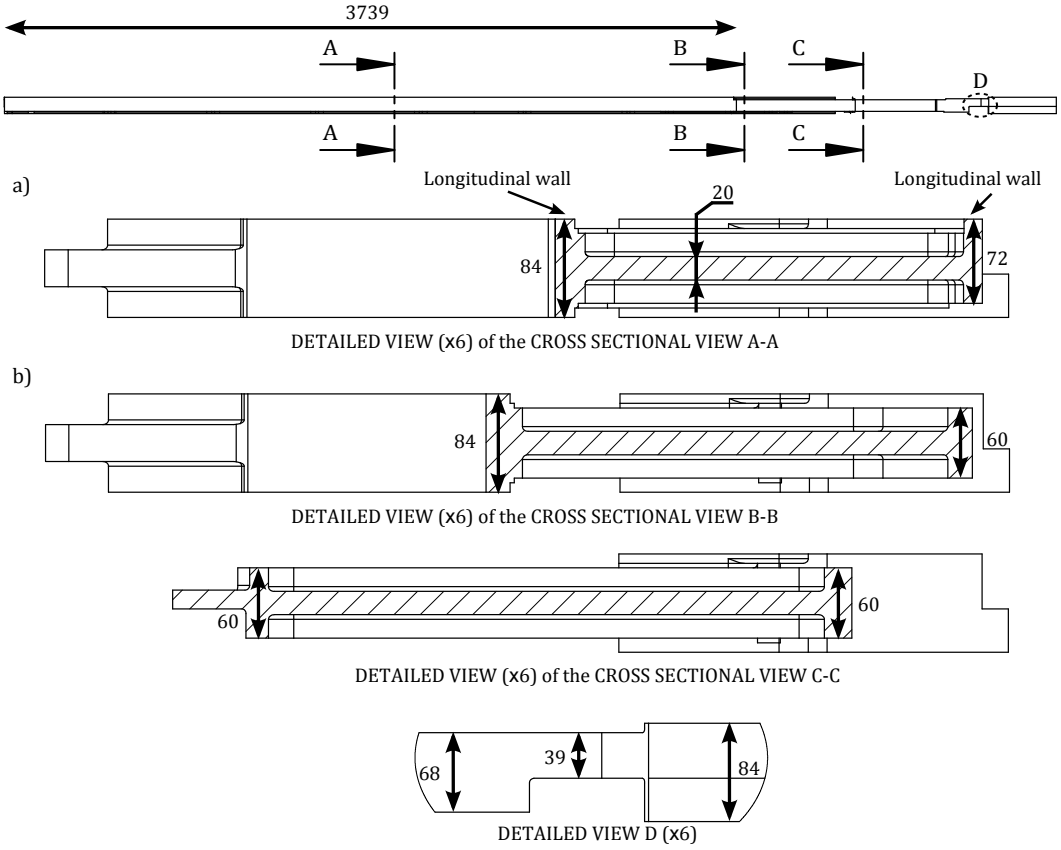

Figure 5.4: Evolution of the geometrical features (walls) depending on the sections of the part

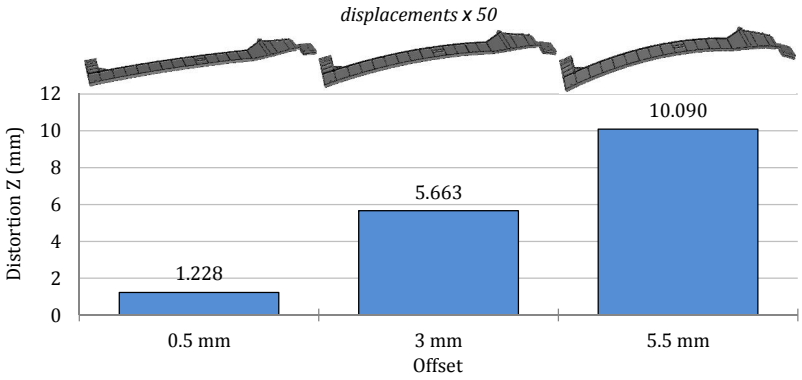

Figure 5.5: Numerical analysis of the offset: maximal distortion measured along one of the longitudinal walls

No optimal offset allowing to prevent post-machining distortion at the end of the two machining steps can be reached using a 90 mm thick rolled plate as initial workpiece. However, it can be observed that even if the maximal offset variation accounts for 5 mm, significant differences in the post-machining distortions can be observed. A maximal distortion value of around 10 mm has been found with an offset of 5.5 mm whereas an offset of 0.5 mm has given

a maximal distortion value of around 1.23 mm, the smallest one. The maximal distortion has therefore been divided by eight by modifying the offset by only 5 mm. This can be explained by the variations of the global bending moment in each section of the part. In Figure 5.6 the residual stress profiles depending on the offset used in the three cross sectional views and the detailed view D (see Figure 5.4) are illustrated.

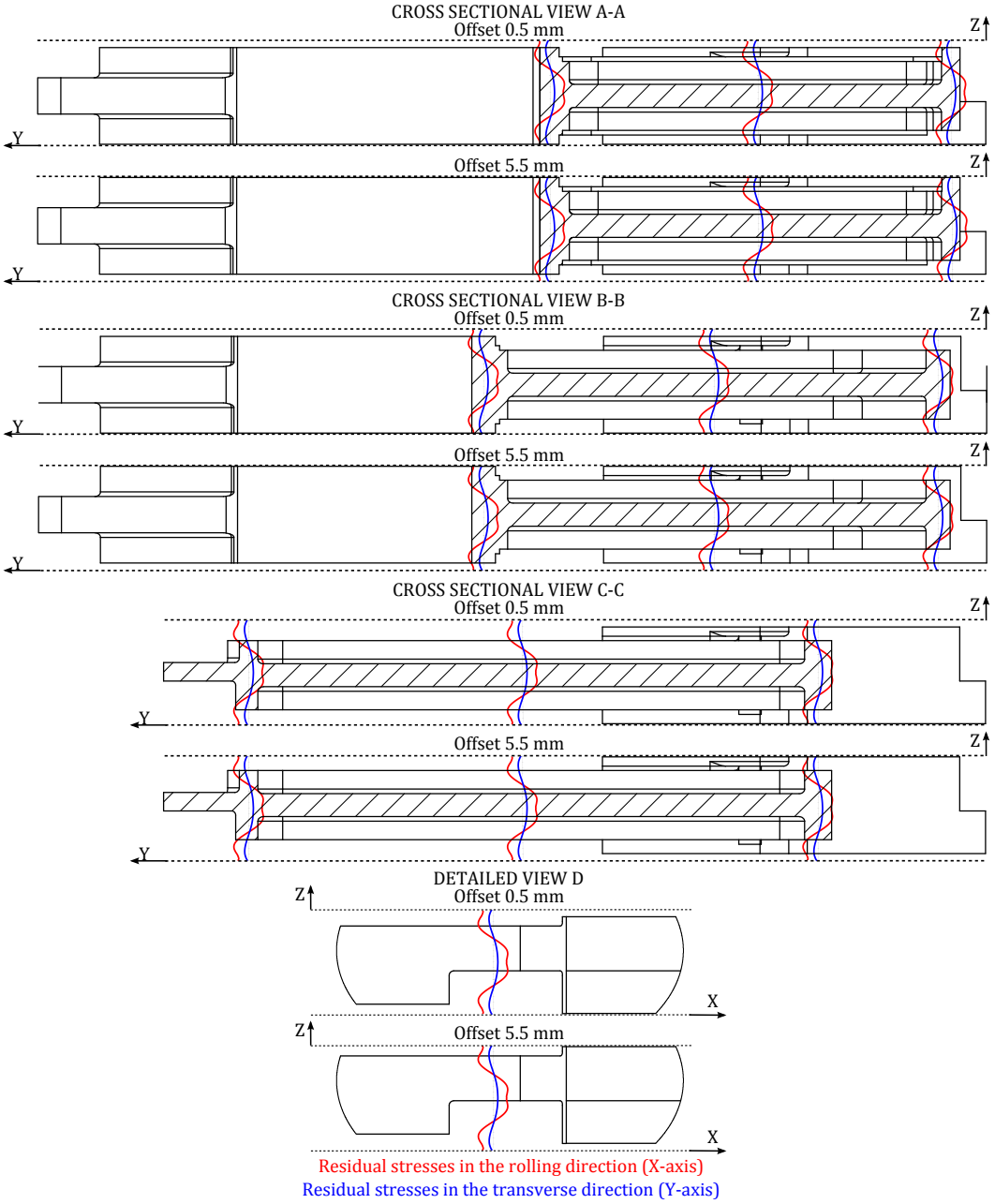

Figure 5.6: Analysis of the residual stresses in the part depending on the offset

First, we introduced the notion of positive and negative bending. When residual stresses evolved from compressive stress on the lower half of the wall to tensile stress on the upper

half, the associated bending is defined as positive and the part will distort in a "∪" shape. A negative bending is defined as being the opposite.

With an offset of 5.5 mm, it can be observed that the same bending moment on each section of the part occurs. Indeed, in the first, second and third section of the part negative bending occurs in the three walls, resulting in a distortion in a "∩" shape. As all the sections have the same negative bending, a significant distortion magnitude is reached.

With an offset of 0.5 mm, different bending moments in the walls can be observed. In the first section of the part, a positive bending occurs in the 84 mm and 20 mm thick walls whereas a negative bending occurs in the last one. However, the bending moment observed in the third wall being more significant, a global and relatively small negative bending of this section occurs. In the second section of the part, the same bending moment as the one in the first section of the part is observed in the 84 mm thick and the 20 mm thick walls. Yet a positive bending moment due to the reduction of the thickness of the 72 mm thick wall occurs, resulting in an overall positive bending of this section of the part. In the third section only positive bending can be observed in the three walls. A distortion in a "∩" shape therefore occurs in the first section whereas a distortion in a "∪" shape occurs in the second and third sections.

In addition, it can be seen in section D in Figure 5.4 that the geometry becomes strongly asymmetric. A significant negative bending therefore occurs in this section. When an offset of 5.5 mm is used, only negative bending occurs in each section of the part, this last section therefore has as an effect to even increase the global distortion of the part. When an offset of 0.5 mm is used, variations in the bending of each section occur. Negative bending occurs in the first section, then positive bending in the second and third one and again negative in the last section, as illustrated in Figure 5.7. These variations thus allow to limit the maximal amplitude of distortion and are the reason of such a difference in the maximal distortion with only a 5 mm difference in the offset. For the following steps, an offset of 0.5 mm is therefore chosen.

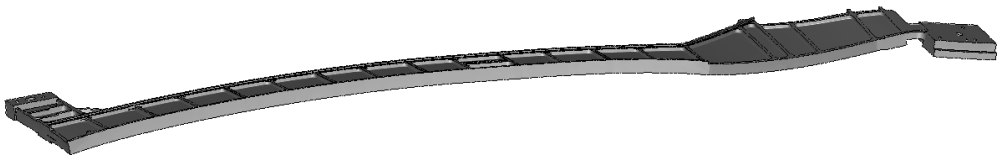

Figure 5.7: The post-machining distortion of the part with an offset of 0.5 mm: changes in the bending of the different sections of the part (deformation amplified × 100)

5.1.3.2 Machining

The first step of the simulation consists in the application of the initial residual stresses on the initial workpiece. The initial mesh is composed of around 1,650,000 nodes and 10,000,000 elements and has been adapted to the configuration of the machining and to the geometry of the part (mesh size of 7 mm in the part areas and 10 mm everywhere else), as illustrated in Figure 5.8.

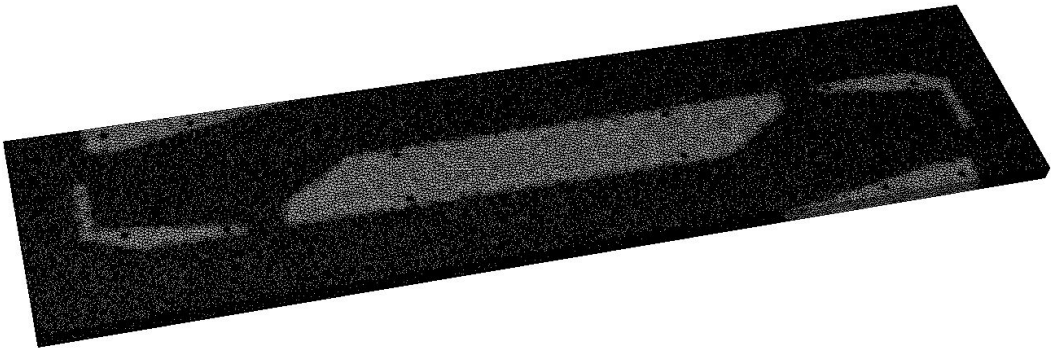

Figure 5.8: The initial mesh of the prepared workpiece

After the preparation step and due to the offset, the workpiece is slightly distorted ($\backsim$ 2.75 mm). Using the ten grooves machined and twelve of the holes drilled during the preparation step the workpiece is clamped, as illustrated in Figure 5.9. The clamping force is set to 15 kN for each fixture element (screws and clamps). After clamping, maximal deflections of around 0.12 mm can be observed at the two ends of the workpiece, the rest of the workpiece being in contact with the fixture body.

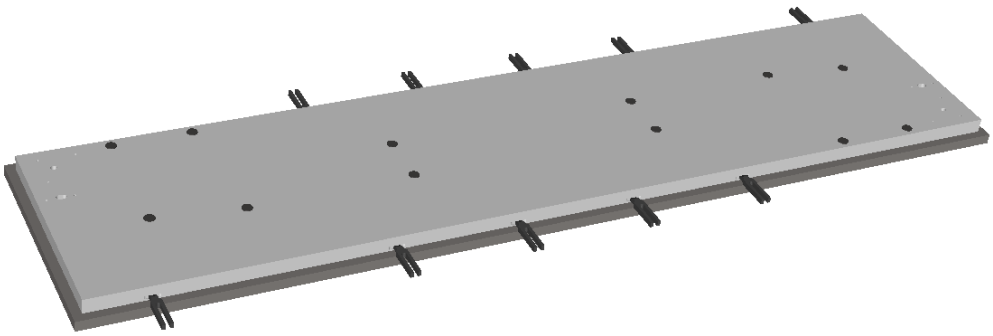

Figure 5.9: The fixture layout used for the first machining step: 12 screws and 10 clamps

The machining of the workpiece is then simulated using the 137 removal steps representing the machining sequence. The removals are performed alternatively on both parts and when the first 134 removal steps have been realised, all the pockets have been machined. The three last removals describe the machining of the contour of the parts. Both the longitudinal residual stress state evolution and workpiece deflections can be observed in Figure 5.10. Significant workpiece deflections occur at each end of the workpiece. At the end of the machining, the maximal deflection amplitude reaches 2.35 mm. Significant overcuts are therefore obtained during this first machining step. Such significant deflections are thus a problem for the part quality but also for the tool. Usually, cutting conditions are computed to decrease costs (compromise between productivity and tool life), such variations in the depth of cut could therefore lead to premature tool wear or even tool failure.

At the end of the machining, the workpiece is unclamped and post-machining distortions are measured on the bottom surface of the workpiece and along the two parts. Results obtained

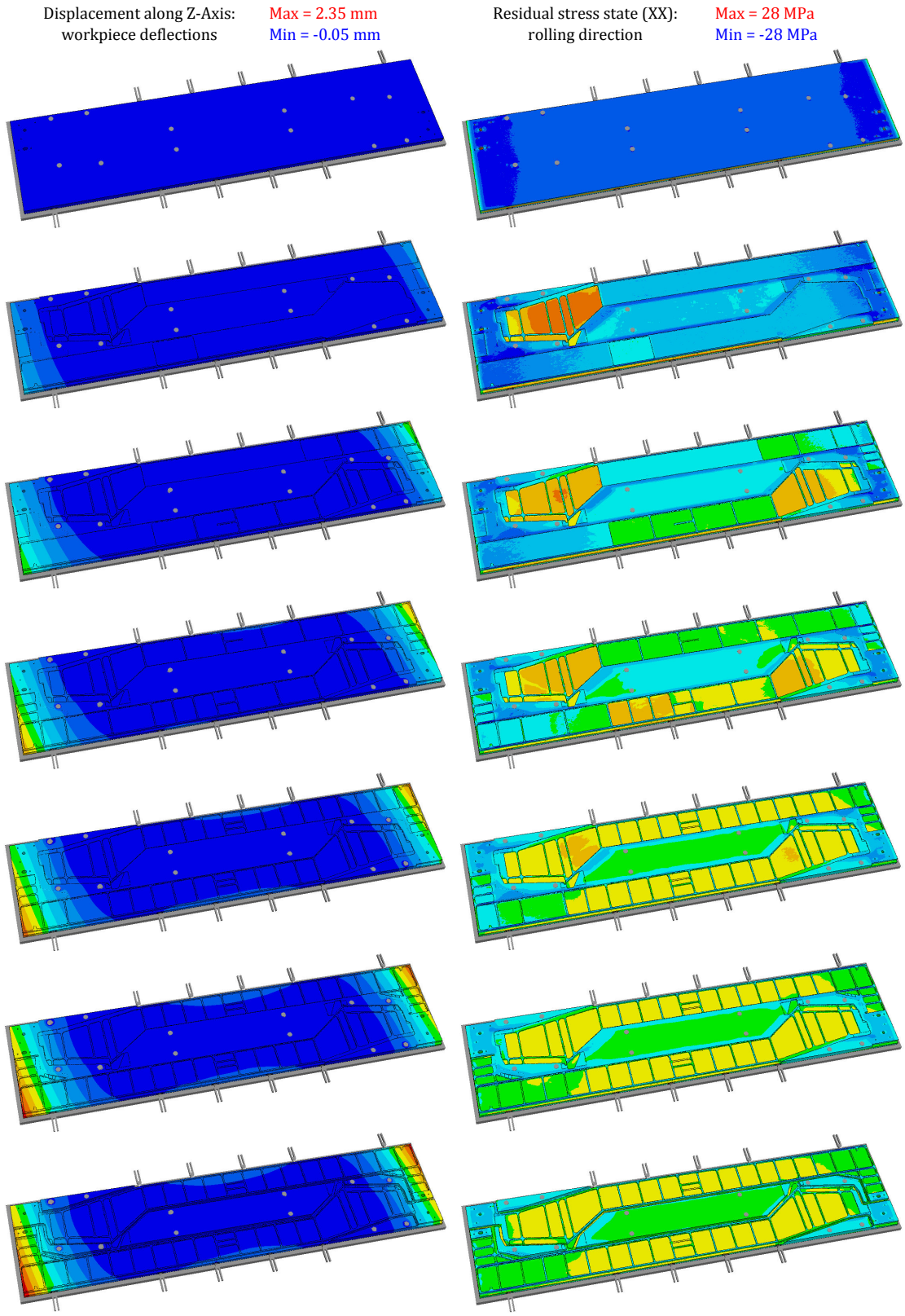

Figure 5.10: Evolution of the deflections and stress state of the workpiece during the first machining step

are depicted in Figure 5.11. It can be observed that the same post-machining distortions are obtained along the two parts and that the maximal amplitude of post-machining distortion is relatively significant as it accounts for around 16 mm.

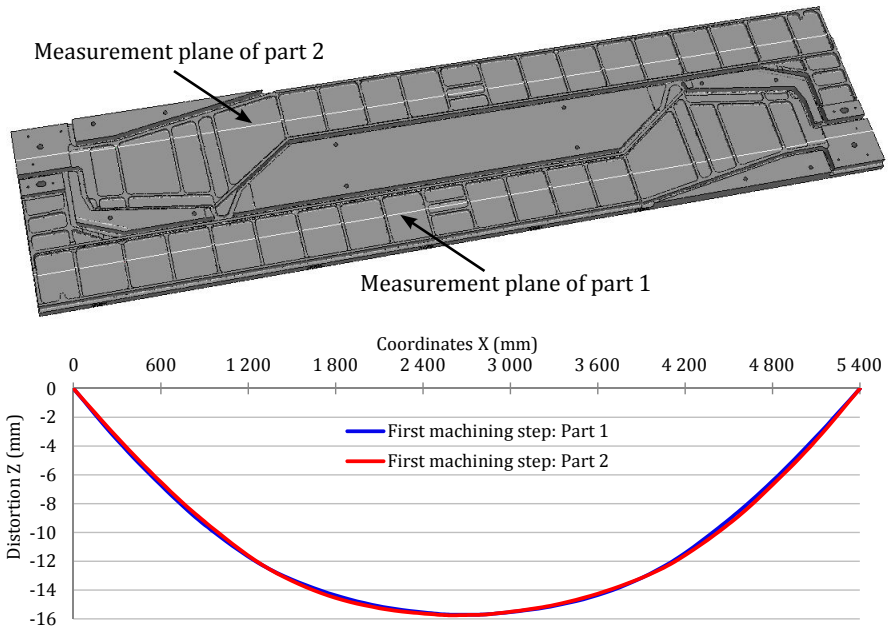

Figure 5.11: Post-machining distortion after the first machining step

Then, the part is flipped and clamped for the second machining step. Only screws are used for the clamping due to the fact that the areas were the grooves have been performed are going to be totally machined. A total of 22 screws are thus used to hold the part in the desired position, as illustrated in Figure 5.12. As for the first clamping step, a clamping force of 15 kN is applied on each screw.

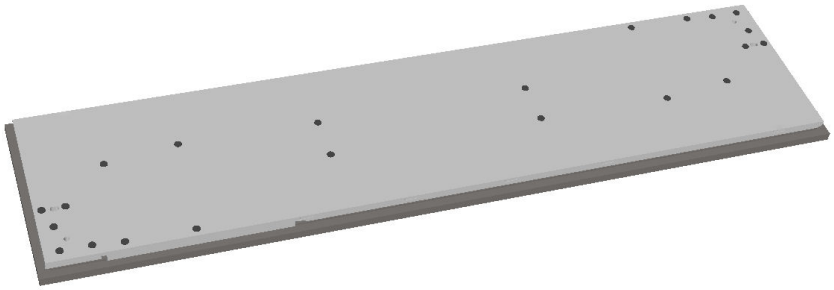

Figure 5.12: The fixture layout used for the second machining step: 22 screws

After the clamping, the workpiece deflections are measured in order to evaluate the capability of the fixture layout to suppress the 16 mm post-machining distortion observed after the first machining step. The workpiece deflections observed are depicted in Figure 5.13. The maximal amplitude being of approximately 0.19 mm, the fixture layout can be considered to suppress

efficiently the post-machining distortions. However, if tight tolerance requirements have to be met, the fixture layout would have to be optimised to obtain smaller and more steady deflections. It can also be observed that similar deflections occur along the two parts (note that the curves are reversed due to the top and tail machining).

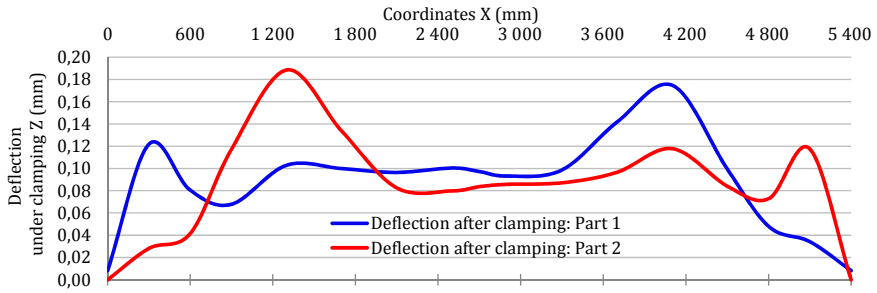

Figure 5.13: Deflection of the workpiece at the beginning of the second machining step (after clamping)

Following the second clamping step, the second machining step is performed. The machining of the workpiece is simulated using a mesh size of 6.5 mm and the 167 removal steps representing the machining sequence. The removals are, like for the first machining step, performed alternatively on both parts. When the first 164 removal steps have been realised, all the pockets have been machined. The three last removals describe the separation of the parts from the workpiece by completing the machining of the contour started in the first machining step.

As for the first machining step, both the longitudinal residual stress state evolution and the workpiece deflections can be observed for the first 164 removals in Figure 5.14. Relatively small workpiece deflections occur during the machining but both overcuts and undercuts are observed. At the end of the machining of the 164^{th} removal, the maximal deflection amplitude reaches 0.37 mm.

In the last three removals, the parts are detached from the rest of the workpiece. During this step, bigger workpiece deflections can be observed, as illustrated in Figure 5.15. These deflections are close to 1 mm which can create some inaccuracies and machining problems. Moreover, workpiece deflections along the Y-axis can also be observed, leading to variations in the width of the longitudinal walls.

At the end of the machining, the two parts are unclamped and post-machining distortions can be measured. A similar post-machining distortion to the one predicted during the offset analysis is obtained on both parts. However, the final post-machining distortions are slightly minimised, due to some numerical diffusion linked to the large amount of material removals and thus field transfers. The fact that a coarser mesh size had to be used with such large parts can also provoke more numerical diffusion compared to the previous cases studied and presented in Chapter 3 and Chapter 4.

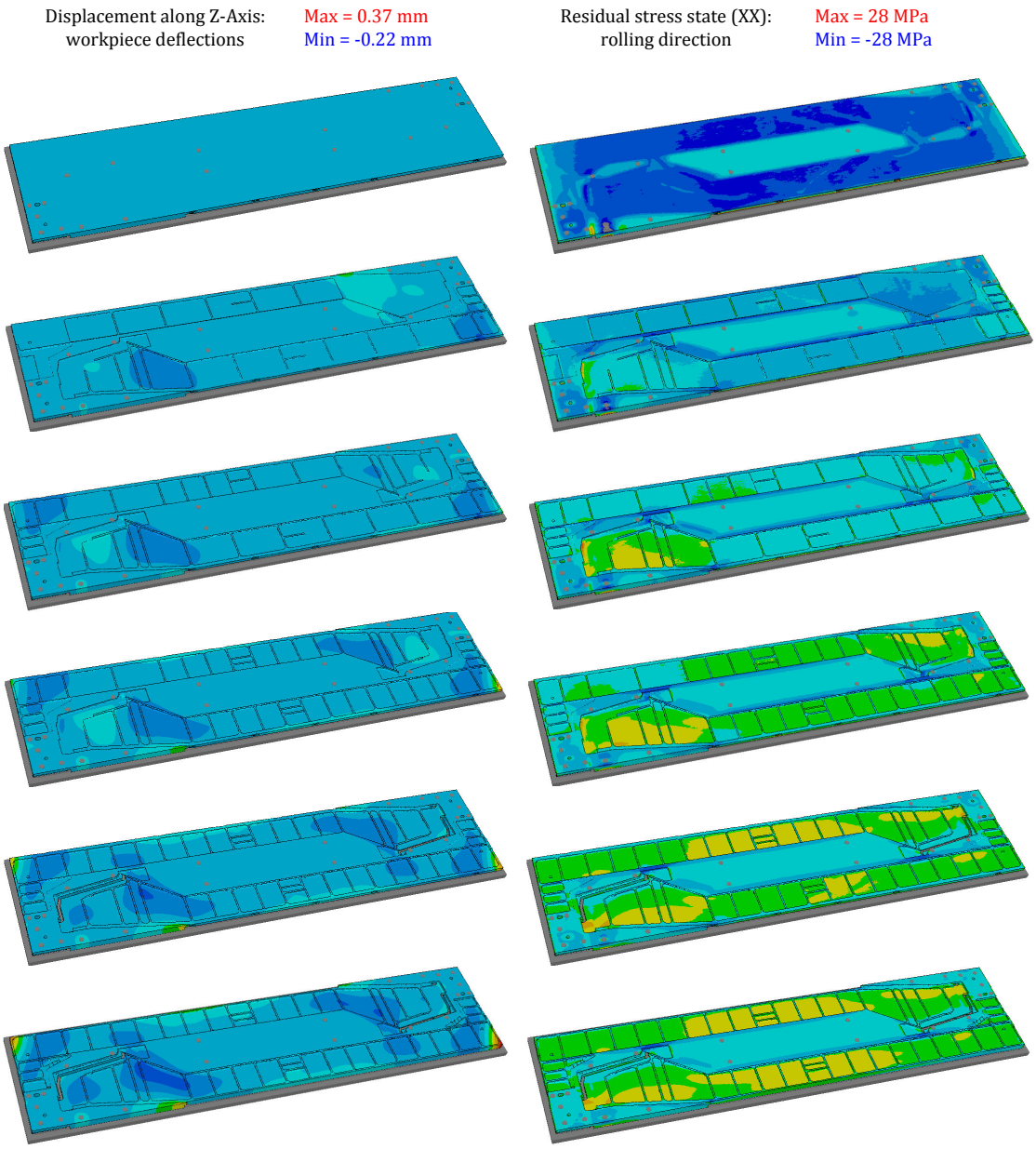

Figure 5.14: Evolution of the deflections and stress state of the workpiece during the second machining step

5.1.4 Discussion

During these simulations, conclusions on both the machining process plan used and the capabilities of the numerical tool can be drawn.
The conclusions on the machining process plan are:

- No optimal offset can be defined in a 90 mm thick rolled plate. Thicker plates should therefore be tested to determine an optimal offset allowing to obtain a post-machining distortion of almost zero.

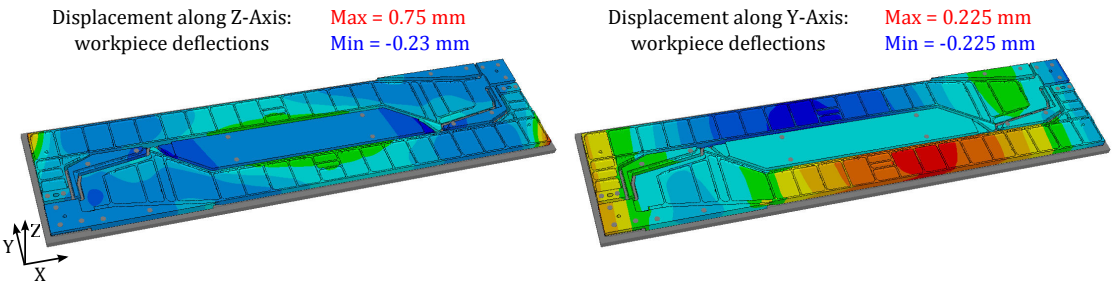

Figure 5.15: Evolution of the deflections during the last removals of material

- Significant workpiece deflections during the first machining step occur (2.35 mm), leading to significant overcuts in some areas. The machining sequence should therefore be modified in order to limit these deflections or clamps should be added. For example, a slightly longer plate should be used in order to have an excess material allowing the machining of other clamping grooves in these sections. This excess material could then be machined as the other sections where clamping grooves are located. Another option would be the use of a vacuum clamping system which would allow to strictly constrain the workpiece and therefore to prevent deflections.
- Apart from the last removals where the parts are detached, only small deflections occur during the second machining step. To prevent the deflections of the workpiece during the last removals, clamps could be added and particular attention could be paid during the detachment of the parts. For example, the tool path used to detach the parts could be optimised to obtain a more gradual redistribution of the residual stresses.

The machining process plan therefore needs further analysis in order to be optimised and to allow the machining of almost error-free parts.

This first study has nevertheless allowed to show that it was possible to perform the simulation of such complex and large parts with FORGE OFELIA. From this study, the following conclusions on the numerical tool can also be drawn:

- A complex machining process plan can be considered and meshes with a large amount of nodes and elements can be used.
- Complex machining sequences can be described by a large amount of massive removals and can be simulated using FORGE OFELIA.
- Such simulations required long computations times (~250 h per machining step) which make the evaluation of multiple machining process plans difficult. Numerical diffusion due to the mesh size and a large number of material removal steps can lead to the minimising of the phenomena and can therefore be sources of uncertainties.

FORGE OFELIA thus allows to simulate the machining of large and complex industrial parts machined from rolled plates. However, the optimisation of such cases seems complicated as long computation times and a large number of material removal steps are required.
In order to make FORGE OFELIA even more applicable to industrial cases, improvements to

decrease computation times, minimise the numerical diffusion and make the optimisation of the machining process plan easier could be performed. Several solutions have been proposed and are presented later in the Conclusion and Perspectives section.

5.2 Machining of a Forged Part

5.2.1 Presentation of the Case

The structural part machined from a forged part is shown in Figure 5.16. The initial worpiece has been manufactured as described previously in section 1.1.3 of Chapter 1. Four principal operations have thus been performed: forging, quenching, mechanical stress relief and aging.

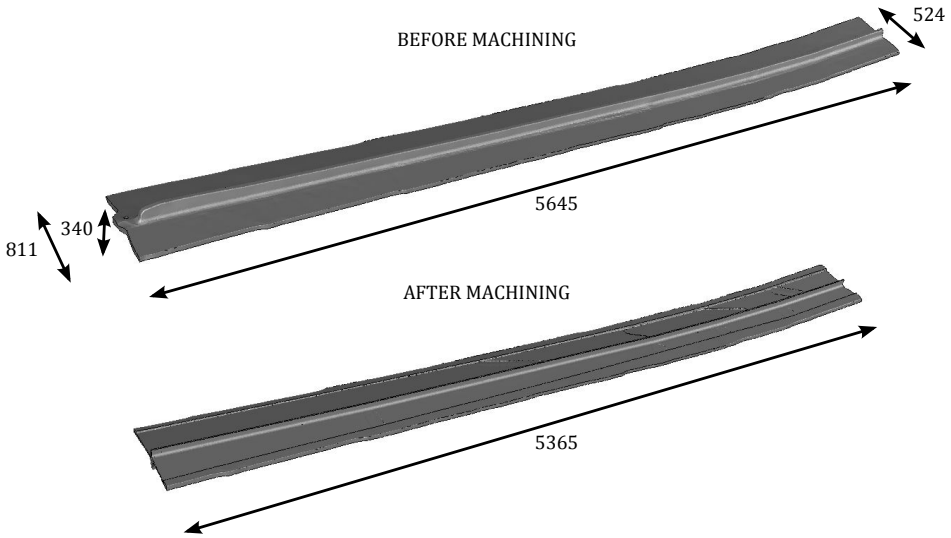

Figure 5.16: Illustration of the initial and machined geometry

The initial residual stress determination has been performed (by Aubert&Duval) using finite element simulations with several validation steps. Several parts have been manufactured and residual stress measurements have been realised on specimens taken from different sections of the part using the layer removal method. Whereas a good agreement has been achieved between the predicted and measured residual stresses after quenching, a relatively poor agreement has been reached after the mechanical stress relief operation. A heterogeneous residual stress field (sections of the part with only compressive or tensile stress) is obtained after the simulation of the mechanical stress relief operation, as shown in Figure 5.17. Experimentally the stress distribution shows the same trends as the ones observed after quenching but with smaller amplitudes. One of the reasons which has lead to such differences in the residual stress profiles could be the mechanical behaviour law of the material used in the simulation which might not describe the material behaviour to capture the final residual stress state in the part well enough. Further work will have to be carried out in order to solve this problem.

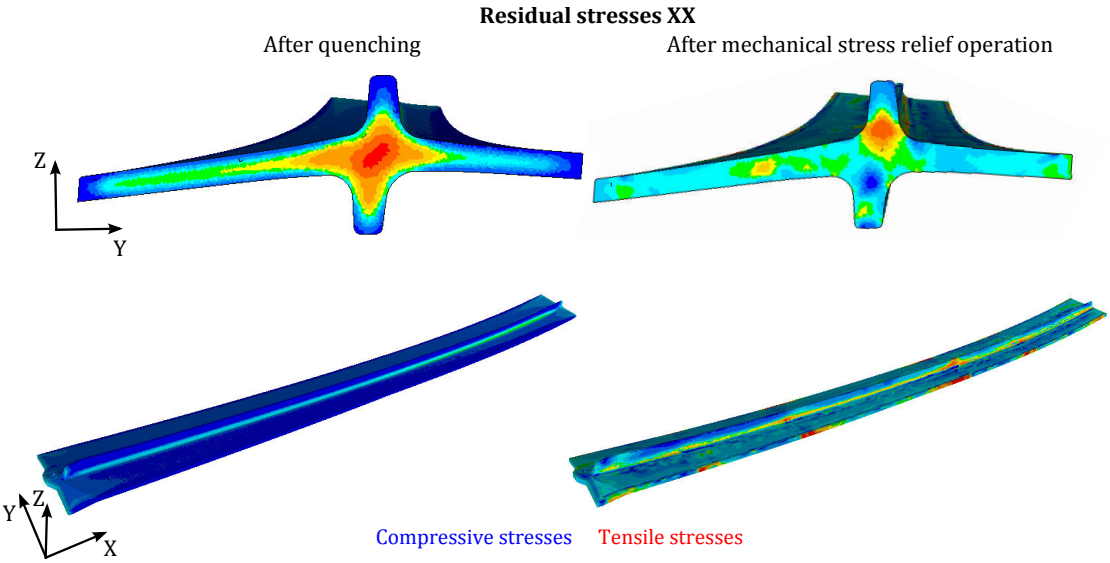

Figure 5.17: Difference between the predicted residual stress state after the quenching and after the mechanical stress relief operation

Despite the fact that the residual stress state obtained does not represent accurately the real one, a simulation of the machining of the part has been performed in order to test the capability of the numerical tool to simulate such a machining case.

5.2.2 Results

The first step of the simulation consists in the clamping of the part. The fixture layout used is shown in Figure 5.18 and is composed of 22 clamps and several supports. A clamping force of 14 kN is applied on each clamp. At the end of the clamping simulation, the correct position of the workpiece within the fixture layout is achieved and the contact between the workpiece and all the fixture elements is modelled correctly.

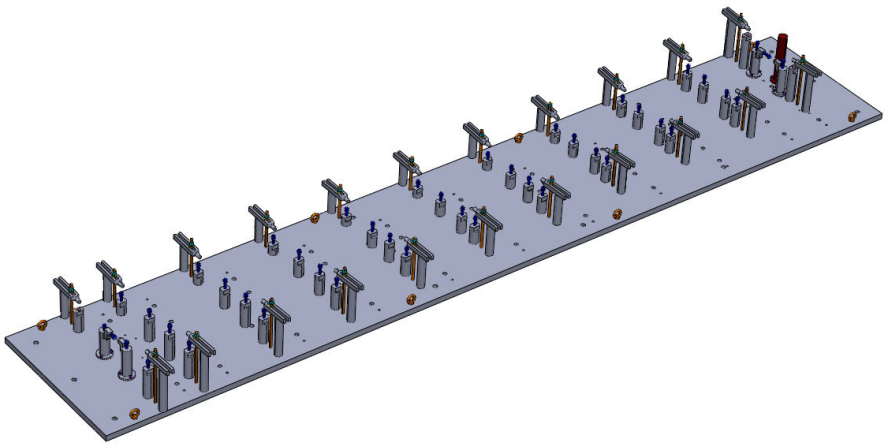

Figure 5.18: The fixture layout used

The machining of the forged part is performed in one step. As illustrated in Figure 5.19, the machining can be represented by 13 main machining areas. The first removal represents a cutting operation, then the machining is performed with a first depth of cut (roughing) from removal 2 to 13. These removals (from removal 2 to 13) are performed another two times with other depths of cut (reroughing and finishing). A total of 44 removal steps are required to simulate the machining sequence with such a discretization.

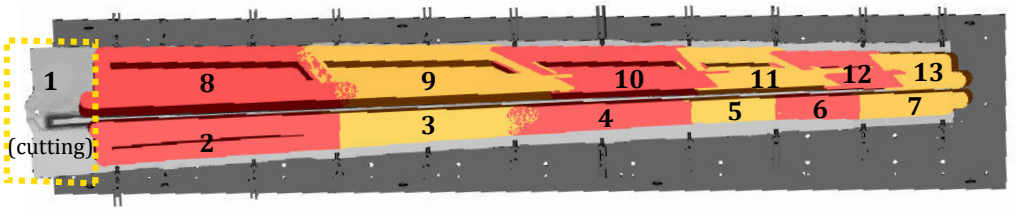

Figure 5.19: The principal machining areas

Using an initial mesh composed of around 1,250,000 nodes and 6,520,000 elements the machining simulation with 44 removal steps has been realised on 24 cores. During the simulation 10 numerical sensors have been placed into the workpiece in order to evaluate the workpiece deflections during machining, as illustrated in Figure 5.20. The evolution of the geometry and of the mesh subdomains is shown in Figure 5.21.

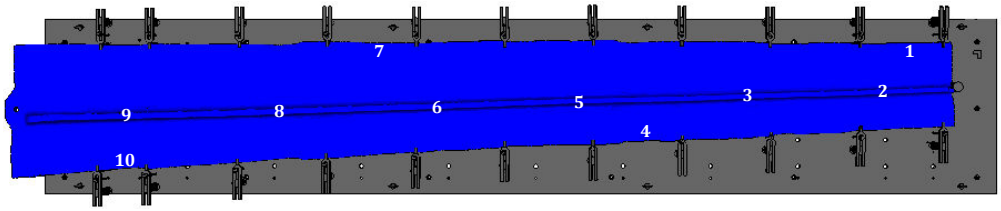

Figure 5.20: Position of the sensors for the evaluation of the workpiece deflections

After all removal steps, the part can be unclamped and the analysis of the machining quality can be performed.

In parallel, an experimental test with the same machining process plan has been performed. In order to evaluate the workpiece deflections holes have been drilled at the position of the numerical sensors (see Figure 5.20) and measurements at these points have been realised during the machining, as shown in Figure 5.22. More precisely, nine measurements at each point are performed, as detailed in Table 5.1.

A comparison between predicted and measured workpiece deflections during the machining can then be performed. The displacements observed for the sensors 2, 5 and 9 are depicted in Figure 5.23.

As expected, due to the difference between the experimental and predicted initial residual stress state of the workpiece, significant deviations between predicted and measured deflections can be observed. No conclusion on the machining quality achieved with such a machining process plan has thus been drawn.

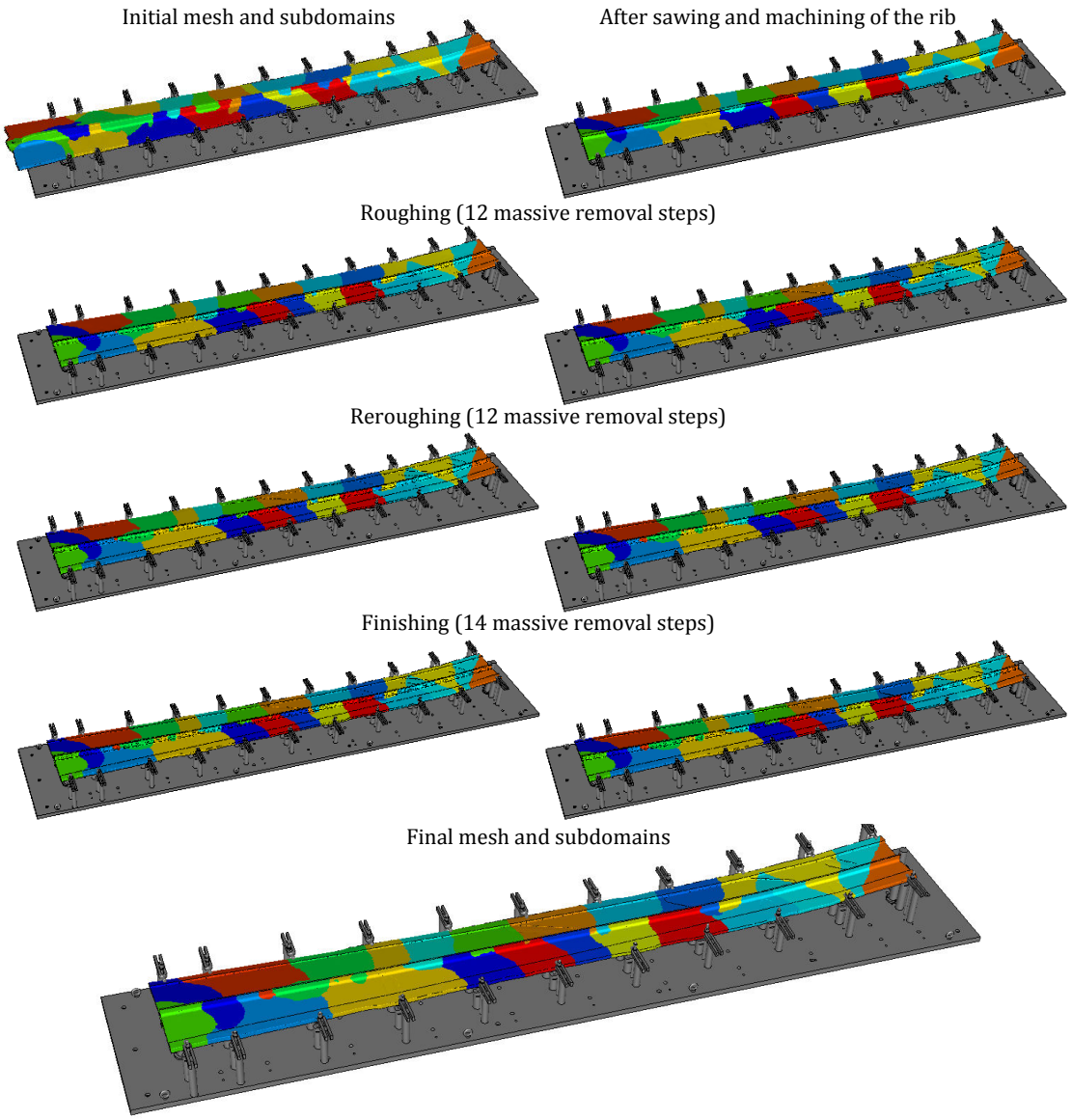

Figure 5.21: Machining of the forged part: Evolution of the geometry of the part and of the 24 mesh subdomains during the machining (each color represents a core)

5.2.3 Discussion

This study has shown the feasibility to simulate the machining of large and complex forged parts using the developed numerical tool. However, no validation of the predicted part geometry with the experimental one has been performed due to the difference in the residual stress state of the initial workpiece. Further studies therefore have to be performed in order to be able to accurately predict the residual stress state in a forged part made of AIRWARE® 2050 alloy as well as to validate the developed numerical tool and its predictions of the behaviour of the workpiece during the machining and of the final part geometry.

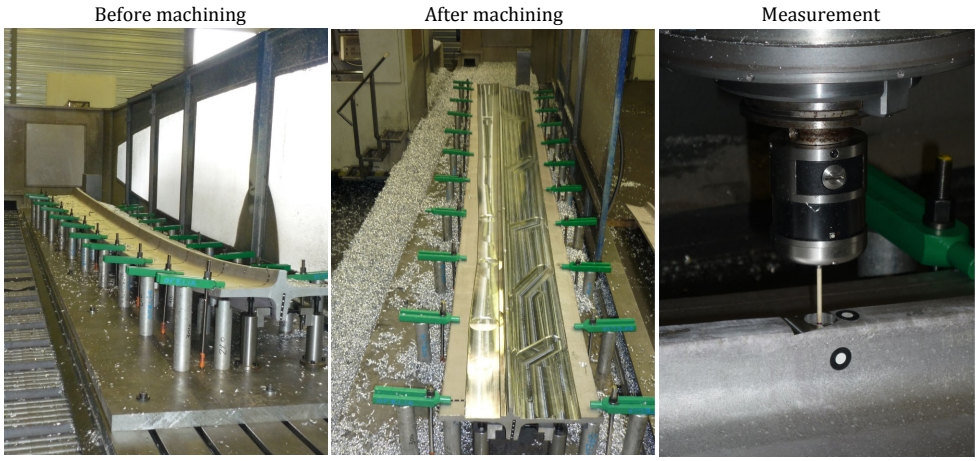

Figure 5.22: Experimental machining of the forged part: machining and measurements

Table 5.1: The different measurement steps performed during the machining

Step 0	After the clamping
Step 1	After the sawing
Step 2	After the machining of the rib
Step 3	After the machining of half of the roughing step
Step 4	After the machining of the roughing step
Step 5	After the machining of half of the reroughing step
Step 6	After the machining of the reroughing step
Step 7	After the machining of half of the finishing step
Step 8	After the machining of the finishing step
Step 9	After the unclamping

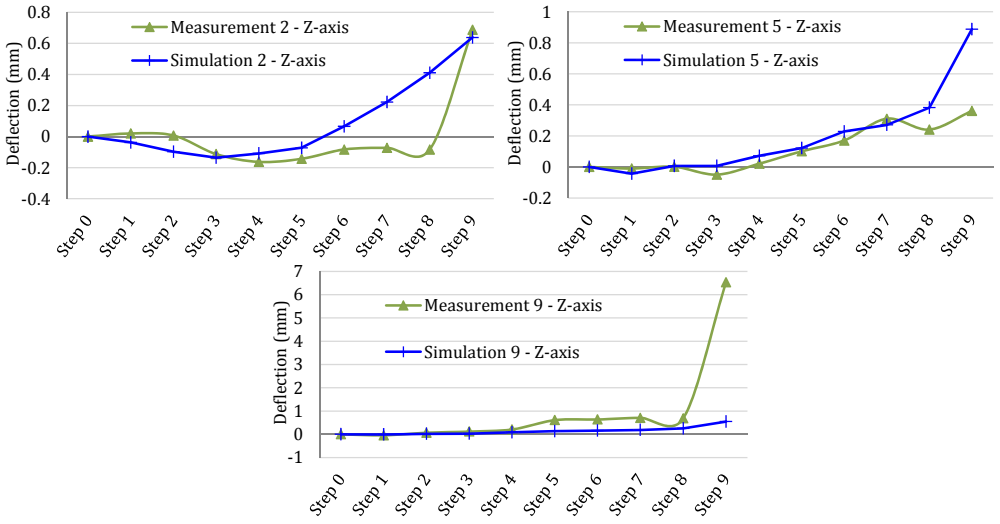

Figure 5.23: Comparison between the predicted and measured workpiece deflections along the Z-axis for the sensors 2, 5 and 9

5.3 Conclusion

In this chapter, two typical cases of large aerospace parts are studied. They represent real industrial machinings and have been used as a final validation of the developed numerical tool.

The first case is a part machined from a rolled plate. In this case a particularly complex machining process plan is used as the parts are machined in pairs (top and tail). In a first step, an analysis of the geometry of the part as well as an offset analysis have been realised in order to determine the optimal offset when dealing with a 90 mm thick AIRWARE® 2050 alloy rolled plate. Then, in a second step, the simulations of the two required machining steps have been performed, showing the capability of the developed numerical tool to simulate such large and complex machining cases. Results are then briefly analysed and advices to improve the machining quality are given. However, no experimental result was available to validate the predicted machining quality.

In the second case, the machining of a forged part is considered. This case is also complex as the geometry of the initial workpiece is a forged part and requires a specific fixture layout. One of the difficulties of such a simulation is thus to deal with the complex fixture-workpiece contact analysis. The machining simulation has been performed, showing again the capability of the developed numerical tool to simulate such large and complex aerospace parts. However, due to the difference observed between the predicted initial residual stresses of the workpiece and the measured ones, no validation of the model has been performed.

The numerical tool FORGE OFELIA therefore allows to simulate the machining of industrial aerospace parts machined from both rolled plates and forged parts. Complex material removals can be performed and meshes with a significant number of nodes and elements can be used.

5.4 Résumé en Français

Dans ce chapitre, deux cas de grandes pièces aéronautiques sont étudiés. Ces cas représentent de réels usinages industriels et ont été utilisés comme validation finale de l'outil numérique développé.

Le premier cas étudié est un cas d'usinage d'une tôle laminée. Une gamme d'usinage particulièrement complexe est utilisée dans ce cas car les pièces sont usinées par deux (tête-bêche). Dans un premier temps, une analyse de la géométrie de la pièce ainsi que de l'offset ont été réalisées afin de déterminer l'offset optimal lorsqu'une tôle laminée en AIRWARE 2050 de 90mm est utilisée. Puis, dans un deuxième temps, les simulations des deux phases d'usinage nécessaires pour ces pièces ont été réalisées, montrant la capacité de l'outil numérique développé à simuler de tels cas d'usinage (grandes pièces avec des géométries complexes. Les résultats sont ensuite rapidement analysés et des conseils en vue de l'amélioration de la

gamme d'usinage sont donnés. Cependant, la qualité d'usinage prédite n'a pu être validée car aucun essai expérimental n'a encore été réalisé.

Le deuxième cas est un cas d'usinage d'une pièce forgée. Ce cas est également complexe car la géométrie de la pièce avant usinage est celle d'une ébauche forgée, nécessitant un montage adapté. Une des difficultés liée à de telles simulations est notamment la gestion du contact entre le montage, composé de nombreux éléments et la pièce de géométrie complexe. La simulation d'usinage a été réalisée, montrant à nouveau la capacité et la flexibilité de l'outil numérique à simuler de telles pièces aéronautiques. Cependant, aucune validation du modèle n'a pu être réalisée. En effet des écarts ont été trouvés entre l'état de contraintes résiduelles prédit en simulation et celui mesuré expérimentalement sur l'ébauche. Il s'ensuit que les distorsions prédites après usinage et débridage sont en désaccord entre les essais et les calculs.

L'outil numérique FORGE OFELIA permet donc de simuler l'usinage de pièces industrielles, qu'elles proviennent de tôles laminées ou de pièces forgées. Des enlèvements de matière complexes peuvent être réalisés afin de décrire les séquences d'usinage et d'importants maillages peuvent être utilisés afin de traiter le cas de pièces de grandes dimensions.

Conclusion and Perspectives

Conclusion

This thesis aimed at providing a better understanding of the phenomena which affect the machining quality when dealing with the machining of large and complex aluminium alloy aerospace parts. It also intended to offer an evolution in the machining process plan definition by taking into consideration the mechanical behaviour of the workpiece linked to the redistribution of the initial residual stresses.

To reach this objective, the work has been organised in two main steps:

- Numerical development step: The development of a numerical tool allowing to predict the final machined part geometry and thus the machining quality.
- Mechanical analysis step: The analysis of the residual stress redistribution during machining and its combined influence with the machining parameters on the machining quality.

The numerical tool is based on a modelling approach which has been defined based on assumptions deduced from literature reviews on aluminium alloys, on the machining process and on residual stresses. The principal assumptions are:

I The initial residual stresses are the main reason for machining non-quality.

II The cutting loads and milling-induced residual stresses can be ignored for such parts.

III The fixture layout and the machining sequence can have an important influence on the machining quality.

A numerical material removal procedure (massive material removal approach) has then been developed (computation of signed distance functions, tetrahedral mesh cutting algorithm, automatic remeshing) as well as parallelized and implemented into FORGE 2011®. The machining is performed by massive removal steps which depend on the discretization of the real machining program. The solver parameters have also been adapted for the machining simulation, e.g. the penalty distance and coefficient have been decreased to ensure an accurate contact modelling and a faster convergence. Several types of models can be defined using the developed numerical tool. These models present different ratios between computation time and accuracy of results and therefore offer a maximal flexibility to the user. A first numerical validation of the numerical tool FORGE OFELIA has then been performed by comparing the

results obtained with FORGE OFELIA with results found in literature with another modelling approach.

The residual stress distributions of a 70 mm thick and a 90 mm thick rolled plate made of AIRWARE® 2050-T84 alloy have been determined using the layer removal method (performed by the Constellium Technology Center). Results have shown a strong anisotropy in the residual stress distribution in both rolled plates. Using the developed numerical tool, simulations of the layer removal method have been performed, as well as the machining simulations of simple parts. A good agreement between the simulations and the experimental results has thus allowed to validate both the initial residual stress profiles and the numerical tool. It has also demonstrated the necessity to define machining process plans in function of the residual stresses.

Through two main studies, the residual stress redistribution during machining and its combined influence with the machining parameters on the machining quality have been analysed. The two principal effects leading to a bad machining quality have then been highlighted. The first one is the post-machining distortions, obtained after unclamping. The second one is the workpiece deflections, observed after clamping as well as during the machining. They lead to geometrical and dimensional errors (overcuts and/or undercuts). The results obtained have also been compared to experimental observations, showing again a good agreement both in terms of post-machining distortions and dimensional variations (final geometry). These comparisons have allowed to demonstrate the capability of the developed numerical tool and the associated models to accurately predict the machining quality. It is thus possible to analyse the influences of the initial workpiece, the fixture layout and the machining sequence. It has been shown that the post-machining distortion can be almost suppressed by using an appropriate initial workpiece with an optimal offset. Both the machining sequence and the fixture layout can have an influence on the machining accuracy (workpiece deflections). They play therefore an important role in the machining quality.
Based on the influence analysis, a procedure using the developed numerical tool for the definition of machining process plans ensuring the desired machining quality by taking into consideration the effects of the initial residual stresses has been created. This procedure is composed of four main steps:

1. The initial workpiece and offset analysis
2. The workpiece deflection analysis after clamping
3. The workpiece deflection analysis during the machining
4. The optimisation

Basic guidelines completing the already existing ones (classic definition of machining process plans) have also been defined.

Such procedure and guidelines form a first methodology for the definition of machining process plans depending on the workpiece residual stress state (mechanical behaviour of the workpiece). This methodology enables the user to choose the best initial workpiece in function of the desired part geometry as well as to define the machining parameters appropriate for

it. Therefore the methodology allows to develop optimised machining sequences and fixture layouts. It also allows to avoid the realisation of machining trials, reducing the cost linked to the definition of the different machining process plan parameters and to the design of the fixture system.
The use of the methodology is even more relevant when dealing with materials presenting excellent recycling properties, like the AIRWARE® alloys and when considering the optimisation of the eco-efficiency of the global manufacturing sector.

To conclude, the capability of the numerical tool to predict the machining quality of large and complex aerospace parts has been validated by simulating two industrial parts, one machined from a rolled plate and another one from a forged part using the industrial machining process plans.

Perspectives

This Ph.D. work has initiated the development of a numerical tool allowing to predict the machined part quality depending on the machining process plan parameters used and depending on the initial residual stresses. Using the developed numerical tool a methodology taking into consideration the mechanical behaviour of the workpiece during the machining to define machining process plans allowing to improve the machining quality has been created. However, the methodology and the numerical tool have only been validated for large and thick aluminium alloy parts. Further work still has to be performed in order to make them more robust and applicable for all challenges of machining industries. Both numerical tool improvements and mechanical analyses therefore have to be realised in the future.

Improvement of the Numerical Tool
In order to make FORGE OFELIA more efficient, flexible and accurate, the following numerical improvements could be performed:

- The material removal procedure could be improved by the use of anisotropic meshes which could be particularly well adapted for the simulation of large and complex machining parts. An analysis on the use of such meshes on the results and computation times could therefore be realised.
- In order to improve the accuracy of results, a procedure allowing the remeshing and associated field transfer only on the subdomains affected by the removal of material could be developed. This would limit the numerical diffusion (smoothing of the P0 variables) provoked by the field transfer at each material removal, which is especially observed when dealing with large parts where coarser meshes have to be used. In addition, the field transfer method could also be improved to limit the numerical diffusion (SPR method for example).
- The automatic mesh adaptation technique (refinement depending on the geometry of the volume removed) could be optimised to reduce the computation time and could then be applied more easily to the machining simulation of large and complex aerospace parts. Currently, in this first version two remeshing steps are performed for each removal, a first one for the mesh refinement and the second one after the cutting of the mesh to improve the mesh quality. The same procedure could be used, yet restricting the remeshing to one step per material removal.
  In the optimised version of the mesh adaptation technique, only the first removal step would require two remeshing steps. A first remeshing adapted to the first material removal geometry would be performed first. After cutting and before the second remeshing, the next material removal file describing the geometry which has to be removed during the following step would be read. The refinement adapted to the next material removal would then be performed during the second remeshing step. All the following removal steps would therefore consist in the cutting and remeshing with refinement for the next removal step (one remeshing step for the refinement and the mesh quality improvement). In Figure 5.24, a simplified flow chart describing the procedure is shown.

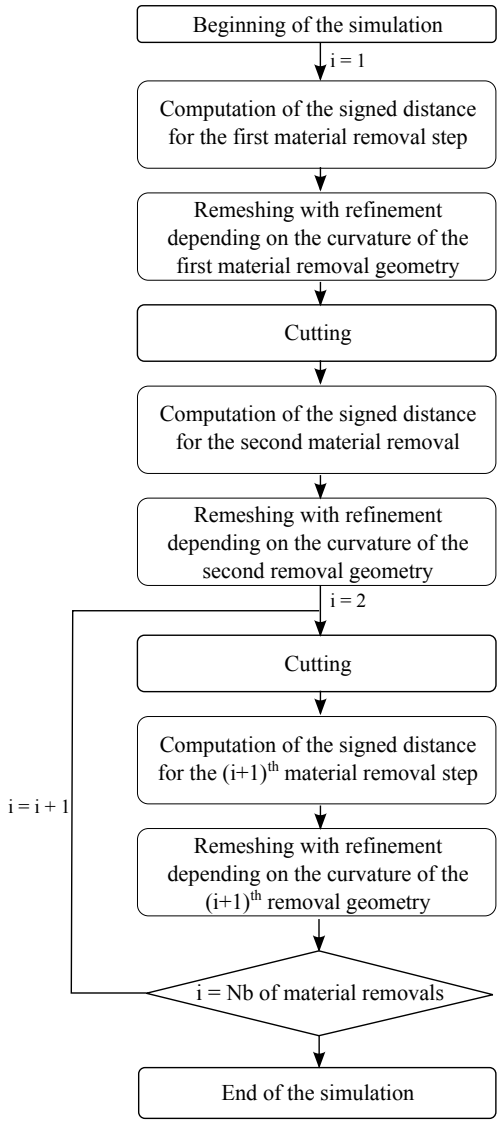

Figure 5.24: Flow chart of the optimised automatic mesh adaptation procedure

- Using the anisotropic remeshing capability as well as the optimised automatic mesh refinement procedure, the possibility to adapt the numerical tool to the machining simulation of thin walled parts, where the cutting conditions cannot always be ignored, could be studied. By remeshing finely the mesh close to the machined surfaces, simplified milling-induced residual stress profiles could be applied onto the machined sub-surface after each material removal step. Deflections during the machining depending on the cutting conditions and the initial residual stresses could then also be predicted.
- The development of a module for the automatic optimisation of the machining sequence could be studied. For each new removal step, several possibilities should be evaluated and the one minimising the deflection of the workpiece would be chosen. However, the feasibility of such a module would have to be studied, especially regarding the

computation time which could be significant. The optimisation of the computation time should therefore be studied first.

Mechanical Analysis of the Machining

In order to develop a better understanding of the machining processes and of the influence of the different parameters on the machining quality the following studies could be performed:

- A literature review as well as tests should be performed to evaluate if the modelling approach (without adaptation) and the methodology are applicable to other materials.
- As shown in Chapter 5, the machining simulation of forged parts can be realised using FORGE OFELIA. A detailed and specific study should therefore be performed in order to develop a specific methodology to improve the machining quality of such parts.
- An experimental study on the measurements of workpiece deflections during machining using linear variable differential transformer (LVDT) sensors and digital image correlation measurements should be realised. These experiments should allow to compare the predicted and measured workpiece deflections during the machining and to add a validation step of the developed numerical tool. In addition, these experiments would also provide more insight information on the behaviour of the workpiece during the machining. Thermocouples could also be placed into the workpiece to determine its temperature evolution during the machining depending on the cutting conditions, the machining sequence and the fixture layout (position of the fixture elements and materials of which they are made). Several types of part geometries (thin or thick walls, open or closed pockets) could be tested and an analysis of the phenomena occurring during the machining could be realised in order to determine which phenomenon has the biggest influence on the machining quality depending on the geometry of the part.
- A study on the fixture-workpiece system compliance should be performed, especially on large forged parts where a high number of fixture elements can be used. An evaluation of the most appropriate modelling approach could be performed (as discussed in Section 4.1.4.3), the influence of the deformation of the global system on the machining quality could thus be analysed and guidelines for the fixture design could be defined.
- The definition of a procedure for the design of appropriate fixture system as well as the automatic generation of a report summarising the main required characteristics of a fixture system should be realised. The procedure would help to design the fixture layout (location and number of fixture elements) whereas the report would provide information regarding the required clamping forces and the evolution of the force applied on each fixture element during the machining. As discussed in Section 4.1.4.3, each fixture element could then be designed depending on the required forces to clamp a distorted workpiece and on the maximal force applied on the fixture elements during the machining (evolves with the redistribution of the residual stresses). This procedure could therefore allow to ensure the design of fixture systems which are able to withstand the mechanical forces linked to the behaviour of the workpiece without any trials, reducing the time needed to design fixtures and minimizing their costs.

Before and After Machining Analysis

Using the developed numerical tool, studies on steps required before (input data) and after (other processes) the machining could be performed. For example, the following studies could be realised using FORGE OFELIA:

- A study of the influence of the residual stress determination method on the accuracy of the residual stress profiles could be realised. Simulations of several destructive methods could be performed (Layer Removal, Hole-Drilling and Slitting method) to validate the residual stress profiles found and a comparison of the results obtained depending on the residual stress profiles used for the machining quality prediction could be drawn. The most adapted and accurate method could then be determined. As discussed in Chapter 3, the development of an inverse method allowing to obtain more accurate residual stress profiles could also be aimed at.
- Relating to the scientific challenges described in the Introduction, future work could also focus on the influence of the residual stresses and machining errors on the assembly process and on the mechanical properties of the global structure.

Bibliography

[1] Airbus. http://www.airbus.com/company/market/gmf2013/. *Global Market Forecast 2013-2032*, 2013.

[2] J. Fernandez Diaz and M. Arizmendi. Machines for the aeronautical industry. In *Machine Tools for High Performance Machining*, pages 399–420. Springer London, 2009.

[3] Airbus. http://www.airbus.com/support/publications/. *Airbus technical magazine: June 2013*, 2013.

[4] Boeing. http://www.boeing.com/commercial/aeromagazine/. *Boeing AERO magazine (QTR 04 2006): Boeing 787*, 2006.

[5] F.C. Campbell. *Manufacturing Technology for Aerospace Structural Materials*. Aerospace Engineering Materials Science. Elsevier Science, 2011.

[6] REXIAA LUSINA. Website of the company specialised in the manufacturing of aerospace parts. *http://www.lusina.eu/*.

[7] E. A. Starke Jr and J.T. Staley. Application of modern aluminum alloys to aircraft. *Progress in Aerospace Sciences*, 32(2–3):131–172, 1996.

[8] J. C. Williams and E. A. Starke Jr. Progress in structural materials for aerospace systems. *Acta Materialia*, 51(19):5775–5799, 2003.

[9] E. A. Starke Jr. Historical development and present status of aluminium-lithium alloys. In N. Eswara Prasad, A. Gokhale, and R.J.H. Wanhill, editors, *Aluminum-Lithium Alloys: Processing, Properties and Applications*. Butterworth-Heinemann, 2013.

[10] R. J. Bucci, C. J. Warren, and E. A. Starke. Need for new materials in aging aircraft structures. *Journal of Aircraft*, 37(1):122–129, 2000.

[11] R. K. Gupta, N. Nayan, G. Nagasireesha, and S. C. Sharma. Development and characterization of Al–Li alloys. *Materials Science and Engineering: A*, 420(1–2):228–234, 2006.

[12] P. Lequeu, K. P. Smith, and A. Danielou. Aluminum-copper-lithium alloy 2050 developed for medium to thick plate. *Journal of Materials Engineering and Performance*, 19(6):841–847, 2010.

[13] F. Klocke and A. Kuchle. *Manufacturing Processes 1: Cutting*. RWTHedition. Springer, 2011.

[14] Y. Wei and X. W. Wang. Computer simulation and experimental study of machining deflection due to original residual stress of aerospace thin-walled parts. *The International Journal of Advanced Manufacturing Technology*, 33(3-4):260–265, 2006.

[15] S.P. Wang and S. Padmanaban. A new approach for FEM simulation of NC machining processes. In *AIP Conference Proceedings*, volume 712, pages 1371–1376, 2004.

[16] Z.T. Tang, Z.Q. Liu, and X. Ai. Optimization of Bulkhead Processing Sequence for Multi-Frame Monolithic Components by FEM. *Advanced Materials Research*, 24-25:355–360, 2007.

[17] J.K. Rai and P. Xirouchakis. Finite element method based machining simulation environment for analyzing part errors induced during milling of thin-walled components. *International Journal of Machine Tools and Manufacture*, 48(6):629–643, 2008.

[18] J.K. Rai and P. Xirouchakis. FEM-based prediction of workpiece transient temperature distribution and deformations during milling. *International Journal of Advanced Manufacturing Technology*, 42:429–449, 2009.

[19] S. Das and U. Chandra. *"Residual Stress and Distortion," in Handbook of Aluminum Metallurgy: Processes and Equipment*, volume 1. G. E. Totten and D. S. Mackenzie, Marcel Dekker, Inc., New York, NY, 1999.

[20] S. Hashmi. *Comprehensive Materials Processing*. Elsevier Science, 2014.

[21] G.E. Totten and D.S. MacKenzie. *Handbook of Aluminum: Vol. 1: Physical Metallurgy and Processes*. Handbook of Aluminum. Taylor & Francis, 2003.

[22] V. Hauk. *Structural and Residual Stress Analysis by Nondestructive Methods: Evaluation - Application - Assessment*. Elsevier Science, 1997.

[23] H. K. D. H. Bhadeshia. Residual stress: Material factors. *Handbook of Residual Stress and Deformation of Steel, ASM International*, pages 3–10, 2002.

[24] U. Dilthey. Lecture notes: Welding technology 2 - welding metallurgy. *ISF – Welding and Joining InstituteRWTH – Aachen University*, pages 21–30, 2005.

[25] P.J. Withers and H.K.D.H. Bhadeshia. Residual stress. part 1 – measurement techniques. *Materials Science and Technology*, 17(4):355–365, 2001.

[26] W. Sim. Challenges of residual stress and part distortion in the civil airframe industry. *International Journal of Microstructure and Materials Properties*, 5:446–455, 2010.

[27] J.R. Davis, J.R.D. Associates, and A.S.M.I.H. Committee. *Aluminum and Aluminum Alloys*. ASM specialty handbook. ASM International, 1993.

[28] G. Hammersley, L. A. Hackel, and F. Harris. Surface prestressing to improve fatigue strength of components by laser shot peening. *Optics and Lasers in Engineering*, 34(4–6):327–337, 2000.

[29] T.J. Drozda, C. Wick, R.F. Veilleux, and Society of Manufacturing Engineers. *Tool and Manufacturing Engineers Handbook: Materials, finishing and coating*. TMEH series. Society of Manufacturing Engineers, 1985.

[30] F. Heymes, B. Commet, B. Dubost, P. Lassince, P. Lequeu, and G.M. Raynaud. Development of new Al alloys for distortion free machined aluminium aircraft components. *ASM International(USA)*, pages 249–255, 1997.

[31] J. Lu and Society for Experimental Mechanics (U.S.). *Handbook of measurement of residual stresses*. Fairmont Press, 1996.

[32] M.B. Prime. Residual stress measurement by successive extension of a slot: the crack compliance method. *Applied Mechanics Reviews*, 52(2):75–96, 1999.

[33] H. Ernst. The use of patent data for technological forecasting: The diffusion of CNC-technology in the machine tool industry. *Small Business Economics*, 9(4):361–381, 1997.

[34] X.W. Xu and S.T. Newman. Making CNC machine tools more open, interoperable and intelligent - A review of the technologies. *Computers in Industry*, 57(2):141–152, 2006.

[35] J. A.C Bokhorst, J. Slomp, and N. C. Suresh. An integrated model for part-operation allocation and investments in CNC technology. *International Journal of Production Economics*, 75(3):267–285, 2002.

[36] S.T. Newman, A. Nassehi, X.W. Xu, R.S.U. Rosso Jr., L. Wang, Y. Yusof, L. Ali, R. Liu, L.Y. Zheng, S. Kumar, P. Vichare, and V. Dhokia. Strategic advantages of interoperability for global manufacturing using CNC technology. *Robotics and Computer-Integrated Manufacturing*, 24(6):699–708, 2008.

[37] M. Weck and D. Staimer. Parallel kinematic machine tools – current state and future potentials. *CIRP Annals - Manufacturing Technology*, 51(2):671–683, 2002.

[38] H. Chanal, E. Duc, and P. Ray. A study of the impact of machine tool structure on machining processes. *International Journal of Machine Tools and Manufacture*, 46(2):98–106, 2006.

[39] M. Safaieh, A. Nassehi, and S. T. Newman. A novel methodology for cross-technology interoperability in CNC machining. *Robotics and Computer-Integrated Manufacturing*, 29(3):79–87, 2013.

[40] H.K. Toenshoff and B. Denkena. *Basics of Cutting and Abrasive Processes*. Springer, 2013.

[41] D.A. Stephenson and J.S. Agapiou. *Metal Cutting Theory and Practice*. Manufacturing Engineering and Materials Processing. Taylor & Francis, 2005.

[42] M. E. Merchant. Mechanics of the metal cutting process. *Journal of Applied Physics*, 16(5):267–318, 1945.

[43] A.P. Markopoulos. *Finite Element Method in Machining Processes*. SpringerBriefs in Applied Sciences and Technology. Springer, 2012.

[44] E.H. Lee and B.W. Shaffer. The theory of plasticity applied to a problem of machining. *ASME Journal of Applied Mechanics*, 73:405–413, 1951.

[45] G.C.I. Lin. Prediction of cutting forces and chip geometry in oblique machining from flow stress properties and cutting conditions. *International Journal of Machine Tool Design and Research*, 18(3):117–130, 1978.

[46] P.L.B. Oxley. *The mechanics of machining: an analytical approach to assessing machinability*. Ellis Horwood series in mechanical engineering. E. Horwood, 1989.

[47] S. Hoppe. *Experimental and numerical analysis of chip formation in metal cutting*. PhD thesis, Fakultät für Maschinenwesen der Rheinisch-Westfälischen Technischen Hochschule Aachen, 2003.

[48] P.J. Arrazola, T. Özel, D. Umbrello, M. Davies, and I.S. Jawahir. Recent advances in modelling of metal machining processes. *CIRP Annals - Manufacturing Technology*, 62(2):695–718, 2013.

[49] H.T. Young, P. Mathew, and P.L.B. Oxley. Predicting cutting forces in face milling. *International Journal of Machine Tools and Manufacture*, 34(6):771–783, 1994.

[50] H.Q. Zheng, X.P. Li, Y.S. Wong, and A.Y.C. Nee. Theoretical modelling and simulation of cutting forces in face milling with cutter runout. *International Journal of Machine Tools and Manufacture*, 39(12):2003–2018, 1999.

[51] X.P Li, A.Y.C Nee, Y.S Wong, and H.Q Zheng. Theoretical modelling and simulation of milling forces. *Journal of Materials Processing Technology*, 89–90(0):266–272, 1999.

[52] H.Z. Li, W.B. Zhang, and X.P. Li. Modelling of cutting forces in helical end milling using a predictive machining theory. *International Journal of Mechanical Sciences*, 43(8):1711–1730, 2001.

[53] H.A.G. El-Hofy. *Fundamentals of Machining Processes: Conventional and Nonconventional Processes*. Taylor & Francis, 2006.

[54] J. Fleischer, R. Pabst, and S. Kelemen. Heat flow simulation for dry machining of power train castings. *CIRP Annals - Manufacturing Technology*, 56(1):117 – 122, 2007.

[55] R. Pabst, J. Fleischer, and J. Michna. Modelling of the heat input for face-milling processes. *CIRP Annals - Manufacturing Technology*, 59(1):121 – 124, 2010.

[56] M. B. Da Silva and J. Wallbank. Cutting temperature: prediction and measurement methods—a review. *Journal of Materials Processing Technology*, 88(1–3):195–202, 1999.

[57] N.A. Abukhshim, P.T. Mativenga, and M.A. Sheikh. Heat generation and temperature prediction in metal cutting: A review and implications for high speed machining. *International Journal of Machine Tools and Manufacture*, 46(7–8):782–800, 2006.

[58] L.R. de León García. *Residual Stress and Part Distortion in Milled Aerospace Aluminium*. PhD thesis, Universität Hannover, 2010.

[59] Z.T. Tang, Z.Q. Liu, Y. Wan, and X. Ai. Study on residual stresses in milling aluminium alloy 7050-T7451. In *Advanced Design and Manufacture to Gain a Competitive Edge*, pages 169–178. Springer London, 2008.

[60] D.J. Richardson, M.A. Keavey, and F. Dailami. Modelling of cutting induced workpiece temperatures for dry milling. *International Journal of Machine Tools and Manufacture*, 46(10):1139–1145, 2006.

[61] C. Ming, S. Fanghong, W. Haili, Y. Renwei, Q. Zhenghong, and Z. Shuqiao. Experimental research on the dynamic characteristics of the cutting temperature in the process of high-speed milling. *Journal of Materials Processing Technology*, 138(1–3):468–471, 2003.

[62] B. Denkena, L. de Leon Garcia, and J. Köhler. FEM-simulation of high-performance-milling. In *Proceedings of the 10th CIRP International Workshop on Modeling of Machining Operations*, pages 149–156, 2007.

[63] K.H. Fuh and C.F. Wu. A residual-stress model for the milling of aluminum alloy (2014-T6). *Journal of Materials Processing Technology*, 51(1–4):87–105, 1995.

[64] J.C. Su, K.A. Young, K. Ma, S. Srivatsa, J.B. Morehouse, and S.Y. Liang. Modeling of residual stresses in milling. *The International Journal of Advanced Manufacturing Technology*, 65(5-8):717–733, 2013.

[65] B. Denkena, L. de León-García, and J. Köhler. Influence of high performance cutting operations on the residual stresses of aluminum structural workpieces. In *25th Congress of International Council of the Aeronautical Sciences*, 2006.

[66] B. Denkena, D. Boehnke, and L. León. Machining induced residual stress in structural aluminum parts. *Production Engineering*, 2(3):247–253, 2008.

[67] B. Denkena and L. de León. Machining induced residual stress in wrought aluminium parts. In *Proceedings of 2nd International Conference on Distortion Engineering*, pages 107–114, 2008.

[68] B. Denkena and L. De Leon. Milling induced residual stresses in structural parts out of forged aluminium alloys. *International Journal of Machining and Machinability of Materials*, 4(4):335–344, 2008.

[69] F. Valiorgue, J. Rech, H. Hamdi, P. Gilles, and J.M. Bergheau. A new approach for the modelling of residual stresses induced by turning of 316l. *Journal of Materials Processing Technology*, 191(1–3):270–273, 2007.

[70] N. Guillemot, B. Beaubier, T. Braham, C. Lartigue, and R. Billardon. A hybrid approach to predict residual stresses induced by ball-end tool finishing milling of a bainitic steel. *Advanced Materials Research*, 223:391–400, 2011.

[71] A.Y.C. Nee, Z.J. Tao, and A.S. Kumar. *An Advanced Treatise On Fixture Design And Planning*. Manufacturing Systems and Technology Series. World Scientific, 2004.

[72] A.Y.C. Nee, K. Whybrew, and A.S. Kumar. *Advanced Fixture Design for FMS*. Advanced Manufacturing. Springer London, 2011.

[73] E. Hoffman. *Jig and Fixture Design*. Delmar learning drafting series. Cengage Learning, 2003.

[74] W.E. Boyes and R. Bakerjian. *Handbook of Jig and Fixture Design*. Society of Manufacturing Engineers, 1989.

[75] P.H. Joshi. *Jigs and Fixtures*. Tata McGraw-Hill Education, 2010.

[76] W. Zhong and S. J. Hu. Modeling machining geometric variation in a n-2-1 fixturing scheme. *Journal of Manufacturing Science and Engineering*, 128(1):213–219, 2006.

[77] E.C. De Meter. Min-max load model for optimizing machining fixture performance. *Journal of Engineering for Industry*, 117(2):186–193, 1995.

[78] B. Li and S.N. Melkote. Improved workpiece location accuracy through fixture layout optimization. *International Journal of Machine Tools and Manufacture*, 39(6):871–883, 1999.

[79] B. Li and S. N. Melkote. Optimal fixture design accounting for the effect of workpiece dynamics. *The International Journal of Advanced Manufacturing Technology*, 18(10):701–707, 2001.

[80] J.N. Asante. A combined contact elasticity and finite element-based model for contact load and pressure distribution calculation in a frictional workpiece-fixture system. *The International Journal of Advanced Manufacturing Technology*, 39(5-6):578–588, 2008.

[81] J.D. Lee and L.S. Haynes. Finite-element analysis of flexible fixturing system. *Journal of Engineering for Industry*, 109(2):134–139, 1987.

[82] S. Satyanarayana and S.N. Melkote. Finite element modeling of fixture–workpiece contacts: single contact modeling and experimental verification. *International Journal of Machine Tools and Manufacture*, 44(9):903–913, 2004.

[83] S.P. Siebenaler and S.N. Melkote. Prediction of workpiece deformation in a fixture system using the finite element method. *International Journal of Machine Tools and Manufacture*, 46(1):51–58, 2006.

[84] Y. Wang, X. Chen, N. Gindy, and J. Xie. Elastic deformation of a fixture and turbine blades system based on finite element analysis. *The International Journal of Advanced Manufacturing Technology*, 36(3-4):296–304, 2008.

[85] K.S. Kumar and G. Paulraj. Analysis and optimization of fixture under dynamic machining condition with chip removal effect. *Journal of Intelligent Manufacturing*, 25(1):85–98, 2014.

[86] H. Dong and Y. Ke. Study on Machining Deformation of Aircraft Monolithic Component by FEM and Experiment. *Chinese Journal of Aeronautics*, 19(3):247–254, 2006.

[87] H.C. Kim and M.Y. Yang. Incomplete mesh-based tool path generation for optimum zigzag milling. *The International Journal of Advanced Manufacturing Technology*, 35(7-8):803–813, 2008.

[88] V. Pateloup, E. Duc, and P. Ray. Corner optimization for pocket machining. *International Journal of Machine Tools and Manufacture*, 44(12–13):1343–1353, 2004.

[89] M.B. Bieterman and D.R. Sandstrom. A curvilinear tool-path method for pocket machining. *Transactions-American Society of Mechanical Engineers Journal of Manufacturing Science and Engineering*, 125(4):709–715, 2003.

[90] J. Mayr, M. Ess, S. Weikert, and K. Wegener. Compensation of thermal effects on machine tools using a FDEM simulation approach. *Proceedings Lamdamap*, 9, 2009.

[91] F. Poulhaon, M. Rauch, A. Leygue, J.Y. Hascoet, and F. Chinesta. Toward a real time control of toolpath in milling processes. *Key Engineering Materials*, 554:706–713, 2013.

[92] F. Poulhaon, M. Rauch, A. Leygue, J.Y. Hascoet, and F. Chinesta. Online prediction of machining distortion of aeronautical parts caused by re-equilibration of residual stresses. In *Key Engineering Materials, Proceeding of the 17th annual ESAFORM Conference on Material Forming, Espoo, Finland*, volume 611-612, pages 1327–1335, 2014.

[93] Q.C. Wang, X.D. Hu, W. Li, and J.L. Yuan. Numerical Simulation of Machining Distortion of Residually Stressed Aircraft Aluminum Components. *Key Engineering Materials*, 315-316:235–238, 2006.

[94] Y.B. Bi, H.Y. Dong, Q.L. Cheng, and Y.L. Ke. Distortion Prediction of Aerospace Monolithic Components due to Milling Process. *Key Engineering Materials*, 392-394:841–847, 2009.

[95] W. Bai, R. Hu, and X. Zhu. Finite element simulation and analysis of part deformation induced during milling of thin-walled aerospace monolithic structure parts. In *proceedings of the International Conference on Intelligent Computing and Intelligent Systems (ICIS)*, volume 2, pages 440–444, 2010.

[96] Y. Yang, Y. Wang, and C. Li. Study on Machining Distortion of Titanium Alloy Aircraft Monolithic Component by Finite Element Method and Experiment. *Advanced Science Letters*, 4(8):3206–3210, 2011.

[97] Y.W. Liu. Numerical Simulation of the Machining Distortion of Aircraft Aluminum Part Caused by Redistribution of Residual Stress. *Advanced Materials Research*, 142:122–125, 2011.

[98] M. Zhongyi and W. Yunqiao. Analyzing distortion of aircraft Structural part in NC machining based on FEM simulation. In *proceedings of the International Conference on Mechanical and Electrical Technology*, pages 1–5, 2010.

[99] K. Ma, R. Goetz, and S.K. Svrivatsa. Modeling of Residual Stress and Machining Distortion in Aerospace Components. *ASM Handbook, Metals Process Simulation*, 22B:386–407, 2010.

[100] T.D. Marusich, S. Usui, and K.J. Marusich. Finite element modeling of part distortion. In *Intelligent Robotics and Applications*, volume 5315 of *Lecture Notes in Computer Science*, pages 329–338. 2008.

[101] O. Pierard, J. Barboza, M. Duflot, and L. D'Alvise. Relaxation of residual stresses during multi-passes machining: Simulation with the level-set method and process optimization. In 8^{th}. *World Congress on Computational Mechanics (WCCM8)*, pages 623–629, 2008.

[102] O. Pierard, J. Barboza, M. Duflot, L. D'Alvise, and A. Perez-Duarte. Distortions prediction during multi-pass machining simulations by using the level-set method. *International Journal of Material Forming*, 1(1):563–565, 2008.

[103] B. Wucher1, P. Martiny1, O. Pierard1, H. Minnebo1, and Lani1 F. Simulation de cuisson et d'usinage de composites à fibres longues. In $10^{\text{è}me}$ *colloque national en calcul des structures, Giens - France*, 2011.

[104] A. Del Prete, A. A. de Vitis, and R. Franchi. Numerical-Experimental Correlation of Distortions Induced by Machining Process on Thin-Walled Nickel Super Alloy Forged Components. *Key Engineering Materials*, 504-506:1299–1304, 2012.

[105] J.K. Rai. FEM-*MILL: A Finite Element Based 3D Transient Milling Simulation Environment for Process Plan Verification and Optimization.* PhD thesis, Federal Polytechnic School of Lausanne, 2008.

[106] L. Masset and J.F. Debongnie. Machining processes simulation: specific finite element aspects. *Journal of Computational and Applied Mathematics*, 168(1–2):309 – 320, 2004.

[107] Y. Yang, M. Li, and K.R. Li. Comparison and analysis of main effect elements of machining distortion for aluminum alloy and titanium alloy aircraft monolithic component. *The International Journal of Advanced Manufacturing Technology*, 70(9-12):1803–1811, 2014.

[108] J.L. Chenot. Three dimensional finite element modeling of forging process. In *Computational Plasticity: Models, Software and Applications*, pages 793–816. Proceedings of the Second International Conference Held in Barcelona, Spain, 1989.

[109] D.N. Arnold, F. Brezzi, and M. Fortin. A stable finite element for the stokes equations. *CALCOLO*, 21(4):337–344, 1984.

[110] T. Coupez, H. Digonnet, and R. Ducloux. Parallel meshing and remeshing. *Applied Mathematical Modelling*, 25(2):153–175, 2000.

[111] FORGE® TRANSVALOR S.A. http://www.transvalor.com/en/. *Finite element software*, 2011.

[112] M. Rappaz, M. Bellet, and M. Deville. *Modélisation numérique en science et génie des matériaux*. Traité des matériaux. Presses polytechniques et universitaires romandes, 1998.

[113] C. Gay. *Contribution à la simulation numérique tridimensionnelle du forgeage à froid*. PhD thesis, MINES ParisTech, 1995.

[114] J. Barboza. *Traitement de contact entre corps déformables et calcul parallèle pour la simulation 3D du forgeage multicorps*. PhD thesis, MINES ParisTech, 2004.

[115] E. Perchat. *Mini element et factorisations incomplètes pour la parallélisation d'un solveur de stokes* 2D. *Application au forgeage*. PhD thesis, MINES ParisTech, 2000.

[116] C. Aliaga. *Simulation numérique par éléments finis en 3D du comportement thermomécanique au cours du traitement thermique d'aciers : application à la trempe de pièces forgées ou coulées*. PhD thesis, MINES ParisTech, 2000.

[117] K. Mocellin. *Contribution à la simulation numérique tridimensionnelle du forgeage à chaud : étude du contact et calcul multigrille*. PhD thesis, MINES ParisTech, 1999.

[118] P. Wriggers. *Computational Contact Mechanics*. John Wiley and Sons, 2002.

[119] L. Fourment, J. L. Chenot, and K. Mocellin. Numerical formulations and algorithms for solving contact problems in metal forming simulation. *International Journal for Numerical Methods in Engineering*, 46(9):1435–1462, 1999.

[120] J.-L. Chenot, L. Fourment, and K. Mocellin. Numerical treatment of contact and friction in FE simulation of forming processes. *Journal of Materials Processing Technology*, 125–126(0):45–52, 2002.

[121] S. Fayolle. *Modélisation numérique de la mise en forme et de la tenue mécanique des assemblages par déformation plastique: application au rivetage auto-poinçonneur*. PhD thesis, MINES ParisTech, 2008.

[122] T. Coupez, L. Fourment, and J.L. Chenot. Adaptive solutions in industrial forming process simulation. In P. Ladevèze and J.T. Oden, editors, *Advances in Adaptive Computational Methods in Mechanics*, volume 47 of *Studies in Applied Mechanics*, pages 365–381. Elsevier, 1998.

[123] R. Boussetta. *Estimateurs d'erreur et ramaillage adaptatif: application à la simulation 3D des procédés de mise en forme des matériaux*. PhD thesis, MINES ParisTech, 2005.

[124] X. Cerutti and K. Mocellin. Parallel finite element tool to predict distortion induced by initial residual stresses during machining of aeronautical parts. *International Journal of Material Forming*, pages 1–14, 2014.

[125] M.B. Prime and M.R. Hill. Residual stress, stress relief, and inhomogeneity in aluminum plate. *Scripta Materialia*, 46(1):77–82, 2002.

[126] S. Marie. *Un modèle de parallélisation SPMD pour la simulation numérique de procédés de mise en forme de matériaux*. PhD thesis, MINES ParisTech, 1997.

[127] H. Digonnet. *Repartitionnement dynamique, mailleur parallèle et leurs applications à la simulation numérique en mise en forme des matériaux*. PhD thesis, MINES ParisTech, 2001.

[128] M. Snir, S. Otto, S. Huss-Lederman, D. Walker, and J. Dongarra. *MPI-The Complete Reference, Volume 1: The MPI Core*. MIT Press, Cambridge, MA, USA, 2nd. (revised) edition, 1998.

[129] S. Osher and R.P. Fedkiw. Level set methods: An overview and some recent results. *Journal of Computational Physics*, 169(2):463–502, 2001.

[130] K. Y. Lervag, B. Muller, and S. T. Munkejord. Calculation of the interface curvature and normal vector with the level-set method. *Computers & Fluids*, 84:218–230, 2013.

[131] S. Van Der Veen, F. Heymes, J. Boselli, P. Lequeu, and P. Lassince. Low internal stress Al-Zn-Cu-Mg plates, 2006. US Patent App. 11/299,683.

[132] P. Lequeu, P. Lassince, T. Warner, and Raynaud G.M. Engineering for the future: weight saving and cost reduction initiatives. *Aircraft Engineering and Aerospace Technology*, 73:147–159, 2010.

[133] R.W. Schultz and M.E. Karabin. Characterization of machining distortion by strain energy density and stress range. In *Materials Science Forum Vols. 6th European conference on residual stresses*, volume 404–407, pages 61–68, 2002.

[134] R. G. Treuting and W. T. Jr. Read. A mechanical determination of biaxial residual stress in sheet materials. *Journal of Applied Physics*, 22(2):130–134, 1951.

[135] A.V. Virkar. Determination of residual stress profile using a strain gage technique. *Journal of the American Ceramic Society*, 73(7):2100–2102, 1990.

[136] Ph. Jeanmart and J. Bouvaist. Finite element calculation and measurement of thermal stresses in quenched plates of high–strength 7075 aluminium alloy. *Materials Science and Technology*, 1(10):765–769, 1985.

[137] R. Tandon and D.J. Green. Residual stress determination using strain gage measurements. *Journal of the American Ceramic Society*, 73(9):2628–2633, 1990.

Appendix A

OFELIA Project

In this appendix, the partners as well as the five principal tasks of the project are presented.

Industrial Partners

Constellium is the company which has developed the new AIRWARE® alloys and which is specialised in the manufacture of foundry, rolled and extruded aluminium alloy products. The AIRWARE® alloys represent the new generation of materials for aviation and space. Many investments and studies have been made. However, the cost of these alloys is high, particularly due to the alloying elements used (silver, lithium). The OFELIA project's objective being to improve the eco-efficiency of the AIRWARE® alloys sector has therefore allowed to improve the competitive position of the AIRWARE® alloys as well as to obtain a better mastery of the whole manufacturing chain.

In this project two entities of Constellium are employed. The Constellium Technology Center, the most important center of R&D in Western Europe on aluminium and its alloys and the production site of Issoire. The Constellium Technology Center is specialised in the design of new aluminium alloys, their production and metallurgical processing, as well as material characterization (microstructure, rheology, thermal properties, etc.) and numerical simulation of manufacturing processes. The production site of Issoire is one of the Constellium sites specialised in machining.

Aubert&Duval is a company specialised in the manufacture of forged and stamped products made of aluminium alloys as well as of steels, of titanium alloys or of superalloys. The manufacturing is usually performed by hot forging or stamping, followed by possible thermal treatments, stress relieving or machining. The R&D department of Aubert&Duval realises also numerical simulations of these different manufacturing steps in order to optimise

them. The finite element software FORGE® is one of the programs used to perform these studies.

Aubert& Duval is the first company to offer forged and stamped parts made of AIRWARE® 2050 alloy. The OFELIA project has enabled Aubert&Duval to increase their knowledge and mastery of the manufacturing of forged and stamped parts made of AIRWARE® 2050 alloy. It has also given the company the opportunity to offer their customers a service as complete as possible, including consulting services on the machining of forged and stamped AIRWARE® 2050 alloy parts.

REXIAA is a group specialised in machining. LUSINA is a company which has become part of the REXIAA group during the project and which is specialised in the machining of very large dimensions. It has capabilities for machining parts up to 12 m in length and 3.7 m in width. REXIAA-LUSINA has therefore been able to provide all its experience in the machining of large aerospace parts. The OFELIA project has allowed them subsequently to improve the treatment and the recycling chain of the machining chips as well as to increase their knowledge of the machining of large AIRWARE® 2050 alloy parts.

Academic Partners

The Centre for Material Forming (Cemef) is the research center of the Mines ParisTech school where the work presented in this dissertation has been performed. The Centre for Material Forming is specialized in the development of numerical methods for modelling manufacturing processes of all kind of materials. In the past, the work of Cemef has in particular given rise to the development of the finite element software FORGE®, which is a software allowing simulations of manufacturing processes with conditions as close as possible to the industrial ones. With this finite element software the work presented in this dissertation has been realised.

The OFELIA project has allowed to develop and to integrate a new approach and a new numerical tool for the machining simulation of large aerospace AIRWARE® 2050 alloy parts into the software FORGE®. These developments have therefore extended the software FORGE® with the ability to simulate the whole manufacturing line of large and complex aerospace AIRWARE® 2050 alloy parts (from rolled plates or forged parts). All the important information about the manufacturing steps of the parts (geometry, possible default, stress state, etc.) can be obtained, giving the possibility to optimise the entire manufacturing line and to study the operating performance and lifetime of the parts in taking into account the whole manufacturing history.

The French Institute for Advanced Mechanics (IFMA) is a research laboratory that conducts research on machining and on methods to determine optimal machining paths (CAM software). The OFELIA project has enabled IFMA to continue its work with the implementation of a specification tool for machining process plans for aerospace parts. Moreover, the OFELIA project has offered a direct link to the industrial reality and problematic as well as the possibility to compare the results on industrial cases.

The Center for Chemical Engineering (SPIN) of the Ecole des Mines de Saint-Etienne is a laboratory specialised in the transformation processes of materials and energy. The laboratory SPIN is particularly specialised in the kinetic modelling of heterogeneous transformations involving a solid phase. The OFELIA project has enabled the laboratory SPIN to increase its expertise in the techniques of physico-chemical characterisation of the AIRWARE® 2050 alloy with the objective to optimise the recycling of the machining chips.

OFELIA Project Tasks

The OFELIA project has been structured in five tasks which are presented below.

TASK 1: Mastery of the residual stresses of thick products before machining
Objective: To master and to model the residual stresses of thick AIRWARE® 2050 alloy products
Stakeholders: Aubert&Duval and Constellium

TASK 2: Optimisation of the machining process plan of AIRWARE® 2050 alloy aerospace parts with numerical simulations
Objective: To predict the quality of the parts and the accuracy of the machining process in function of the machining process plan used
Stakeholders: Cemef, IFMA, Aubert&Duval, Constellium, REXIAA and LUSINA

TASK 3: Characterization of an optimised machining chip for recycling improvements
Objective: To define the specifications of an optimised recyclable machining chip and to determine the technical and economic optimum (machining and recycling)
Stakeholders: IFMA, Constellium and SPIN

TASK 4: Development of an optimised alloy for the sector of thick products
Objective: To define an optimised alloy for thick products allowing to improve the eco-efficiency of the sector (improve the chemical pollution tolerance)
Stakeholders: Aubert&Duval and Constellium

TASK 5: Global optimisation of the AIRWARE® 2050 alloy sector: eco-efficiency of the machining process plan and recycling
Objective: To incorporate the conclusions of the previous tasks to identify and to validate one

or more sectors with maximum eco-efficiency and to develop an eco-efficient optimisation tool for the definition of machining process plans
Stakeholders: Cemef, IFMA, SPIN, Aubert&Duval, Constellium, REXIAA and LUSINA

A review of the project organisation and collaboration between the different stakeholders is illustrated in Figure A.1.

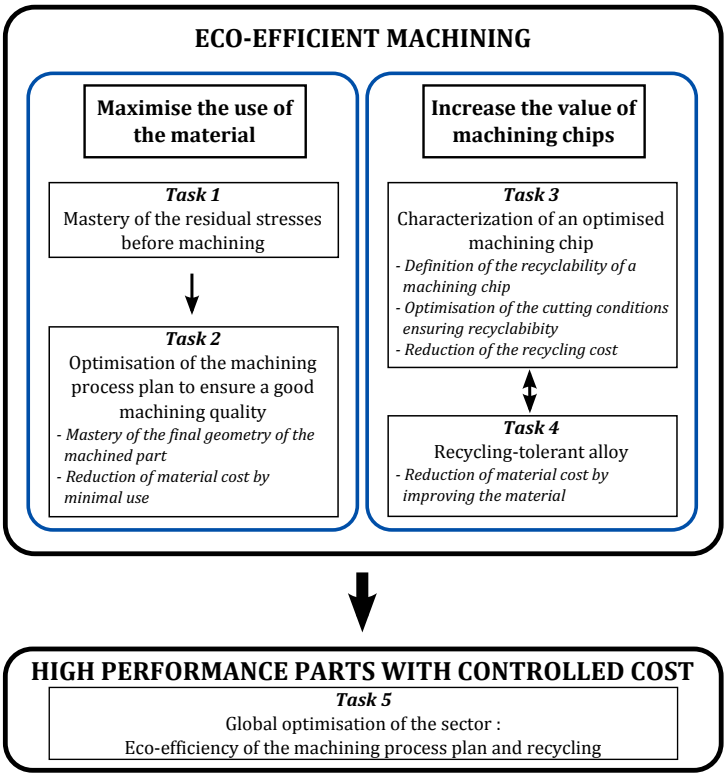

Figure A.1: Illustration of the organization of the OFELIA project and the interactions between each task and their stakeholders

Appendix B

The Layer Removal Method: Residual Stress Redistribution

The layer removal method, introduced by Treuting & Read [134], allows to estimate residual stresses (Type I) in sheet materials. It is based on the successive removal of layers and on strain or curvature measurements of the samples due to the redistribution of the residual stresses after each removed layer. These operations are realised through the whole thickness of the samples taken from the rolling and transverse directions. Using the elastic theory the residual stress profiles inside the plate are computed. However, this method is based upon the following assumptions:

1. Young's modulus and Poisson's ratio are constant in the specimens.
2. The removal of successive layers does not disturb the initial residual stresses in the samples (no machining-induced residual stress).
3. Residual stresses vary only throughout the thickness.

More precisely, the layer removal method using a strain gauge technique has been used in this study (Section 3.1).

A simplified example of layers removed from a panel is considered. The analysis allowing to relate the residual stress distribution to the measured strain as well as the analysis of the phenomenon of the redistribution of residual stresses and the associated distortion due to the material removal are briefly explained.

Let h and b denote respectively the height and width of a panel sampled from a rolled plate. A strain gauge has been bonded on it. Assuming plane stress conditions ($\sigma_{zz} = 0$), the strains ϵ_{xx} and ϵ_{yy} in the x- and y-direction can be expressed as

$$\epsilon_{xx} = \frac{\sigma_{xx} - \nu\sigma_{yy}}{E} \qquad \text{and} \qquad \epsilon_{yy} = \frac{\sigma_{yy} - \nu\sigma_{xx}}{E} \tag{B.1}$$

where σ_{xx} and σ_{yy} are the stresses in the x- and y-direction.

For the sake of simplicity, it is assumed that $\sigma_{xx} = \sigma_{yy} = \sigma(z)$. $\sigma(z)$ is the residual stress profile evolving only through the thickness of the plate. Using this assumption the strains in both the x- and y-directions are given by

$$\epsilon(z) = \frac{(1-\nu)\sigma(z)}{E} \tag{B.2}$$

The forces and bending moments associated with the initial residual stress profiles being balanced, the following conditions can be written

$$\begin{aligned} F_x = F_y = b\int_0^h \sigma(z)dz = 0 \\ M_x = M_y = b\int_0^h \sigma(z)zdz = 0 \end{aligned} \tag{B.3}$$

with F_x and F_y being the forces and M_x and M_y the bending moments in the x- and y-direction.

When the material is removed layer by layer, a new state of equilibrium is reached and therefore a new residual stress profile is obtained. If one layer with a thickness of a is removed, the new residual stress σ' can be expressed as

$$\sigma^{'}(z) = \sigma(z) + \sigma_{l1}(a) \tag{B.4}$$

with $\sigma_{l1}(a)$ being a uniform balancing stress due to the removal of the first layer.
Considering balanced forces in the resulting specimen, the following equation can be written

$$b\int_0^{h-a} \sigma^{'}(z)dz = 0 \tag{B.5}$$

Whereas the forces will be balanced, the bending moments will not be due to the new asymmetric residual stress profile. A moment has to be created to counterbalance the moment $M(a) = b\int_0^{h-a}\sigma^{'}(z)zdz \neq 0$ [135]. The new residual stress profile that will satisfy both the force and moment equilibrium can be written as

$$\sigma_{new}(z) = \sigma^{'}(z) + \frac{M(a)\left(\frac{h-a}{2} - z\right)}{I} \tag{B.6}$$

with I being the moment of inertia expressed as

$$I = \frac{b \times (h-a)^3}{12}$$

In order to reach a new state of equilibrium (of the forces and moments) the residual stresses are redistributed leading to the deformation of the sample. Figure B.1 illustrates the evolution of the residual stress profile, starting from the initial residual stress profile $\sigma(z)$ to the residual

stress profile allowing to obtain the force equilibrium $\sigma'(z)$ and then to the residual stress profile allowing to fulfil both the force and moment equilibrium $\sigma_{new}(z)$. It is the re-equilibrium of the moment which provokes distortion, as also illustrated in Figure B.1.

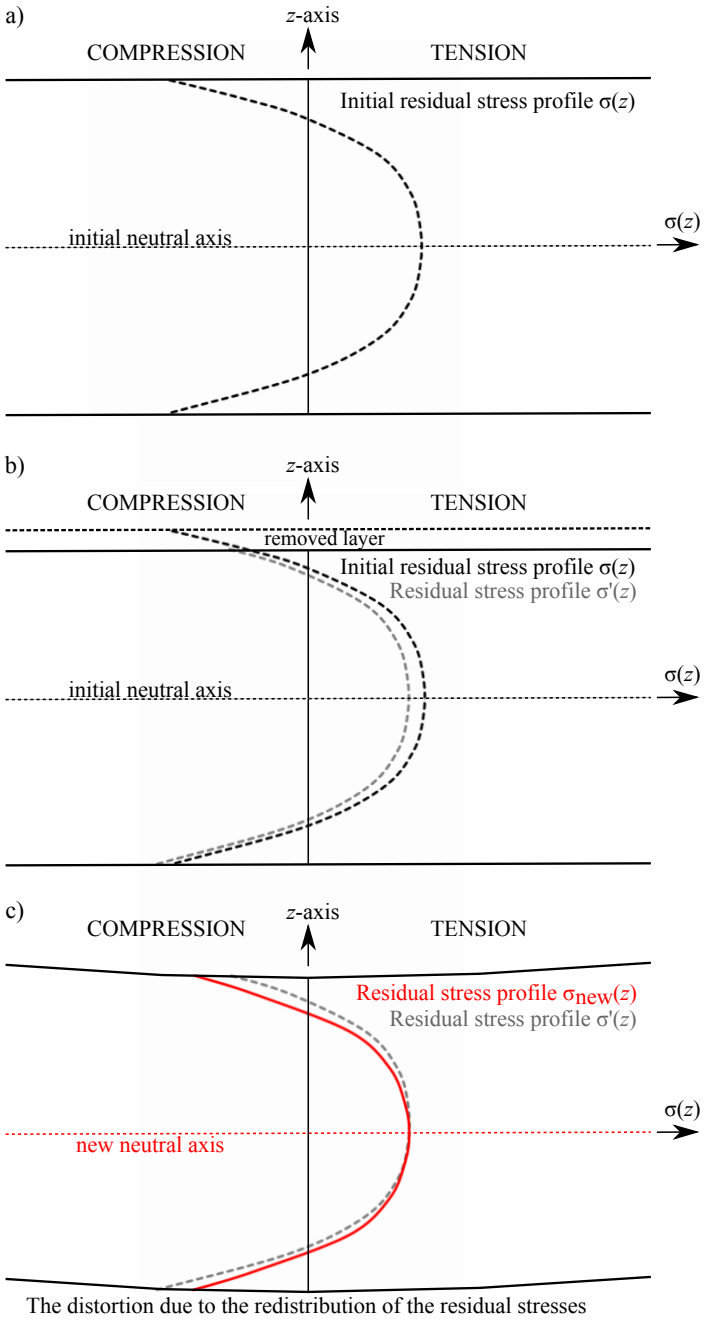

Figure B.1: Illustration of the residual stress redistribution after the removal of a layer with a simplified residual stress distribution: a) The initial residual stress profile ; b) The residual stress profile after the layer removal with only balanced forces ; c) The new residual stress profile after the layer removal respecting both the force and moment equilibrium

The strain gauge is bonded at the center of the lower surface of the sample and is used to measure the evolution of the strain linked to the redistribution of the residual stresses after each layer removal. Using this method, authors in [135, 136, 137] have demonstrated that it is possible to link the initial residual stress profiles to the measured strain. Equation B.7 represents this relation and gives the measured strain depending on the thickness of the layer removed. For more details on this technique and the theoretical analysis, readers can refer to [135, 137].

$$\epsilon(a) = \frac{1-\nu}{E(h-a)^2} \int_0^{h-a} [6z - 4(h-a)]\, \sigma(z)\, dz \tag{B.7}$$

with $\epsilon(a)$ being the strain detected by the strain gauge due to the removal of a layer of thickness a and $\sigma(z)$ the initial residual stress profile.

Appendix C

Machining of a "Closed Pockets" Case

This case deals with the study of the part illustrated in Figure C.1, for which almost 80% of the volume of the initial workpiece is removed during the machining. This value is representative of the amount of material usually machined on aeronautics parts. The same preparation steps as for the test presented in section 3.3.1 are performed in order to obtain the same initial geometry shown in Figure 3.18.

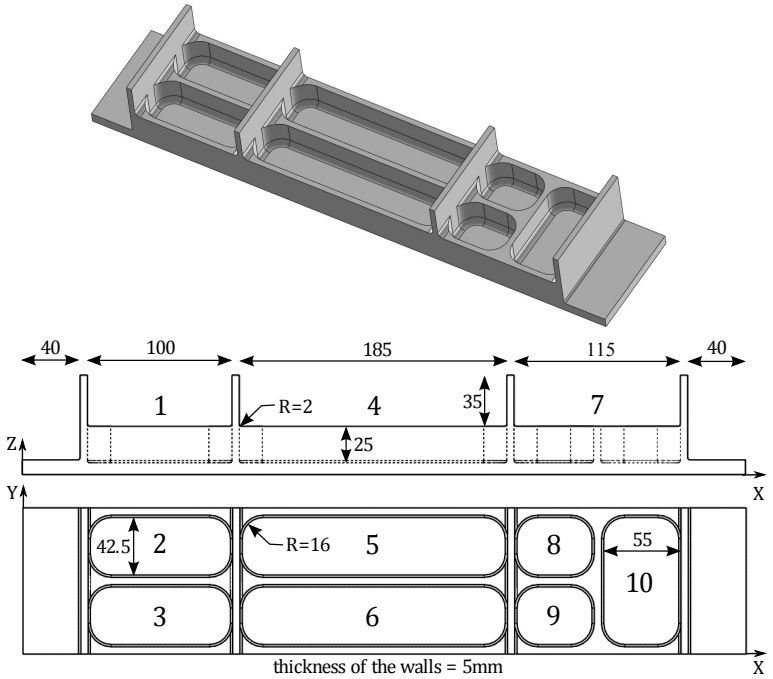

Figure C.1: The part geometry and the pocket numbers

The same fixture layout as the one represented in Figure 3.20 is used. The machining of the ten machining features shown in Figure C.1 has been performed with forty-three material

removal steps. The material removal depths are defined in function of the machining depths of cut (equivalent to a model of Level 5), which are representative of what can be used in industry. The features 1, 4 and 7 have been numerically machined with five layers of material removal steps each (7 mm thick layers), whereas the features 2, 3, 5, 6, 8, 9 and 10 have been machined with four material removal steps each, three of 7 mm and one of 4 mm (the last one). Figure C.2 shows the evolution of the von Mises stress state and the distortions which can be observed during the machining simulation at three different steps.

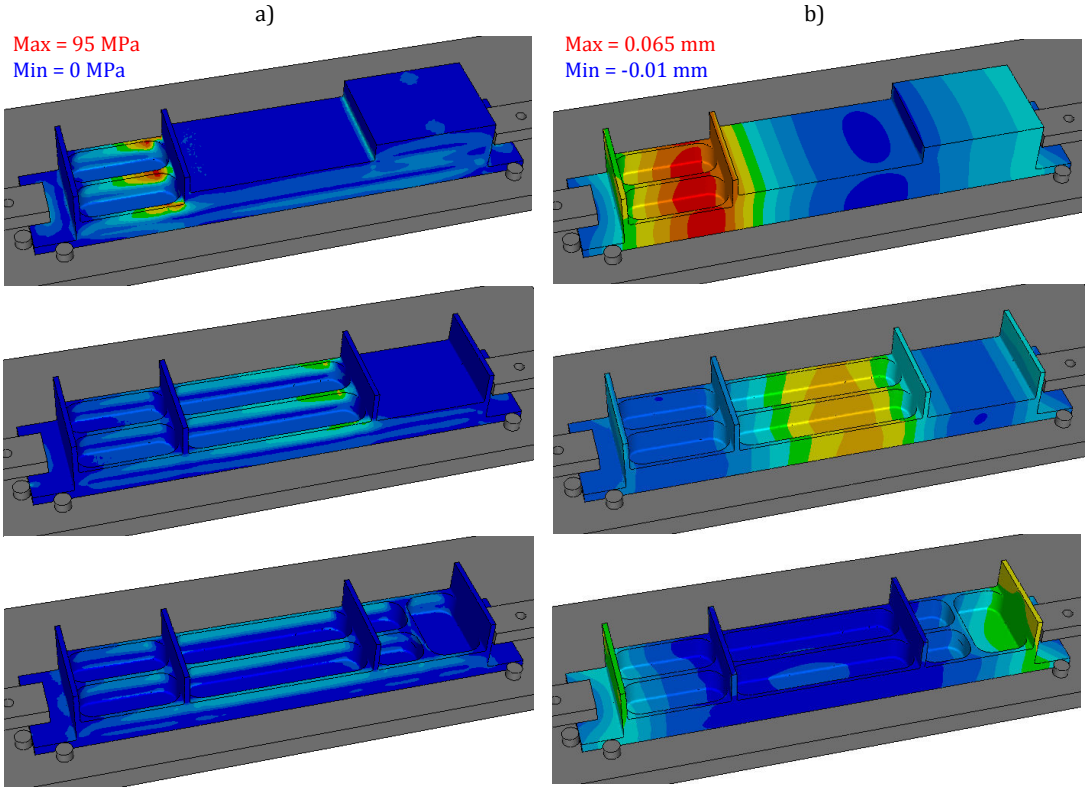

Figure C.2: Evolution of the workpiece during the machining: a) The residual stress state (von Mises stress field); b) The displacements along the Z-axis linked to the changing geometry of the part during the machining simulation

The predicted machined part geometry with amplified distortion can be observed in Figure C.3a. In parallel, experimental machining has been performed twice using the machining process plan described for the simulation (depth of cut, radius of the tool, fixture layout and machining sequence). Distortion measurements have been performed on the bottom surface of the part using a CMM. The curvature of the part can then be compared to the one resulting from the simulation. In Figure C.3b the distortion observed on the bottom surface of the part is plotted for simulation and experimental results. For both experiments similar distortions have been obtained, showing again a good repeatability of the test. A good agreement between the numerically predicted distortion and the measured one can be also observed in this case showing the capability of the developed approach to predict accurately the evolution of the residual stress state in the workpiece during the whole machining process.

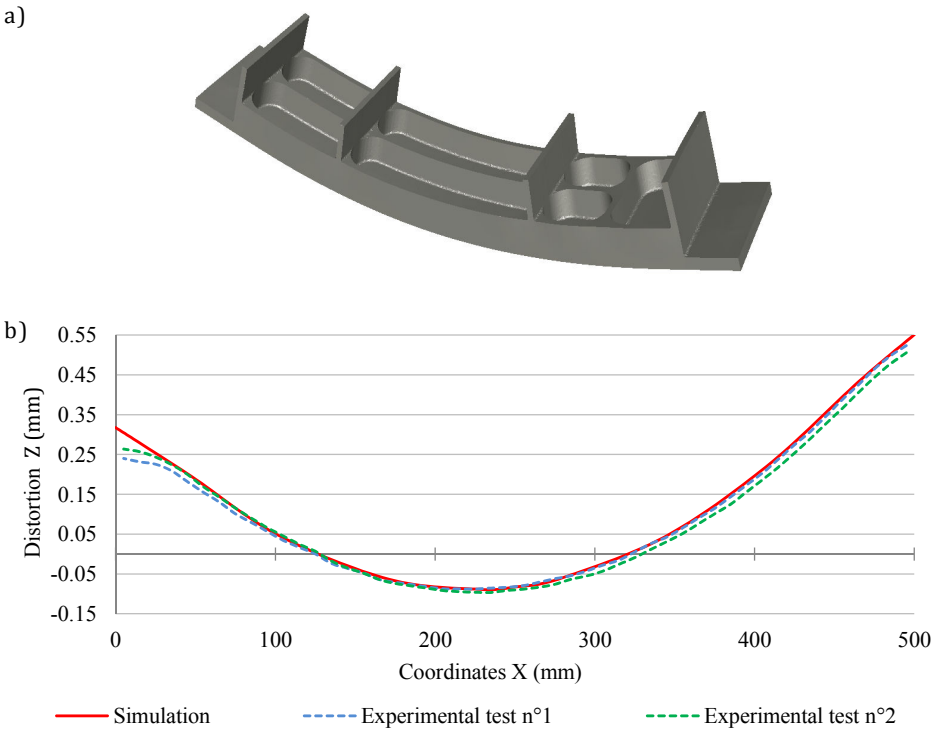

Figure C.3: The post-machining distortion of the part: a) The machined part with amplified distortion ; b) Comparison between experimental and simulation distortion

Appendix D

Results Presented in Chapter 4

D.1 70mm Thick AIRWARE® 2050-T84 Alloy Rolled Plate: Thickness Variations

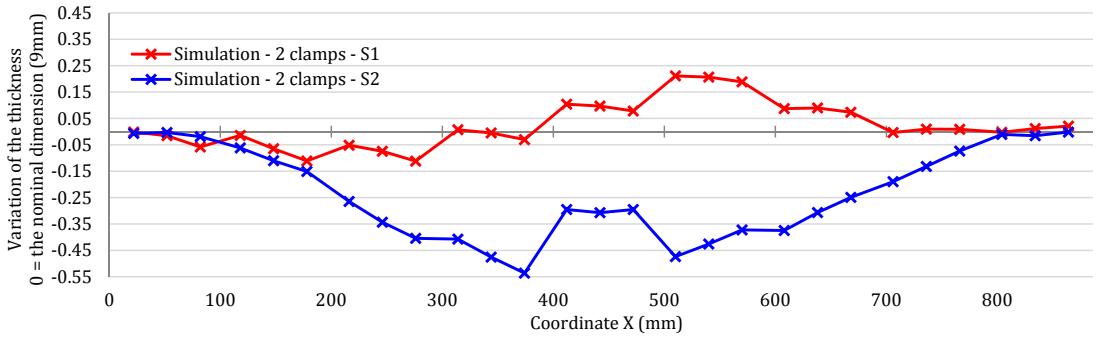

Figure D.1: Thickness variations of the wall with a nominal dimension of 9 mm with the fixture layout with two clamps and two different machining sequences

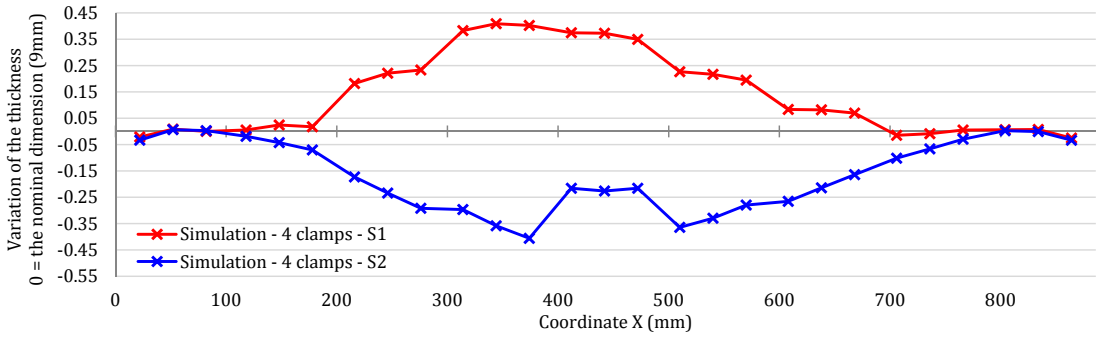

Figure D.2: Thickness variations of the wall with a nominal dimension of 9 mm with the fixture layout with four clamps and two different machining sequences

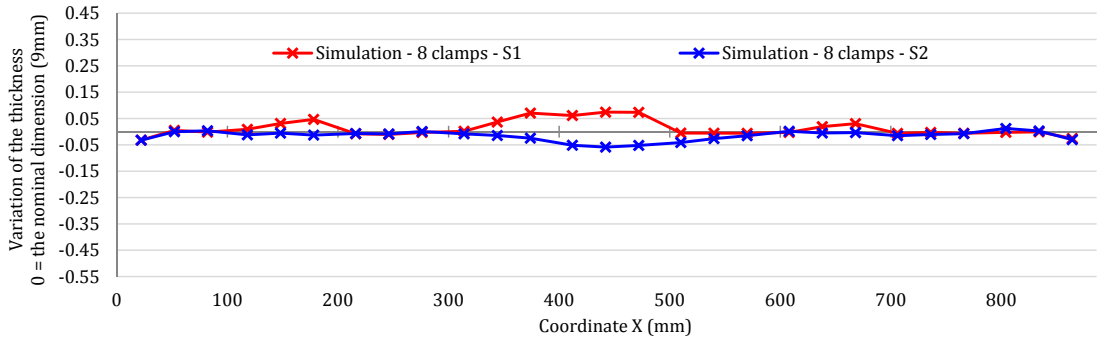

Figure D.3: Thickness variations of the wall with a nominal dimension of 9 mm with the fixture layout with eight clamps and two different machining sequences

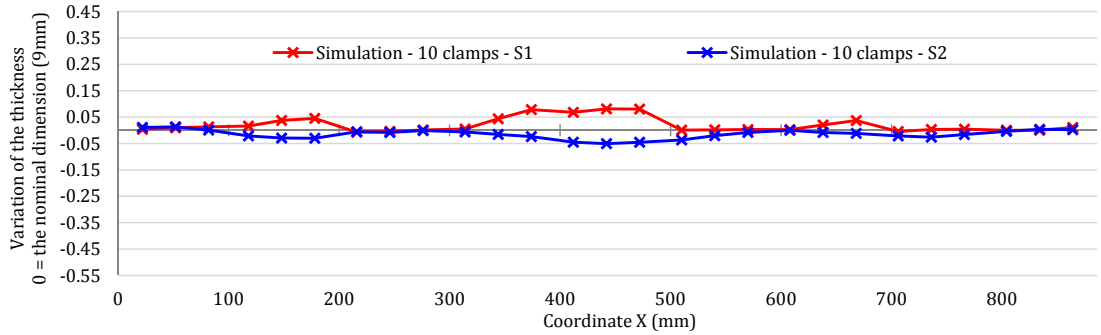

Figure D.4: Thickness variations of the wall with a nominal dimension of 9 mm with the fixture layout with ten clamps and two different machining sequences

D.2 90mm Thick AIRWARE® 2050-T84 Alloy Rolled Plate

D.2.1 Post-Machining Distortions

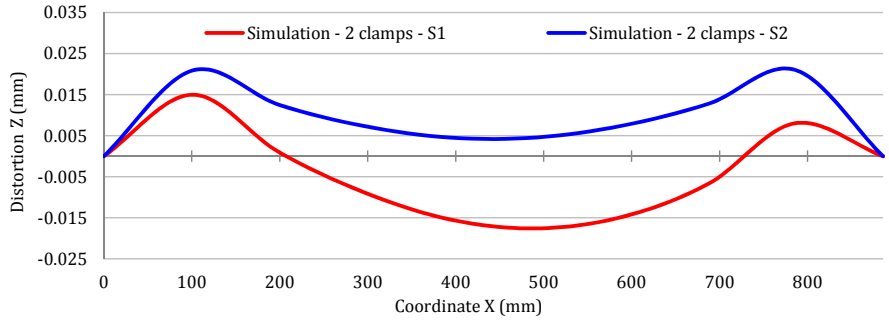

Figure D.5: Post-machining distortion after the second machining step with the fixture layout with two clamps and two different machining sequences

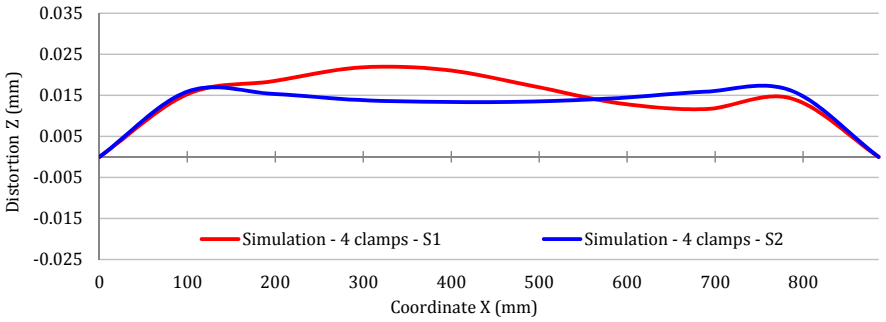

Figure D.6: Post-machining distortion after the second machining step with the fixture layout with four clamps and two different machining sequences

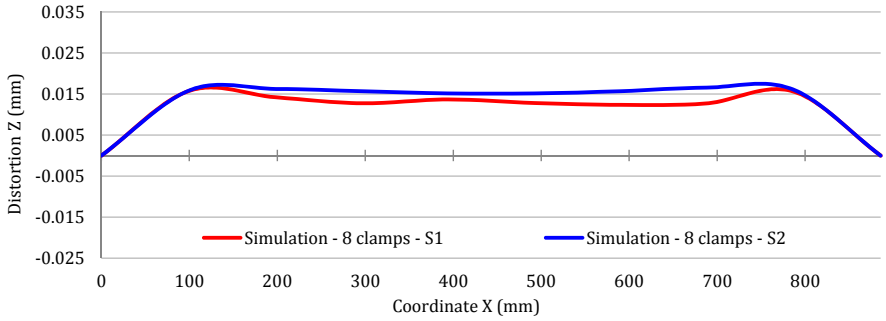

Figure D.7: Post-machining distortion after the second machining step with the fixture layout with eight clamps and two different machining sequences

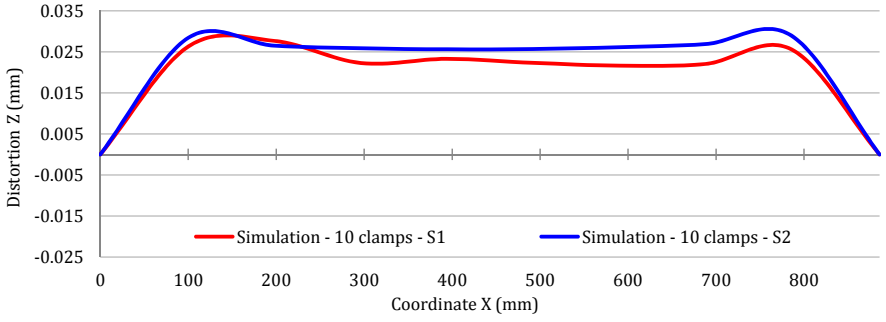

Figure D.8: Post-machining distortion after the second machining step with the fixture layout with ten clamps and two different machining sequences

D.2.2 Thickness Variations

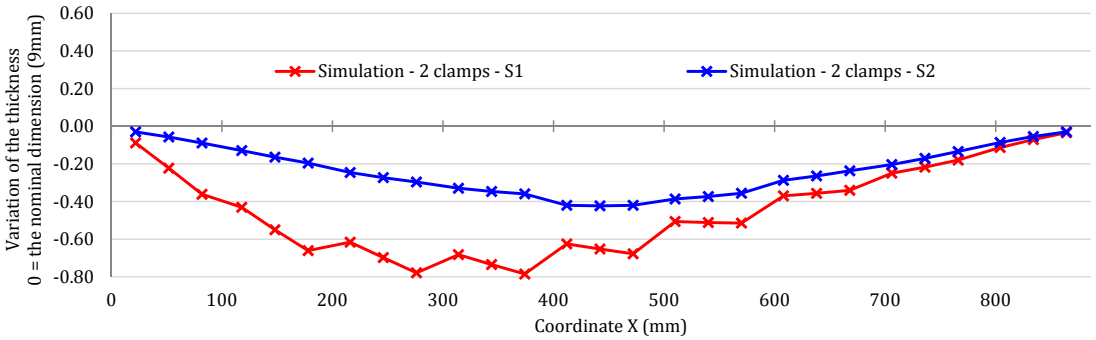

Figure D.9: Thickness variations of the wall with a nominal dimension of 9 mm with the fixture layout with two clamps and two different machining sequences

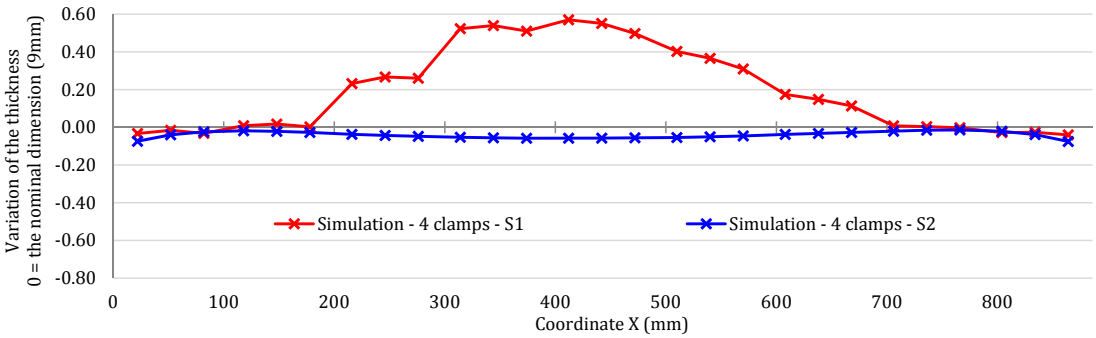

Figure D.10: Thickness variations of the wall with a nominal dimension of 9 mm with the fixture layout with four clamps and two different machining sequences

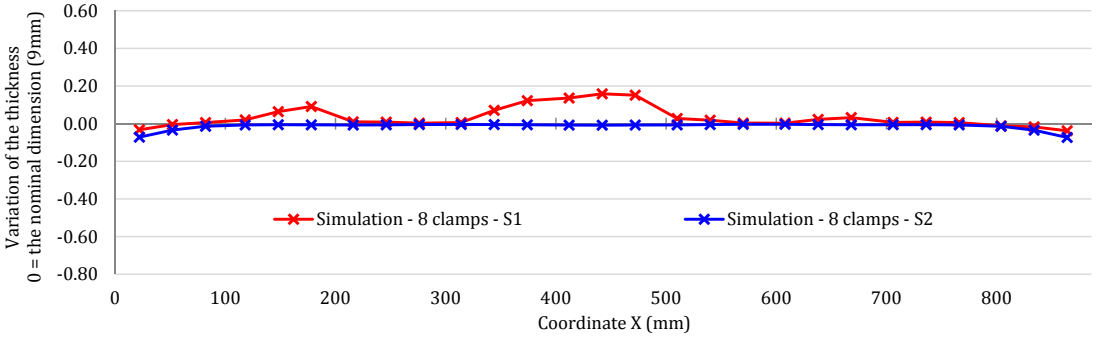

Figure D.11: Thickness variations of the wall with a nominal dimension of 9 mm with the fixture layout with eight clamps and two different machining sequences

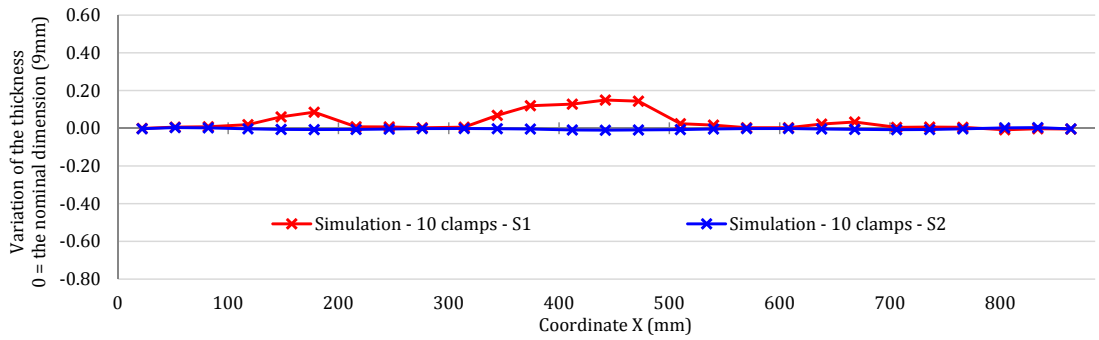

Figure D.12: Thickness variations of the wall with a nominal dimension of 9 mm with the fixture layout with ten clamps and two different machining sequences

Modélisation numérique et analyse mécanique de l'usinage de grandes pièces aéronautiques : Amélioration de la qualité d'usinage

RÉSUMÉ : La fabrication des grandes pièces structurelles aéronautiques en alliage d'aluminium nécessite la réalisation de multiples étapes de mises en forme (laminage, matriçage, etc...) et de traitements thermiques. Les différents chargements mécaniques et thermiques subis par les pièces pendant ces étapes de fabrication induisent des déformations plastiques ainsi que des modifications de la microstructure, qui sont sources de contraintes résiduelles. La géométrie finale des pièces est obtenue par usinage, qui est généralement la dernière étape de fabrication. Jusqu'à 90% du volume de matière initial peut être enlevé durant l'usinage de grandes pièces aéronautiques, qui peuvent également présenter des géométries complexes. La redistribution des contraintes résiduelles pendant l'usinage est une des principales causes de non-conformité des pièces avec les tolérances géométriques et dimensionnelles et donc de non-acceptation de celles-ci.
De nos jours, les contraintes résiduelles et leurs effets pendant l'usinage ne sont généralement pas pris en compte lors de la définition des gammes d'usinage. Ce travail de thèse vise donc à proposer une évolution dans l'établissement des gammes d'usinage des pièces de structures en alliage d'aluminium et a été construit autour de deux principaux axes de recherche : un axe numérique et un axe d'analyse mécanique.
L'axe numérique est basé sur la mise en place d'une approche de modélisation et le développement d'un outil numérique adapté à la simulation de l'usinage. L'approche de modélisation a été définie à partir d'hypothèses déduites d'études bibliographiques sur les alliages d'aluminium, le procédé d'usinage et les contraintes résiduelles. Une approche numérique d'enlèvements massifs de matière a ainsi été développée et tous les développements ont été intégrés dans les codes sources du logiciel FORGE® dans un environnement parallèle.
L'axe d'analyse mécanique est basé sur l'étude de la redistribution des contraintes résiduelles et des déformations associées lors de l'usinage. Une première étude appliquée à la méthode expérimentale utilisée pour déterminer les profils de contraintes résiduelles dans des tôles laminées en alliage AIRWARE® 2050-T84 a été réalisée. Les simulations de ces essais ont permis une première validation de l'outil numérique développé et ont démontré la nécessité de définir des gammes d'usinage en fonction des contraintes résiduelles. D'autres études sur l'influence de certains paramètres définis dans les gammes d'usinage sur la qualité d'usinage ont également été menées. Les simulations réalisées ont été validées par de multiples comparaisons avec des résultats expérimentaux, montrant la capacité de l'outil numérique à prédire précisément la géométrie finale des pièces. A l'aide des résultats obtenus sur les précédentes études, une procédure numérique et de premières recommandations pour la définition de gammes d'usinage permettant d'obtenir la qualité d'usinage souhaitée en tenant compte des contraintes résiduelles initiales ont été mises en place.

MOTS CLÉS : contraintes résiduelles, éléments finis, usinage, distorsions, tolérances finales, aluminium-lithium

Numerical modelling and mechanical analysis of the machining of large aeronautical parts : Machining quality improvement

ABSTRACT : The manufacturing of aluminium alloy structural aerospace parts involves multiple forming (rolling, forging, etc.) and heat treatment steps. The mechanical and thermal loads that the workpieces undergo during these manufacturing steps result in unequal plastic deformation and in metallurgical changes which are both sources of residual stresses. Machining is usually the last manufacturing step during which the final geometry of the parts is obtained. Up to 90% of the initial volume of the workpiece can be removed during the machining of aerospace structural parts which can furthermore have complex geometries. The residual stress redistribution is one of the main causes of the non-conformity of parts with the geometrical and dimensional tolerance specifications and therefore of the rejection of parts.
Nowadays, initial residual stresses and their effect during the machining are often not taken into account in the definition of the machining process plan. This work aims to propose an evolution in the establishment of machining process plans of aluminium structural parts. It has been organised along two principal lines of research : a numerical line and a mechanical analysis line.
The numerical line is based on the development of a modelling approach and of a numerical tool adapted to the simulation of the machining process. The modelling approach has been defined based on assumptions deduced from literature reviews on aluminium alloys, on the machining process and on residual stresses. A massive material removal approach has then been developed. All the numerical developments have been implemented into the finite element software FORGE® and are suited to a parallel computing environment.
The mechanical analysis line is based on the study of the residual stress redistribution and its effect on the workpiece deflections during the machining as well as on the post-machining distortion. A first study on the layer removal method used to determine the initial residual stress profiles in an AIRWARE® 2050-T84 alloy rolled plate has been realised. The simulation of these experiments has allowed a first validation of the numerical tool and to demonstrate the necessity to define machining process plans in function of the residual stresses. Other studies on the influence of some machining process parameters on the machining quality have then been performed. Simulation results have been validated by multiple comparisons with experimental tests, showing the capability of the numerical tool to predict the final machined part geometries. Using the results of the studies mentioned above, a numerical procedure and first recommendations for the definition of machining process plans allowing to obtain the desired machining quality depending on the initial residual stresses have been established.

KEYWORDS : residual stresses, finite element, machining, distortions, tolerance specifications, aluminium-lithium

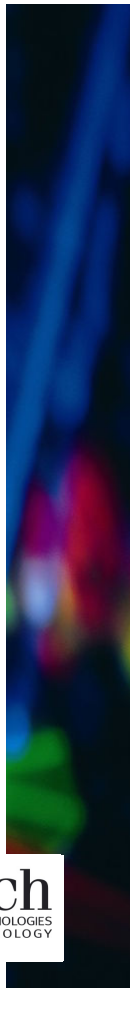

MINES ParisTech

ParisTech
INSTITUT DES SCIENCES ET TECHNOLOGIES
PARIS INSTITUTE OF TECHNOLOGY